British Geological Survey
Expert | Impartial | Innovative

Characterising the hyporheic zones in the Skerne Catchment

Groundwater Science Programme

Commercial Report CR/19/004

BRITISH GEOLOGICAL SURVEY

GROUNDWATER SCIENCE PROGRAMME

COMMISSIONED REPORT CR/19/004

Characterising the hyporheic zones in the Skerne catchment

B Palumbo-Roe, VJ Banks, B Brauns

Contributors

J Elsome, D Mallin Martin, S Gregory

Keywords

Hyporheic zone; groundwater-surface water interaction; Magnesian Limestone; sulphate; mine water; Co Durham.

Front cover

A tributary of the River Skerne.

Bibliographical reference

PALUMBO-ROE, B, BANKS, VJ, BRAUN, B 2019. Characterising the hyporheic zones in the Skerne Catchment. *British Geological Survey Commissioned Report*, CR/19/004. 173 pp.

Keyworth, Nottingham British Geological Survey 2019

BRITISH GEOLOGICAL SURVEY

The full range of our publications is available from BGS shops at Nottingham, Edinburgh, London and Cardiff (Welsh publications only) see contact details below or shop online at www.geologyshop.com

The London Information Office also maintains a reference collection of BGS publications, including maps, for consultation.

We publish an annual catalogue of our maps and other publications; this catalogue is available online or from any of the BGS shops.

The British Geological Survey carries out the geological survey of Great Britain and Northern Ireland (the latter as an agency service for the government of Northern Ireland), and of the surrounding continental shelf, as well as basic research projects. It also undertakes programmes of technical aid in geology in developing countries.

The British Geological Survey is a component body of UK Research and Innovation.

British Geological Survey offices

BGS Central Enquiries Desk

Tel 0115 936 3143 Fax 0115 936 3276

email enquiries@bgs.ac.uk

Environmental Science Centre, Keyworth, Nottingham NG12 5GG

Tel 0115 936 3241 Fax 0115 936 3488
email sales@bgs.ac.uk

The Lyell Centre, Research Avenue South, Edinburgh EH14 4AP

Tel 0131 667 1000 Fax 0131 668 2683
email scotsales@bgs.ac.uk

Natural History Museum, Cromwell Road, London SW7 5BD

Tel 020 7589 4090 Fax 020 7584 8270
Tel 020 7942 5344/45 email bgslondon@bgs.ac.uk

Cardiff University, Main Building, Park Place, Cardiff CF10 3AT

Tel 029 2167 4280 Fax 029 2052 1963

Maclean Building, Crowmarsh Gifford, Wallingford OX10 8BB

Tel 01491 838800 Fax 01491 692345

Geological Survey of Northern Ireland, Department of Enterprise, Trade & Investment, Dundonald House, Upper Newtownards Road, Ballymiscaw, Belfast, BT4 3SB

Tel 028 9038 8462 Fax 028 9038 8461

www.bgs.ac.uk/gsni/

Parent Body

Natural Environment Research Council, Polaris House, North Star Avenue, Swindon SN2 1EU

Tel 01793 411500 Fax 01793 411501
www.nerc.ac.uk

UK Research and Innovation, Polaris House, Swindon SN2 1FL

Tel 01793 444000
www.ukri.org

Website www.bgs.ac.uk
Shop online at www.geologyshop.com

Foreword

This report is the published product of a study by the British Geological Survey (BGS). It comprises a review of the methodology developed to improve the understanding of connectivity between the River Skerne and the Magnesian Limestone aquifer. This research was supported by the Environment Agency, the Coal Authority, Anglian Water Services and Nortumbrian Water Group with BGS co-funding in order to inform the scheduling of design measures to protect the groundwater resource in the context of the River Basin Management Plan. The research is necessarily multi-disciplinary, drawing from the skills of a range of colleagues in the BGS and EA to provide field and laboratory support.

Acknowledgements

In addition to the authors, the contribution of a number of people is gratefully acknowledged. In particular BGS staff Michael Watts, Simon Chenery, Tom Barlow, Elliott Hamilton, Tom Kelly, Aurelie Devez, and Andy Marriott are thanked for providing the chemical analysis. The student Tim Roth and BGS colleagues Mike Bowes, Jack Elsome and Dan Mallin Martin are thanked for field work contribution and Simon Gregory for the microbiological analysis. Pauline Smedley is thanked for reviewing the report. The Environment Agency colleagues including Ms Diane Steele, Ms Sally Gallagher contributed to generating the research outputs and therefore to the production of this report. In addition to the collection of data, many individuals have freely given their advice, and provided the local knowledge so important to the process understanding and we would particularly like to thank colleagues at JBA in this regard.

Contents

FIGURES

TABLES

1 Introduction

1.1 PURPOSE AND STRUCTURE OF REPORT

This report describes the progress of a BGS-Environment Agency (EA) co-funded project aimed at contributing to the assessment of the potential contaminant pathways in the hyporheic zone of the Skerne catchment in Co. Durham, UK. The study forms stage II of a three year programme led by the EA. The programme's main goal is to understand connectivity between the River Skerne and the Magnesian Limestone aquifer, in order to design measures to improve protection of the groundwater resource in the context of the River Basin Management Plan. The zone of groundwater–surface water connectivity is often referred to as the hyporheic zone, defined as the region beneath and alongside the streambed, where there is mixing of groundwater and surface water. Over the past two years the EA has been monitoring the quality of the surface waters to determine whether they have been impacted, via baseflow, by an eastwards moving mine water plume. The mine water plume is related to the recovery of groundwater levels in the Coal Measures within the Durham Coalfield to the south of the Butterknowle Fault and following closure of the Mainsforth and Fishburn Collieries. It has been confirmed that the sulphate-rich groundwater is entering the Woodham Burn, a tributary of the River Skerne, with observed concentrations of sulphate greater than 300 mg/l.

This project aims:

i) to review the conceptual model of groundwater–surface water interaction in the study catchment (Chapter 1) and draw a first-pass conceptual ground model of selected sites (up to 5 sites) (Chapter 2) for more detailed investigation at the "local" metre scale of hyporheic flow and geochemical processes.

ii) to characterise the hyporheic zone chemistry in areas of groundwater–surface water connectivity and provide an understanding of the biogeochemical interactions taking place in the hyporheic zone, with a focus on mine water-related sulphate and iron, and nutrient pollution (phosphate, and nitrate).

The approach and the methods to deliver the project's aims are covered in this progress report (Chapters 3 and 4) and the results presented (Chapters 5, 6 and 7).

1.2 SUMMARY OF PREVIOUS RESEARCH ON THE RIVER SKERNE AND THE MAGNESIAN LIMESTONE AQUIFER

A number of previous studies have been carried out on the River Skerne and the Magnesian Limestone aquifer and the findings are summarised in this section. The key reports informing this study are:

1. JBA 2017. Skerne Magnesian Limestone. Skerne catchment assessment, 46 pp.
2. Environment Agency, 2012. Hydrology Flow Investigation Stage 2. Northumbria River Basin District Investigation: NE2010-10005.

3. Bearcock, J. and Smedley, P.L. 2009. Baseline groundwater chemistry: the Magnesian Limestone of County Durham and North Yorkshire. BGS Groundwater Programme Open Report OR/09/030.
4. Price, S.J., Merritt, J.E., Whitbread, K., Lawley, R.S., Banks, V., Burke, H, Irving, A.M. and Cooper, A.H. 2007. Superficial geology and hydrogeological domains between Durham and Darlington Phase 1 (Durham South). BGS Commissioned Report CR/07/002 N.

A number of key papers are listed below and these and other relevant papers informing this study are referenced throughout the text and at the end of the report.

1. Cairney, T., and Hamill, L. 1977. Interconnection of surface and underground water resources in southeast Durham. *Journal of Hydrology*, 33, 73 – 86.
2. Hamill, L. 1978. Evaluation of induced infiltration between the River Skerne and the Magnesian Limestone in south east Durham. Journal of the Institute of Water Engineers and Scientists, 34, 2, 161-71.
3. Kortas, L. and Younger, P.L. 2013. Fracture patterns in the Permian Magnesian Limestone Aquifer, Co. Durham, UK. Proceedings of the Yorkshire Geological Society, 59, 3, 161 – 171.
4. Neymeyer, A., Williams, R.T. and Younger, P.L. 2007. Migration of polluted minewater in a public supply aquifer. Quarterly Journal of Engineering Geology and Hydrogeology. 40, 75-84.

1.2.1 The River Skerne catchment

The River Skerne is a tributary of the River Tees which flows through County Durham in North East England (Figure 1). It forms one of the 6 operational catchments of the River Tees management catchment in the Northumbria River Basin District. The Skerne rises near Trimdon Village where it is impounded at Hurworth Burn reservoir immediately upstream of some natural swallow holes in the bed of the Skerne. Variable thicknesses of impermeable drift and groundwater levels produce a complex pattern of flow interaction. Rivers have been diverted and channelised for the purposes of agricultural land drainage. Villages such as the Trimdons, Fishburn, Ferryhill and Chilton and the more industrial Newton Aycliffe discharge treated sewage and trade effluents into the river. The river continues south where it is heavily modified through the centre of Darlington before joining the Tees at Croft-on-Tees [from http://environment.data.gov.uk/catchment-planning/OperationalCatchment/3406/Summary].

Permanent flow gauging stations on the River Skerne are: from upstream to downstream Bradbury, Preston-Le-Skerne, John St Darlington and South Park (Figure 1). Flows are known to be naturally low throughout most of the year, though the catchment is flashy, and flooding can occur. A general increase in flow downstream from Bradbury to South Park is recorded. When the flow is normalised by catchment area, a complex pattern of gains and losses is recognised.

In the past there were significant discharges into surface watercourses from mine dewatering. Minewater discharges from Chilton, Mainsforth, Thrislington and Fishburn Collieries particularly affected flows in the River Skerne, above Bradbury or between Bradbury and Preston-le-Skerne (tributary to Rushyford Beck). Some of the discharges will have been lost to the Magnesian Limestone aquifer, as estimated by Cairney and Hamill (1977).

Surface water quality data has highlighted elevated concentrations of phosphate and nitrate, which have been identified as the primary reason for the ecological failures down the catchment. Secondary reasons for the ecological failures include elevated sulphate concentrations and low flows.

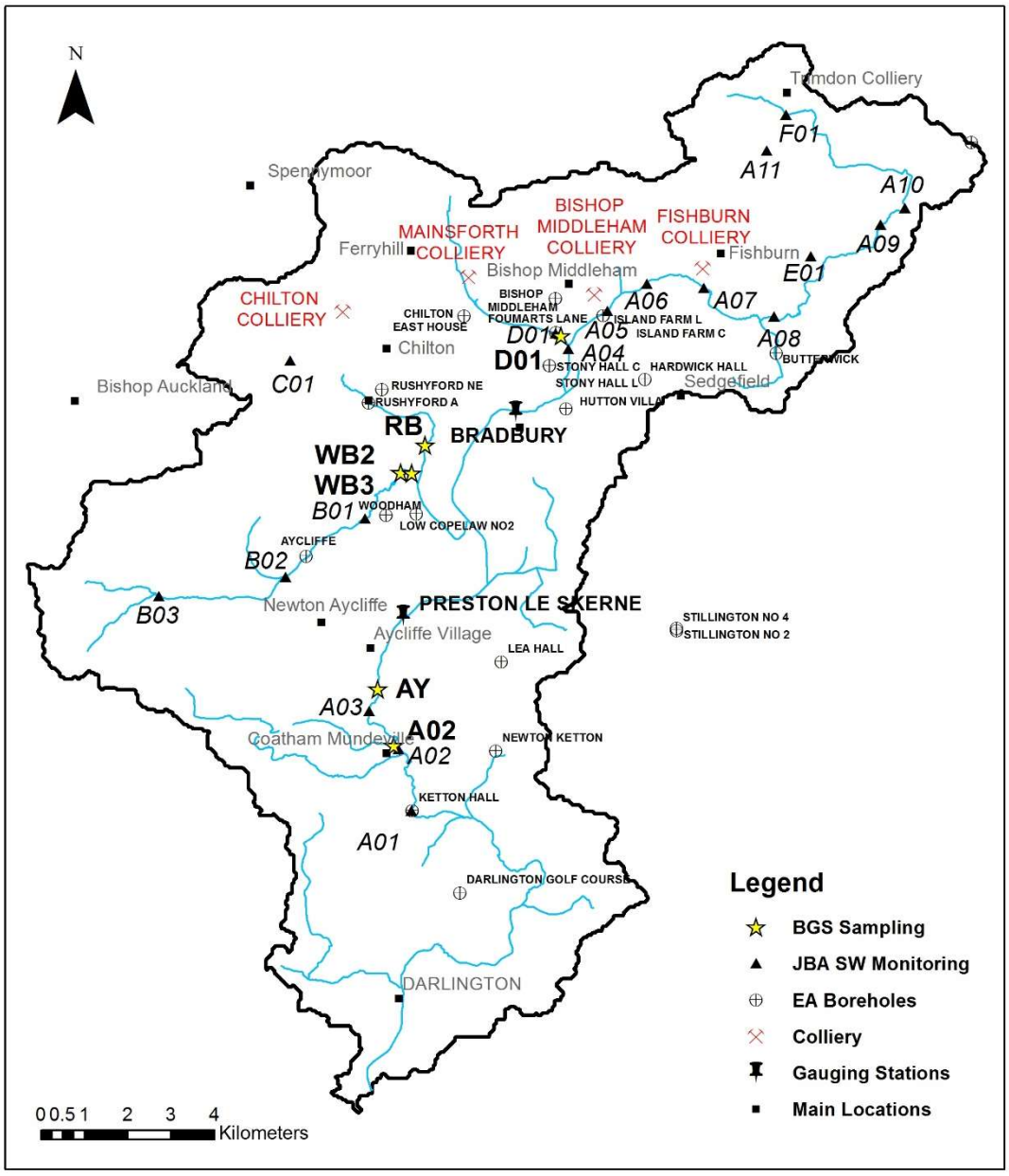

Figure 1: Study area. Location of BGS hyporheic zone (HZ) sampling sites, surface water (SW) monitoring carried out by JBA (JBA, 2017) , and EA borehole (BH) monitoring.

1.2.2 The Magnesian Limestone aquifer: geology and hydrogeology

The River Skerne flows across the Permian Zechstein Group (Magnesian Limestone) for almost all of its length. The Magnesian Limestone aquifer is an important source of water for potable supplies and for industrial, commercial and recreational uses. The aquifer also supports a number of water dependent features including springs, wetlands and rivers. Many

anthropogenic activities, including rising sulphate-rich mine water pollution, and licensed abstractions, are known to pose a risk to, or are already impacting on the quality and/or quantity of groundwater in the aquifer.

The Environment Agency manages the Magnesian Limestone Principal Aquifer which comprises the Permian Zechstein and Rotliegendes groups. The groups are hydrogeologically connected because the Marl Slate Formation at the base of the Zechstein Group is laterally impersistent. The Magnesian Limestone comprises a series of marine limestones and dolomites, marls and evaporites deposited in response to changes in the level of shallow tropical seas (Stone et al., 2010). The limestones form a thin north–south trending outcrop between South Shields and Nottingham. Figure 2 presents the major mapped formation described in this section and Figure 3 presents a cross section marked in Figure 2. The regional variation and the current and traditional nomenclature of the Permian stratigraphy are compared in Table 1 (after Bearcock and Smedley, 2009).

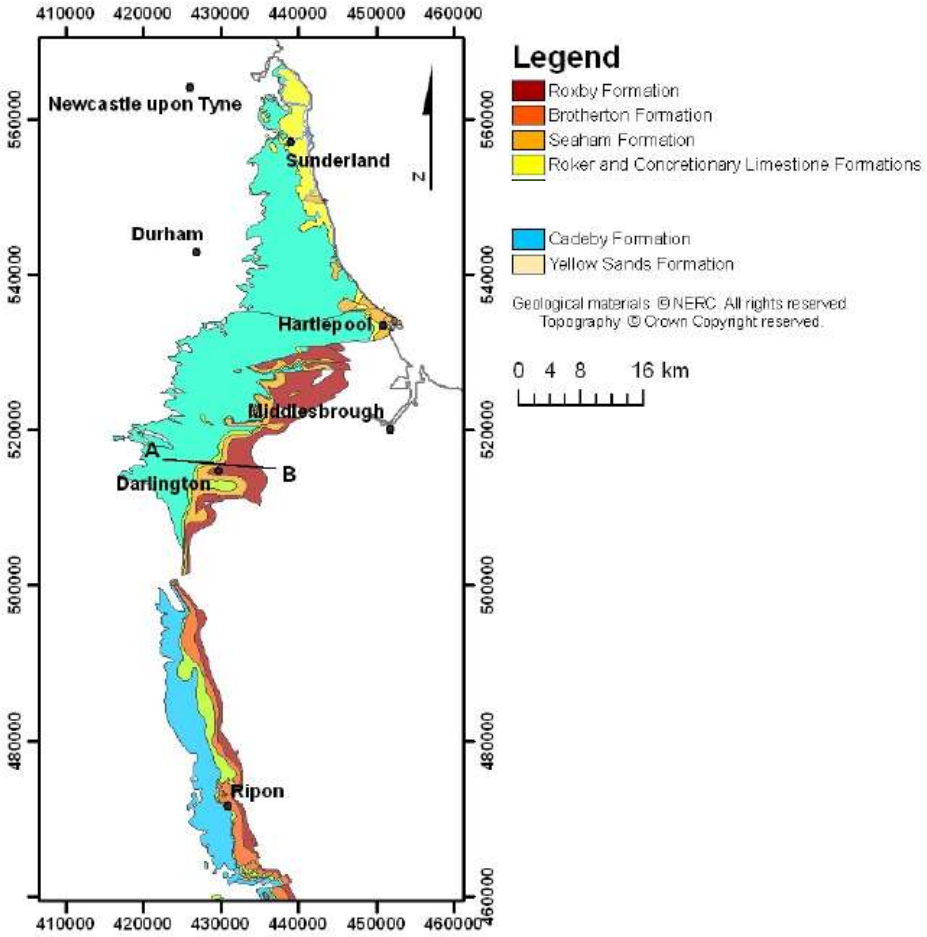

Figure 2: Mapped formations within Magnesian Limestone (from Bearcock and Smedley, 2009). Contains Ordnance Survey data © Crown Copyright and database right 2019. Ordnance Survey Licence no. 100021290

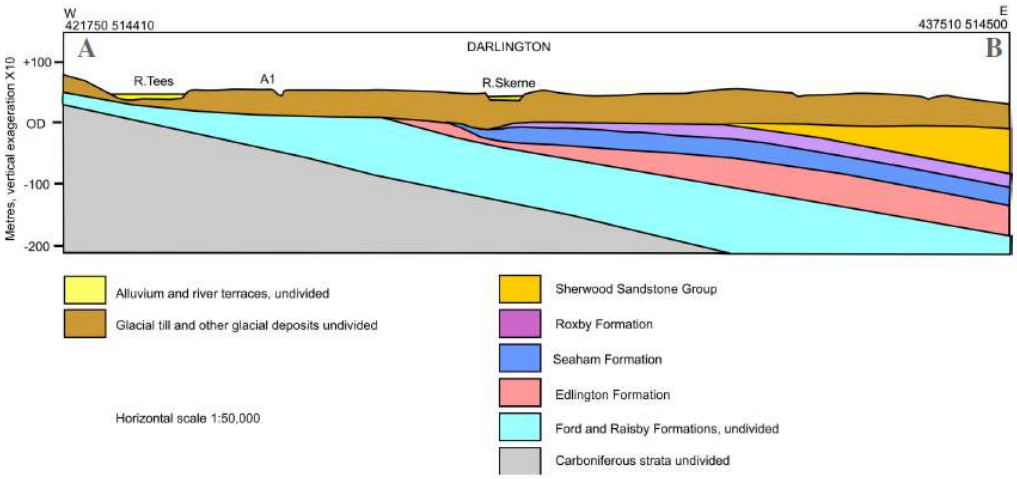

Figure 3: Cross section, east to west, across the Magnesian Limestone outcrop in Darlington (from Cooper and Gordon, 2000).

Table 1: Correlation of the Permian Groups and Formations (Bearcock and Smedley, 2009).

	Group	Durham Province		Yorkshire Province		English Zechstein Cycle
		Old Nomenclature	New Nomenclature	New Nomenclature	Old Nomenclature	
Triassic	Sherwood Sandstone Group	Bunter Sandstone	Sherwood Sandstone		Bunter Sandstone	
Permian	Zechstein Group	Upper Permian Marl	Roxby Formation		Upper Permian Marl	EZ5
						EZ4
		Upper Magnesian Limestone	Seaham Formation	Brotherton Formation	Upper Magnesian Limestone	EZ3
			Seaham Residue	Edlington Formation (also in south of Durham Province)	Middle Permian Marl	EZ2
			Roker Formation			
			Concretionary Limestone Formation			
		Middle Permian Marl	Hartlepool Anhydrite Formation			EZ1
		Middle Magnesian Limestone	Ford Formation	Cadeby Formation	Lower Magnesian Limestone	
		Lower Magnesian Limestone	Raisby Formation			
		Marl Slate Formation	Marl Slate Formation		Marl Slate Formation	
	Rotliegendes Group	Basal Permian Sands/ Breccia	Yellow Sands Formation		Basal Permian Sands/ Breccia	

The Zechstein Group comprises six formations that overlie the Rotliegendes Group Basal Permian Yellow Sands Formation (Table 1). A brief description of each follows. The Raisby Formation rests on the Marl Slate, an evenly laminated carbonaceous, dolomitic and calcareous siltstone, and is the first major carbonate rock unit of the English Zechstein. It crops out along a narrow belt forming a prominent west-facing escarpment (Smith, 1994), extending eastwards beneath younger strata. The thickness of the formation is variable, being less than 10 m in the north of the Durham Province, increasing to 70 m west of Hartlepool in the central region, and about 30 m in the south of the province (Bearcock and Smedley, 2009). It comprises cream, brown and grey, fine-grained dolostone with grey, fine-grained limestone.

The Permian strata rest unconformably on the Carboniferous strata to the west of the Skerne catchment. The Ford Formation overlies the Raisby Formation and is a wedge-shaped carbonate shelf complex composed of dolomites, calcitic dolomites and dolomitic limestones (Smith and Francis, 1967; Mills and Hull, 1976). The formation comprises three distinct facies: shelf-edge reef that separates a broad belt of back-reef and lagoonal beds to the west from a belt of fore-reef talus aprons and off-reef beds to the east. It crops out in a north-south belt up to 3–10 km wide, occupying most of the outcrop of Permian rocks north of Hartlepool (Smith and Francis, 1967; Smith, 1994) and predominates in the area of the Skerne catchment. The formation is often considered together with the Raisby Formation because both are dolomitic and commonly indistinguishable in boreholes. Their combined thickness varies from 5–82 m (Cooper and Gordon, 2000). The variation in thickness reflects the topography of the underlying strata (Cooper and Gordon, 2000).

The Edlington Formation (up to 65 m thick) incorporates the Hayton Anhydrite at its base. Overlying the Hayton Anhydrite is the Kirkham Abbey Formation, a thin sequence (≤5 m) of lenticular dolomitic limestone (Bearcock and Smedley, 2009). The upper 20 m of the Edlington Formation is mainly siltstone and mudstone containing thin anhydrite and gypsum beds. This formation is equivalent to the Hartlepool Anhydrite, Concretionary Limestone and Roker formations, and the Seaham Residue found in the north of the Durham Province. It represents the latter parts of the first Zechstein cycle and most of the second cycle (Table 1; Cooper and Burgess, 1993). Boreholes downdip of the outcrop show that the anhydrite is up to 40 m thick.

The Seaham Formation comprises the carbonate phase of EZ3, representing renewed marine incursion (Cooper and Burgess, 1993; Smith, 1994). Although the Seaham Formation is locally variable, it is the most uniform of all the carbonate deposits of the English Zechstein sequences (Bearcock and Smedley, 2009).

The Roxby Formation is the uppermost unit of the English Zechstein sequence. It is 10–18 m thick in the few outcrops that occur in the south of the Durham Province. It comprises silty mudstones and fine-grained sandstones.

The superficial deposits consist of glacial and associated glaciolacustrine and glacio-fluvial sediments of Late Devensian age overlain by younger Flandrian deposits. The Late Devensian deposits have been divided using the lithostratigraphic nomenclature outlined in Stone et al. (2010) and described in Price et al. (2007). However, for this report the more generic lexicon terms of the BGS digital mapping have been used for consistency.

More details of the geology at each study site are included in subsequent sections of this report.

As noted by Price et al. (2007) the superficial deposits influence recharge and aquifer vulnerability. Tills predominate throughout the Skerne catchment with smaller areas of glacio-fluvial deposits, and pockets of lacustrine deposits and peat. Geological sections presented by Price et al. (2007) confirmed that broadly the superficial deposits thin to the west, as noted by Cairney and Hamill (1977), and such that they form an increasingly confining layer to the east. The glacio-fluvial deposits are largely associated with the northern, eastern and downstream parts of the catchment, whilst the glaciolacustrine and peat deposits occur to the north of Preston-le-Skerne. The absence of the Quaternary deposits (a hydraulic window) in the area of Aycliffe Village has also been noted. Connectivity of the River Skerne and the bedrock was demonstrated by Cairney and Hamill (1977). They identified two such areas, one was suggested in the areas of the hydraulic window referenced above and the other in the bed of the Rushyford Beck. More recent research (JBA, 2017) has further developed this concept.

The hydrogeology of the Zechstein Group has been considered by Allen et al. (1997), Bearcock and Smedley (2009), and Kortas and Younger (2013). The combined thickness of the Ford and Raisby formations is 5-82 m. The regional hydraulic gradient is to the east; however, Kortas and Younger (2013) have shown that the dominant fracture sets impose a permeability tensor to the NNE to ENE. Transmissivity values within the Zechstein Group aquifer range from 6–4300 m^2 day^{-1}, but more generally range between 60 and 800 m^2 day^{-1} (Younger, 1995; Allen et al., 1997). Typically, higher values are associated with fault zones (Allen et al., 1997). However, lithological variation and variability in the density of discontinuities results in variable hydraulic conductivity (Bearcock and Smedley, 2009). For example, the reef structures of the Ford Formation are commonly permeable and therefore a focus for groundwater resources (Bearcock and Smedley, 2009). Secondary dolomitisation has been a significant factor in increasing the matrix permeability of the limestones (Machel, 1999).

Neymeyer et al. (2007) undertook conceptual and numerical modelling of the recovery of dewatering in the southern part of the Durham Coalfield since 1974. Their modelling suggests that both point (unlined mineshafts and boreholes) and diffuse (widely distributed) upward flow is required to explain the patterns of pollutant migration to 2003.

1.2.3 Baseline groundwater geochemistry

The main chemical properties of groundwater in the Magnesian Limestone are determined by rainwater recharge reacting with the carbonate rock and evaporite deposits. Mineral reactions involving calcite and dolomite dominate the groundwater chemistry, resulting in Ca-Mg-HCO_3 type waters. Dissolution of evaporite minerals such as gypsum and anhydrite results in high levels of SO_4 in some groundwaters. These are generally samples from confined areas of the Magnesian Limestone where there is leakage from the overlying evaporite-rich marls, e.g. the Edlington and Roxby Formations as part of the English Zechstein evaporite deposits.

Minewater rebound in the Ferryhill area has given rise to groundwaters with high concentrations of SO_4 and Fe, as well as Ca, Na and Cl.

The complex lithology and variable chemistry of the strata mean that sites with groundwaters of a very different chemistry occur in close proximity. Concentrations of Fe, Mn and SO_4 are particularly variable and (along with nitrate and fluoride), potentially the most problematic from a supply point of view (Bearcock and Smedley, 2009).

1.2.4 Conceptual model of surface water–groundwater interaction within the Skerne (including tributaries).

The eastern and larger part of the Skerne catchment is covered by thick (>30 m) superficial deposits consisting of glacial clays which are essentially impermeable and thus confine the Magnesian Limestone. Because of this clay blanket, the Skerne and the Magnesian Limestone have originally been considered to be isolated water resources. Cairney and Hamill (1977) were the first to re-examine this assumption and described the connectivity between the River Skerne and the Magnesian Limestone. Groundwater provides base flow to the River Skerne and its tributaries at a number of locations along its length. Marsh and Hannaford (2008) reported that the base flow index (BFI) of the river ranges from 0.39 in the upper reaches to 0.5 close to its confluence with the River Tees. Superficial drift (primarily Glacial Till and Sand and Gravel deposits) is understood to significantly vary in thickness across the catchment. In areas of thinner drift deposits groundwater–surface water connectivity is likely, with surface waters either being lost to ground or receiving baseflow, with loss or gain being controlled by the differences in the ground and surface water levels. For example lower groundwater levels in the northern part of the catchment are likely associated with loss from the stream. High groundwater levels in the area of Swan Carr, Low Copelaw, Great Isle and Ketton Hall are likely to be confined by the thicker cover of superficial deposits. In this setting there is a potential for recharge via faults, e.g. at Coatham Mundeville to the north of Ketton Hall. The presence of springs along the edge of the River Skerne and its tributaries in the area of Bishop Middleham, where the thickness of the superficial deposits is less than farther east, may be indicative of groundwater discharge to the river. It is plausible that the situation is similar along stretches of Woodham Burn.

EA (2012) concluded that there has been an increase in the rate of groundwater discharge downstream of Preston-le-Skerne since recovery of groundwater levels in the late 1970s, with discharges likely via windows in the cover of superficial deposits. The BGS report Superficial Geology and Hydrogeological Domains between Durham and Darlington Phase 1 (Durham South) prepared for the Environment Agency has further informed the surface water-groundwater interaction assessment reported in the Northumbrian Magnesian Limestone Aquifer study (EA, 2012). Figure 4 from EA, 2012 summarises the conceptual model of potential losses and gains to the river from groundwater, based on groundwater levels and superficial deposit distribution.

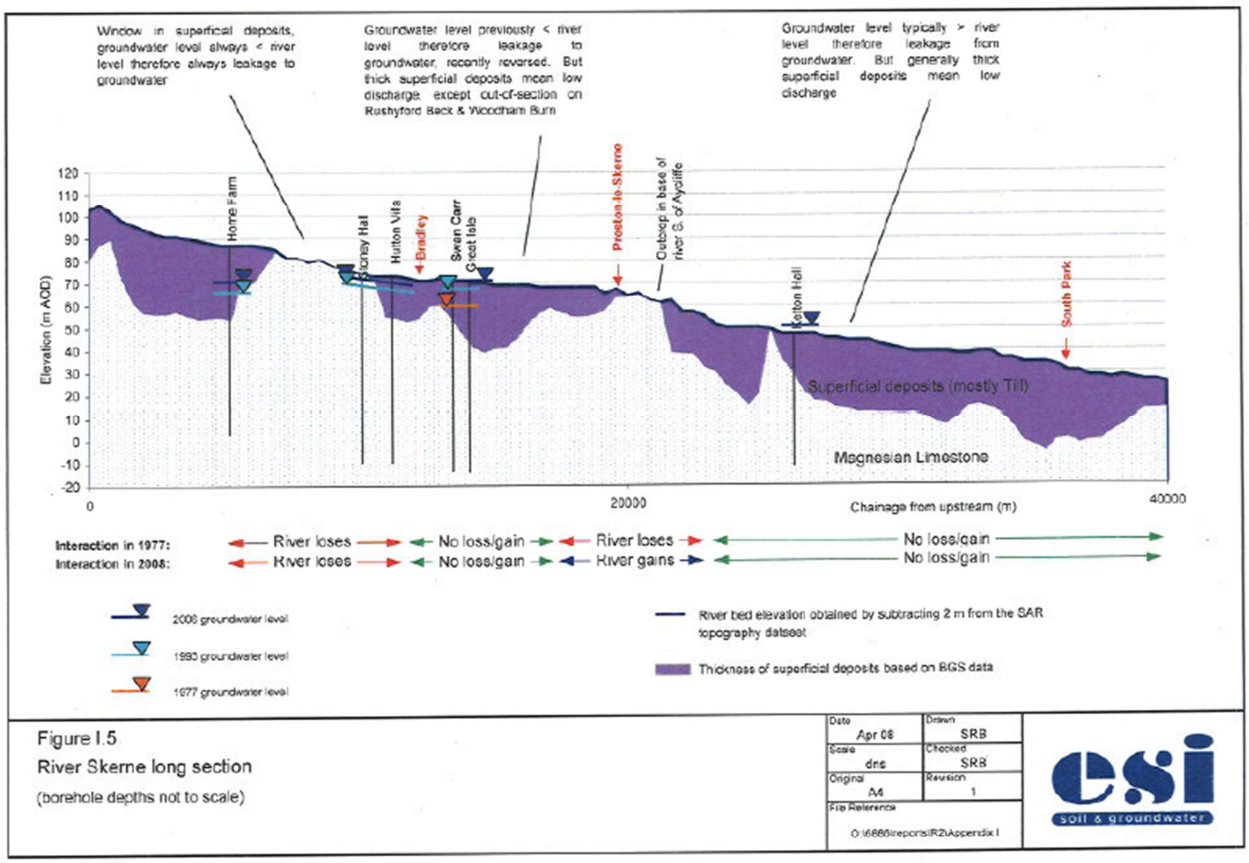

Figure 4: from EA (2012) Appendix I: river–aquifer interaction: long section of River Skerne.

More recently as part of the EA study, a broad River Connectivity Classification Scheme (Figure 5, JBA, 2017) was developed by JBA on behalf of the EA, based on two key hydrogeological factors:

- depth to groundwater within the Magnesian Limestone (ML) relative to surface elevation, estimated from EA borehole hydrographs and the Digital Terrain Model (DTM) for the area;

-thickness of superficial geology from BGS (2007).

Connectivity includes both the potential to lose and/or gain water from/to the ML aquifer.

The following broad river reach divisions were recognised in the Skerne catchment and tributaries (JBA, 2017):

- Small tributaries on areas of higher ground near the topographic ridge line on thin, low permeability till, or areas free of superficial deposits; these are prone to losing water to the bedrock where the ML is unconfined and the thickness and permeability of the superficial that underlie the bed vary;

- Skerne and tributaries on thick superficial deposits in the east, isolated from the ML aquifer; these reaches have limited potential for connection with the ML aquifer;

- Skerne (and tributaries) through the centre of the catchment on thin till and alluvium, or with alluvium directly on bedrock. These reaches are more likely to interact with

groundwater in the underlying ML aquifer, gaining or losing depending on the local groundwater levels in the aquifer relative to riverbed level and local superficial geology.

A further monitoring program of spot flow gauging at selected sites in the catchment, carried out by JBA, indicates a complex spatial and temporal pattern of gaining and losing reaches in the river. Their conclusions are as follows (JBA, 2017):

- The pattern of gaining and losing behaviour in the Skerne in the study area is complex and cannot be attributed to changes in groundwater levels in the Magnesian Limestone alone.

- Though artificial discharges might aid in partly explaining why certain sections gain, the losing reaches have to be as a result of losses to the underlying groundwater system.

- It is possible that there are two groundwater systems which influence flow conditions in the river:

- A shallow rapidly responding system within the superficial deposits which is responsible for the increases in baseflow observed in the winter when ML borehole hydrographs indicate that water levels in this aquifer are still recovering. However, there are no groundwater monitoring data available for the superficial deposits within the entire catchment to fully evaluate the interaction of the superficial deposits with the river.

- A deeper system of recharge from the ML aquifer which supplies a greater proportion of baseflow in the late spring after a winter of recharge. EA borehole hydrographs indicate that groundwater levels in the ML aquifer are at their maximum in the late spring.

- Superimposed upon this is the possible contribution to baseflow from artificial discharges, the influence of which it is not possible to accurately assess as detailed discharge volumes are not available.

- This means that baseflow is not a good proxy for ML input into the rivers.

- Losses and gains are greatest in reaches with strong connection to the ML aquifer.

- Some areas of superficial aquifers are prone to drying out. This could be explained by the water table in these areas falling beneath the river level so water can be lost to them in dry periods.

Figure 5 illustrates the JBA River Reach Connectivity Classification and Gaining/Losing Reach Classification (Map 4-4: JBA, 2017), which has guided the selection of the hyporheic zone study sites, outlined in Section 2.

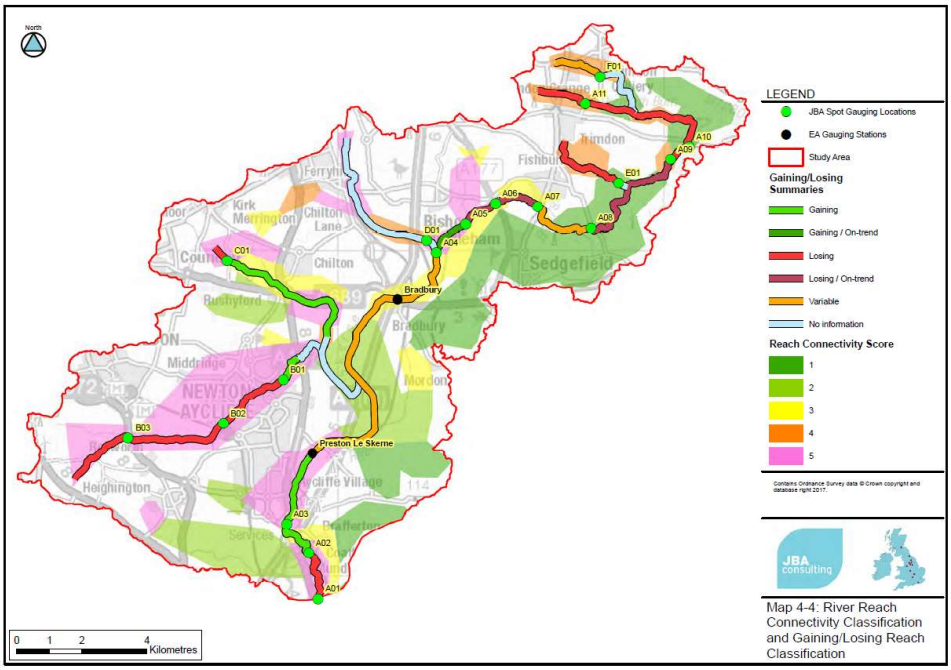

Figure 5: JBA River reach connectivity classification and gaining and losing reach classification (JBA, 2017).

2 Site selection and initial conceptual site models

2.1 OVERVIEW

During an initial field visit on 08/06/2017, in consultation with JBA, the EA guided BGS to a number of gaining reaches within the Skerne catchment that were suspected to be zones of groundwater contributions. Five locations (Table 2) in the catchment have been selected for the hyporheic zone data collection.

Table 2: Site selection for hyporheic zone characterisation

Location	Point name	Easting	Northing	Classification of Connectivity (JBA, 2007)
Mainsforth Stell Tributary	D01	482683	530306	Unclassified
Woodham Burn Tributary	WB/2 WB/3	429388 429134	527080 527086	High Connectivity
Rushford Beck Tributary	RB	429703	527719	High Connectivity
Skerne at Aycliffe	AY (A03)	428609	522106	High Connectivity
Skerne at Coatham Mundeville	A02	429087	520710	High Connectivity

A quick review of each of these sites has enabled the development of a "first pass" conceptual ground model for the design of the subsequent field experiments and revision of the conceptual models in the light of the new data. Furthermore, a number of sampling sites were chosen for the hyporheic zone study (Figure 1).

2.2 MONITORING POINT FOUMARTS LANE (D01)

2.2.1 Location, geomorphology and land use

Site D01 falls in the "Carrs from Source to Skerne" catchment. The source of this tributary lies to the north–east of Ferryhill. It flows south and then south–east to join the River Skerne at 432997 530001. It is accessed via Foumarts Lane, which is a public pathway and track that extends south from Bishop Middleham village. In this area the geomorphology has been influenced by both geological and anthropogenic processes. The stream is canalised in this stretch and lies towards the northern edge of a wide floodplain. To the south of the stream the

extensive floodplain comprises flat pasture for sheep and cattle, interrupted by areas of carr woodland (seasonally wet woodland), field boundaries and drainage ditches. To the north of the stream the ground rises from the floodplain to the escarpment (approximately 130 m OD). Hummocky ground at the edge of the floodplain comprises mounds of glacio-fluvial deposits (Table 3), giving rise to the term "island landscape" (Durham County Council, 2012) and quarry spoil. To the west of Foumarts Lane the land sustains arable farming, to the east the ground level slopes towards a sewage treatment works and the grounds of the former Middleham Castle, which was the principal residence of the Bishops of Durham from the Conquest to the end of the 14th century. It is understood that this was more of a manor house than a castle, however its situation afforded good protection and the area of wet land to the south was, in part, given over to fish ponds, a swannery and medieval deer park (Durham County Council, 2012). Several historic quarries were opened on the escarpment. The historic maps also show an old quarry at 432735 530376, which was worked for dolostone and was known as Nunstainton Carr.

The JBA monitoring point is accessed via a poached area on the south side of the stream, which provides a gentler slope into the water course. At this location JBA found the stream bed to be too silty for flow gauging. BGS staff explored the stream in the order of 90 m downstream of this point and despite the high water levels at the time of the reconnaissance visit confirmed the silty nature of the stream bed.

2.2.2 Geology

Geological data obtained from BGS digital data, BGS (2008) and borehole records (Foumarts Lane Borehole; Appendix 1) are summarised in Table 3 and shown in Figure 6 and Figure 7.

Table 3: Geology in the vicinity of monitoring location D01

	Mapped Unit	**Lithology**
Superficial (0-15 m)	Alluvium	Organic clay
	Glacio-fluvial sand and gravel	Sand and gravel
	Devensian Till	Gravelly silty sandy clay
Bedrock	Ford Formation of the Zechstein Group (Permian); formerly Middle Magnesian Limestone	Dolostone (very vuggy in field walls)

The glacio-fluvial sand and gravel deposits are shown to the north of the stream (BGS, 2008), whilst Alluvium underlies the extensive flood plain to the south of the channel with another ribbon extending to the north–east. Here the Alluvium underlies the surface water depressions in this area and forms the area of wet ground that formerly lay within the grounds of Middleham Castle. This ribbon of alluvium extends to Bishop Middleham village and then closes round, marking the route of a former meander that closes in the order of metres downstream of monitoring point D01 and surrounding the area centred on Island Farm at 43347 531051.

The BGS geology field slip (NZ 33 SW, G.D. Gaunt 1953-1987) provides more detail on the distribution of arisings from the former Bishop Middleham Colliery (433676 531273), including: the presence of coke storage tips (433855 430702); red silty clay (433871 531154), and much tipped shale at 433676 531119. Durham County Record Office indicates that the Colliery was opened in 1846 (NCB 24/117) and closed in 1934–8. This followed an explosion on March 2 1930 (recorded in *The Northern Daily Mail and South Durham Herald* on 27 March 1930). A detailed log of the geology can be accessed via: http://www.largeimages.bgs.ac.uk/iip/mapsportal.html?id=1003581. However, little is known of the groundwater conditions in the mine. The groundwater conditions in the flooded mines are monitored jointly by the Coal Authority and EA, at the few remaining unfilled mine shafts, and a good network of purpose drilled monitoring boreholes, several of which are paired with boreholes into the overlying limestone aquifer.

2.2.3 Hydrology and hydrogeology

Evidence for potential groundwater recharge in the alluvial deposits comes from the presence of springs, e.g. at 432033 530464 and 433771 531305 (Figure 7). Both of these springs appear to be associated with inferred faults of unknown displacement (BGS, 2008). Any groundwater rising in this area would be focused on this reach of the channel. The spring at 433771 531305 is also shown on the field slip, indicating that it is a natural feature that may be recharged by resurgences from the escarpment or by deeper groundwater upwelling on a fault zone (see dotted lines in Figure 7) in response to head generated by recharge to the escarpment. Both springs occur in close proximity to the glacio-fluvial deposits and therefore it is equally plausible that they are fed by "perched water" in the glacio-fluvial strata. Input into the river may also occur via Castle Lake (which has an outlet into the river about 100 m upstream from D01) and from the nearby sewage treatment works. Island farm boreholes, Fishburn, Mainsforth, Moor Lane and Millwood, Chilton boreholes can be used to provide groundwater conditions for the area in future further assessments.

2.2.4 EA/JBA reach connectivity classification

In the Phase 1 study, this area was given a Reach Connectivity score of 4 out of 5 (5=highest connectivity), while no information is available in terms of losing/gaining reach. Flow monitoring conducted by JBA on behalf of the EA in the Skerne between A04 and A05 (near Bishop Middleham) indicated that there were significant gains in flows, which were assumed to originate from inflow from the Magnesian Limestone aquifer (JBA, 2017). Relatively high flow was also measured in January and February, when the groundwater level in the Magnesian Limestone aquifer was still low. It was therefore hypothesized that a more superficial (and shallow) aquifer within the superficial deposits may be present in some locations, delivering further inflow into the riverbed. Due to its proximity and similar hydrogeological setting, this could also be the case at monitoring point D01, but no clear conclusion and either gaining or losing conditions could be drawn near D01 in the previous phase of the study.

2.2.5 Initial conceptual site model

The desk study indicates that at the sampling position the stream may encounter groundwater that is impacted by the rising groundwater levels associated with the Mainsforth Colliery. The evidence from the Fourmarts Lane borehole and the Hutton Villa Borehole (Appendix 1) indicate that the groundwater is confined. Although the boreholes indicate sub-artesian conditions, the Fourmarts Lane borehole is raised above river level. This, and the presence of the Carrs, indicates the potential for groundwater interaction with the river. Springs in the area

may be fed by drainage of the superficial deposits, in particular recharge to the glacio-fluvial sands and gravels that are situated immediately to the north and north–west of the sampling point. High groundwater levels may contribute to spring function. Confined flow paths could develop within the Alluvium at any of the sampling positions, providing that it is stratified and of sufficient thickness.

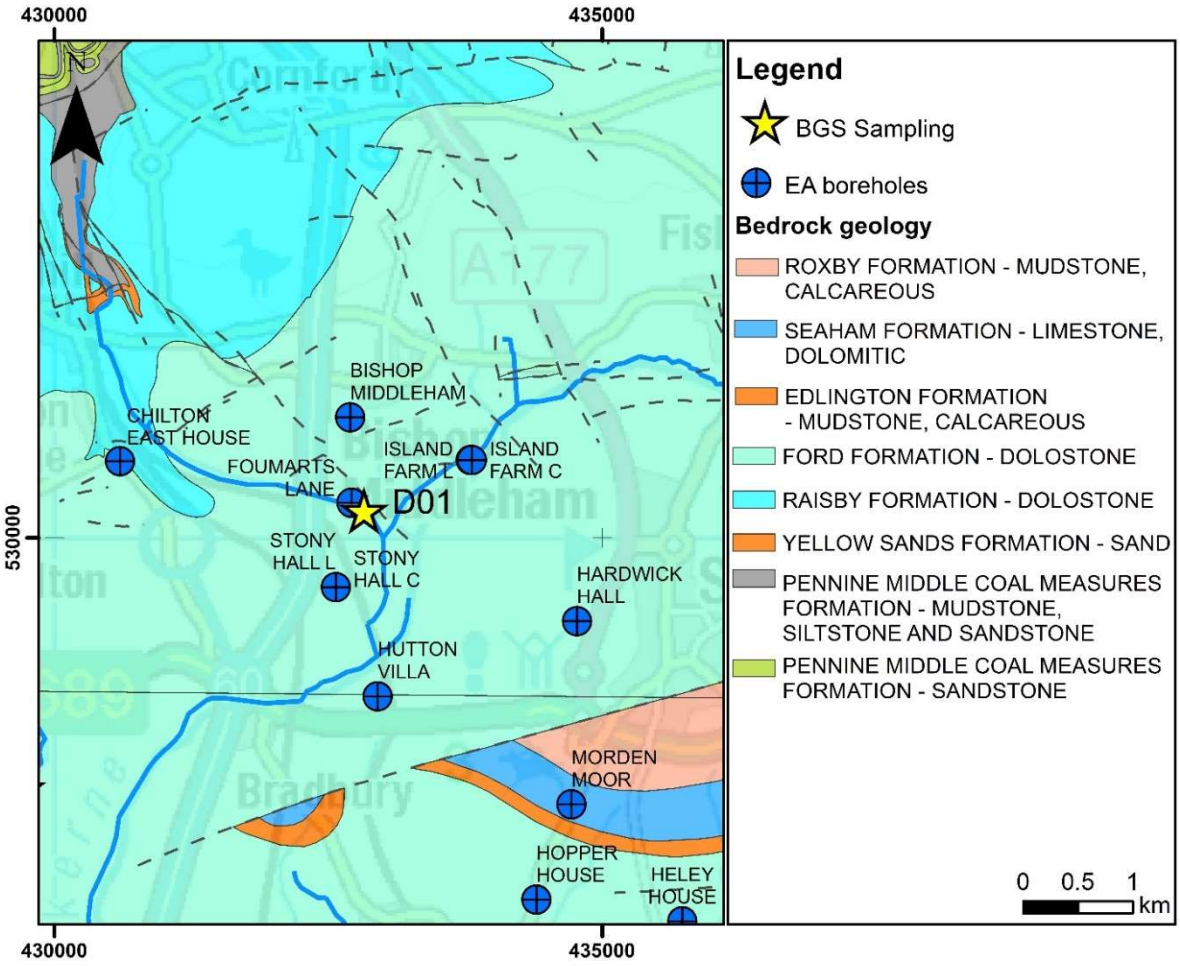

Figure 6: Bedrock geology and EA boreholes near monitoring point D01. Dotted lines indicate inferred faults. ***Contains Ordnance Survey data © Crown Copyright and database right 2019. Ordnance Survey Licence no. 100021290.***

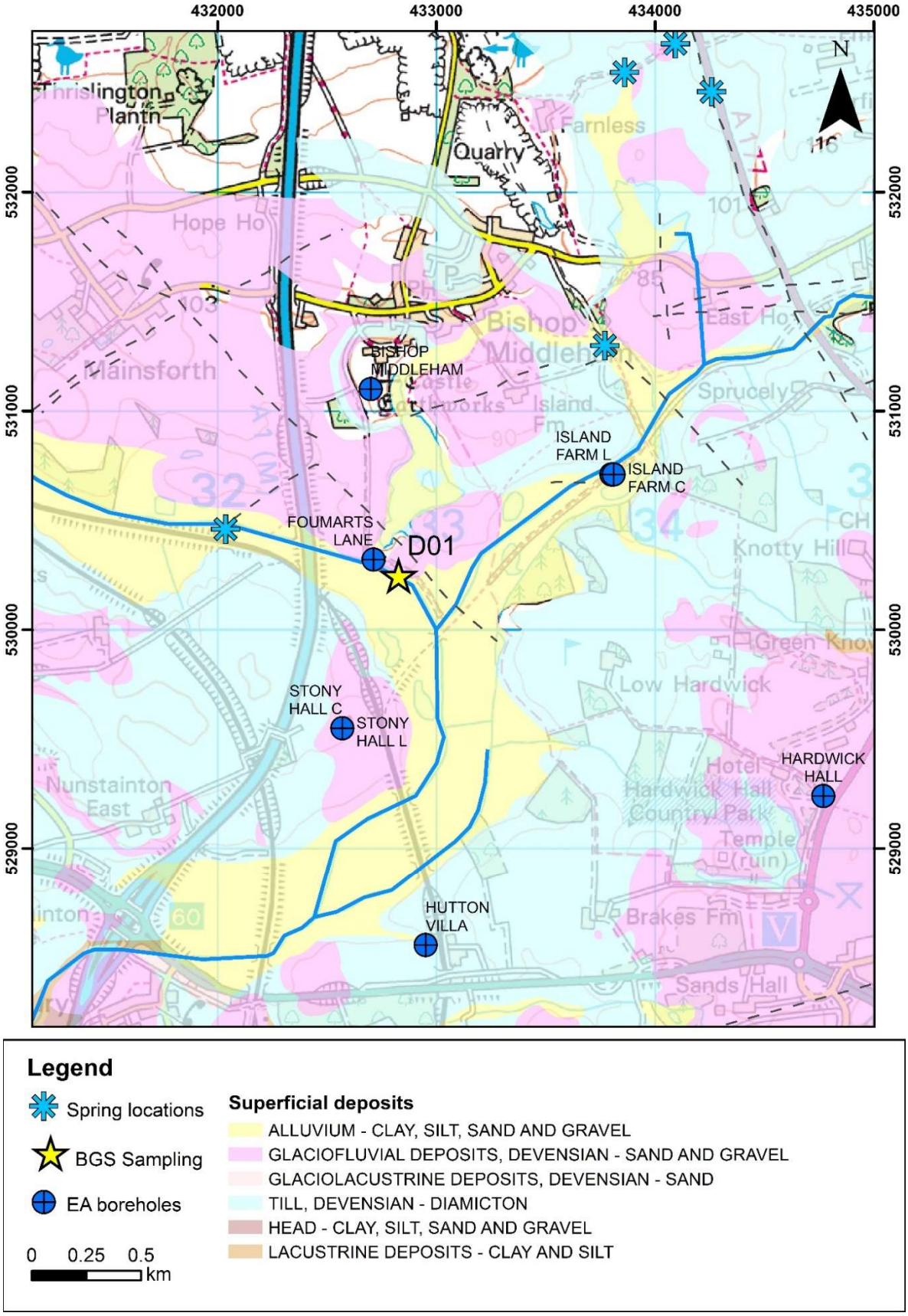

Figure 7: Superficial deposits at monitoring D01. Dotted lines indicate inferred faults. ***Contains Ordnance Survey data © Crown Copyright and database rights 2019. Ordnance Survey Licence no. 100021290.***

2.3 MONITORING POINTS ALONG WOODHAM BURN (WB) AND RUSHYFORD BECK (RB)

2.3.1 Location and geomorphology

The investigated sites are located about 1 km north-east of the JBA monitoring point B01; near and at the confluence of Rushyford Beck (RB) and Woodham Burn (WB).

2.3.2 Geology

The bedrock geology (Figure 8) comprises south-easterly dipping Raisby Formation cream, brown and grey, fine-grained dolostone with grey, fine-grained limestone, overlain to the south–east by the dolomitised platform limestones of the Ford Formation. Towards its source, the western end of Woodham Burn is incised through the Ford Formation into the underlying Raisby Formation, whereas Rushyford Beck is underlain by the Ford Formation. Glacial till and Glaciofluvial sand and gravel deposits overlie the bedrock geology with ribbons of alluvium along the course of the river and its tributaries (Figure 9). To the east of approximately easting 429435, the alluvial deposits give way to lacustrine clays and silts. Within the lacustrine clay deposits, isolated ponds with bulrushes were observed at NZ 29528 27127 and NZ 29445 27127 75 and 76 m OD, respectively.

Table 4: Geology in the vicinity of monitoring locations RB and WB

	Mapped Unit	**Lithology**
Superficial (0-30 m)	Alluvium	Organic clay
	Lacustrine deposits	Peaty, silty clays
	Glacio-fluvial sand and gravel	Sand and gravel
	Devensian Till	Gravelly silty sandy clay
Bedrock	Ford Formation of the Zechstein Group (Permian); formerly Middle Magnesian Limestone	Dolostone (very vuggy in field walls)

2.3.3 Hydrology and hydrogeology

There are a small number of springs in the area that are associated with the till and the boundary between the till and the glacio-fluvial sand and gravel deposits. The spring at Carrsides (429607 527534) is at the boundary between the till and lacustrine clay and silt deposits (to the east). For part of its course the Rushyford Beck follows the boundary between the till and the lacustrine deposits, before turning south to flow across the lacustrine deposits. The association of Rushyford Beck and, to the east the River Skerne, with the lacustrine deposits, likely reflects

their lower vertical permeability and propensity to support surface water above the groundwater table.

Boreholes to the north of Rushyford Beck (Rushyford to Bradbury Beck) indicate an unsaturated zone of at least 5 to 7 m in thickness; whilst Low Copelaw borehole (700 m to the south-east of the confluence of Rushyford Beck with Woodham Burn, indicates an unsaturated thickness of 21.95 m [in 1968], with the groundwater water table reaching the basal 12 m of the superficial deposits that extend to 33.53 m below ground level and are underlain by the Ford Formation extending to 49.38 m and, in turn, underlain by the less permeable Raisby Formation (Figure 12). Although not evident in the mapped structural geology, it would seem that bedrock faulting compartmentalises the groundwater conditions.

The geological setting suggests that groundwater recharge enters the streams as baseflow from the glacial and fluvioglacial deposits. The streams are more likely to be losing streams upstream of lacustrine deposits. It may be more than coincidental that the source of the streams lies above the Raisby Formation.

2.3.4 Initial conceptual site model

Borehole groundwater levels (Rushyford NE and Low Copelaw No 2; Figure 9 and Appendix 1) are indicative of confined, sub-artesian groundwater conditions. The desk study indicates that at sampling positions WB 2 and RB, where the stream is likely fed by base-flow from the lacustrine deposits, it is plausible that the base-flow enters the stream by more permeable laminae within the lacustrine sequence with additional storage in the Alluvium. In the lacustrine deposits some of the flow paths are likely to be confined by overlying, lower permeability laminae and the head would be controlled by the local topography. Depending on the detail of the topography, there is also a potential for subsurface connectivity via the superficial deposits with the River Skerne. If there is any groundwater connectivity there is a possibility of it being connected with the former Chilton Colliery.

Sample point WB 3 lies beyond the exposure of the lacustrine deposits. Here, it is much more likely that, at least seasonally, the stream is a losing stream with recharge via the Till.

Confined flow paths could develop within the Alluvium at any of the sampling positions, providing that it is stratified and of sufficient thickness.

2.3.5 Previous findings

2.3.5.1 RUSHYFORD BECK

Results from JBA spot gauging indicate that Rushyford Beck has higher flows than assumed to occur naturally. This was concluded to be likely due to discharges from the Windlestone STW. Another possibility could be that the springs indicated in the BGS database recharge the beck.

2.3.5.2 WOODHAM BURN

In previous EA studies the Woodham Burn is considered a losing watercourse, as there are several sinkholes reported to be located along its flow path (not mapped in the BGS database). However, intermittent gaining sections may also occur. Based on previous flow measurements by the EA, a gaining section is suspected near the location of a spring immediately downstream

of Aycliffe. Additional gauging by JBA indicated the Woodham Burn gains flow near the spring location during lower flows, but loses when flows are higher. An interaction of groundwater and surface water is expected based on the previous findings.

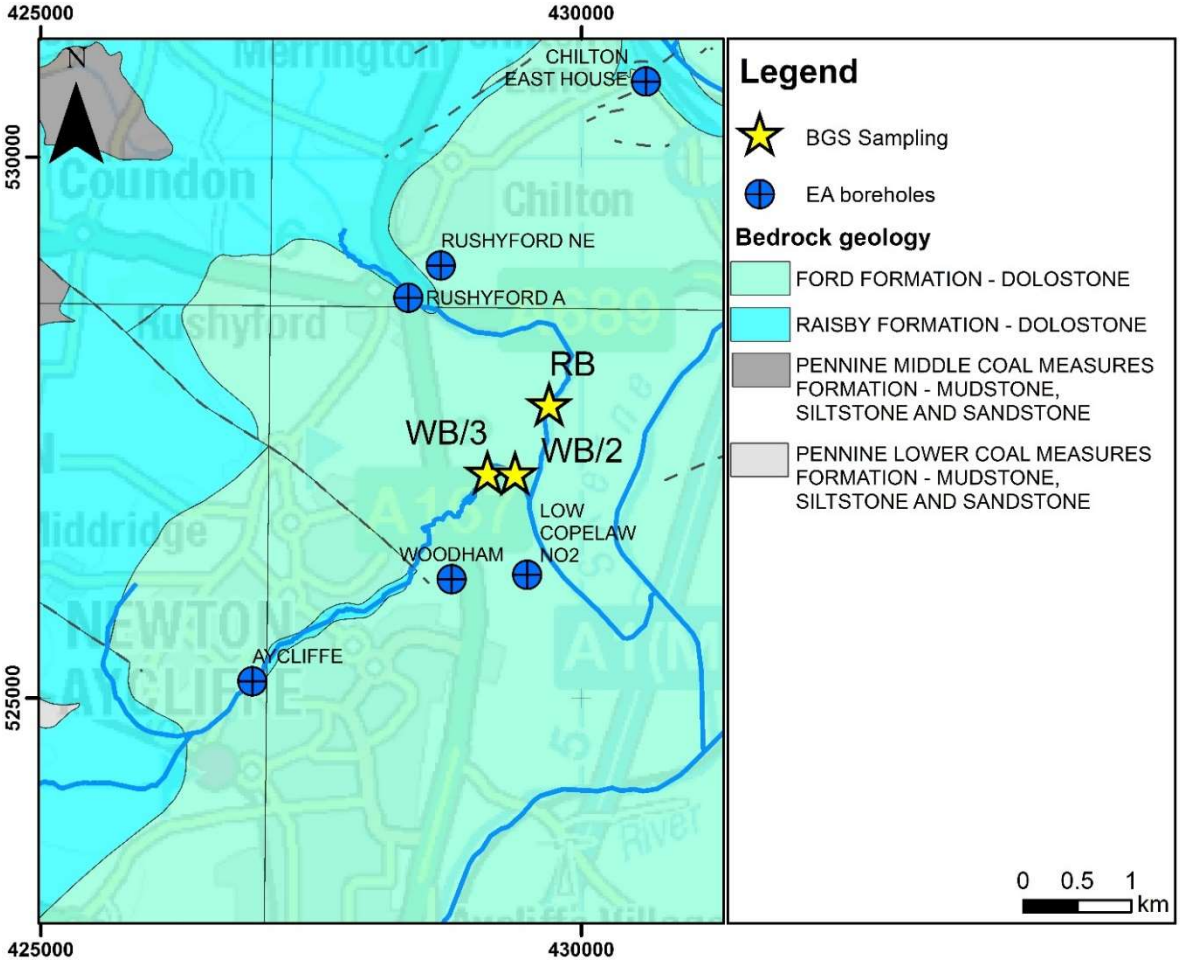

Figure 8: Bedrock geology and EA boreholes at monitoring point RB/WB. Dotted lines indicate inferred faults. ***Contains Ordnance Survey data © Crown Copyright and database right 2019. Ordnance Survey Licence no. 100021290.***

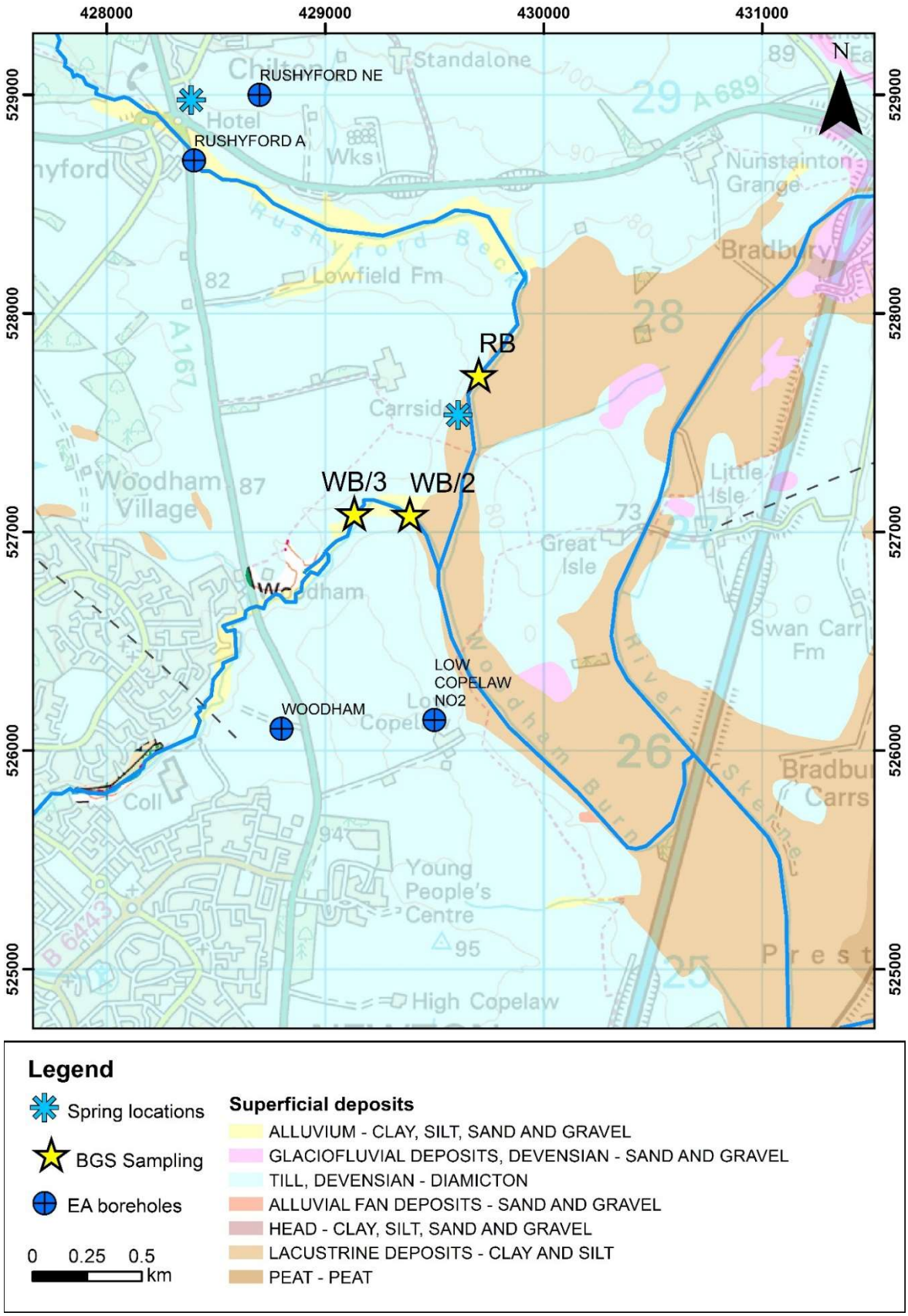

Figure 9: Superficial deposits at monitoring site RB/WB. Dotted lines indicate inferred faults. ***Contains Ordnance Survey data © Crown Copyright and database rights 2019. Ordnance Survey Licence no. 100021290.***

2.4 MONITORING POINT AY (SOUTH OF AYCLIFFE VILLAGE)

2.4.1 Location and geomorphology

This monitoring point was located approximately 250 m to the south-west of the southern edge of Aycliffe Village at 428609 522106. The relatively straight form of this stretch of the river and the presence of the sharp meander and former mill (Holme Mill) 290 m to the south-southwest, suggest that this stretch of the river has been canalised. The wooded (Banks Wood) eastern bank of the river rises by about 5 to 10 m to a plateau at about 90 m OD. To the west the ground is flatter.

Historic maps (1898 and 1923) indicate that quarrying was undertaken immediately to the east of this location (Aycliffe Quarries). Associated with the quarrying there were a number of lime kilns and also a Smithy at 428683 522011. More recently the quarry has been partially restored with landfill and is currently used for waste recycling. There are therefore, a number of additional factors that might impact on groundwater quality.

2.4.2 Geology

The bedrock geology (Figure 10) comprises the north–easterly dipping Raisby Formation, which is capped to the north east by the Ford Formation. The Raisby Formation comprises cream brown and grey fine grained dolostone with grey fine grained limestone. The Ford Formation also comprises limestone but it is oolitic with reef structures. However, it too is shown as dolostone in the vicinity of the monitoring point. There are no superficial deposits mapped at this location (Figure 11). The area of quarries is mapped as artificially modified ground. Ribbons of alluvium occupy the bed of the river and its tributaries south of Holme Mill, where the Alluvium reaches a width of 100 m.

2.4.3 Hydrology and hydrogeology

Indicative of the high groundwater levels and the absence of tills from this area historically there were a number of wells, including: 428478 522100 and 428525 521780 (Holme Mill). The BGS records include a Water Well at Windmill House (429010 521920; Appendix 5) where groundwater was encountered at 68.27 m OD in 1960. For the regional context see section 1.4.1. At this location the aquifer is unconfined. The Environment Agency (2016) noted that the groundwater levels at the EA Aycliffe Borehole average 83 m OD, in the order of 5.5 m below ground level and therefore below the surface water, but that the groundwater becomes artesian in a southerly direction.

Table 5: Geology in the vicinity of monitoring point AY

	Mapped Unit	Lithology (BGS Lexicon)
Bedrock	FML-DOLO Ford Formation of the Zechstein Group (Permian); formerly the Middle Magnesian Limestone	Dolomite that comprises three distinct facies: shelf-edge reef that separates a broad belt of back-reef and lagoonal beds to the west from fore-reef talus aprons and off-reef beds to the east
	RML-DOLO Raisby Formation of the Zechstein Group (Permian); formerly the Lower Magnesian Limestone	Cream, brown and grey, fine-grained dolostone with grey, fine-grained limestone

2.4.4 Previous findings

The BGS monitoring point AY is located between the JBA monitoring points A03 (upstream) and A02 (downstream). Flow gauging undertaken by JBA indicated the Skerne River was overall gaining across this section of the Skerne River at all gauging rounds (in January, February, and May 2017).

2.4.5 Initial conceptual site model

Sampling point AY was situated to the south of Aycliffe village, within the hydrological window through the superficial deposits, i.e. area where there are no mapped superficial deposits over the Raisby Formation dolostone. The alluvium associated with the southerly flowing stream is relatively narrow and incised into the till deposits. The alluvium widens as the river bends to the southeast parallel to a north–west to south–east trending fault. Glaciofluvial deposits are sparse. The alignment of the river with the fault indicates a potential for structurally guided groundwater discharge to the stream. However, there is no borehole evidence to substantiate this.

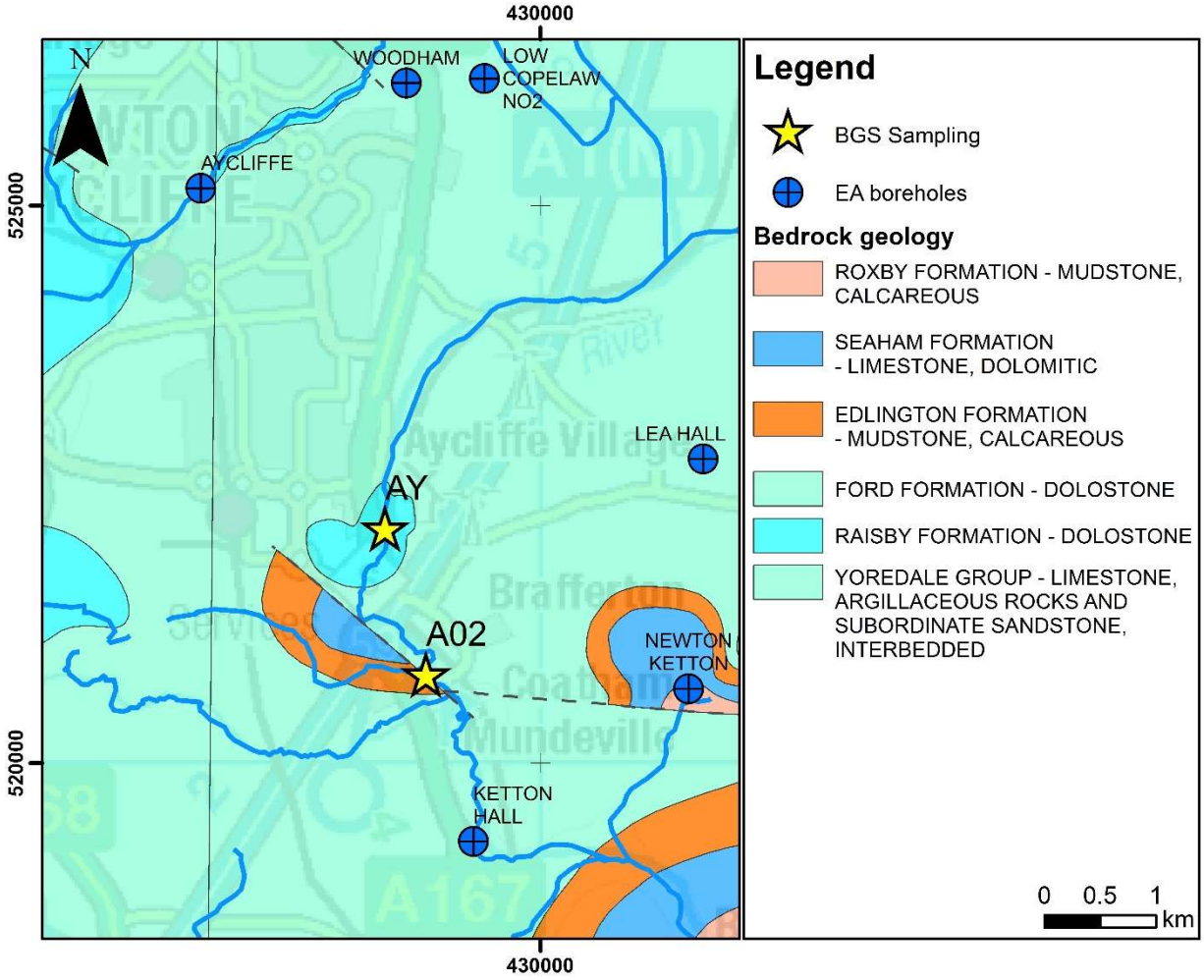

Figure 10: Detailed bedrock geology at monitoring site AY (and A02). Dotted lines indicate inferred faults. ***Contains Ordnance Survey data © Crown Copyright and database rights 2019. Ordnance Survey Licence no. 100021290.***

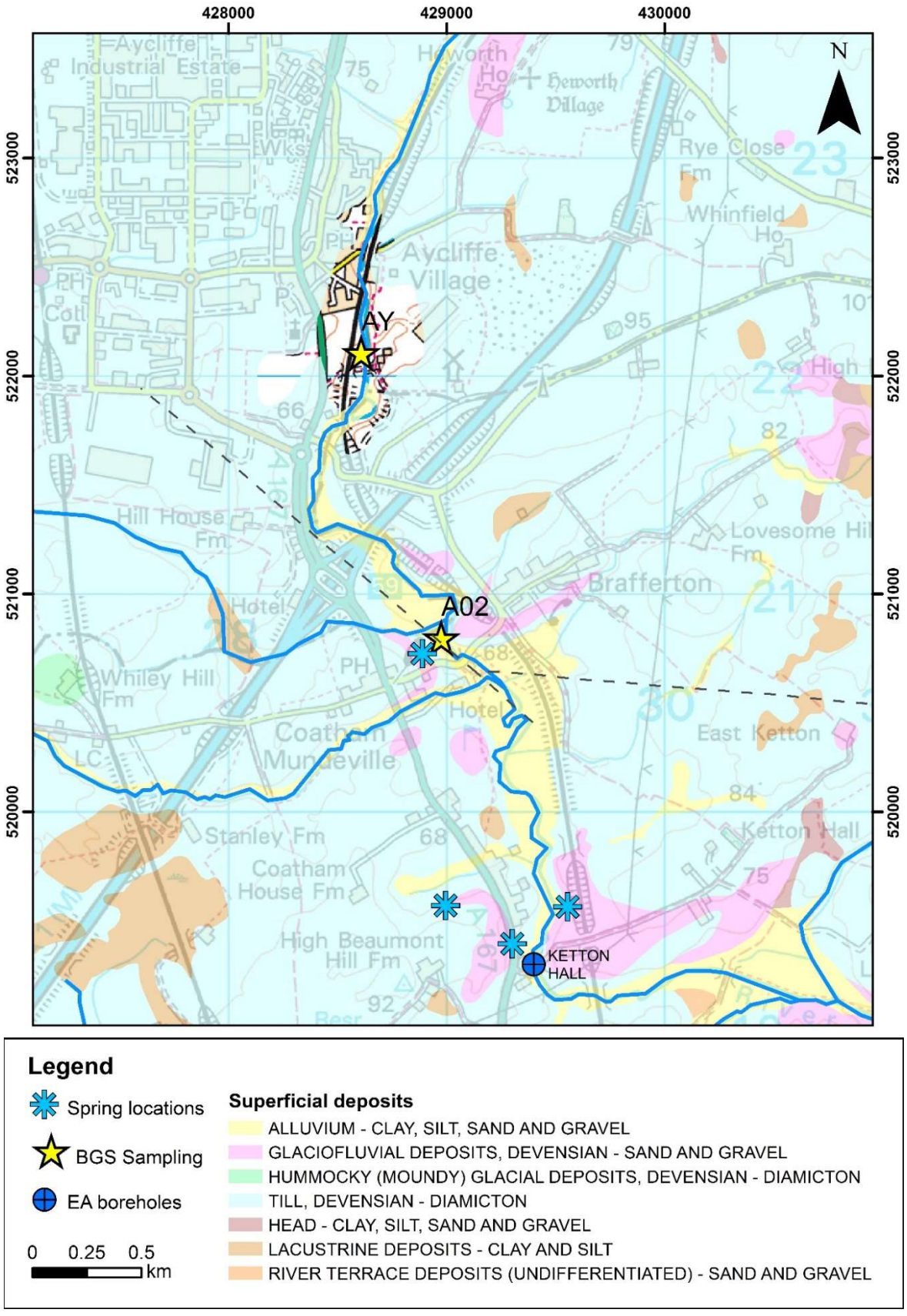

Figure 11: Superficial deposits at monitoring sites AY and A02. Dotted lines indicate inferred faults. ***Contains Ordnance Survey data © Crown Copyright and database right 2019. Ordnance Survey Licence no. 100021290.***

2.5 MONITORING POINT COATHAM MUNDEVILLE VILLAGE (A02)

2.5.1 Location, geomorphology and land use

This monitoring point is situated towards the southern end of the River Skerne, adjacent to the Mill Bridge on Brafferton Lane, Coatham Mundeville. Here JBA monitor flow on the downstream side of the bridge. The stream is about 8–10 m in width with a stable bed. The river is wider with an overspill channel at the location of the bridge. It is understood that this area is prone to flooding. Immediately upstream of the bridge the channel flows through an area of deciduous woodland that gives way to grazing land to the north. The woodland is bound by a stone wall on its southern side adjacent to Brafferton Lane.

On the southern edge of the woodland, near the wall there is a depression that might be the surface expression of a sinkhole in the Edlington Formation (see below).

Coatham Mill, which was first mentioned in the list of Bishop Hatfield tenants in 1377, was originally a flax mill. It was rebuilt between 1754 and 1761 for spinning flax, hemp and wool and then subsequently corn (Coatham Mundeville Conservation Area Draft Character Appraisal, Darlington Borough Council, February 2009). It went on to be partly operated by steam and then during the Second World War the mill pond was infilled and the mill converted to electricity. The area of the former Mill Dam forms a substantial part of the footprint of land that was advertised for sale at the time of the site visit.

2.5.2 Geology

The bedrock geology comprises northerly dipping Ford, Edlington and Seaham formations downthrown along a north–west- to south–east- trending fault against the Ford Formation (Figure 12). Glacial till and glacio-fluvial sand and gravel deposits overlie the bedrock with ribbons of alluvium along the course of the river and its tributaries (Figure 11). The Alluvium reaches a width of 450 m downstream of the Mill Bridge.

Immediately upstream of the Mill Bridge the alignment of the bedrock faulting is coincident with the northern side of the river. North of 428965 520785 the river course moves away from the fault alignment.

A water supply borehole (borehole No. 1 at Hill House [2830 2137]) penetrated the Zechstein Group and went into the top of the Carboniferous at approximately 58 m depth. There was very poor core recovery in this borehole between 18 and 35 m depth, which suggests a significant degree of karst in the Ford Formation, where it is capped by the Till.

Table 6: Geology in the vicinity of monitoring site A02.

	Mapped unit	Lithology
Superficial (40 m)	Alluvium	Peaty clay
	Glacio-fluvial sand and gravel	
	Devensian Till	
Bedrock	Seaham Formation of the Zechstein Group (Permian)	
	Edlington Formation of the Zechstein Group (Permian)	
	Ford Formation of the Zechstein Group (Permian); formerly Middle Magnesian Limestone	Dolostone (very vuggy in field walls).

2.5.3 Hydrology and hydrogeology

Information provided in the Coatham Mundeville Conservation Area Draft Character Appraisal (2009) indicates that the former Mill Pond was situated immediately upstream of the Mill Bridge and formerly the river in the stretch upstream of the Mill Pond meandered and has subsequently been re-aligned (straightened), likely at the time that the Mill Pond was infilled.

There are a small number of springs in the area that are associated with the glacio-fluvial sand and gravel deposits. Of particular note is the spring at 428889 520726, which is on the down slope contact of the glacio-fluvial sand and gravel with the till. North–easterly flowing tributaries enter the river at 429230 520602 and 428997 520884. Both of these tributaries are associated with ribbons of alluvium.

2.5.4 Initial conceptual site model

Groundwater levels in the Ketton Hall and Newton Ketton boreholes (Figure 14, Appendix 1) indicate that groundwater is confined and subartesian. There is a significant east– west trending fault between these boreholes with the Newton Ketton borehole being situated immediately to the north of it. The geological setting suggests that seasonally groundwater recharge might enter the stream along the line of the fault, but the best chance of monitoring the chemical impact is upstream of the infilled Mill Pond and downstream of the point where the stream channel deviates from the line of the fault. This is the area that was targeted for sampling. The accumulation of alluvium suggests a significant contribution of overland flow during periods of high rainfall. It is likely that an additional baseflow contribution to the stream comes from the glacio-fluvial deposits. However, their limited occurrence in this area indicates that this is only a minor component of the stream water.

2.5.5 EA/JBA reach connectivity classification

In Phase 1 of the study, this area was given a Reach Connectivity score of 5 out of 5 (5=highest connectivity) (Figure 5). Flow gauging undertaken by JBA indicated the Skerne River was overall gaining between the nearest upstream point and A02 in January, February, and May 2017, and losing between A02 and the nearest downstream point in January and May (no measurement was taken downstream of A02 in February 2017).

Unlike most EA monitoring boreholes, the borehole at Ketton Hall (south of A02, see Figure 12) has been known to show significant annual variation.

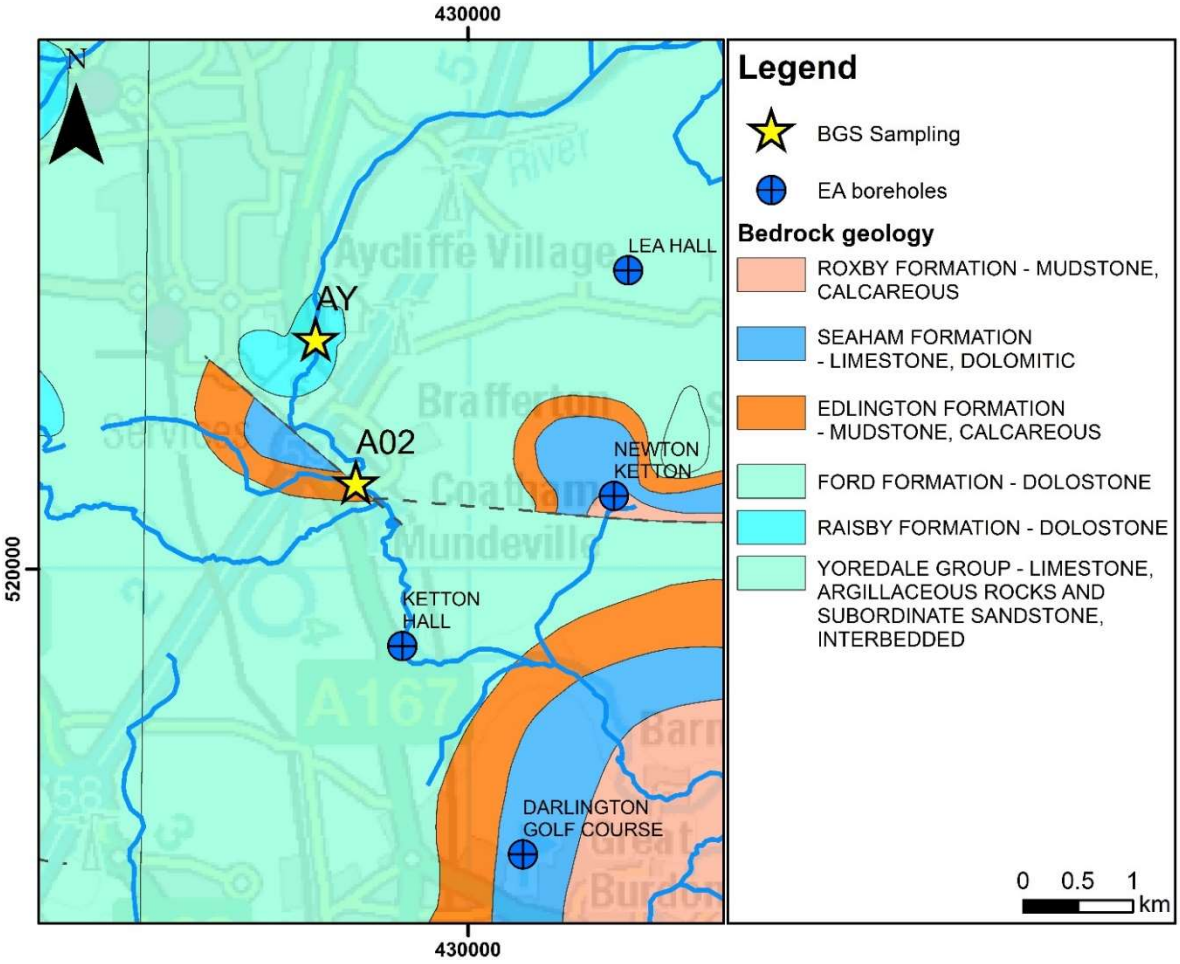

Figure 12: Bedrock geology and EA boreholes at monitoring point A02. Dotted lines indicate inferred faults. ***Contains Ordnance Survey data © Crown Copyright and database right 2019. Ordnance Survey Licence no. 100021290.***

2.6 OTHER MONITORING POINTS VISITED

2.6.1 Monitoring Point A01 [429384 519294]

This location was accessed via Ketton Lane. The monitoring point was immediately upstream of the bridge. The pasture land is owned by the farm. Dense sedge-like vegetation in the bed of the stream has the potential to impact on flow monitoring at this monitoring point. The

bedrock geology comprises the Ford Formation of the Zechstein Group (Permian). It is overlain by glacial till and glacio-fluvial sand and gravel deposits with ribbons of Alluvium along the course of the river and its tributaries. Here the Alluvium is in the order of 60 m in width. Northumbrian River Authority Borehole No 26 proved Till to about 21 m depth overlying vuggy dolomitised limestone.

There are a number of springs associated with the glacio-fluvial sand and gravel deposits close to their contact with the Glacial Till, including the springs at 428995 519569; 429302 519398 and 429556 519566. The groundwater in the borehole was reported to be standing at about 11.5 m depth. Ground level at the borehole position is in the order of 1 m above that of the river level. This suggests that there is an unsaturated zone of about 10 m beneath the river at this point, i.e. it is potentially a losing stretch, as indicated by JBA (Figure 5).

3 Data Collection

3.1 SAMPLING PROGRAMME: SCOPE AND LIMITATIONS

Our survey of the hyporheic zone provided a snapshot in time of the spatial variation over stretches of 1 to 5 m in hyporheic zone pore water chemistry and overlying surface water at selected sites in the Skerne catchment, using a network of minipiezometers and grab sampling.

The hyporheic zone is viewed as a temporally and spatially dynamic saturated transition zone between surface water and groundwater bodies that derives its specific physical (e.g. water temperature) and biogeochemical (e.g. steep chemical gradients) characteristics from mixing of surface and groundwater to provide a dynamic habitat and potential refugia for obligate and facultative microbial species (Krause et al. 2011). The elucidation of hyporheic zone process dynamics and their importance for surface water and groundwater hydrology and ecology and biogeochemical cycling requires an interdisciplinary multi-scale approach considering the hyporheic zone process dynamics, spatio-temporal patterns and scales. This is, however, outside of the scope and resources available to this project. Instead, in this study we provide a direct measurement using multilevel samplers of the hyporheic zone composition at given locations, presenting a broad assessment of the hydrochemical variations observed within and across the selected locations. A detailed investigation at each site, although limited in spatial extent and restricted to one sampling episode per site, aims to provide a mechanistic understanding of the main biochemical process at the time of sampling, and baseline data to inform future research.

The main limitation of the approach is therefore that the measurements may not be extrapolated spatially and temporally. A further limitation of the method using minipiezometers is that not all riverbeds are conducive to the installation of minipiezometers with ideal locations being represented by areas containing sediments with few cobbles or stones.

3.2 HYDROLOGICAL CONDITIONS DURING SAMPLING

The hyporheic zone sampling of the selected sites took place on four occasions during the summer period from June to September 2017.

The aim of this study was to sample both river water and the HZ water during low-flow conditions. Figure 13 shows the Skerne river levels at the EA monitoring station Preston-Le-Skerne throughout the hydrological year 2016/17 and Figure 14 shows the hydrological conditions (including rainfall data) from seven days before the first sampling (which took place on 20th June 2017) until the last sampling (26th September 2017).

The data presented in Figure 16 comprise daily precipitation data from the EA monitoring station Harpington Hill Farm at 433631 526654, and average daily water level data from the EA monitoring station Preston-Le-Skerne at 429196 523796, which was the closest monitoring station to monitoring sites A02 and AY. The closest monitoring site to RB/WB and D01 was Bradbury station 431798 528500, which is located about 0.5 and 5.5 km (respectively) closer to the RB/WB and D01 than the Preston-Le-Skerne station. Water levels at Bradbury and Preston-Le-Skerne station were relatively similar during the study period, and therefore only

levels from Preston-Le-Skerne will be used in this chapter. More detailed information about the location of the rainfall and gauging stations in comparison with the HZ monitoring points, as well as a comparison of river levels at Preston-Le-Skerne and Bradbury station can be found in Appendix 4.

The most stable low-flow conditions could be observed from April to June 2017 (Figure 14), but for logistical reasons, sampling during this period was not possible. Some higher flow episodes occurred from June to September 2017 (which corresponds to the time period during which sampling took place), but these were relatively minor compared to the much more extreme flows from November 2016 to April 2017. All sampling took place during periods with normal river stages (normal being used in this context as the defined usual range of river stage at Preston-Le-Skerne by riverlevels.co.uk).

During the week prior to the first sampling round (26–29 June ‘17, D01), little rainfall (15.8 mm) was recorded at the nearby Harpington Hill Farm monitoring station, and water levels were on the low end of normal conditions at the time of sampling. A heavy rainstorm occurred on the last day of sampling (see Appendix 4 for more details).

Similarly, little rainfall (19.6 mm) occurred in the week prior to sampling at monitoring station A02 on 12–14 July ‘17. However, the impact of a wetter period prior to this (see Appendix 3) had led to slightly higher water levels compared to the first sampling round. No further heavy rainfall occurred during sampling (Appendix 4).

The third sampling (RB/WB, 24–26 July 2017) took place after a week with a total of 38.8 mm of precipitation. Most of this rainfall (30.6 mm) occurred three and two days before sampling started, but no further rainfall took place on the day prior to sampling. Nevertheless, the third sampling round is clearly the most affected by prior rainfall, and water levels were on the higher end of the normal range on both sampling days (Appendix 3 and Appendix 4).

In contrast, the last sampling round (monitoring point AY, 25—27 September ‘17) was conducted again during low flow with a river stage of only 0.15 m (Figure 14 and Appendix 3). Water levels prior to sampling had been declining continuously, and very little (4 mm) rainfall occurred during the seven day period before the site visit. No rainfall occurred on the day of sampling.

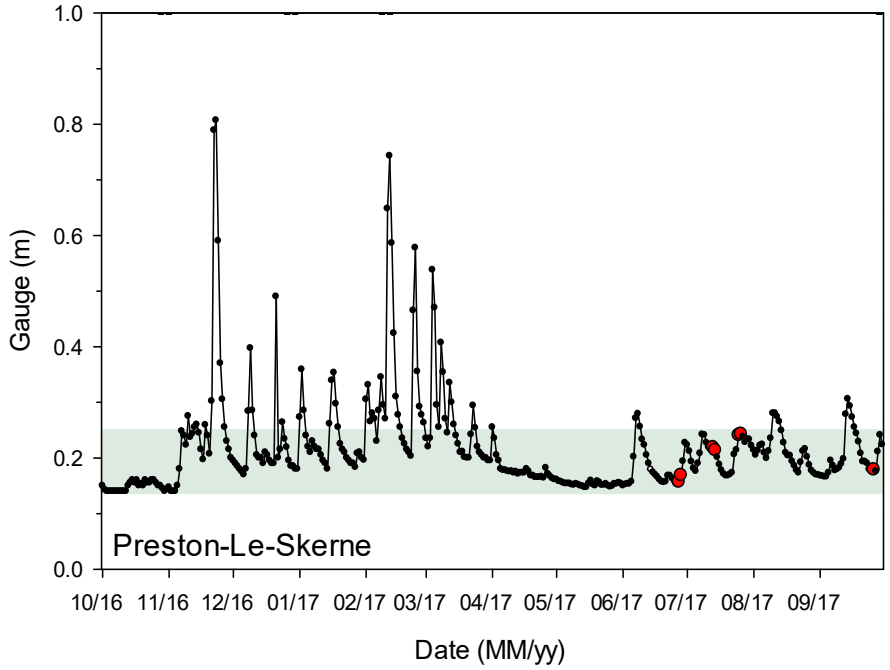

Figure 13: Water levels at Preston-Le-Skerne monitoring station in the hydrological year 2016/17. Dates of hyporheic zone sampling are indicated by the red dots. Green shading refers to the normal water level in average weather conditions.

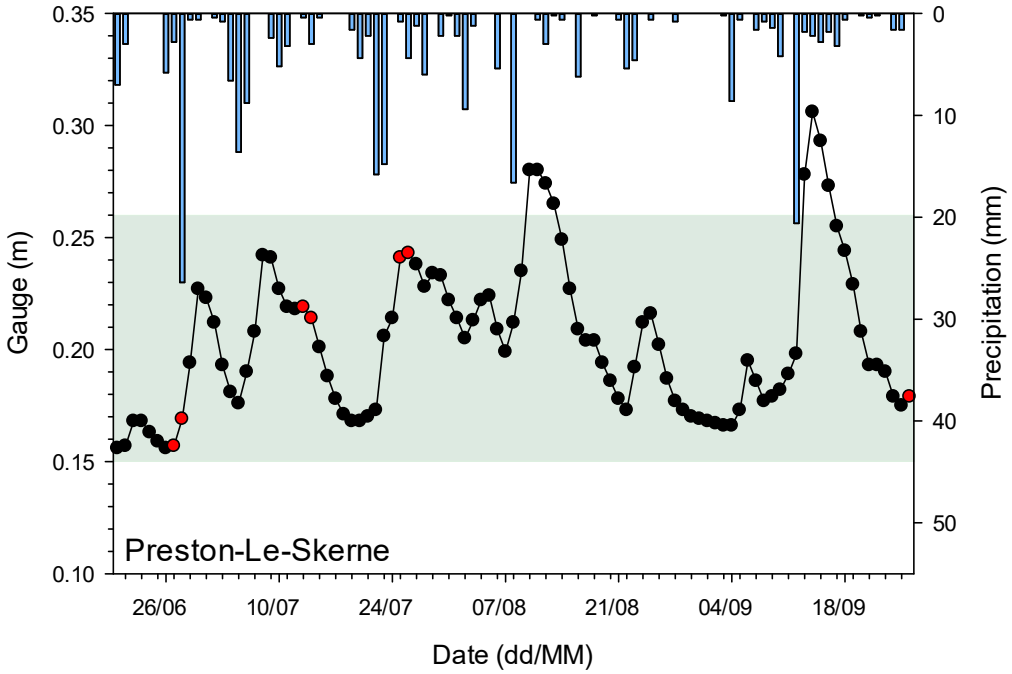

Figure 14: Water levels at Preston-Le-Skerne monitoring station from 20th June to 26th September 2017. Red dots indicate the days on which sampling took place and green shading refers to the normal water level in average weather conditions. Secondary Y-axis: daily precipitation data from the EA monitoring station Harpington Hill Farm at 433631 526654.

3.3 HYPORHEIC ZONE SAMPLING METHOD

Pore water samples were collected using multilevel samplers or mini drive-point samplers. The hyporheic zone multilevel sampler designs adopted in this study are based on those described by Rivett et al. (2008). The hyporheic zone multilevel samplers comprise a 12 mm ID, 16 mm OD, 1200 to 1800 mm long, HDPE tube, fitted at one end with a machined, stainless steel drive-point that assists penetration of the device into sediments. Four discrete, depth sampling ports were installed around the central stock of the hyporheic zone multilevel sampler, comprising Teflon tube (1.6 mm ID, 3.2 mm OD) measuring ~200 mm in length and fitted at one end with nylon mesh screen (e.g. 45 μm mesh size) to prevent blockages due to sediment ingress. The sampling ports were installed at 10 cm intervals and marked at the top end of the Teflon tubes with different colour tape according to this scheme: yellow=3 mm from datum (top of metal bolt of the stainless steel drive-point); green= 100 mm from datum; red=200 mm from datum; black=300 mm from datum).

To install the sampler into the hyporheic zone, the device was inserted into a 1500 or 2000 mm long, metal drive tube (29 mm ID, 31.5 mm OD), leaving the 36 mm diameter drive-point protruding from the pipe end. During installation, the drive tube rests on the lip of the widest part of the drive-point cone. In order to drive the sampler into the hyporheic zone a sledge hammer was used to apply force to a metal cap placed on the top of the drive tube. The metal cap was designed to limit metal fatigue and deformation. The samplers were driven into the hyporheic zone to a variable depth below the riverbed, depending on the riverbed resistance or river level. The drive tube was then removed. In clay/organic-rich sediments the sampler and drive tube readily parted leaving the sampler in the ground.

Alternatively, and in parallel, we used stainless steel mini drive-points (0.64-cm inside diameter (ID)) with slots (0.04 x 1.0 cm) sawn into the tube near the tip to remove pore water below the streambed. Elastic tubes are attached to the drivepoints and connected to either a 50 ml syringe or a vacuum bottle. Vacuum was applied to withdraw the pore water at a relatively low rate of 4 ml/min.

In order to drive the minidrive point sampler into the hyporheic zone a sledge hammer was used to apply force to a metal cap placed on the top of the rod. The mini drive-point sampler was used in preference to the multilevel sampler when installation of the multilevel samplers of larger diameter proved to be too difficult in zones of more resistant consolidated riverbed. Porewater samples were drawn from the Teflon tubes directly into either 250 ml DURAN glass bottles where vacuum was created using a hand vacuum pump or into 60 ml syringes. The sample tubes were purged before sampling by collecting and discarding 3 times the volume of water present in the sample tube. The water extracted from each depth was analysed in the field for dissolved oxygen (DO), specific conductance, redox potential, and temperature, immediately after collection and avoiding contact with air for the DO measurements. Samples for major- and trace-element analysis, alkalinity and Fe(II) analysis were filtered through 0.45 μm filters and collected in plastic 60 ml bottles. The aliquots for cation and trace elements were acidified to 1% v/v HNO_3 immediately.

3.3.1 Field measurements

Of all the field parameters measured in the pore water (temperature, dissolved oxygen, specific conductance, Eh), specific conductance is the parameter whose measurements are least likely to be affected by the sampling method.

The reliability of measurements of dissolved oxygen concentrations and Eh may have varied during the study, potentially being affected by a change in the sampling method from drawing water samples using a low volume peristaltic pump, when DO was measured after enough volume was collected in a 30 ml tube (only for D01 site), to sampling under vacuum in syringes/bottles and carrying out the measurement immediately after pouring the water from the syringe in a 30 ml tube with no headspace (for all the remaining sites). The first sampling method possibly was less reliable than the latter, given that it was not possible to use a flow-through cell to prevent loss of oxygen gas dissolved in the samples.

Some concern over the reliability of the temperature measurements was also associated to the fact that the measurements were taken after the sample bottle/syringe was full with a variable time of ~ 20 to 60 minutes, depending on the piezometer yield. The bottles could have then equilibrated with air temperature before the measurement and not representing the in situ sample condition.

Low yield from the mini rods made it occasionally difficult to obtain a sufficient volume for field measurement of physico-chemical properties.

As recommended by Nordstrom and Wilde (2006), measurements of Eh are used for qualitative delineation of strong redox gradients and gaining insights on the evolution of water chemistry. Different sensitive redox elements (iron, manganese, sulphur, selenium, arsenic) tend not to reach overall equilibrium in most natural water systems; therefore, a single Eh measurement generally does not represent the system. Also Nordstrom and Wilde (2006) warn about the limitation of the Eh measurements indicating that many elements with more than one oxidation state do not exhibit reversible behaviour at the platinum electrode surface and some systems will give mixed potentials, depending on the presence of several different couples. Methane, bicarbonate, nitrogen gas, sulphate, and dissolved oxygen generally are not in equilibrium with platinum electrodes.

3.4 **CHEMICAL ANALYSIS**

Alkalinity was determined by titrating 25 ml filtered water sample against 1.6 N H_2SO_4, using a bromocresol green indicator solution. For colorimetric Fe(II) analysis of a sample subset, 15 ml of the filtrate was added to 1.5 ml of a pre-made reagent containing the colour-forming agent 2,2’ dipyridyl.

Determination of Cl, SO_4 and F was by ion chromatography (IC) and major and trace elements were determined by inductively-coupled plasma mass spectrometry (ICP-MS), with independent QC checks providing 96 +/- 3 % accuracy (in-house QC solution) and 98 +/- 4 % accuracy (NIST SRM 1643e). The Non Purgeable Organic Carbon (NPOC) content was determined using a Shimadzu TOC-V CPH analyser with an associated ASI-V auto-sampler.

Concentrations of major and trace elements determined in procedural blanks were negligible when compared with the reported data. Repeatability of the field measurements estimated from the results of surface water duplicate (D) determinations and reported as relative percent difference RPD = (D1-D2)100/[(D1+D2)/2] was < 25 % for NPOC, < 15 % for bicarbonate (HCO_3), sulphate (SO_4) and chloride (Cl), < 10 % for iron (Fe), < 5 % for manganese (Mn). Field duplicates for the hyporheic pore water at various depths had higher RPD, as has been observed by other authors (Nagorski and Moore, 1999).

4 Data processing

4.1 INTRODUCTION

The statistical summary of the field parameters and analytical chemical data of the surface water (SW), hyporheic zone (HZ) and groundwater (GW) samples is reported in Table 16 to Table 29 in Appendix 7.

Furthermore the data were processed and described as follows:

i. Hydrochemistry of the hyporheic zone: spatial variation of hyporheic water composition across the Skerne catchment.

ii. Comparison of hyporheic zone chemical data with the Magnesian Limestone aquifer.

iii. Hyporheic mixing and geochemical controls on hyporheic zone composition: inferring hyporheic zone exchange and processes using vertical gradients of hydrochemical parameters.

4.2 VERTICAL GRADIENTS

In describing the hydrochemical vertical changes in the hyporheic zone we present the results distinguishing between conservative and reactive elements in order to assess respectively, Hyporheic Exchange Flow (HEF) and chemical processes accounting for elemental gradients with depth. Vertical porewater gradients of element concentrations from surface water throughout the hyporheic zone can occur due to:

i) mixing of downwelling surface water with upwelling groundwater or stagnant or low-flow zone water, characterised by dilution/enrichment;
ii) water-sediment interaction, governed by dissolution kinetics, composition, rate and direction of water flow and sediment composition, leading to precipitation/ sorption/ dissolution/ desorption and redox changes.

Measurements of porewater chloride (Cl) through the streambed with respect to surface water were used for making assessments of HEF. It is worth mentioning that, even under gaining conditions and upward pressure gradients, such as those expected in some reaches of the Skerne, surface water can migrate down into the shallow hyporheic zone. In this case down-welling of river water superposes the regional hydraulic regime. Assuming the conservative nature of Cl, porewater Cl concentration would reflect the mixing process of downwelling surface water with groundwater, either with stagnant zone/low flow, upwelling flow or lateral flow (Engelhardt et al., 2011); the vertical gradients in the streambed would vary mainly as a result of the extent of mixing and the number of end-members (mostly surface water and groundwater, but also complicated by lateral flow, which can also be either diffuse or focused). Reactive solutes, when compared with the non-conservative solutes, may have identical patterns, suggesting that either no reaction occurred or the balancing of source and sink processes was ongoing. If the reactive solute has a higher concentration above the simple mixing ratio then that site in the hyporheic zone is a source for the reactive solute, and vice versa, the hyporheic location is a sink for the reactive solute.

5 Spatial variation of hyporheic zone hydrochemical composition across the Skerne catchment

5.1 INTRODUCTION

This section presents a description of the hydrochemical characteristics of the hyporheic zone in the study sites and its spatial variation. The data are presented in Piper diagrams, Schoeller diagrams, and box and whisker plots to present and compare chemical distributions in the hyporheic zone across the sites and with selected boreholes and spring waters from the Skerne catchment.

5.2 WATER TYPES AND PHYSICOCHEMICAL CHARACTERISTICS

The hyporheic zone waters are mostly Ca-Mg-HCO_3 types, similarly to the Magnesian Limestone groundwaters from the area (Bearcock and Smedley, 2009) (Figure 15). The waters are well buffered with median pH values in the alkaline range (7.9 to 8.0) (Figure 17). The waters contain generally low concentrations of dissolved oxygen (median values ranging from 1.9 to 4.3) and have Eh median values ranging from 120 to 390 mV indicating moderately reducing conditions, with some exceptions. The electrical conductivity median values range from 918 to 1351 µS/cm, with the highest SEC values found at the WB sites. The range of dissolved organic carbon (NPOC) median concentrations over the study area is 2.37 - 7.75 mg/l.

The elemental distribution pattern is shown in the Schoeller diagram of Figure 16. The diagram clearly indicates that the hyporheic zone waters from D01 are depleted in SO_4 relative to the other sites.

5.3 MAJOR ELEMENTS

Figure 18 and Figure 19 show the box plot distribution of the major elements in the hyporheic zone of the study sites. The bottom and top of the box plots represent, respectively, the first quartile Q1=25% and third quartile Q3=75% of the data values. The lower whisker extends to the lowest value within the lower limit (lower limit = Q1- 1.5 (Q3 - Q1)) and the upper whisker extends to the highest data value within the upper limit (upper limit = Q3 + 1.5 (Q3 - Q1)). The median values are also reported.

Chloride concentrations have a median value ranging between 39–48 mg/l, except for those much higher values at site A02 and AY (71 and 74 mg/l) in the lower reach of the Skerne. Like Cl, the highest median concentrations of K are found at A02 and AY (9.2 and 8.6 mg/l), while for the remaining sites K median concentrations are lower averaging around 4 mg/l. The opposite spatial distribution with the lowest median values at A02 and AY is observed for Ca concentrations. This spatial pattern is not reflected in the Na distribution (narrow Na median range 37–57 mg/l). Magnesium median values range between 31 to 50 mg/l, except for site WB where the median value is of 76 mg/l. The bicarbonate (HCO_3) concentrations show similar median values around 500 to 600 mg/l suggesting carbonate mineral buffering, except

for site A02 whose median HCO_3 is much lower (260 mg/l). Sulphate (SO_4) concentrations have median values ranging 67 to 115 at A02, AY and RB sites, while D01 site and WB site differ, respectively, for the lowest median (16 mg/l) and highest median (301 mg/l) concentrations observed. The latter value is above the maximum value of 250 mg/l permissible in drinking water regulations. The range of nitrate–nitrogen ($N\text{-}NO_3$) median concentrations across the sites is 0.07– 3.15 mg/l, with most of the sites having a median lower than 0.7 mg/l (well below the drinking water limit of 50 mg/l as NO_3/ or 11 mg/l as $N\text{-}NO_3$). Two of the sites, A02 and RB, show relatively high total phosphorus (total P) median values of 0.2 and 0.8 mg/l with the remaining sites lower than 0.08 mg/l. The distribution of phosphate (PO_4) is more homogeneous ranging between 0.05 and 0.1 mg/l (median values over the study area, except for A02 with a higher median of 0.5 mg/l).

5.4 MINOR AND TRACE ELEMENTS

Figure 20 to Figure 22 show the box plot distribution of the minor and trace elements in the hyporheic zone of the study sites. Fluoride (F) median concentrations range from 0.3 to 0.8 mg/l, with AY and D01 sites with distinctively higher concentrations. The other halogen bromide (Br) has a more homogeneous distribution with median values 0.1–0.2 mg/l. The alkaline earth element barium (Ba) has a range of median values of 59–203 µg/l with site WB with the highest median. Strontium (Sr) median values range from 214 to 379 µg/l. Manganese (Mn) median concentrations are high (849–1365 ug/l) for all sites, except for AY with a lower median of 134 µg/l. Iron (Fe) concentrations range vary more significantly across the sites, with sites RB and WB showing very high Fe peaks greatly above 1 mg/l water quality limit. Among other trace elements boron (B) median concentration range is 98–204 µg/l. Uranium (U) median value range is 0.4–2.1 µg/l, with site A02 distinctively higher.

5.5 HIERARCHICAL CLUSTERING

In order to group the samples on the basis of similar characteristics, hierarchical clustering of the hyporheic zone/surface waters and selected boreholes, spring and seepage waters (total of 97 samples) was carried out based on the geochemical data set consisting of the following elements Ca, Mg, Na, K, HCO_3, Cl, SO_4, F, Si, Ba, Sr, Mn, Fe, Li, B, Rb, U. Nitrate and phosphate were omitted to reduce the potential differences among water samples due to point source anthropogenic inputs in agriculture. The samples were clustered using Euclidean distance and the Ward's Linkage method. The data were standardised to convert all variables to a common scale by subtracting the means and dividing by the standard deviation before the distance matrix was calculated, to minimize the effect of scale differences.

Based on the results of hierarchical clustering three distinct hyporheic zone hydrochemical facies are identified (Appendix 5): Foumarts Lane (D01) makes up a distinct group (Cluster 1: Low SO_4 type) characterised by the lowest SO_4 concentrations. The hyporheic zones at Woodham Burn (WB) and Rushyford Beck (RB) group together with fewer samples than from D01 and have distinctively high Fe concentrations (Cluster 4: High Fe type). The remaining hyporheic zone from site A02 and A03 cluster together characterised by the highest Cl and lowest Fe contents (Cluster 3: High Cl type). The surface waters sampled across the Skerne during the hyporheic zone sampling are associated to the latter cluster (3), showing similarities with A02 and A03 sites, with the exception of surface water at WB. Surface water together

with seepage and springs sampled at WB form in fact a separate cluster (Cluster 2: High Ca-SO_4 type), the highest in SO_4. The boreholes Low Copelaw, Stillington OBH2 and Ketton Hall are part of Cluster 3, while the composition of Stillington and a Magnesian Limestone groundwater sampled at Aycliffe Quarry fall in Cluster 1.

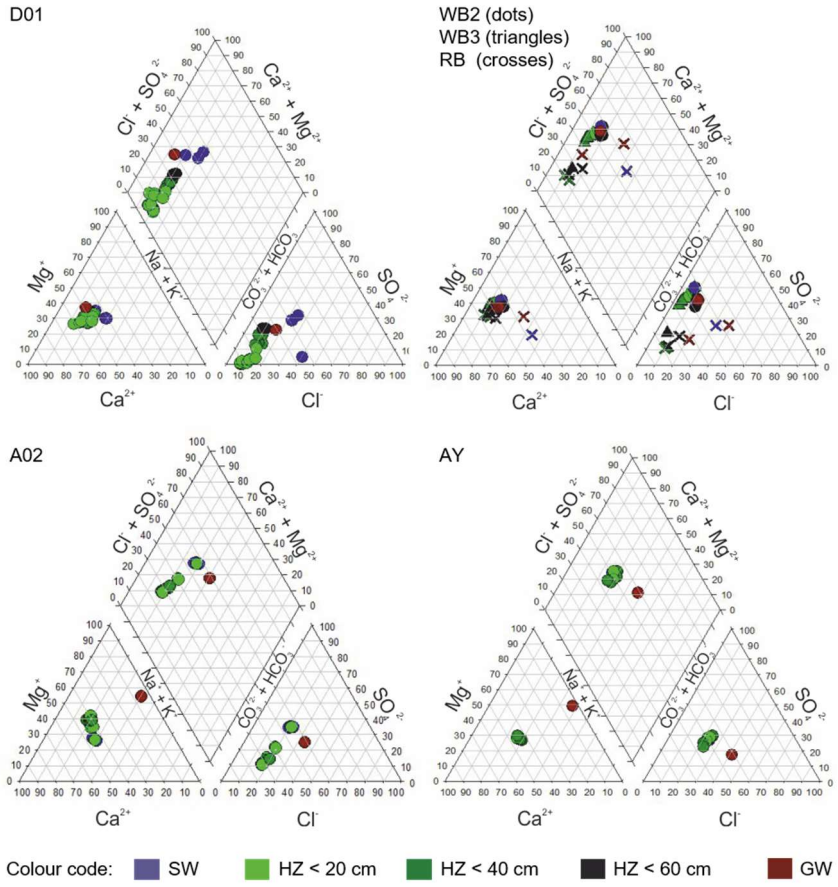

Figure 15: Piper plot diagram for surface water (SW), hyporheic zone porewater (HZ) and selected boreholes (GW): DO1-Foumarts Lane, sampled by EA 05/2017; WB and RB-Low Copelaw, Rushyford NE, sampled by EA 05/2017; A02-Ketton Hall Borehole, sampled by EA 05/2017; AY-Ketton Hall, sampled by EA 10/2017.

5.6 MICROBIOLOGICAL CHARACTERISATION: ENUMERATION OF SULPHATE REDUCING BACTERIA (SRB) USING MOST PROBABLE NUMBER METHOD.

5.6.1 Method

To estimate the number of sulphate reducing bacteria present in samples taken from river sediments, a most probable number (MPN) count was carried out. Samples analysed can be seen in Table 7; they are sediments from site D01, Woodham Burn, Rushyford Beck and site AY.

Approximately 1–2.5 g wet sediment was weighed out into tubes and ten times (volume per mass) 0.9% sterile sodium chloride solution was added to create a slurry. Tubes were vortexed for 30 s to mix and dislodge bacterial cells attached to sediment particles. A ten-fold dilution series was created from this slurry (down to 10^{-7}) and 0.1 ml each dilution added to 0.9 ml Postgate's Medium B in triplicate in a deep well 96-well plate. Work was carried out in an anaerobic cabinet and samples were incubated for ten days at 35˚C in anoxic conditions. Calculation of MPN was done according to Jarvis *et al.* (2010).

5.6.2 Results and discussion

There was considerable variability in number of SRB detected between samples. Cultivable SRB were detected in all sites with the exception of "D01 upper" (note that, because of the probabilistic nature of this method an upper confidence limit can be calculated even though no growth was observed). At D01 and Woodham Burn site 1 the number of SRB in the deeper sediments was higher than in shallower sediments, perhaps reflecting a more suitable reducing environment. The highest number of SRB detected was at site AY; MPN was above the upper limits of this test and therefore not detected (ND), i.e. further dilutions would be needed for determination. The upper range for the test was $1.2x10^9$ MPN/g. MPN was also high in the 20cm sample collected from the Woodham Burn site 2.

For comparison, MPN values for SRB can be variable, for example in one study of mine water treatment SRB MPN values were low in tailings (up to $9x10^2$ MPN/g) but much higher where sulphate rich water entered a carbon-rich permeable barrier (up to $3.7x10^7$ MPN/g), and remained high (>10^6 MPN/g) downstream, where dissolved organic carbon remained high (Benner et al., 2000).

A variety of physical, chemical and biological approaches are available for the remediation of sulphate-rich waters, including the stimulation of sulphate reducing bacteria. Sulphate reducing activity in mine drainage can be improved by addition of organic carbon sources such as sucrose, plant material, manure etc (for example, see Gibert et al., 2004 and Fernando et al., 2018).

Table 7: Results of most probable number count of sulphate reducing bacteria

Sample	MPN/g	95% lower confidence limit	95% upper confidence limit
D01 depth -40 cm	100000	24000	430000
D01 depth 0-40 cm	0	0	1200
Woodham Burn site 1 [429509, 526874] - 60 cm	25000	6100	110000
Woodham Burn site 1 [429509, 526874] - 20 cm	2500	610	11000
Woodham Burn site 2 [429388, 527080] - 20 cm	370000	90000	15000000
Rushyford Beck -30 cm	8100	2000	33000
AY site	above upper limit of test	-	-

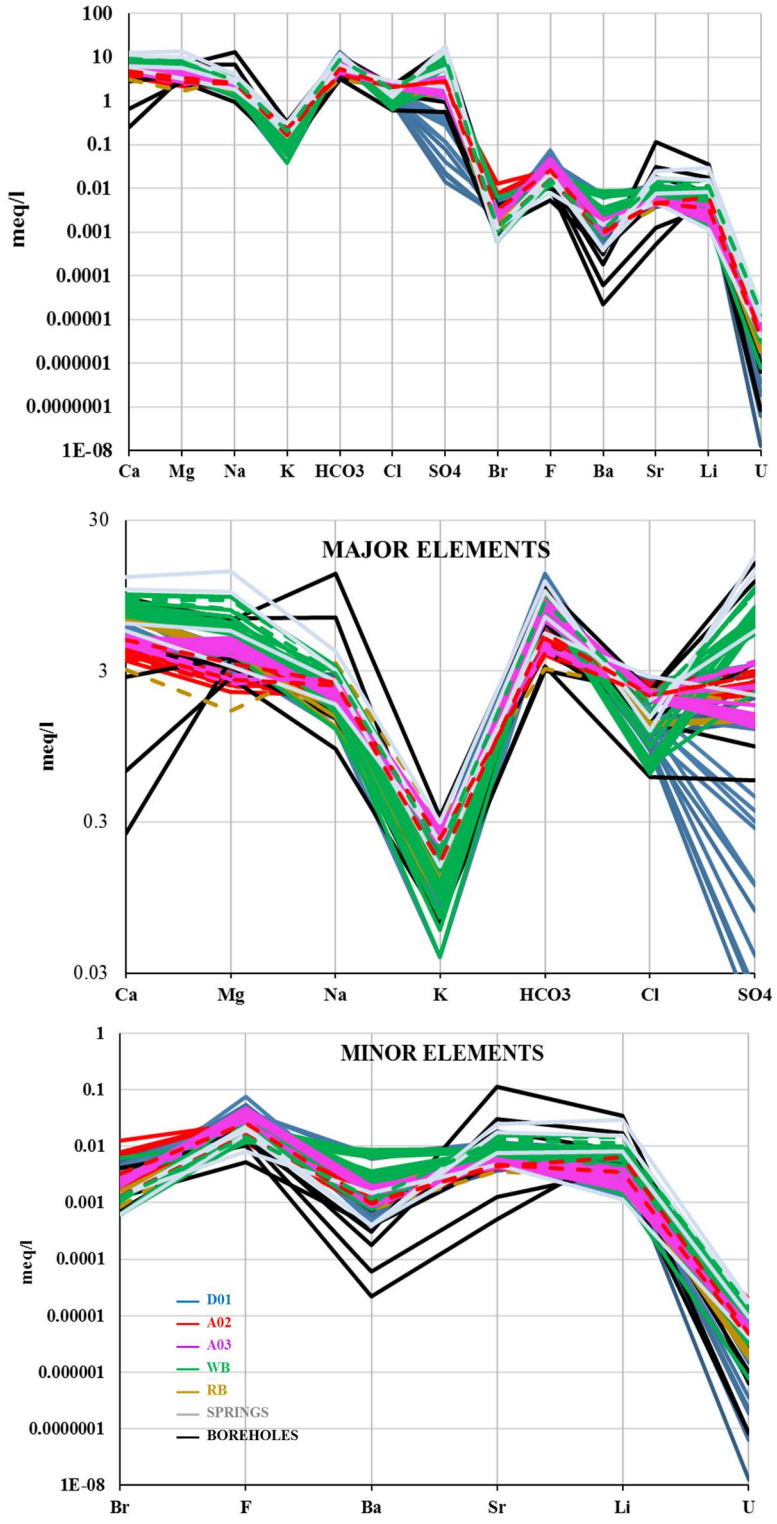

Figure 16: **Schoeller diagram for selected elements (top graph) in the Skerne waters; middle and bottom graphs show respectively the major and minor elements only. Legend – "Coloured Symbols": HZ (continuous line) and SW (broken line) at each site; "SPRINGS": springs and seepage at Woodham site; "BOREHOLES": Foumarts Lane, Stony Hall C & L, Low Copelaw, Stillington OBH2 & OBH4, Ketton Hall, plus Magnesiam Limestone GW sampled at Ayclyffe Quarry.**

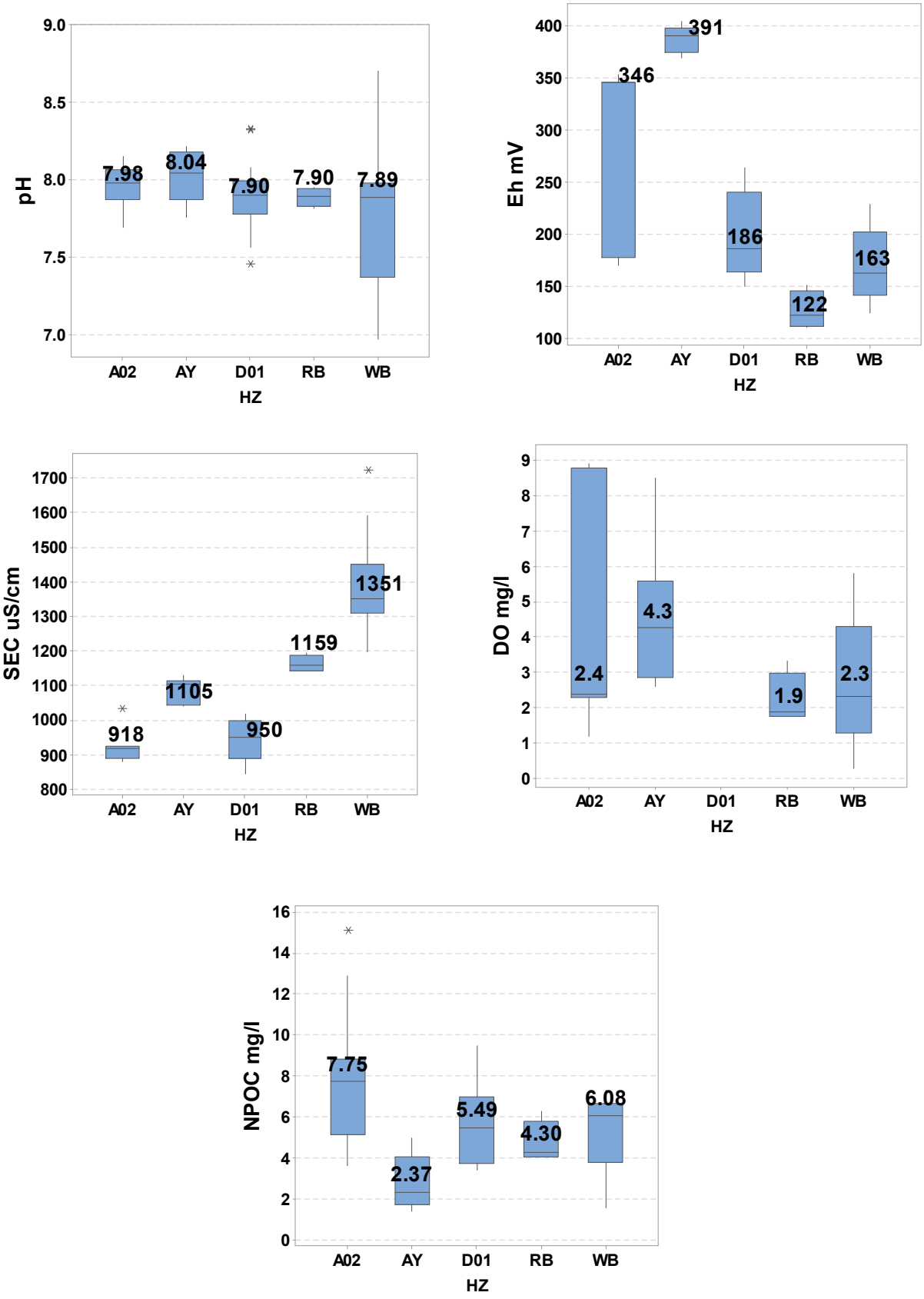

Figure 17: Box plot and median values of physicochemical parameters observed in the hyporheic zones at the study sites.

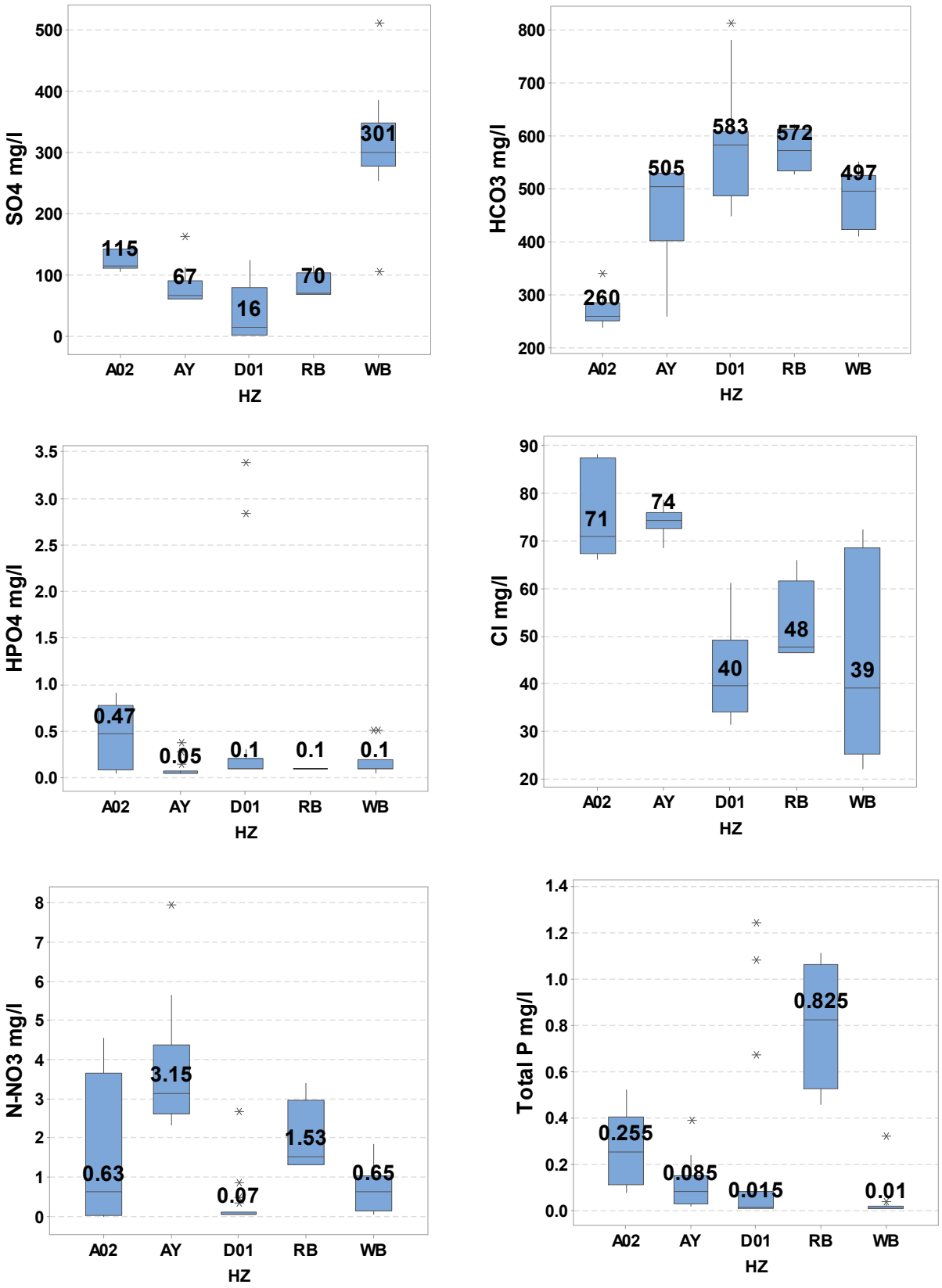

Figure 18: Box plot and median values for the major ions observed in the hyporheic zone over the study area.

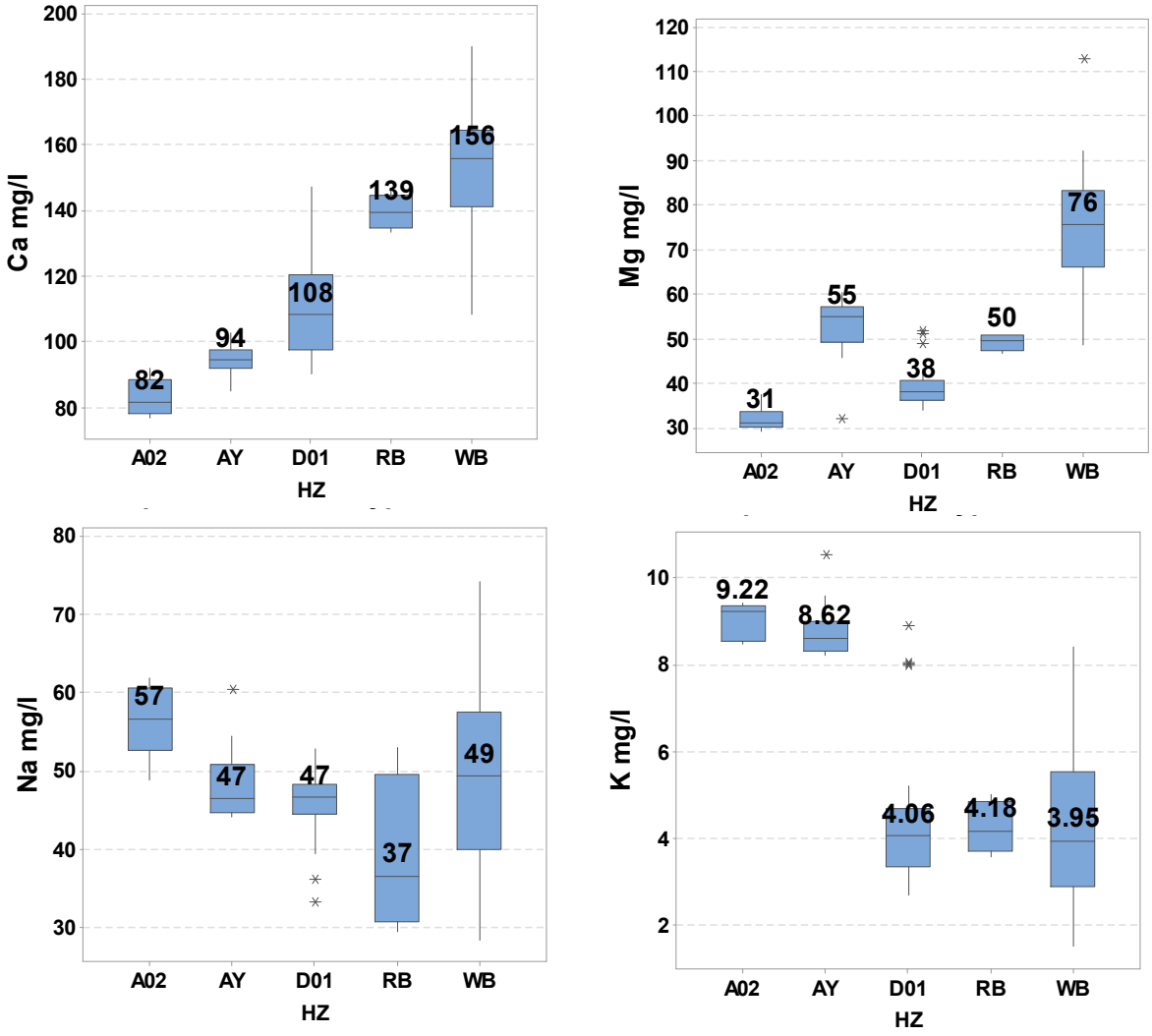

Figure 19: **Box plot and median values for the major ions observed in the hyporheic zone over the study area (continued).**

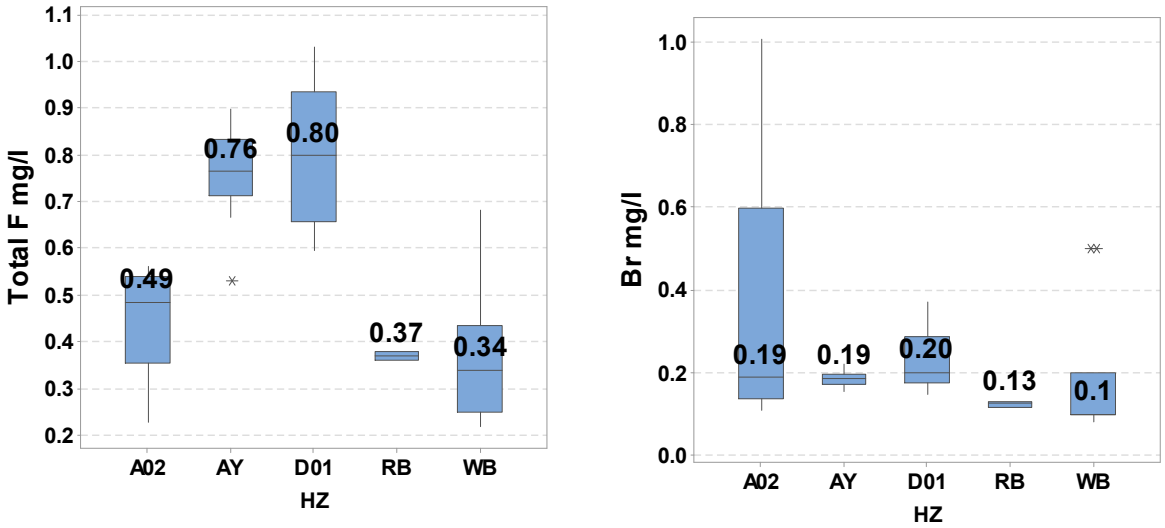

Figure 20: Box plot and median values for the minor halogen elements (F and Br) observed in the hyporheic zone over the study area.

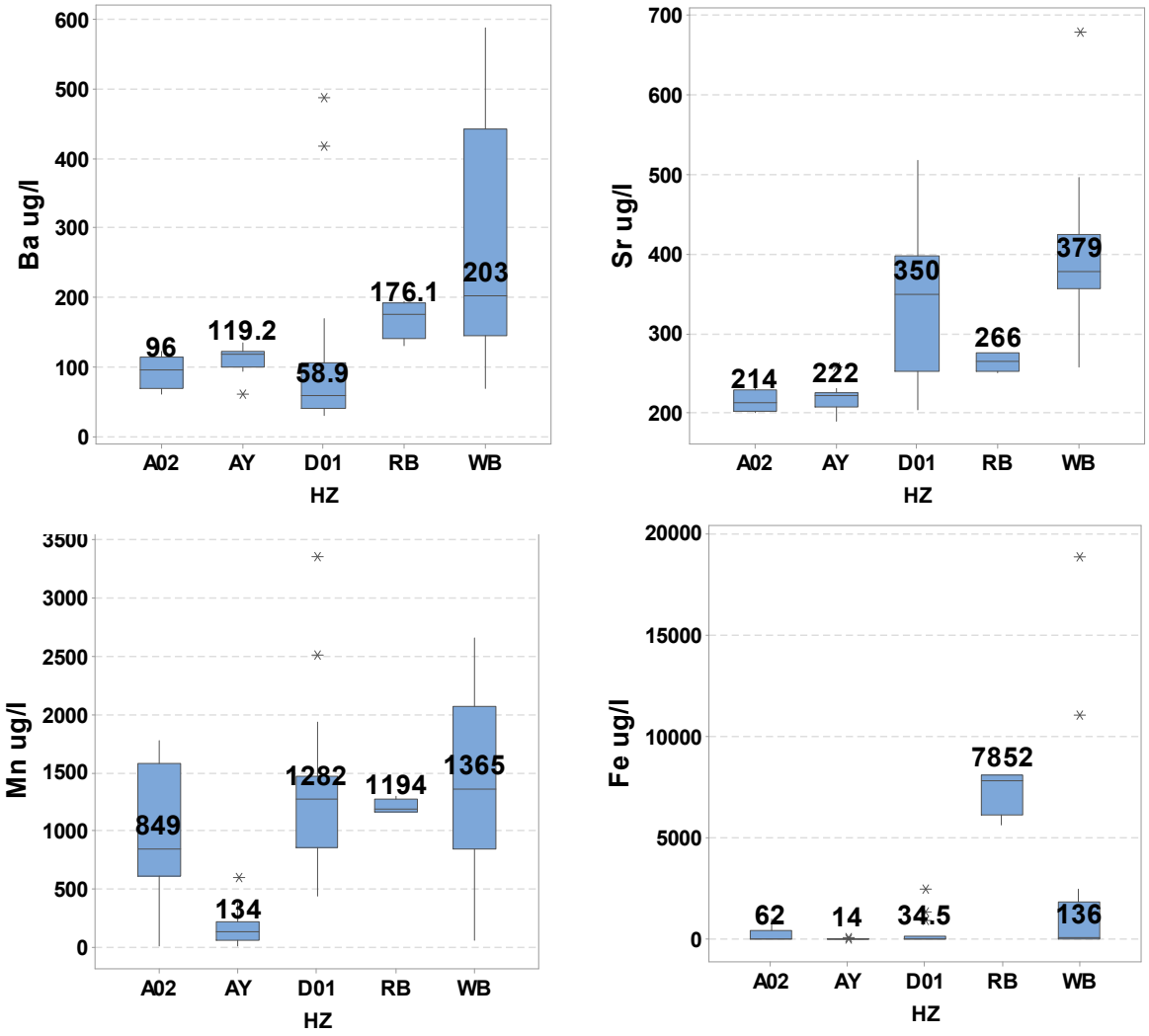

Figure 21: **Box plots and median values for the the minor alkaline earth element barium (Ba) and strontium (Sr) and manganese (Mn) and iron (Fe) elements observed in the hyporheic zone over the study area.**

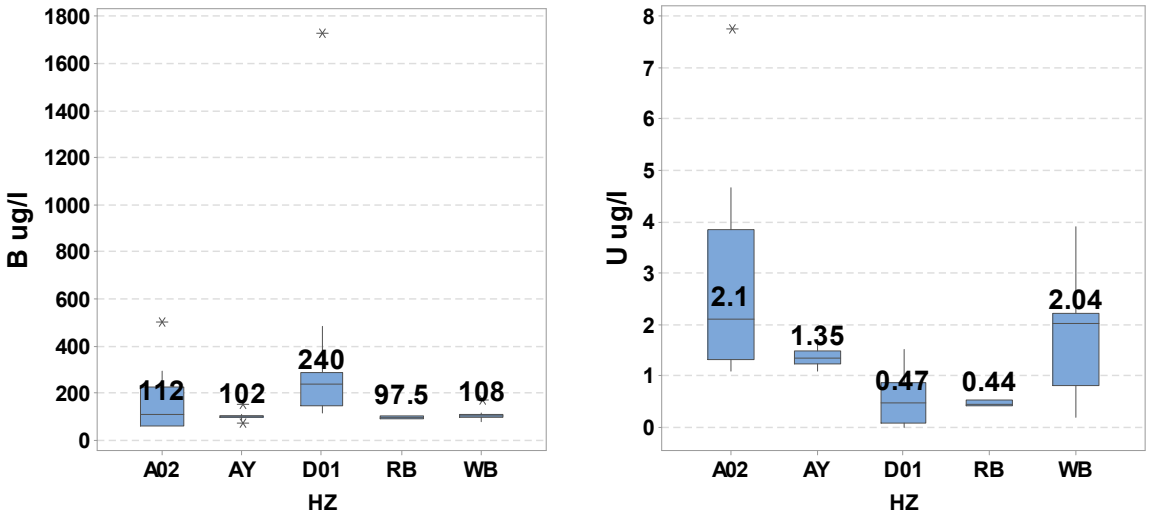

Figure 22: Box plots and median values for boron (B) and uranium (U) in the hyporheic zone over the study area.

6 Comparison of hyporheic zone chemical data with the Magnesian Limestone aquifer

6.1 MAGNESIAN LIMESTONE AQUIFER END-MEMBER

In order to infer inflow of groundwater to the stream using hydrochemical data, knowledge of the groundwater end-members is critical. Furthermore, given the large baseflow contribution expected in the Skerne catchment, a comparison of the composition of groundwater and streams may yield information about chemical processes occurring at the groundwater-surface water interface. For this purpose the EA groundwater data (WIMS water quality database) of potentially related boreholes from the EA monitoring network of the Magnesian Limestone Aquifer were used. The BGS data of the hyporheic zone were compared with this dataset. For some of the considered boreholes, a sample of groundwater was obtained at the time of the hyporheic zone sampling and analysed in the BGS chemical laboratories. Additional surface water data from the spot flow gauging locations established by JBA Consulting on behalf of the EA (during winter of 2017, 24–25 /01 and 27–28/02, and the third in late spring of 2017, 31/05–1/06) have been considered to indicate temporal variability in surface water composition, based on available data.

The EA groundwater monitoring network does not include monitoring of groundwater levels and groundwater quality within the superficial deposits which overlie the Magnesian Limestone aquifer across the catchment, and which may also interact with the hyporheic zone and surface water in the Skerne. This represents a gap in the data collection in order to understand the relative importance of shallow and deeper groundwater in contributing to the hyporheic zone "make-up" and its capacity to attenuate potential contaminants such as nitrate or sulphate.

In this report we show the data as individual value plots limiting the data presentation to a visual qualitative inspection of various elemental distributions in surface water, hyporheic zone waters and groundwater. Further data investigation is necessary to address the understanding of groundwater-surface water connectivity and this will be the focus of future research.

6.2 BOREHOLE FOUMARTS LANE AND SITE D01

The borehole Foumarts Lane [NZ2710030300], (Appendix 1) was selected to provide information on the Magnesian Limestone aquifer hydrochemical characteristics of possible relevance to the site D01. The borehole is part of a cluster of sulphate-rich boreholes north of Newtown Aycliffe, where mine water enters the Magnesian Limestone aquifer through its base, since groundwater levels in the Coal Measures have risen after cessation of mine dewatering in the 1980s. It also demonstrates very high levels of iron, visibly causing extracted water to be orange in colour. The groundwater quality variability for selected major and trace elements across various decades of sampling until the values closest in time to our sampling is shown in Appendix 6.

Although a full interpretation of the borehole hydrochemistry is outside the scope of this report, it is noticeable that high Fe and SO_4 concentrations are present in the groundwater, which can

be interpreted as indicative of mine water impact. The relatively high concentration of $N\text{-}NO_3$ suggests an area of recharge influenced e.g. by nearby fertilizer applications.

6.2.1 Variations across surface water, hyporheic zone and groundwater at site D01

Figure 27 shows the individual values of Cl, SO_4, $N\text{-}NO_3$ and Fe (additional graphs in Appendix 6), respectively, in surface water (SW), hyporheic porewater (HZ) and groundwater (GW) at site D01. Additional surface water data from the spot flow gauging locations set up by JBA Consulting on behalf of the EA was available and also plotted. In addition, the groundwater samples from Foumarts Lane, to the side of site D01 were shown (GW_FO), in order to consider the Magnesian Limestone (ML) aquifer as potential groundwater end-member. The borehole was also sampled at the time of the hyporheic zone sampling and the related chemical analysis results also reported in the same diagrams.

The different composition of the surface water from the hyporheic zone, as observed in the Piper plot (Figure 16) which indicated surface waters as mixed Ca-Mg-Cl type and HZ as Ca-Mg-HCO_3 type water. Surface water Cl is significantly higher than the groundwater concentrations (typically <50 mg/L). This difference permitted Cl to be used as a tracer of surface water / groundwater mixing in the hyporheic zone.

6.3 BOREHOLES LOW COPELAW WITH WOODHAM AND SITE WB

Data from Low Copelaw N01 (LC1) [NZ2940026300], N02 (LC2) [NZ2950026140], and Woodham (W) [NZ2880026100] boreholes were selected, as representative of the Magnesian Limestone Aquifer close to the WB site.

The boreholes are part of a cluster of sulphate–rich boreholes north of Newtown Aycliffe village. Low Copelaw N01 and Low Copelaw N02 have large concentrations of Fe (respectively, in µg/l: median 3845; min-max 81–10600; and median 360; min-max 20 – 120000); Mn (respectively, in µg/l: median 1155; min-max 130–1410, and median 288.5; min-max 11.8–416) and SO_4 (respectively, in mg/l: median 434.5; min-max 200–665, and median 104; min-max 9.98–251). The BGS chemical analysis of Low Copelaw N01 groundwater is within the above range. Woodham borehole has a lower content of SO_4, in mg/l median 46; min-max 5.0–160, Fe median is 380 µg/l and min-max 20-11000 µg/l, while Mn median is 275 µg/l and min-max 215-310 µg/l. Alkalinity as HCO_3 median values are high for Low Copelaw N01 (476.6 mg/l) and relatively lower for Low Copelaw N02 (221.9 mg/l) and Woodham (156 mg/l). BGS analysis of Low Copelaw N01 is $HCO_3$253 mg/l.

6.3.1 Variations across surface water, hyporheic zone and groundwater at site WB

Figure 36 shows the distribution of selected major and trace element concentrations in the SW and HZ at site WB compared with the distribution in the selected boreholes and additional JBA SW samples. For completeness and to consider potential variability in temporal SW composition, the JBA SW samples were included. However, the samples were taken from further upstream (JBA site B01) than the study site and their relevance might be limited.

The individual value plot of Cl across the groups indicates that Cl concentrations for the HZ have a quite broad distribution (22–72 mg/l). SW samples collected at the time of the HZ sampling have Cl concentrations (57–66 mg/l) closer to the higher HZ values. The GW water

types broadly appear to be distributed within the HZ range. However, when the Cl distribution for each borehole is considered across the years (Appendix 6), all boreholes show an increasing trend in Cl concentrations with years. Only Low Copelaw N01 has been sampled continuously up to the more recent years (2010–2017). These GW samples show a fairly narrow range of Cl concentrations (50–56 mg/l). The recent GW sample (BGS analysis) has a value of 51 mg/l. Results from the three SW samples undertaken previously by JBA at the nearby monitoring location B01 indicate two high values (75–85 mg/l) and a low value of 16 mg/l.

HZ SO_4 appears evenly distributed across a range 253–386 mg/l; with one low value at 105 and one high value at 511 mg/l outside the range and a median of 310 mg/l. SW SO_4 ranged 327–498 mg/l (median 411 mg/l), closer to the HZ high range values. The JBA point was measuring lower SO_4 <57 mg/l, but it is located upstream the area of known high SO_4 in SW.

The HZ SO_4 values fall within the Low Copelaw N01 with SO_4 distribution of 200–665 mg/l. Low Copelaw N02 has instead a lower range of SO_4 (12–251 mg/l), and similarly Woodham (5–155 mg/l). When the SO_4 distribution for each borehole is considered across the years (Appendix 6) borehole Low Copelaw N01 shows a decreasing trend in SO_4 concentrations with years. Vice versa, Low Copelaw N02 and Woodham had an increasing trend in the 1990–2000 decade. The recent GW sample (BGS analysis) has a value of 162 mg/l, close to the 2010–2016 distribution of Low Copelaw N01 borehole.

The SO_4 concentration trends through the years for Low Copelaw N01, N02, and Woodham (Appendix 6) indicate that noticeably the most recent GW samples (2010–2016) from Low Copelaw N01 are the lowest, while it appears to be the opposite trend for Copelaw N02, and Woodham boreholes, whose SO_4 values are higher for the 1990-2000 group than the 1969-1980 group.

6.4 BOREHOLES RUSHYFORD AND SITE RB

Data from Rushyford_A (_A), [NZ2840028700], Rushyford_NE (_NE) [NZ2870029000] boreholes were considered as representative of the Magnesian Limestone aquifer close to the RB site. The boreholes have different concentration ranges of total Fe (respectively, in µg/l: median 568; min-max 20–9350; and median 305; min-max 5 –970); total Mn (respectively, in µg/l: median 13.10; min-max 3.65–140, and median 10; min-max 0.33–73) and SO_4 (respectively, in mg/l: median 2015; min-max 7–315, and median 75.10; min-max 33.8–92). Alkalinity as HCO_3 median values are 361 mg/l and 364 mg/l.

Figure 25 shows the distribution of selected major element concentrations in SW and HZ at site RB and allows comparison with the distribution in the selected boreholes. The HZ Cl values fall in the lower range of the Cl values of Rushyford_A. The borehole has very high Cl values up to ~250 mg/l. The small number of HZ samples has also very high concentrations of Fe, reflecting the equally high values of Rushyford_A borehole.

6.5 BOREHOLES KETTON HALL WITH AYCLIFFE AND SITE AY

Data from boreholes Ketton Hall [NZ2940019300] and Aycliffe [NZ2695725157] were considered, as representative of the Magnesian Limestone Aquifer close to the AY site.

Figure 26 shows the distribution of Cl, SO_4, N-NO_3 and Fe concentrations in the SW and the HZ at site AY. The groundwater samples from two boreholes: Ketton Hall and Aycliffe are also shown, in order to consider the Magnesian Limestone aquifer groundwater end-member chemistry. The borehole Ketton Hall was further sampled near to the time of the HZ sampling and the analysis additionally reported in the same diagrams. The groundwater quality variability across various decades of sampling through to the values closest in time to our sampling is shown in Appendix 6 Figure 70. Additional surface water data from the spot flow gauging location A03, immediately downstream AY site, undertaken by JBA Consulting on behalf of the EA was available and also plotted.

6.6 BOREHOLE KETTON HALL AND SITE A02

Data from Ketton Hall [NZ2940019300] borehole were selected, as representative of the Magnesian Limestone aquifer close to the A02 site.

Figure 27 shows the distribution of Cl, SO_4, N-NO_3 and Fe concentrations in the SW and the HZ at site A02. The groundwater samples from Borehole Ketton Hall are also shown, in order to consider the Magnesian Limestone aquifer groundwater endmember chemistry. The borehole was sampled close to the time of the HZ sampling and the analysis additionally reported in the same diagrams. The groundwater quality variability across various decades of sampling until the values closest in time to our sampling is shown in Appendix 6. Additional SW data from the spot flow gauging locations set up by JBA Consulting on behalf of the EA were available and also plotted.

The individual value plots confirm the similar composition of SW and HZ porewater, as observed in the Piper plot, with the exception of NO_3, and Mn values, which spread towards lower (NO_3) or higher (Mn) values than SW.

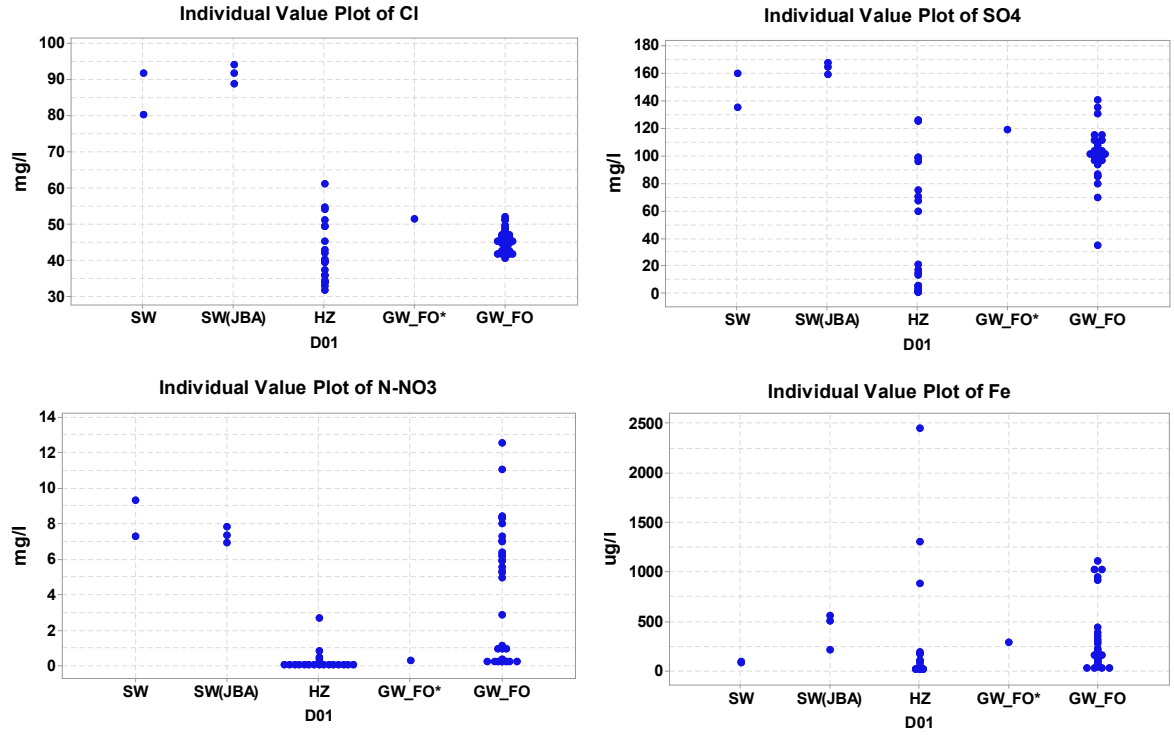

Figure 23: Individual value plot of Cl, SO_4, N-NO_3 and Fe distribution in surface water (SW), hyporheic porewater (HZ) and groundwater (GW) at site D01. GW_FO = EA data for borehole 25-3-330 Foumarts Lane (date of collection 10/6/1992 to 27/2/2017). GW_FO* = BGS data of borehole 25-3-330 Foumarts Lane collected at the same time of SW/HZ. SW(JBA) = EA/JBA surface water data (collected on 24/1, 27/2 and 31/5 2017).

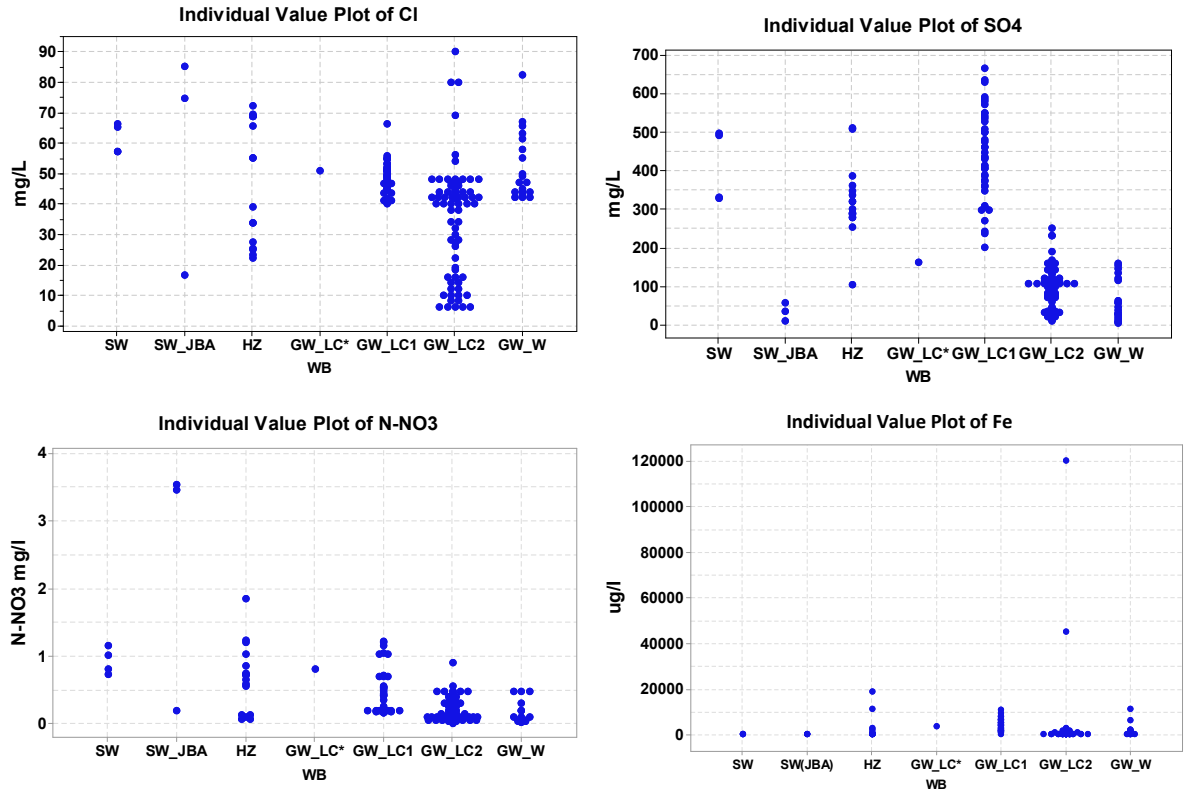

Figure 24: Individual value plot of Cl, SO_4, N-NO_3 and Fe distribution in surface water (SW), hyporheic porewater (HZ) and groundwater (GW) at sites WB2 and 3. Legend: SW at WB1,2,3 SW(JBA): JBA sites B01, B02, B03; GW_LC*= Borehole 25-3-27 Low Copelaw N01 (NRA D)/BGS analysis; GW_LC1= borehole 25-3-27 Low Copelaw N01 (NRA D)/EA analysis; GW_LC2= Borehole 25-3-28 Low Copelaw N02 (NRA 7)/EA analysis; GW_W= Borehole 25-3-26 Woodham (NRA 5)/EA analysis.

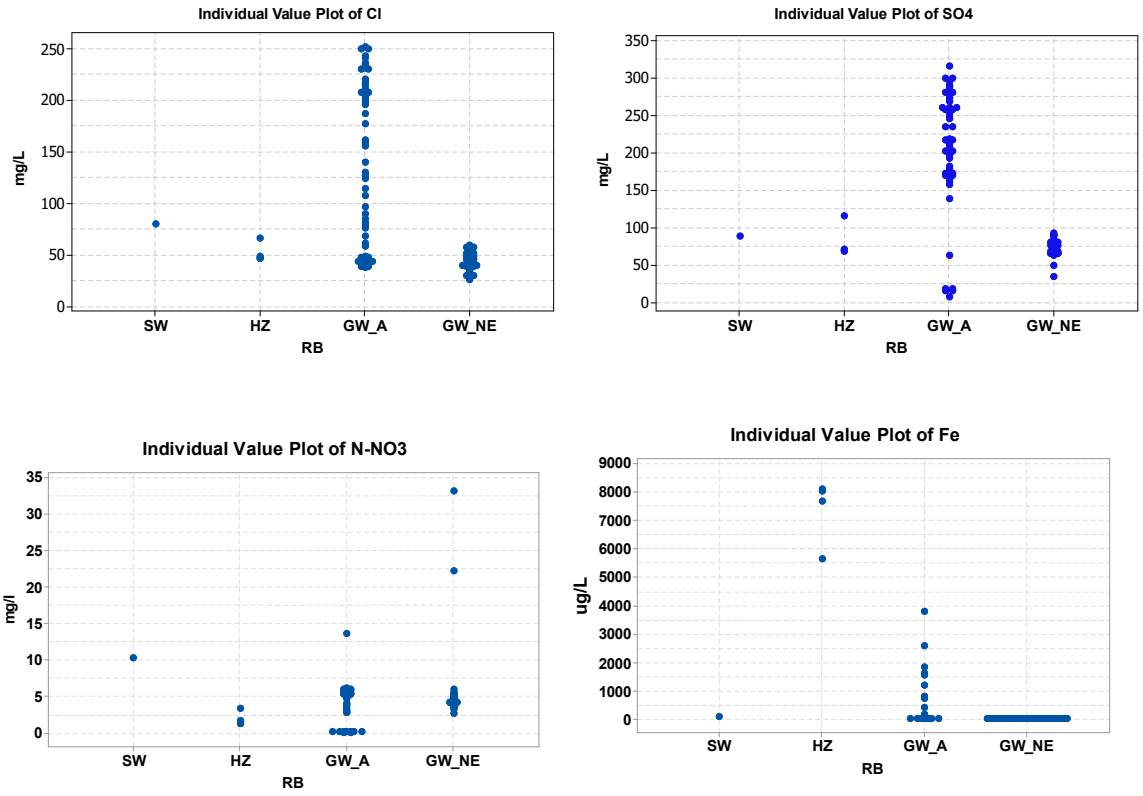

Figure 25: Plot of Cl, SO_4, N-NO_3 and Fe distribution in surface water (SW), hyporheic porewater (HZ) and groundwater (GW) at site RB. Legend: GW_A= Borehole 25-3-21 Rushyford_A , GW_NE= Borehole 25-3-22 Rushyford_NE.

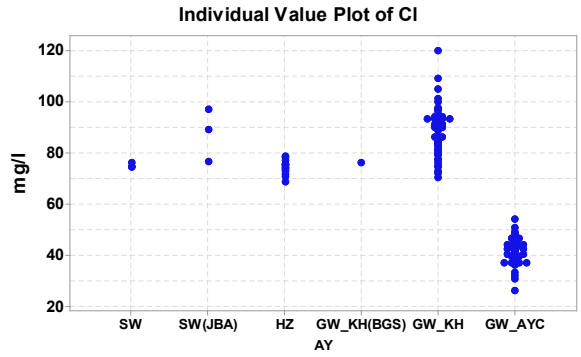

GW_KH=KETTON HALL; GW_AY=AYCLIFFE

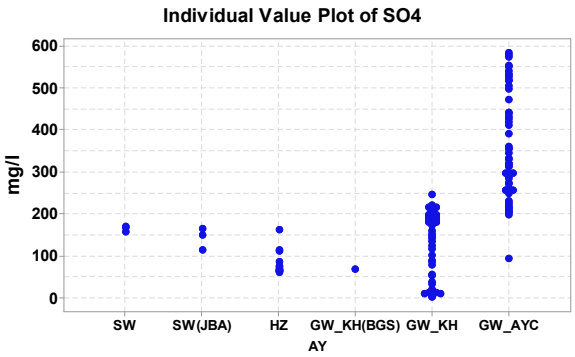

GW_KH=KETTON HALL; GW_AY=AYCLIFFE

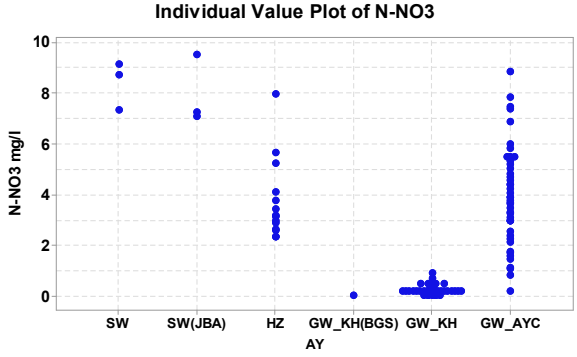

GW KH=KETTON HALL: GW AY=AYCLIFFE

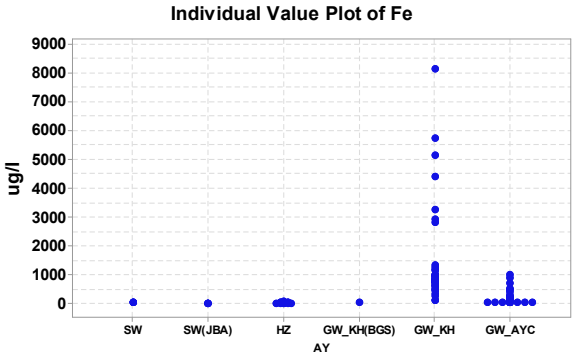

GW_KH=KETTON HALL; GW_AY=AYCLIFFE

Figure 26: Plot of Cl, SO_4, N-NO_3 and Fe distribution in surface water (SW), hyporheic porewater (HZ) and groundwater (GW) at site AY. GW_FO = EA data for Borehole 25-3-76 Ketton Hall (date of collection 10/6/1992 to 27/2/2017). GW * = BGS data of Borehole Ketton Hall collected at the same time of SW/HZ. SW(JBA) = EA/JBA surface water data (collected on 24/1, 27/2 and 31/5 2017). GW_AYC = EA data for Borehole 25-3-41 Aycliffe (NRA 2).

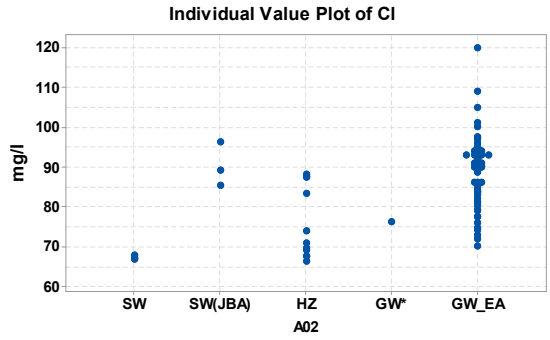

Borehole Ketton hall

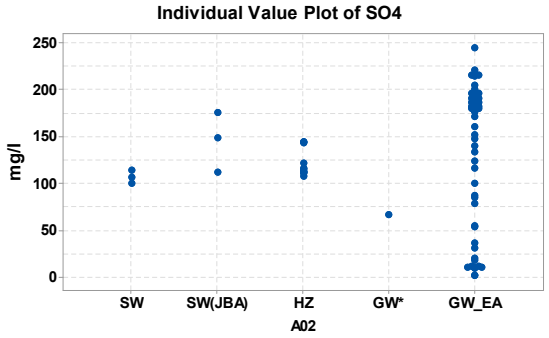

Borehole Ketton hall

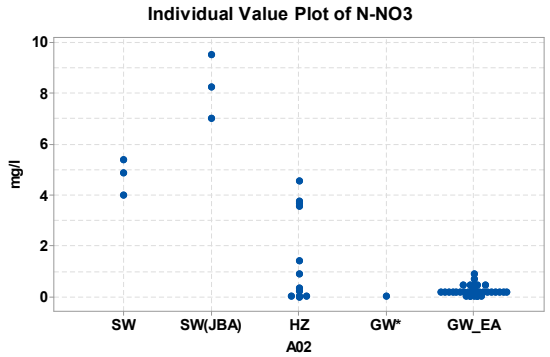

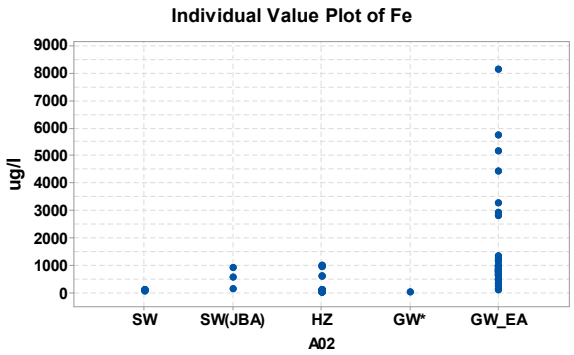

Borehole Ketton hall

Figure 27: Plot of of Cl, SO_4, N-NO_3 and Fe distribution in surface water (SW), hyporheic porewater (HZ) and groundwater (GW) at site A02. GW_FO = EA data for Borehole 25-3-76 Ketton Hall (date of collection 10/6/1992 to 27/2/2017). GW * = BGS data of Borehole Ketton Hall collected at the same time of SW/HZ. SW(JBA) = EA/JBA surface water data (collected on 24/1, 27/2 and 31/5 2017).

7 Hyporheic mixing and geochemical controls on hyporheic zone composition

7.1 INTRODUCTION

This section provides an overview of the role of the hyporheic zone and further presents the evidence of hyporheic mixing and the geochemical processes controlling porewater chemistry. This is done at site level using the approach described in sections 3 and 4.

7.1.1 Why hyporheic mixing is important

The hyporheic zone is the interface region beneath and adjacent to the stream and rivers where surface water (SW) and groundwater (GW) mix and interact. A copious body of literature exists related to the physical processes controlling the hyporheic mixing. Here only a brief summary is given. At the stream reach scale, flow paths originating in the SW may temporarily enter the subsurface and allow for GW–SW mixing in the streambed and the near-channel saturated zone. These flow paths are commonly referred to as hyporheic exchange flows (HEFs). At this scale HEF are related to variability of hydraulic conductivity and differences in hydraulic gradient as a result of streambed geomorphology and turbulent flow (Krause et al. 2011), resulting in a mosaic of path-lengths and -depths. At the catchment scale ambient groundwater discharge (AGD) can dominate over bedform-driven exchange. Superposed on the 1 m scale, aquifer water discharges into and/or is recharged from almost all freshwater rivers and lakes, resulting in a net gain or loss from the water column. Depending on the direction of the net groundwater flow, these are referred to as 'gaining' and 'losing' water bodies (Cardenas and Wilson, 2007). However, even under gaining conditions and upward pressure gradients, such as those expected in some reaches of the Skerne, surface water can migrate down into the shallow hyporheic zone. In this case down-welling of river water superposes the regional hydraulic regime.

Across all scales, hyporheic mixing is of particular importance to the chemical mass balance of a river catchment. In fact, when surface water moves through the hyporheic zone and mixes with groundwater in close contact with geochemically and microbially active sediments, enhanced biogeochemical reactions can change solute composition; this can ultimately affect, through continuous surface water – hyporheic flow exchanges, the solute mass balance at the catchment scale (Harvey and Fuller, 1998; Bencala, 2011). Hyporheic mixing is also important in the attenuation of upwelling groundwater contaminants as well documented in a variety of field studies illustrating e.g. perchloroethene (PCE) degradation or denitrification as a groundwater plume traverses hyporheic sediments before exiting to the river (Conant et al, 2004; Gu et al., 2007).

Natural attenuation of contaminants in the hyporheic zone can be the combined effect of a variety of biogeochemical processes such as redox reaction, precipitation, complexation to organic matter and sorption to sediments. These processes will affect the spatial distribution and fate of inorganic and organic contaminants, nutrients and pathogens during transport through the hyporheic zone. The extent to which biogeochemical processes also affect the hyporheic zone composition depends on the balance between chemical reaction rate versus fluid residence time, as the infiltrating fluids are far from equilibrium and the biogeochemical reactions are kinetically controlled (Stumm and Morgan, 2012). Systems of low hydraulic conductivity are expected to favour transformation and attenuation of contaminants, because

chemical reactions have sufficient time to occur under the relatively slow flow conditions. However, low hydraulic conductivity may also limit hyporheic exchange, thereby potentially reducing the significance of the hyporheic zone as a natural attenuation zone. Ultimately, the extent to which the hyporheic zone affects the surface stream at reach and catchment scale is a function of both its activity and extent of connection (Boulton et al., 1998).

7.1.2 Cycling of pollutants affected by redox gradients

When oxygenated downwelling water enters the streambed, sediment organic matter, through its decay, will drive reduction of the system with an Eh decline as the water moves into the subsurface. By contrast, a reverse sequence of oxidation processes can occur when anoxic groundwater enters a well-oxygenated streambed. This has been observed in ferrous iron and manganese rich mine water plumes entering the hyporheic zone, causing precipitation of Mn and Fe hydroxides in the streambed.

The redox conditions are determined by a balance between i) the supply of oxygen from oxygenated surface water related to the residence time of the flow through the sediment and ii) the consumption of oxygen by microbial decomposition of organic matter in the riverbed sediment, i.e the abundance and reactivity of organic matter. The redox processes along a subsurface flow path proceed sequentially from the highest energy yield downwards (Lovley and Chapelle, 1995). The sequence commonly encountered in subsurface environments shows a sequential reduction of free oxygen (O_2), nitrate (NO_3) reduction, manganese and iron (MnO_2(s), $Fe(OH)_3$(s)) reduction and sulphate (SO_4) reduction and or methane fermentation. Other important reductants along with organic matter are NH_4, H_2S.

Aerobic conditions are defined by free dissolved oxygen (generally in excess of 1 mg/l) and low concentrations of all reduced species. Nitrate (NO_3) reduction can occur even where free oxygen is measured (Pedersen et al., 1991). The processes for aerobic respiration and denitrification are relatively similar. Most known denitrifying microorganisms are able to use oxygen preferentially when available and in some cases the two are used together. These processes can be carried out by a single organism. It is also possible for dissimulatory NO_3 reduction directly to ammonium (NH_4) to occur (Tiedje, 1988).

Ferrous iron is a common constituent of anoxic waters as a result of reductive dissolutions of ferric minerals. Similar behaviour is of manganese, however, Mn-oxides become reduced and then dissolve at higher Eh than Fe-oxides. Although in some natural environments, when the available iron oxide has low solubility, Fe(III) and sulphate reduction can proceed simultaneously, in most environments iron reduction takes place at higher Eh than sulphate reduction (Appelo and Postma, 2005). Strictly anaerobic processes such as SO4-reduction occur only under more extreme redox conditions (usually at Eh < -150 mV, Storey et al, 1999; Mitsch & Gosselink, 1986). When a SO_4-rich water enters an organic matter-rich riverbed in anoxic conditions, SO4 reduction can be accelerated, according to the general reaction $2CH2O + SO_4^{2-} \rightarrow 2HCO_3^- + H_2S$. The net effect of the reduction of sulphate to sulphide is the depletion of soluble sulphate from the water and production of alkalinity. For example the reduction of 100 mg/l SO4 leads to the production of 127 mg/l HCO3-. Sulphate can persist in anoxic water that is generally poor in microbially viable organic matter, though some bacteria are able to use methane as electron donor (anaerobic oxidation of methane, $CH_4 + SO_4^{2-} \rightarrow HCO_3^- + HS^- + H_2O$).

Although a redox zonation can be expected through the hyporheic zone, fine scale heterogeneity in organic matter in the bed sediment, forming patches of dissolved oxygen

(DO)-depleted zones, can result in multiple microbially-mediated redox processes in close proximity (Triska et al, 1993).

7.2 SITE FOUMARTS LANE (D01)

7.2.1 Monitoring set-up

The geomorphological, geological and hydrogeological setting of the site has been described in Section 2. The study reach is shown in Figure 28 alongside a plan of relevant monitoring installations along a cross section from the north bank towards the middle of the stream. The riverbed consists of a consolidated layer which deepens from 1 m above the surface water level near the north bank to 2 m above the water level towards the middle stream overlain by a soft dark layer (containing visibly larger amounts of organic matter) of variable thickness (0.4 to 1.3 m) (Figure 29). Most samplers were installed to sample both from the softer and harder sediment, with the exception of the mini drive-points, which only sampled from the harder sediment layer. The river flow was very low at the time of sampling.

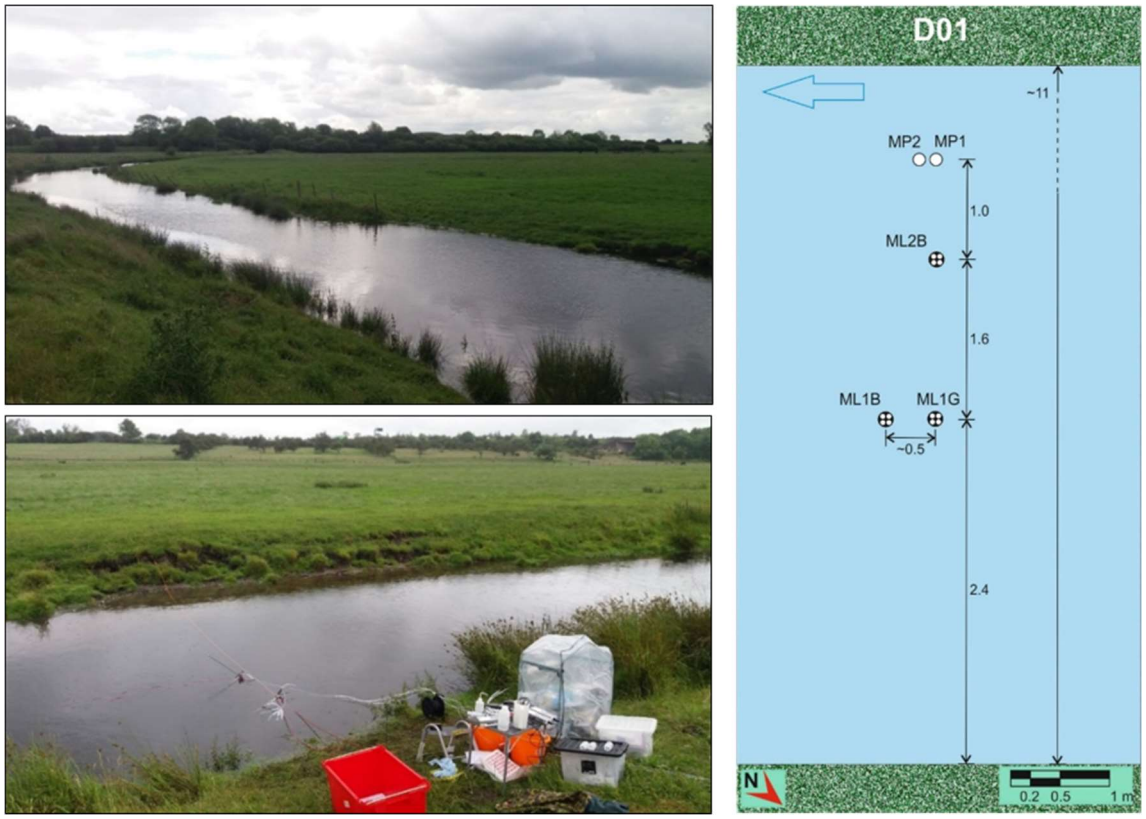

Figure 28: Photo of D01 study reach and monitoring installations from the North bank approached from Foumarts Lane and Plan view of monitoring set-up along a cross section from the North bank towards the middle of the canal (left) and schematic view of the monitoring network (right). ML are multilevel samplers, MP are minidrive points.

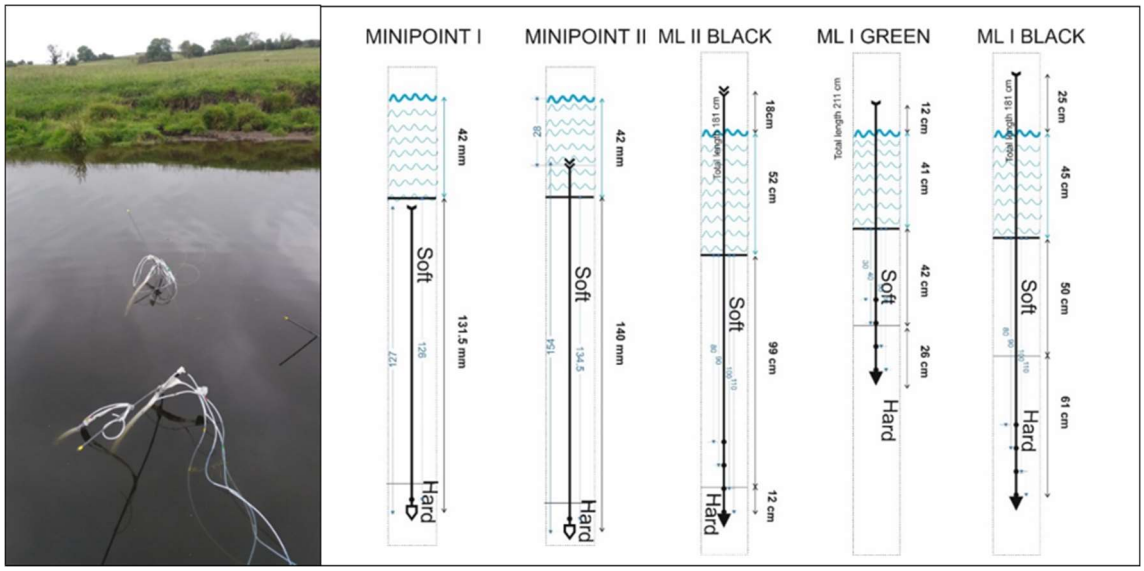

Figure 29: Photo of monitoring installations and Outline of sampler installation depth and details of the soft-hard sediment boundary (Minipoint I being at the centre, and ML I Black closest to the northern side of the canal).

7.2.2 River survey

A brief river survey was undertaken on 29th June 2017 to investigate whether field parameters such as temperature, pH and electrical conductivity vary along the flow path of the tributary, indicative of potential groundwater inflows. For this purpose, grab samples from the river were taken at 10 m intervals from approximately 150 m upstream to about 100 m downstream of the HZ site. Measurements at the nearby pond (432690 530325), and at the confluence of the tributary with the Skerne River (and the Skerne River itself) were included. The data are reported in full in Appendix 3; the measured T, pH, and EC were relatively stable at around 12.5°C, 7.5, and 1050 µS/cm (respectively), failing to show any obvious subsurface inflow able to cause measurable changes in the field parameters.

7.2.3 Field parameters at D01

The distribution of the field parameters of temperature, redox, dissolved oxygen (DO), conductivity and pH are reported in Figure 30. HZ temperatures distributed mostly between 13.7 °C and 14.9 °C, median 14 °C with only one sample at 16.3 °C, and they were relatively higher than the SW (13.6 °C). All HZ Eh measurements were between 264–150 mV, median 186 mV, clearly separating them from the higher SW Eh of 360 mV. On the contrary, the DO values of the HZ and SW were partially overlapping, with some of the HZ values close to the SW DO of 7.6 mg/l; it is suspected (Section 3.3) that some are unreliably high measurement for some of the HZ samples. Only the samples from the minidrive points MP1-MP2 differed substantially with very low DO concentrations of 2 mg/l, indicating almost anoxic conditions. They were the only HZ samples collected with the syringe method from the minidrive points at a sediment depth (the top of the sediment being defined as the top of the softer sediment layer) of 125–135 cm. Both HZ conductivity and most of the pH measurements were close to or lower than SW conductivity and pH (HZ conductivity= 845–1020, median 950 µS/cm; SW conductivity= 1007–1017, median 1012 µS/cm; HZ pH. 7.23–7.80, median 7.33; SW pH 7.36–7.56, median 7.44).

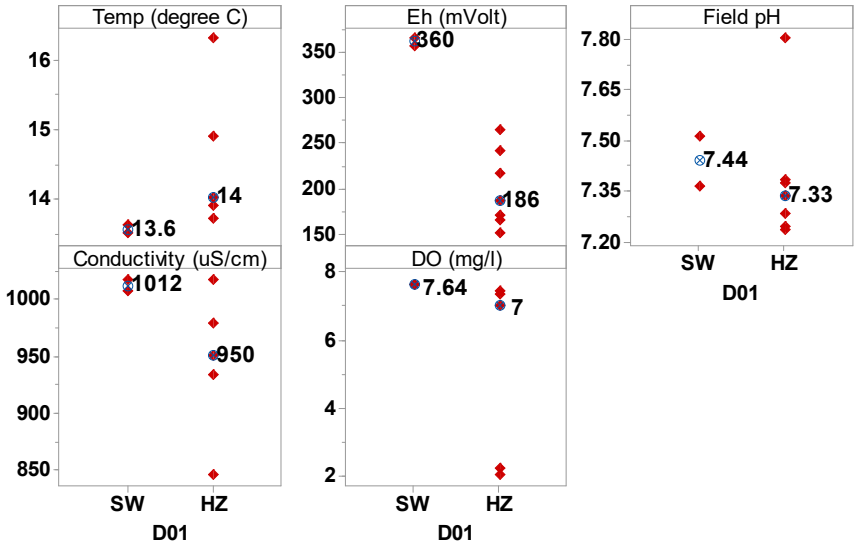

Figure 30: Individual value plots showing the distribution of field parameters in surface water (SW) and hyporheic porewater (HZ) at site D01. Median values indicated by open blue circles.

7.2.4 Chloride depth profile

Figure 31 shows the Cl depth profiles for all piezometers installed at site D01. SW Cl (range 80–92 mg/l) was far more abundant than HZ Cl (range 34–61 mg/l), and similar to the values reported in previous monitoring by JBA. The observed Cl vertical gradients do not show a linear vertical trend with depth. The data are better considered in relation to both the spatial distribution of the piezometers along the stream horizontal transect and the riverbed stratigraphy. ML1G and ML1B are two multilevel piezometers close to the riverbank, installed respectively at shallow and deep (< -80 cm) depth, while ML2B and MP1, MP2 were installed further away from the bank towards the middle of the stream, all at similar depth (120–140 cm). A sharp change in the streambed lithology from a soft sediment layer to a more lithified clayey sediment layer was recorded at the time of the installation (Figure 29). The depth of this boundary varied across the canal section. ML1G and ML2B crossed the soft-hard sediment boundary, respectively at a sediment depth of about -40 cm and -110 cm, and that was marked by a sudden increase in Cl below the boundary. ML1B, near ML1G but installed at deeper depth all in the hard sediments, had relatively lower Cl than ML1G, between 40 and 55 mg/l. The lowest Cl values (32–36 mg/l) were shown by the deepest piezometers MP1 and MP2, almost at the centre of the canal.

The sediment porewater shows therefore a complex Cl concentration pattern. Although significant surface water contribution is excluded, it is difficult to infer unequivocally the source of Cl and possible flow path directions determining the observed gradients. Also, the average Cl (51.4 mg/l) of Foumarts Lane borehole is slightly higher than the deepest porewater Cl points, but interestingly, Cl concentrations in the nearby ponded area showed a low value (Table 16, Cl 34.2 ml/l) that is similar to some of the HZ samples. It is therefore not possible to prove unequivocally the contribution to the HZ make-up of groundwater from the ML and of a superficial aquifer contribution.

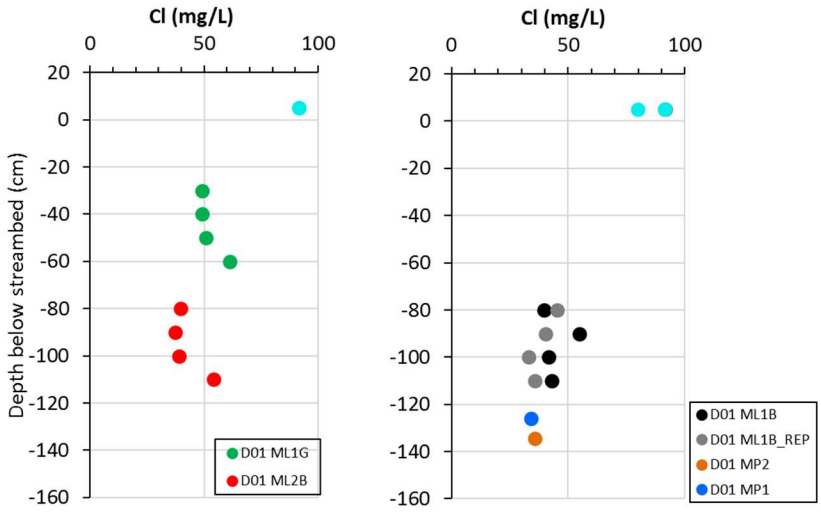

Figure 31: Depth profiles of chloride concentrations. Symbols grouped by piezometer. Light blue circle symbols: grab surface water samples at the time of porewater sampling.

Reactive Solute

Figure 32 and Figure 33 show the SW and HZ porewater vertical profiles measured in the streambed at site D01 for SO_4, NO_3, Mn, and Fe.

N-NO_3 measurements in SW were 7.25–9.3 mg/l, with concentrations very similar to the previous JBA monitoring (6.91–7.81 mg/l). N-NO_3 was much lower through all the monitored HZ, mostly with values <0.01 mg/l. These values are close to the latest N-NO_3 value for Foumarts Lane borehole. At 110 cm depth a noticeable increase in N-NO_3 (0.8–2.7 mg/l) was measured in two of the piezometers, ML1B close and ML2B further away from the bank (refer to monitoring setting Figure 28).

Manganese (Mn) concentration in the hyporheic zone was higher (median 1282 µg/l) relative to that in surface water (median 102 µg/l). The vertical gradients observed for each piezometer were of decreasing Mn concentrations with depth, up to -110 cm. At greater depth mini drive-point piezometers MP1 and MP2 showed instead a large increase in Mn. HZ Mn was always much higher than Foumarts Lane borehole.

Hyporheic zone Fe concentrations were very variable, with a median of 35 µg/l. It is noticeable that very high values (2455 µg/l) during the first sampling of ML1B, which did not repeat during a second sampling few hours later. Hyporheic zone Fe was either higher or lower than Foumarts Lane borehole, due to the high spatial and temporal variability measured.

SW SO_4 concentration was 135-160 mg/l at the time of sampling, with concentrations very similar to the previous JBA monitoring (159-167 mg/l). The HZ SO_4 showed significant vertical gradients. In the shallow piezometer close to the river bank, ML1B (sampling ports at depth -30 to -60 cm below the water-sediment boundary), SO_4 concentration was relatively low (5.55 mg/l) at -30 cm depth and then higher (15-21 mg/l) in the lower ports. The shift corresponds to a change in lithology from a soft sediment layer to a harder clayey sediment layer. In the deeper piezometer (ML1B), drawing porewaters only from the clayey layer, SO_4 was much higher and with an increasing trend with sediment depth (from 65 to 125 mg/l). SO_4 gradients in piezometer ML2B further away from the banks and with the first 100 cm installed in the soft sediments, reflect the pattern of SO_4 concentration-lithology described above. In

fact, a sharp increase in SO_4 was observed at the soft/hard sediment boundary, from very low values (2 to 13 mg/l) in the upper soft layers to a much greater value of 60 mg/l at depth -110 cm in the harder clayey layer. However, SO_4 was very low in the mini drive-points MP1 and MP2, towards the middle of the canal, even though the ports were fully into the hard sediments at depth >120 cm. The highest SO_4 concentrations at 110 cm depth were similar to both SW and Foumarts Lane borehole.

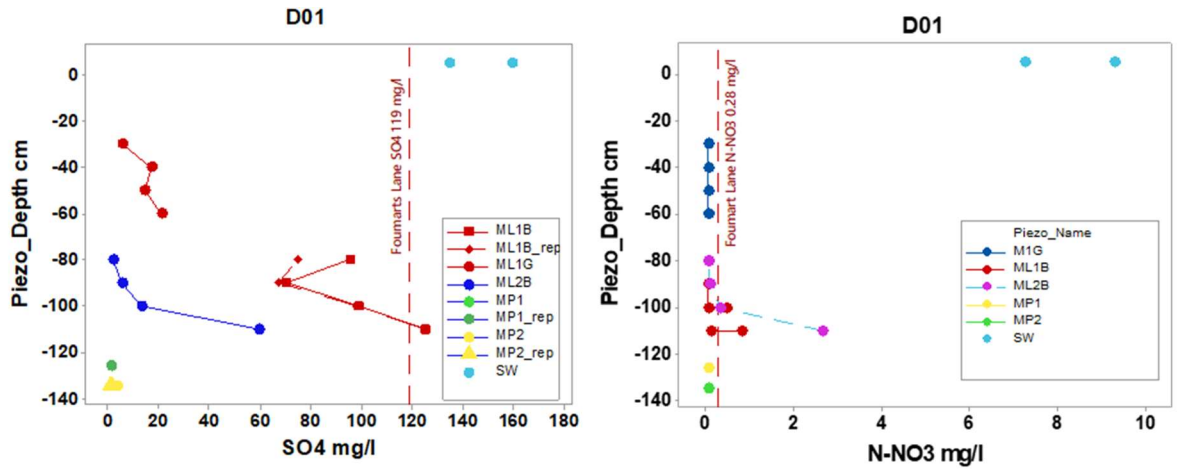

Figure 32: Depth profiles of sulphate (SO_4) and N-NO_3. Symbols grouped by piezometer.

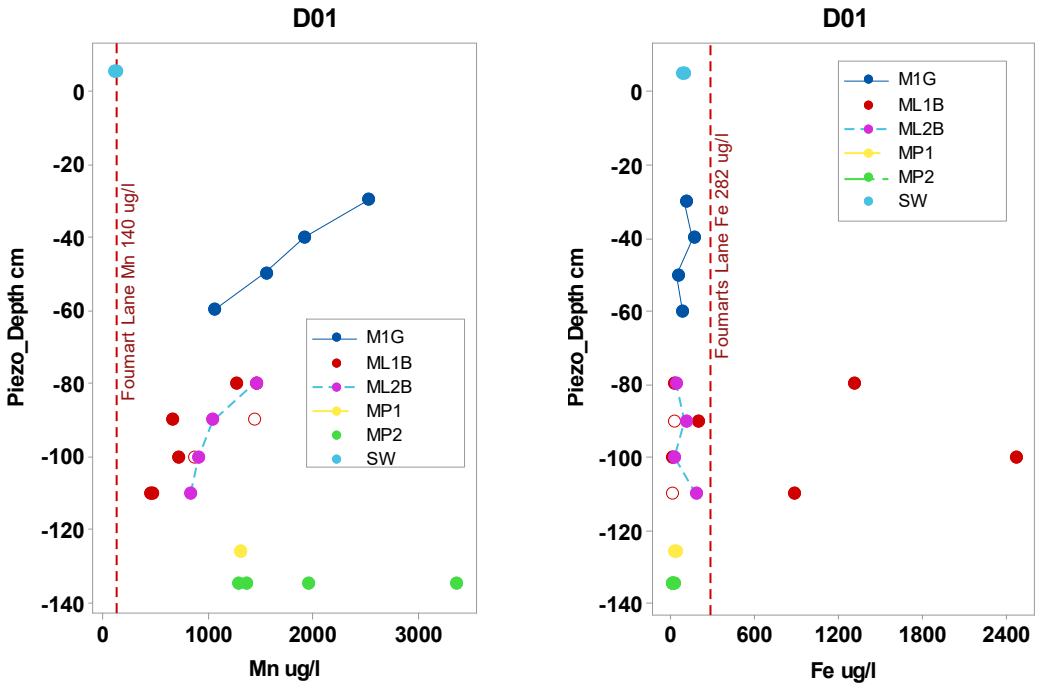

Figure 33: Depth profiles of manganese (Mn) and iron (Fe) concentrations. Symbols grouped by piezometer.

7.2.5 Redox control on reactive solutes

Figure 34 and Figure 35 show elemental correlations for the SW and HZ samples from our sampling and groundwater samples from the EA database; Na and Cl show a strong positive correlation in the HZ samples, with most of these samples aligned between SW and the deepest HZ (MP1 and MP2), suggesting some mixing between SW and the water at greater sediment depth. SO_4 is not correlated with Cl. This indicates that SO_4 concentrations in the hyporheic zone are not simply related to mixing and might suggest that SO_4 does not behave conservatively in the HZ.

Taking Eh measurements was not always possible, but with the data available it is noticeable that for some of the lowest Eh, at around 150 mV, the SO_4 was very low. This was not always the case, however, and at similarly low Eh, much higher SO_4 (80 mg/l) was also present. Mn, a redox sensitive element, at moderately low Eh conditions reduces from Mn^{4+} to soluble Mn^{2+}, and its increased concentration in porewater can be used as an index of moderate reducing conditions. Figure 35 shows that the lowest SO_4 values were mostly associated with the highest Mn values. The correlation Fe-SO_4 is instead weak, possibly due to the instability of dissolved ferrous iron in neutral to alkaline pH waters. SO_4 and HCO_3 are also negatively correlated in the hyporheic zone, with the highest alkalinity shown by the low SO_4-porewaters. For samples with HCO_3 lower than ~ 650 mg/l, the negative gradient SO_4-HCO_3 of the HZ sulphate porewaters closely relates to the "sulphate to alkalinity" stoichiometries of sulphate reduction by organic matter, according to the reaction $2CH_2O + SO_4^{2-} \rightarrow 2HCO_3^- + H_2S$. The observed alkalinity increase of 185 mg/l in alkalinity as HCO_3, from 450 mg/l to 635 mg/l (Figure 35), would in fact correspond to a decrease of 145.6 mg/l SO_4, using the above equation. This is not too dissimilar to the difference between the measured SO_4 values in surface water and the very deep HZ (Figure 32). The findings suggest the removal of SO_4 from porewater solution as a result of redox processes, reducing the soluble sulphate and increasing alkalinity of the porewater.

7.2.6 Summary

Figure 36 presents a schematic cross section summarising the overall solute concentrations in the surface water-hyporheic zone and groundwater system observed at site D01. The main conclusions from this study are: a limited HEF at the time scale of our monitoring (6 to 9 hours) was recognised on the basis of a clear difference in conservative Cl concentrations between SW and HZ zones. The sediment porewater had a complex Cl concentration pattern. It is difficult to infer unequivocally the source of Cl and possible flow path directions determining the observed element gradients with the present data.

In contrast to a high SO_4 (median 147 mg/l) in SW at the time of sampling, the SO_4 measured in the sediment porewater was low (median 15.8 mg/l). On the basis of the available evidence, it is suggested a low porewater SO_4, as a result of attenuation by redox processes in the shallower soft organic–rich streambed. Near the river bank, at depth of ~ 1 m, a distinct high SO_4-high Fe plume was detected. On the basis of the similarities in SO_4 composition with Foumarts Lane borehole a connection with the GW cannot be excluded. However, due to the lack of characterisation of a possible contribution from the superficial deposits, it is not possible to unequivocally distinguish the contribution to the HZ make-up of upwelling groundwater from the ML and of a superficial aquifer contribution. This is therefore only a possible hypothesis to test with further sampling.

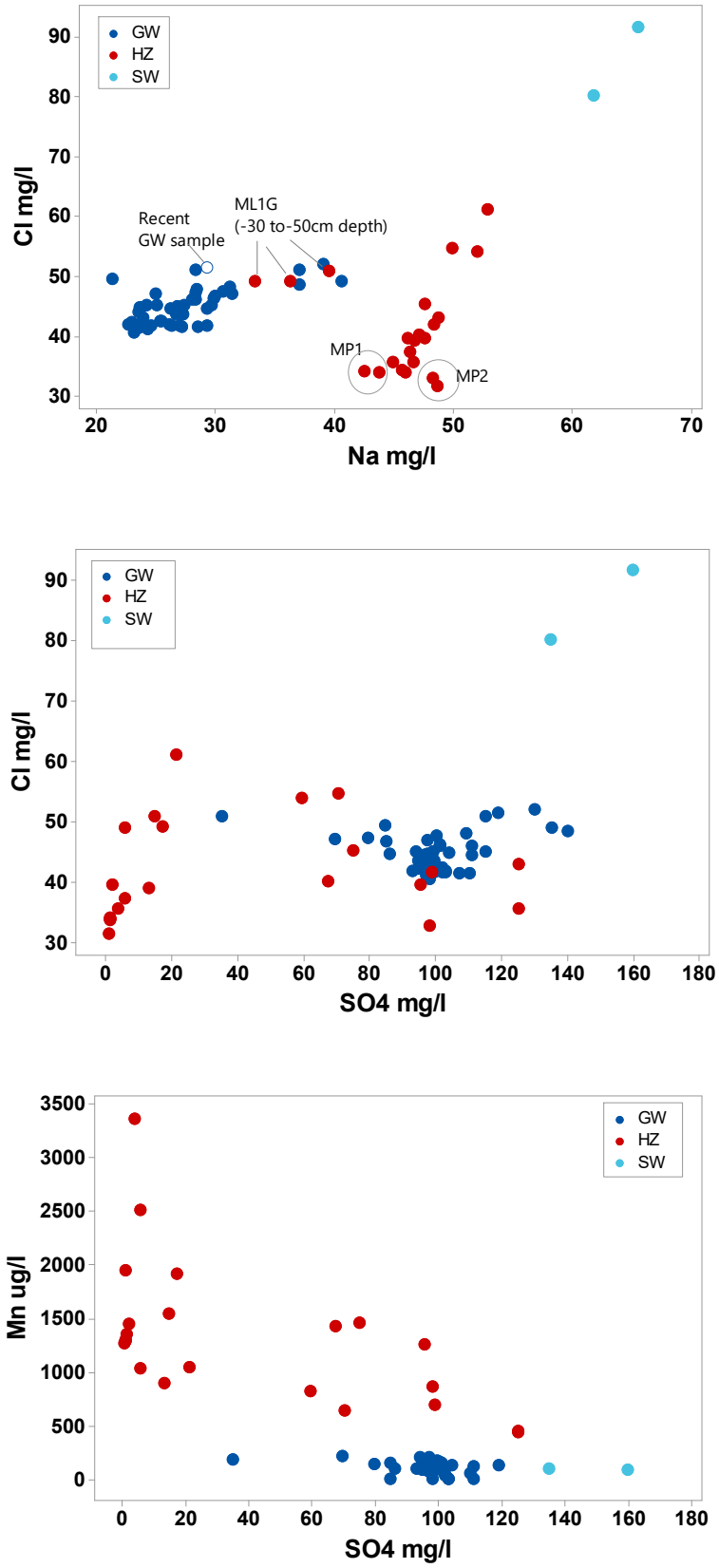

Figure 34: Elemental correlations. Symbols grouped by water type (SW=surface water; HZ= hyporheic zone porewater; GW=Foumarts Lane borehole).

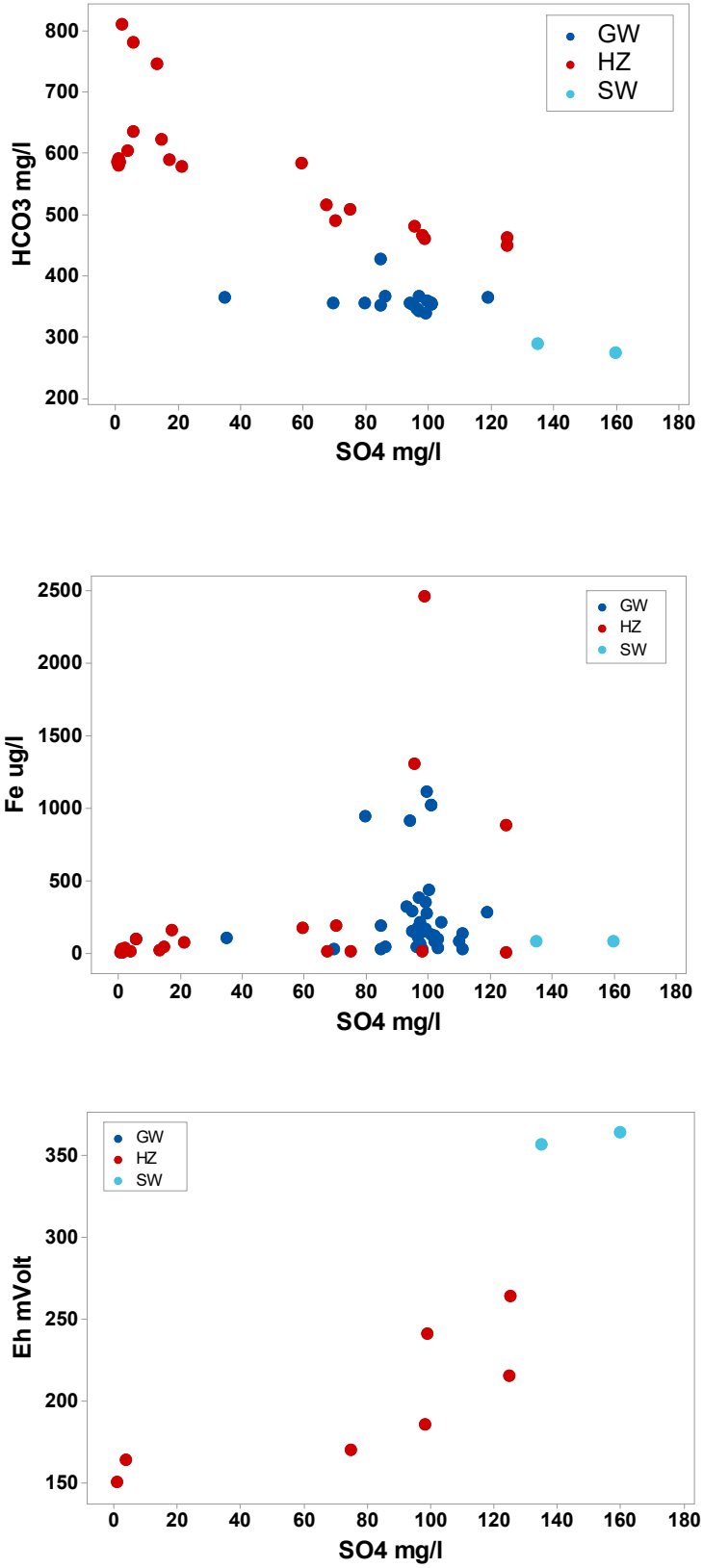

Figure 35: Elemental correlations. Symbols grouped by water type (SW=surface water; HZ= hyporheic zone porewater; GW=Foumarts Lane borehole).

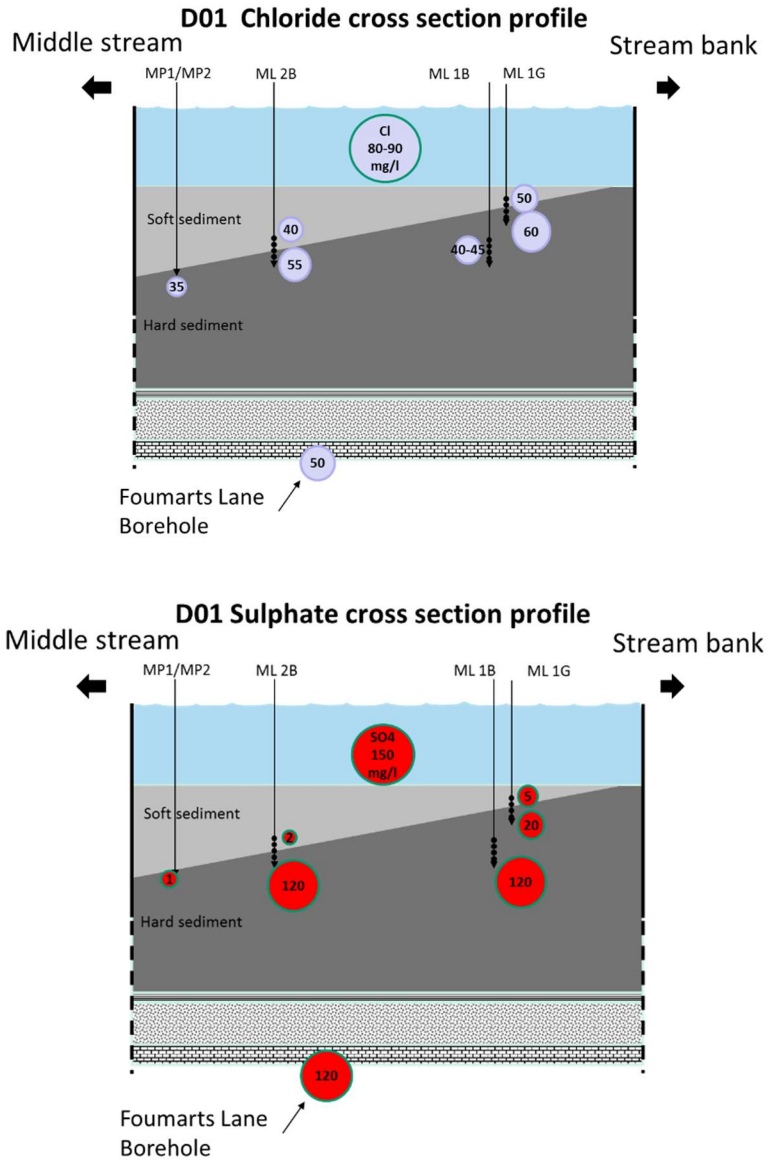

Figure 36: Schematic cross section summarising the overall concentrations of Cl and SO_4 observed at site D01.

7.3 SITE WOODHAM BURN (WB)

7.3.1 Monitoring set-up

The geomorphological, geological and hydrogeological settings have been described in section 2.

The study reaches of the Woodham Burn are shown in Figure 37 alongside the plans of the monitoring installations. The WB 2 and WB 3 sites have a poorly sorted gravel—sand grain size riverbed.

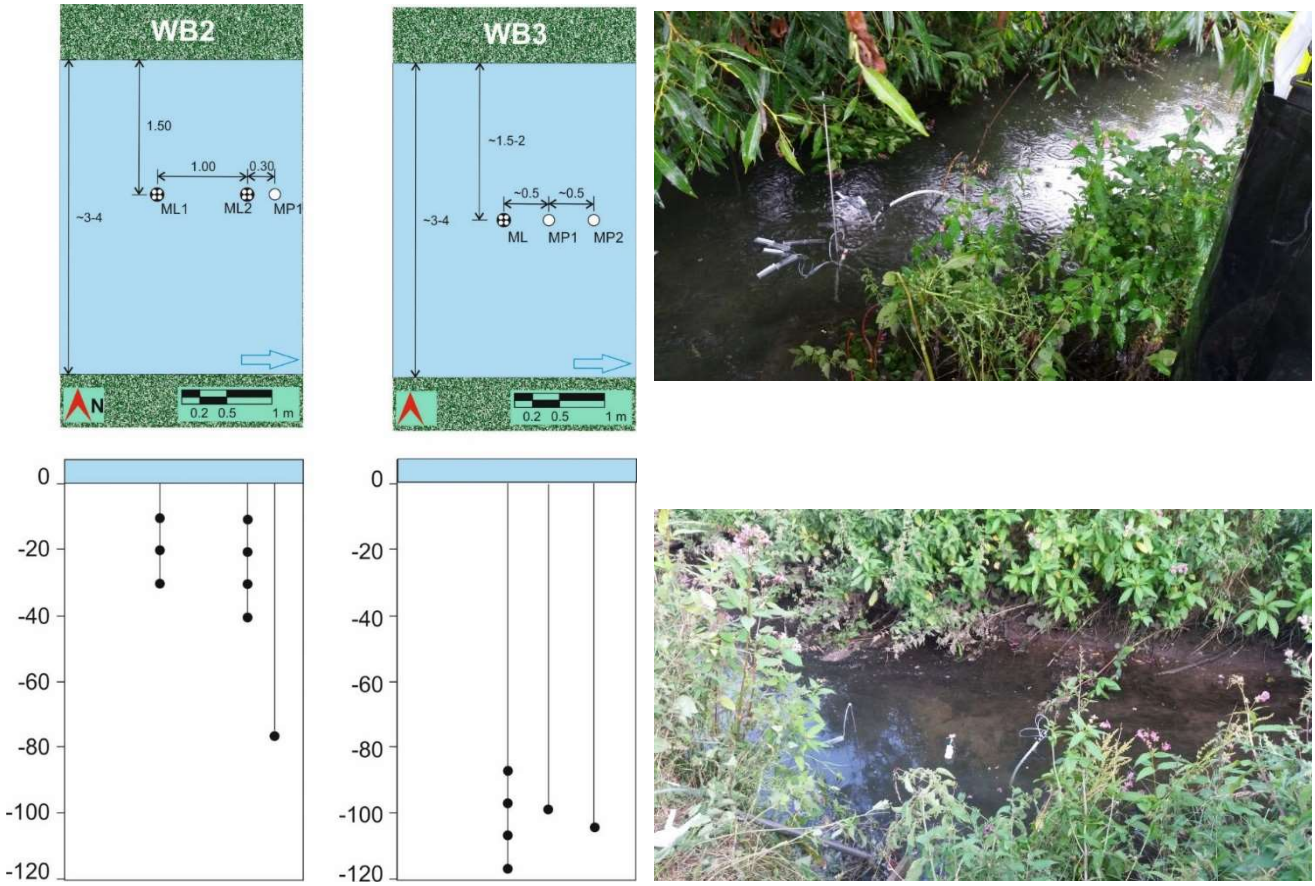

Figure 37: Photos of WB 2 (top) and WB 3 (bottom) sampling locations in the Woodham Burn and outline of monitoring installations.

7.3.2 Field parameters at WB

The distribution of the field parameters of temperature, redox, dissolved oxygen (DO), conductivity and pH at site WB are reported in Figure 38. Temperature in SW ranges from 11.8 to 13.5 °C (median 12.7 °C), while it has a wider range of distribution in the HZ, between 12.9 and 20.3 °C (median 14.5 °C), with some of the temperatures much higher than in SW. Eh distribution is significantly different between the SW and the HZ, with higher values around a median of 348 mV in SW and lower values around a median of 163 mV in the HZ. Similarly, the DO median in the SW (7.6 mg/l) is much higher than the median value in the HZ of 2.3

mg/l. Median values of pH in the SW and HZ were respectively 7.2 and 6.9, while conductivity median values were 1670 uS/cm in the SW and 1350 in the HZ.

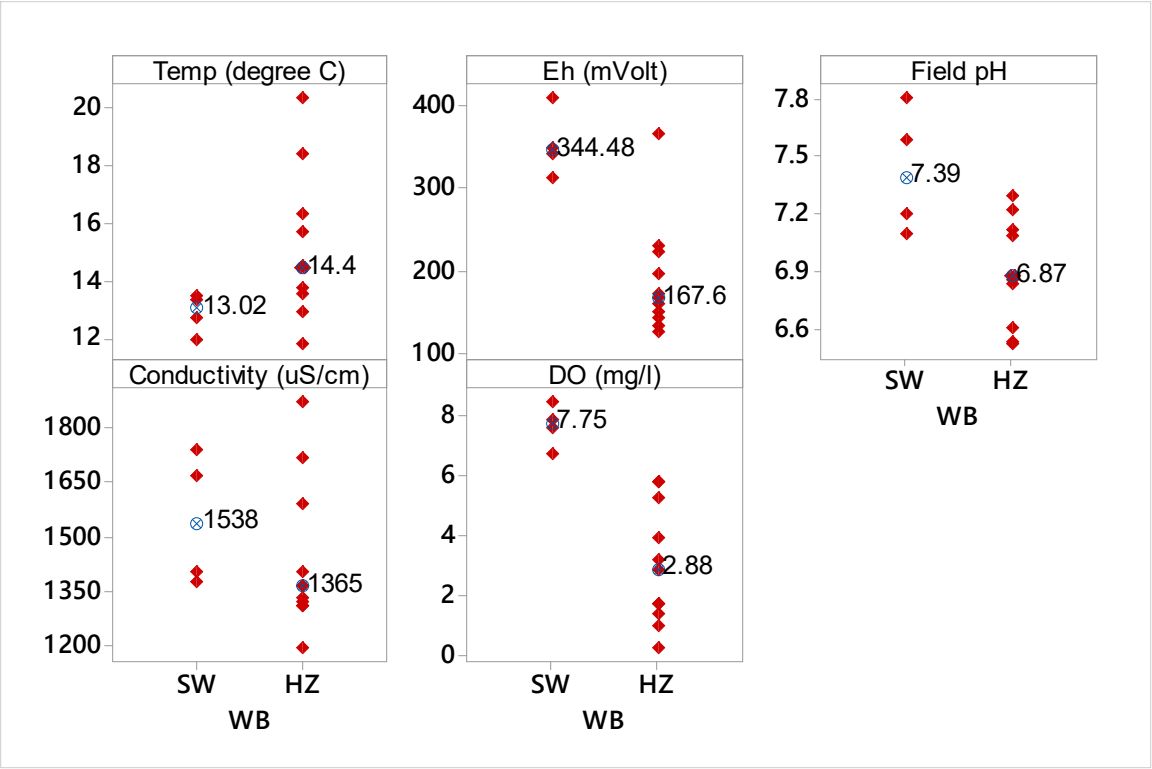

Figure 38: Distribution of field parameters in surface water (SW) and hyporheic porewater (HZ) at site WB. Median values indicated by open blue circles.

7.3.3 Chloride depth profile

Figure 39 shows the Cl distribution in water samples across sediment depth and by sampling location (WB 2 and WB 3) compared to SW. At WB 2, SW Cl concentration was 55–57 mg/l at the time of sampling and a decreasing Cl concentration trend with depth up to -40 cm was visible (Cl ~ 25 mg/l). The deeper port (-75 cm depth) showed a low Cl concentration of 25 mg/l. At WB 3 all piezometer ports had higher Cl concentrations (66–72 mg/l) than WB 2 at equivalent sediment depth and close to the SW concentrations of Cl 65–66 mg/l.

7.3.4 Chloride depth profile interpretation

Assuming the conservative nature of chloride, it is possible to infer HEF of the stream water within the first 30 cm of the riverbed at WB 2. The extent of SW mixing with low Cl porewater decreased with depth. At site WB 3, the shallow sediment depth was not monitored, but the Cl composition of the lower bed (-85 and -115 cm depth) similar to SW could be due to a high HEF. Equally, the observed porewater Cl composition could be the result of a lateral or upwelling water inflow with Cl concentration the same as SW. Further monitoring of the shallow sediment to complete the depth profile would help to validate the hypothesis.

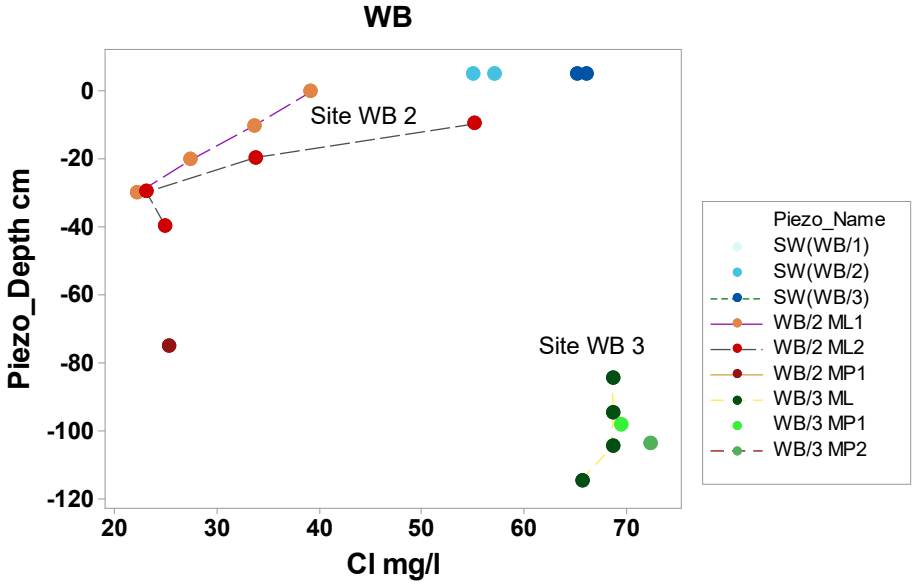

Figure 39: Depth profiles of chloride concentrations. Symbols grouped by piezometer.

7.3.5 Reactive solutes

Figure 40, Figure 41 and Figure 42 show the SW and HZ porewater vertical gradients measured in the streambed in the Woodham Burn at site WB 2 and WB 3 for NO_3, Mn, Fe, and SO_4.

At WB 2, N-NO_3 ranged from 0.1 to 1.0 mg/l, with lower concentrations compared to the SW (0.7 and 0.8 mg/l). The deepest sample at -75 cm depth had a concentration of 0.1 mg/l N-NO_3. At WB 3, the N-NO_3 concentration range was much wider than in the SW, with values both higher and lower than SW (1–1.15 mg/l); N-NO_3 decreased with depth from 1.2 to 0.5 mg/l to increase again at a depth of -120 cm with a value of 1.85 mg/l.

SW was low in Mn with median values 58.9 and 54.4 µg/l, and Fe 25.5 and 58.5 µg/l, respectively, at both WB2 and WB3. At WB2 HZ profiles of both Fe and Mn showed high peaks. For Mn, it was an increasing trend with depth up to -40 cm with values of 2650 µg/l, to return to a lower value of 765 µg/l at greater depth. Fe concentration was relatively low above -20 cm depth, and it peaked, similarly to Mn, at -20 to -40 cm with concentrations up to 19000 µg/l, returning to very low concentrations (10 µg/l) at depth. At site 3, Mn and Fe concentrations in the riverbed remained lower than WB2. Mn concentrations ranged from high values of 1600 to 1000 µg/l in ML in the monitored sediment depth -85 to -115 cm. In contrast, a low concentration of 56 µg/l Mn was measured at one of the minidrive points, at a similar sediment depth. Fe concentrations decreased from 960 to 24 µg/l to increase again to 1850 µg/l at depth.

Consistent with the Cl patterns, at location WB 2, a decreasing SO_4 concentration trend with depth was measured. It is possible to distinguish, from top to bottom, a shallow zone (-10 to -20 cm) with values closer to SW, an intermediate zone (-50 to -20 cm) with a range of SO_4 285-320 mg/l and a relatively low SO_4 zone (105 mg/l) at depth > -50 cm. At WB 3 the HZ SO_4 values (250-340 mg/l) were equal to or only slightly lower than the SW (325 mg/l). The vertical profile from ML indicates a slight increase with depth. However, caution is needed as

the presence of litter (plastic sheet) buried at depth at the site might have altered the natural flow, creating a very specific niche, limited to that location.

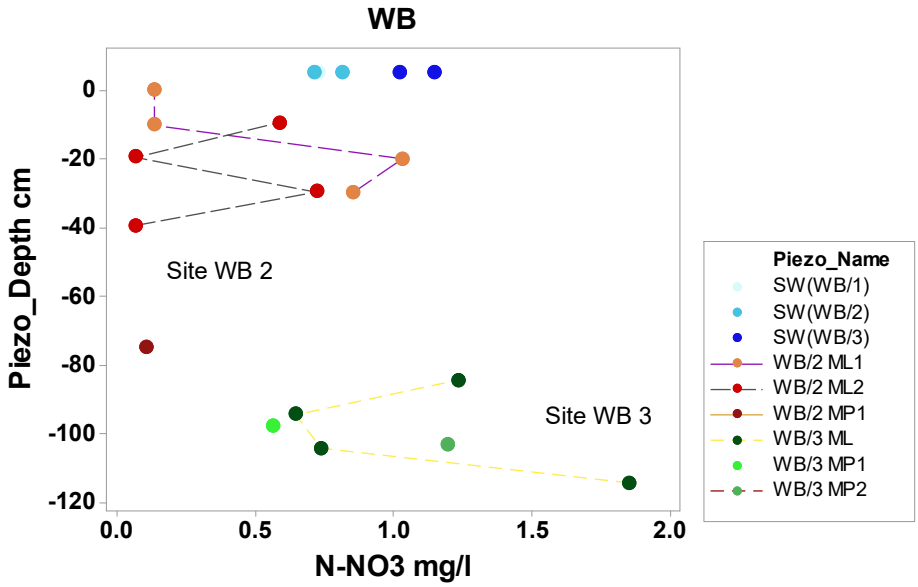

Figure 40: Depth profiles of N as nitrate (N-NO_3) concentrations. Symbols grouped by piezometer.

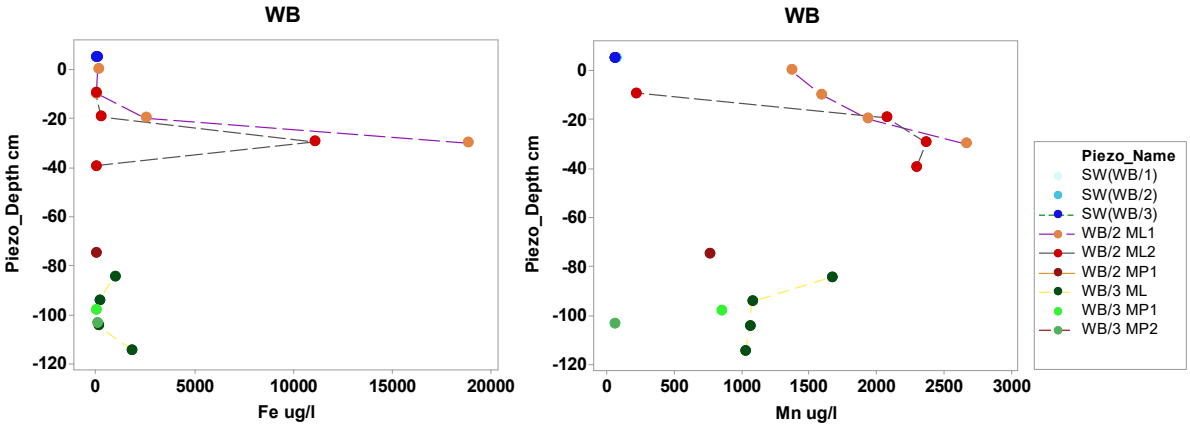

Figure 41: Depth profiles of manganese (Mn) and iron (Fe) concentrations. Symbols grouped by piezometer.

7.3.6 Redox control on reactive solutes

Elemental correlations are better seen grouped by site (Figure 43). While for WB 3 SO_4–Cl concentrations were not correlated, it is noticeable that linear correlations between SO_4–Cl and Na–Cl were evident for site WB 2, with SW and HZ sample points aligned, except for the deep sample. This supports the interpretation from the Cl gradients of mixing of SW in the shallow porewater at the site. The correlation of Cl with SO_4 indicated a conservative behaviour of sulphate in the shallow streambed. At depth pore water SO_4 is lower than in the upper sediment, but remains relatively high of 100 mg/l. It is not possible to interpret the data at depth in terms of reduction mechanisms as field parameters Eh, DO could not be measured due to the low sample volume obtained at this site. More data are needed to understand the processes at depth

in the area of WB 2. At WB 3, the high SO_4 and correspondingly high DO values of the porewater suggest the system did not have a SO_4 reducing capacity.

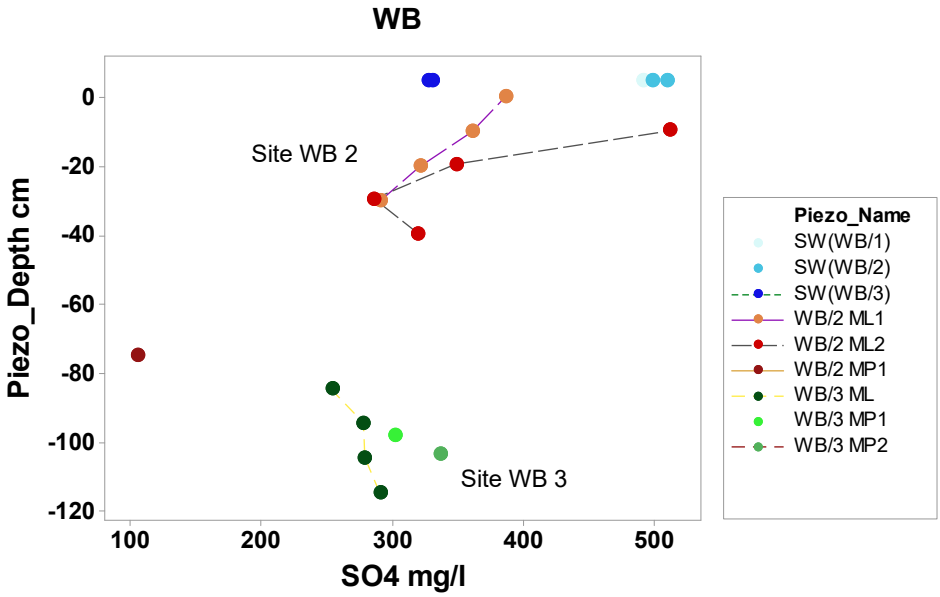

Figure 42: Depth profiles of sulphate (SO_4) concentrations. Symbols grouped by piezometer.

7.3.7 Summary

Figure 44 presents a schematic cross section summarising the overall solute concentrations observed at sites WB 2 and WB 3. HEF of the stream water with the first 30 cm of the riverbed at WB 2 is inferred. The extent of SW mixing with low Cl -porewater decreased with depth. The composition of the deeper GW-dominated hyporheic zone, as compared with the shallow SW-dominated HZ, has a low Cl, distinctively different from Low Copelaw borehole. Further sampling is necessary to confirm these patterns and characterise the groundwater.

SO_4 behaved conservatively with slightly attenuated concentrations in the hyporheic zone as a result of mixing of SO_4 rich SW with moderately less enriched groundwater. However, at greater depth (-80 cm) SO_4 reduced significantly to 100 mg/l. It is not possible to interpret the SO_4 data at depth in terms of reduction mechanisms as field parameters such as Eh, DO are not available. More data are needed to understand the processes at depth at WB 2.

At site WB 3, the shallow sediment depth was not monitored, but the Cl composition of the lower bed (-85; -115 cm depth) similar to SW could be due to a high HEF. Equally, the observed porewater Cl composition could be the result of a lateral or upwelling water inflow with Cl concentrations similar to SW. Further monitoring of the shallow sediment to complete the depth profile would help to validate one of the hypotheses. The HZ SO_4 is similar in concentrations to site WB 2 at a depth of -20 to -40 cm. The high SO_4 and corresponding relatively high DO values of porewater suggest the system did not have a strong reducing capacity.

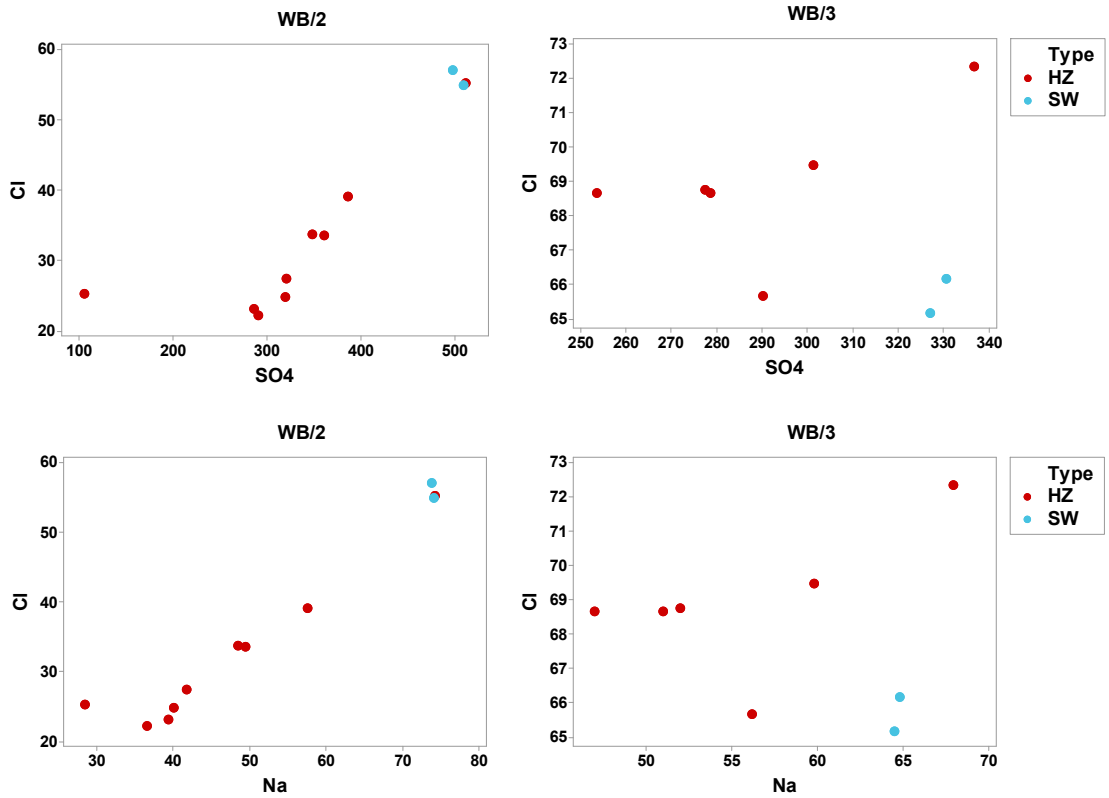

Figure 43: Elemental correlations.

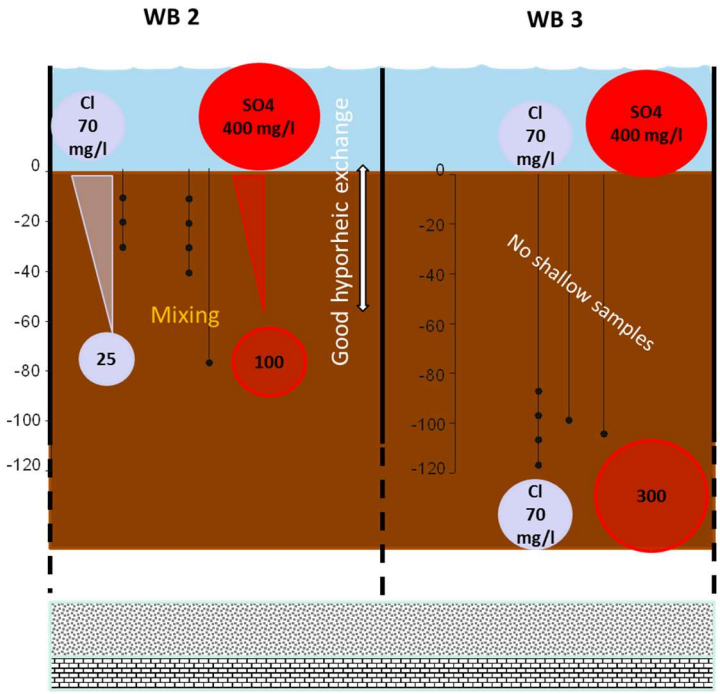

Figure 44: Schematic cross section summarising the overall solute concentrations observed at site WB2 and WB3.

7.4 SITE RUSHYFORD BECK (RB)

7.4.1 Monitoring set-up

The geomorphological, geological and hydrogeological settings have been described in section 2.

The study reach of the Rushyford Beck is shown in Figure 45 alongside the plans of the monitoring installations. The site has a fine sand-silt-clay riverbed.

7.4.2 Field parameters at RB

One multilevel piezometer was inserted in the riverbed to sample water over a 10 cm interval from a depth of -50 to -80 cm. The distribution of the field parameters of temperature, redox, dissolved oxygen (DO), conductivity and pH at site RB are reported in Figure 46. Temperature in the HZ ranged from 16.5 °C to 17.7 °C with a median of 17.5 °C, lower than the SW value of 18.6 °C. Eh in the HZ had a range 110-150 mV (median 122 mV), lower than the SW Eh of 290 mV. Field pH ranged from 6.8 to 7.0 (median 6.9) in the HZ and was 7.3 in SW. HZ conductivity had a narrow range of values between 1140–1200 uS/cm and higher than SW 820 µS/cm. DO was 5.19 mg/l in SW and lower with a range 1.74 – 3.32 mg/l in the HZ.

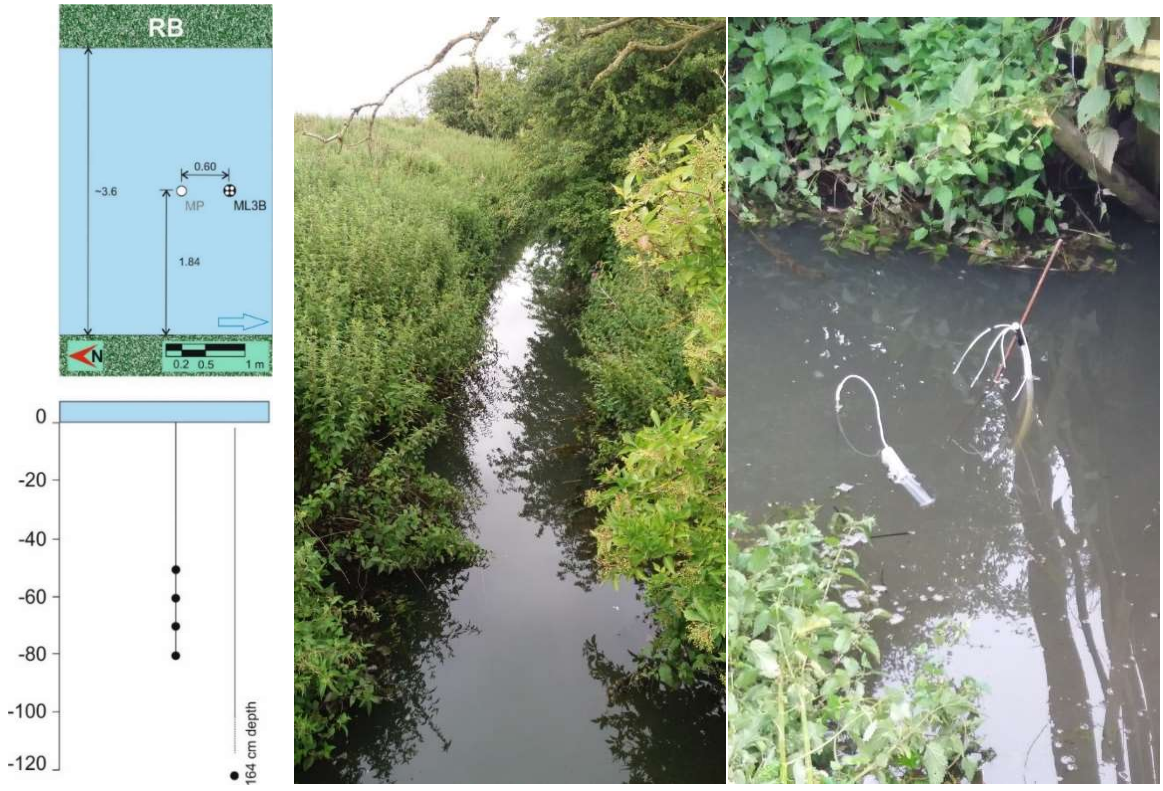

Figure 45: photos of RB sampling location in the Rushyford Beck and outline of monitoring installations.

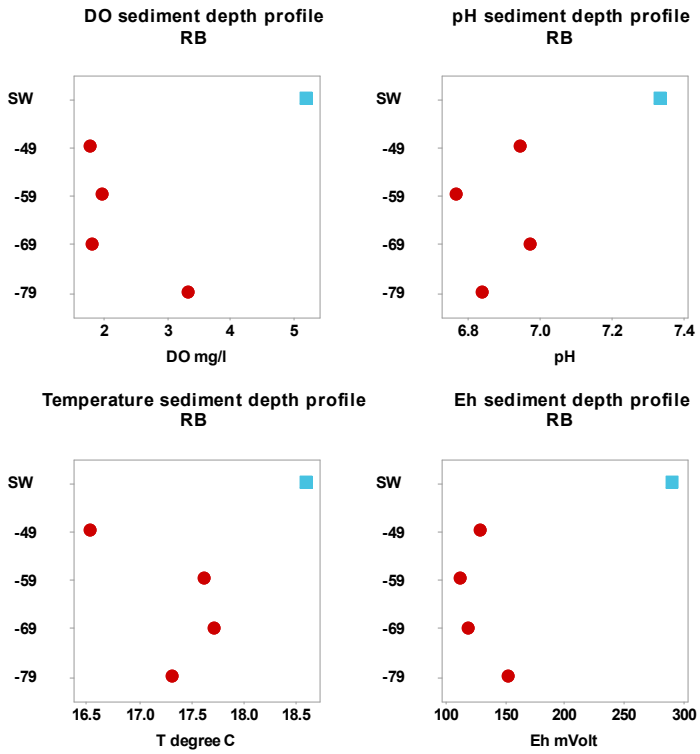

Figure 46: Depth profiles of field parameters at site RB.

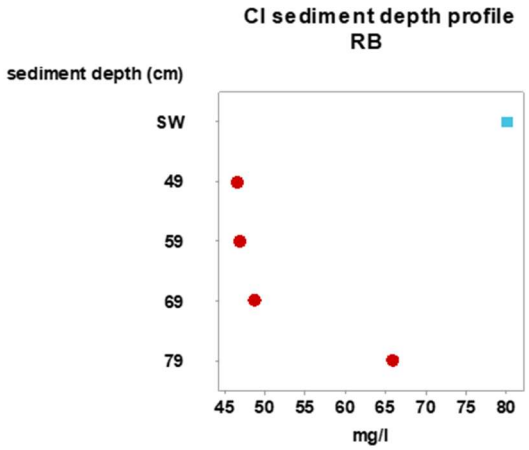

Figure 47: Depth profiles of Cl concentrations at site RB.

7.4.3 RB Hydrochemistry

Figure 47 shows the depth profile for Cl captured by the multilevel piezometer monitoring a sediment depth of -50 to -110 cm. SW Cl was 80 mg/l. At the first piezometer port at depth of -50 cm Cl was much lower (46 mg/l) than in the SW and remained low down to -70 cm, it then increased at -80 cm depth to 66 mg/l. The same trend was observed for SO_4, i.e. lower SO_4 concentrations in the HZ (~ 70 mg/l) than the SW (88 mg/l), but with a noticeable increase at depth of -80 cm when SO_4 was 116 mg/l, higher than SW. HZ N-NO_3 was lower than the SW 10.5 mg/l, with values below 1.7 mg/l throughout the monitored depth until the lowest point,

when it increased to 3.4 mg/l. Both Mn and Fe were much higher in the HZ (median 1194 ug/l and 7852 ug/l) than SW (35 ug/l and 102 ug/l, respectively) (Figure 48).

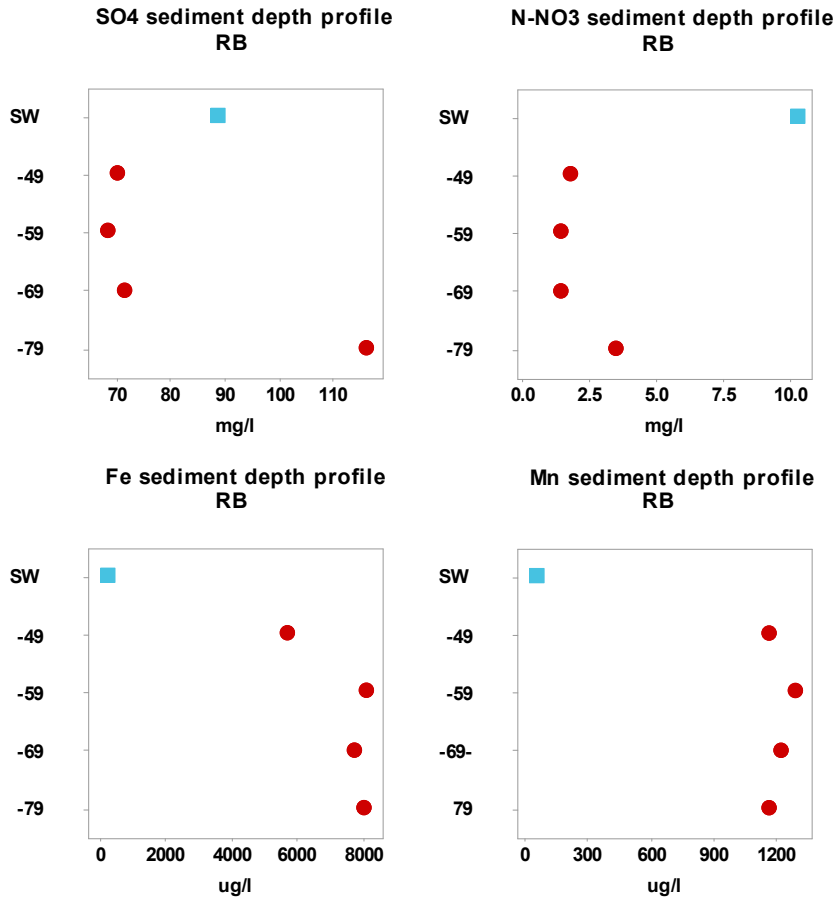

Figure 48: Depth profiles of SO_4, N-NO_3, Fe, Mn at site RB.

7.4.4 Summary

The streambed at the sampling depth of 50 cm to 80 cm below the surface water-sediment interface is close to suboxic conditions and low Eh. Its porewater composition is distinct from the SW and enriched in Fe, Mn, while low in N-NO_3 (for absolute values refer to table and graph Appendix 6), in accordance with the redox conditions. SO_4 is slightly depleted in porewater compared to SW, but not for all samples. The noticeable increase in SO_4 at 79 cm, corresponding to Cl, NO_3, DO increase, although not to the same extent, suggests a potential inflow of water with a different composition.

7.5 SITE AY

7.5.1 Monitoring set-up

The geomorphological, geological and hydrogeological settings have been described in section 2. The study reach of the Skerne is shown in Figure 49 alongside the plans of the monitoring installations. The AY site has a gravelly coarse sand riverbed.

Figure 49: Photos of AY sampling location in the Skerne and outline of monitoring installations.

7.5.2 Field parameters at AY

The distribution of the field parameters of temperature, redox, dissolved oxygen (DO), conductivity and pH are reported in Figure 50.

HZ temperature had a wider distribution range than SW, between 15 °C and 18 °C, and was generally higher than the SW temperature of 14.6-15.6 °C. HZ and SW Eh measurements were similarly distributed with a narrow range between 370 and 410 mV, with only one SW outlier at the relatively lower value of 310 mV. DO values ranged between 2.6–5.6 mg/l in the HZ and were lower than the SW ones (8.6 mg/l). HZ pH ranged from 7.3 to 7.8 with the highest values close to SW pH. On the contrary, HZ conductivity mostly clustered around 1100 µS/cm with two low outliers closer to the SW conductivity of 1040 µS/cm (mean value).

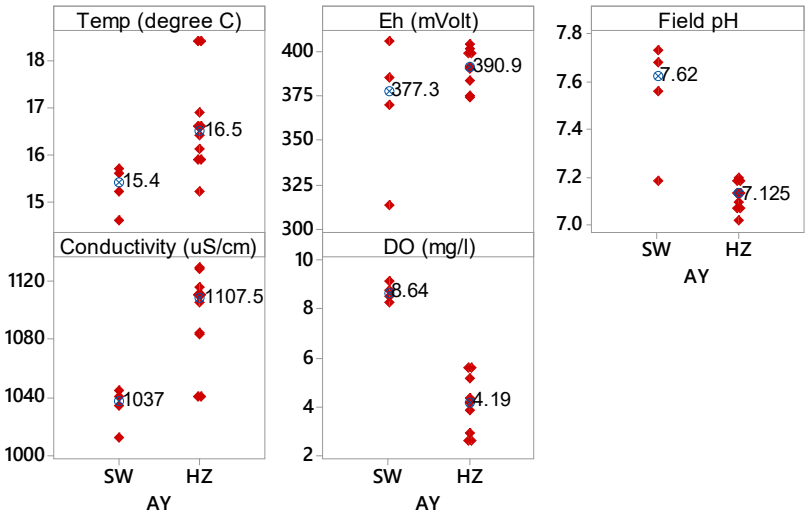

Figure 50: Distribution of field parameters in surface water (SW) and hyporheic porewater (HZ) at site AY. Median values indicated by open blue circles.

7.5.3 Chloride depth profile

Figure 51 shows the Cl depth profiles for all of the piezometers installed at site AY. Cl in most of the HZ samples was similar in concentrations to the SW values. Only one of the multilevel piezometers (ML4R) captured a decreasing trend from SW to a depth of -30 cm. Piezometer ML2G showed slightly higher Cl concentrations than SW. It was located closer to the banks compared to the ML4R (Figure 49). Given the weak or absent Cl vertical gradients, which could be due to similar Cl concentrations of SW and GW, other conservative elements like Br and Na, were used to infer potential HEF (Figure 52, Figure 53). They suggest a mixing zone limited to the first 10 cm for the piezometers ML2G closer to the banks, while a deeper HEF up to a depth of -30 cm for ML4R, placed in the middle of the stream. The extent of mixing decreased with depth, with a GW dominated zone at depth of -45 cm. Ketton Hall borehole Cl had similar value to the deep porewater concentrations, but not Br or Na.

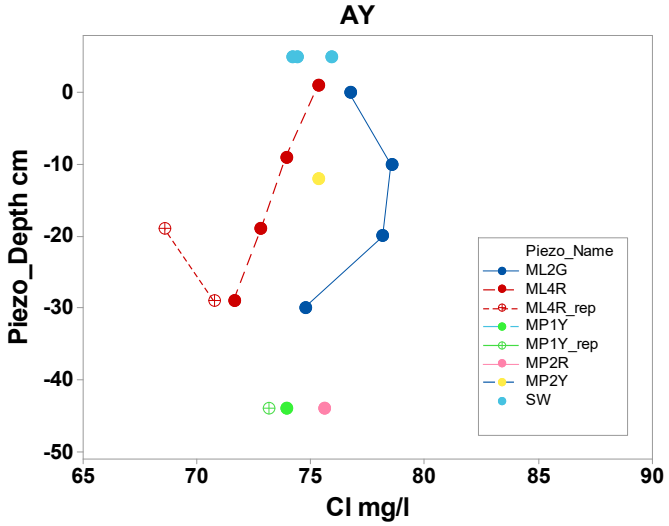

Figure 51: Depth profiles of chloride concentrations. Symbols grouped by piezometer.

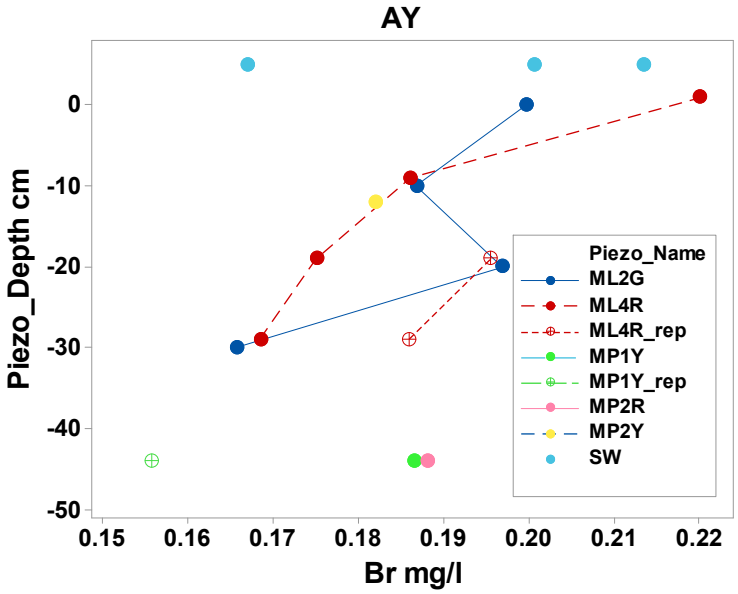

Figure 52: Depth profiles of Br concentrations. Symbols grouped by piezometer.

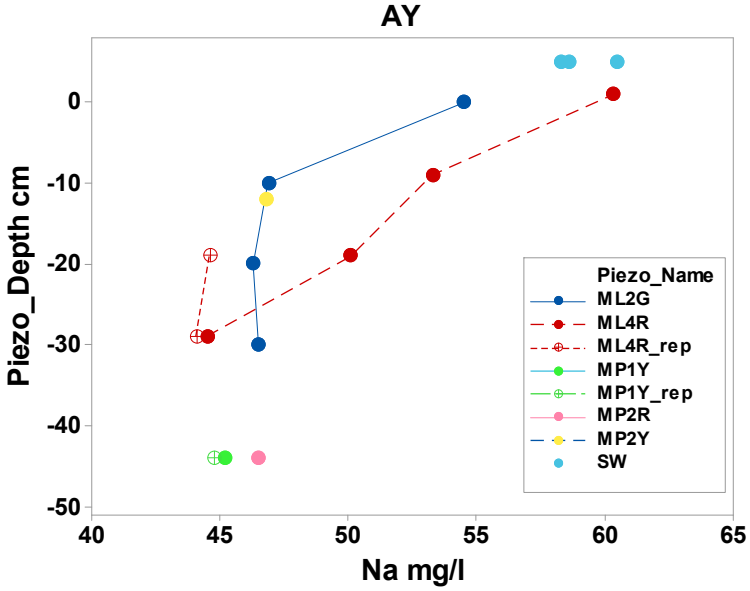

Figure 53: Depth profiles of Na concentrations. Symbols grouped by piezometer.

7.5.4 Reactive solutes

Figure 54 and Figure 55 show the SW and HZ porewater vertical gradients measured in the streambed at site AY for SO_4, N-NO_3, Mn, Fe.

SO_4 distribution through the riverbed showed a decreasing trend in the first -10 to -30 cm depth (depending on the piezometer), from a SW of 157–170 mg/l to 60–75 mg/l. It then remained constant. Ketton Hall borehole SO_4 had similar value to the deep porewater concentrations.

N-NO_3 measurement in SW ranged from 7.3 to 9.1 mg/l, with concentrations very similar to the previous JBA monitoring (7.03–9.5 mg/l). N-NO_3 distribution through the riverbed showed a decreasing trend in the first -10 to -30 cm depth (depending on the piezometer) and then remained constant around 3 to 4 mg/l.

Mn concentration was overall low, but higher (median 134 µg/l) in HZ than SW (10 µg/l). The highest concentrations (380–600 µg/l) were observed at the bottom of the monitored riverbed and at minidrive piezometer MP2Y at shallow depth. Fe was low in SW (median 35 µg/l) and even lower in the HZ (median 14 µg/l).

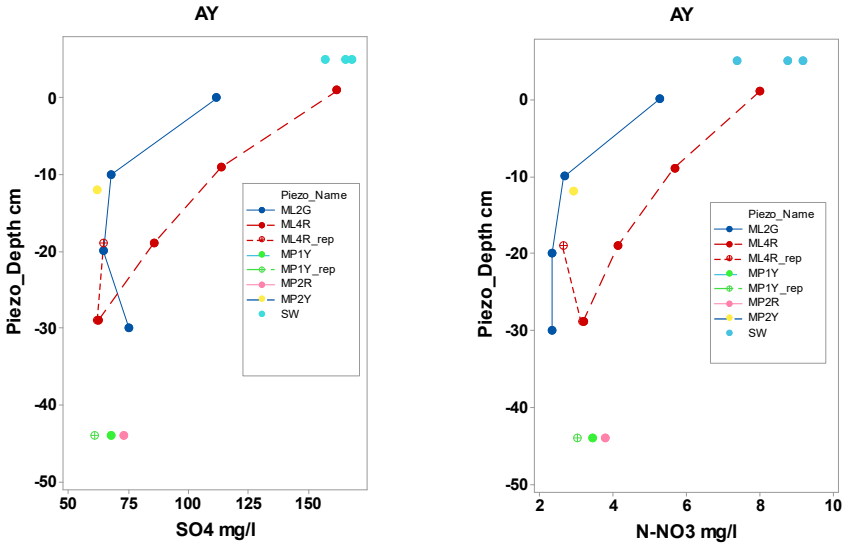

Figure 54: Depth profiles of sulphate (SO_4) and N as nitrate (N-NO_3) concentrations. Symbols grouped by piezometer.

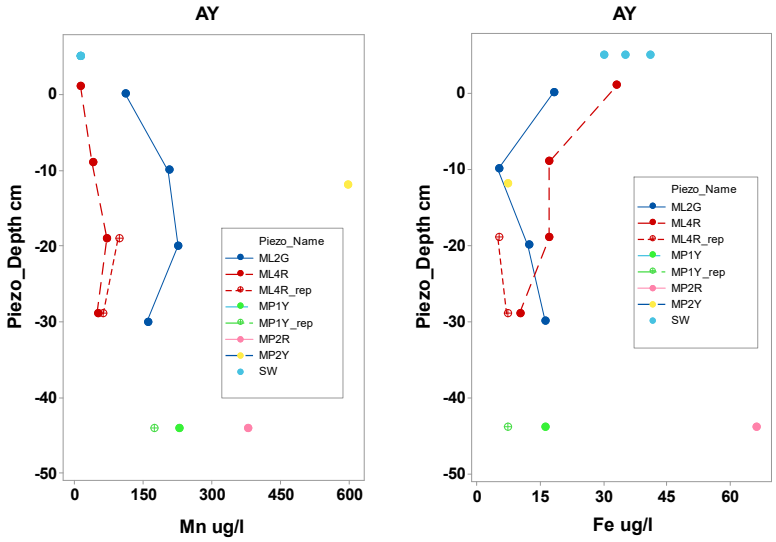

Figure 55: Depth profiles of manganese (Mn) and iron (Fe) concentrations. Symbols grouped by piezometer.

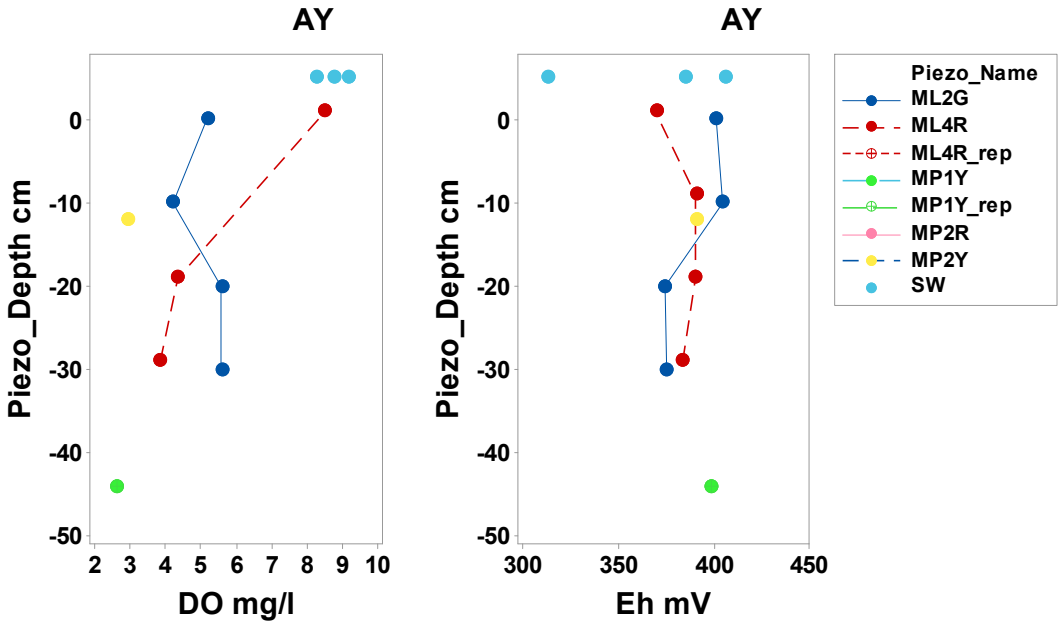

Figure 56: Depth profiles of DO and Eh. Symbols grouped by piezometer.

7.5.5 Summary

The hydrochemical profiles suggest that stream water infiltration extent varies from -10 to -30 cm. The GW dominated deeper zone is poorer in SO_4 compared to the SW. The pore water remains also relatively DO-rich, compared to other sites, which is reflected in relatively high NO_3 concentrations. Fe and Mn concentrations are low.

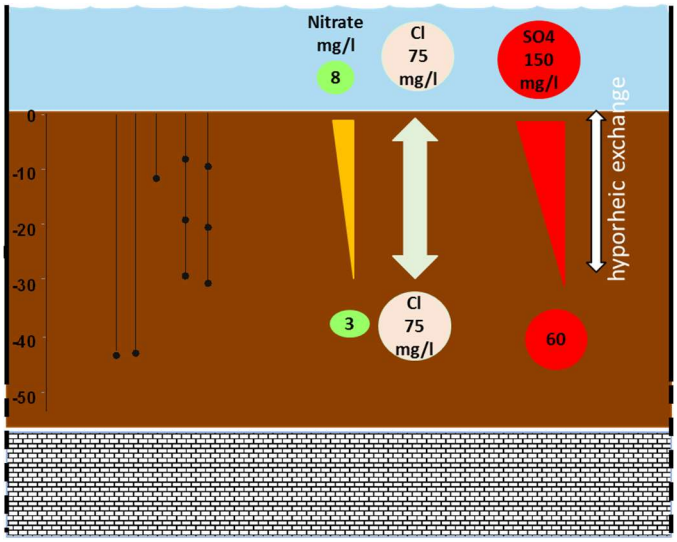

Figure 57: Schematic cross section summarising the overall solute concentrations observed at site AY.

7.6 SITE A02

7.6.1 Monitoring set-up

The geomorphological, geological and hydrogeological settings have been described in section 2. The study reach of the Skerne at site A02 is shown in Figure 58 alongside the plans of the monitoring installations.

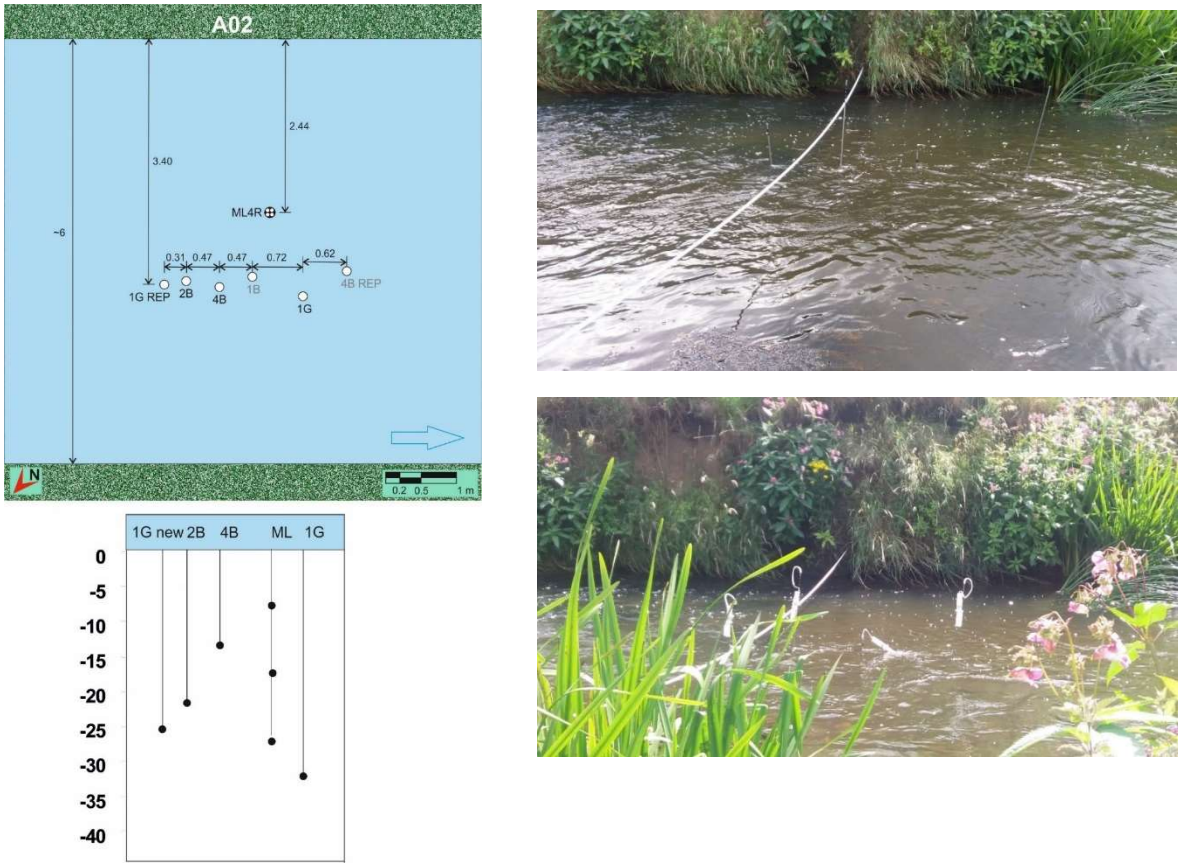

Figure 58: Photos of A02 sampling locations in the Skerne and outline of monitoring installations.

7.6.2 Field parameters at Site A02

The distribution of the field parameters (temperature, redox, dissolved oxygen (DO), conductivity and pH) are reported in Figure 59. HZ temperature distribution covers a wide range between 16 °C and 24 °C, with a number of samples with temperatures noticeably higher than the SW temperature of 17 °C. HZ Eh measurements were not distributed uniformly with two main groups, one at low values of 150 mV and the other at relatively higher values of 350 mV, similar to the SW Eh. A similar bimodal distribution was observed for DO. Some of the DO values clustered around 2 mg/l and lower, while others at 9 mg/l, close to the SW values. HZ pH ranged from 7.3 to 7.8 with the highest values close to SW pH. On the contrary, HZ conductivity had a relatively narrow range around 900 µS/cm and close to the SW conductivity.

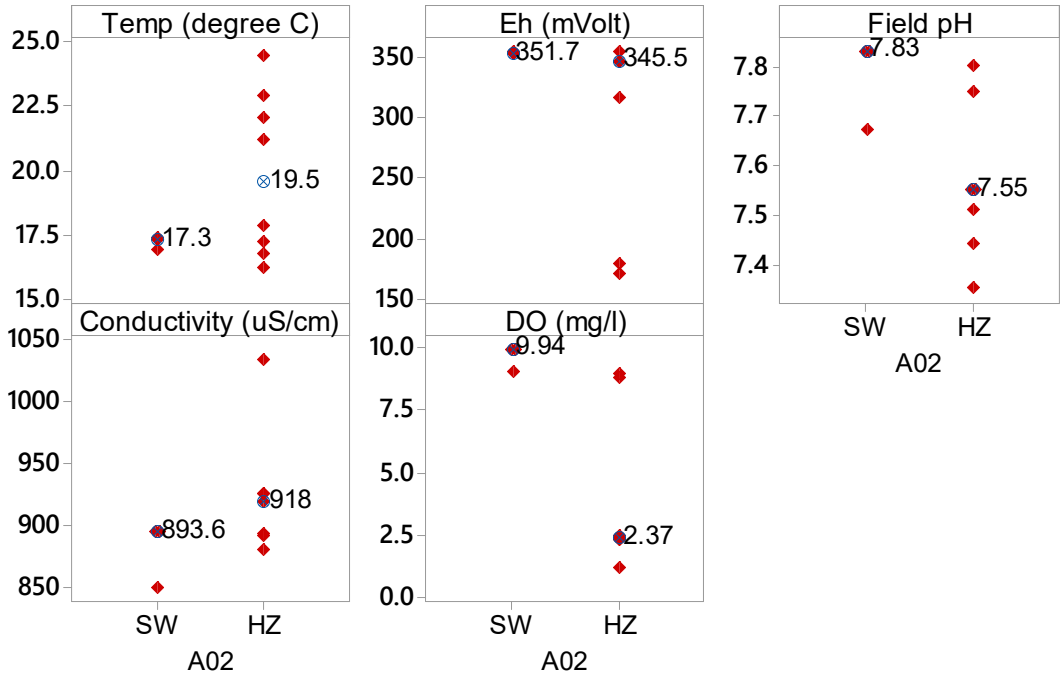

Figure 59: Distribution of field parameters in surface water (SW) and hyporheic porewater (HZ) at site A02. Median values indicated by open blue circles.

7.6.3 Chloride depth profile

Figure 60 shows the Cl depth profiles for all of the piezometers installed at site A02. HZ Cl concentrations remained very similar to the SW (65 mg/l) down to a sediment depth of -20 cm. With depth, an increasing trend was observed, with Cl over 80 mg/l at -35 cm depth. High Cl porewater was drawn by MP1G at ~ -25 cm depth. Assuming the conservative nature of chloride, the first 30 cm of monitored streambed were affected by HEF. The downwelling SW mixed with relatively high Cl waters. The HEF is also confirmed by Na gradients. The Ketton Hall borehole GW Cl falls between the SW and bottom sediment porewater Cl compositions.

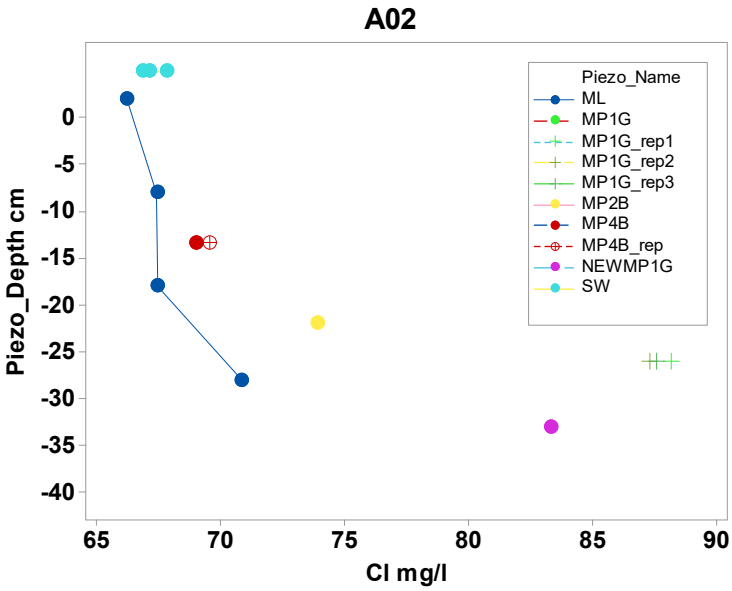

Figure 60: Depth profiles of chloride concentrations at site A02. Symbols grouped by piezometer.

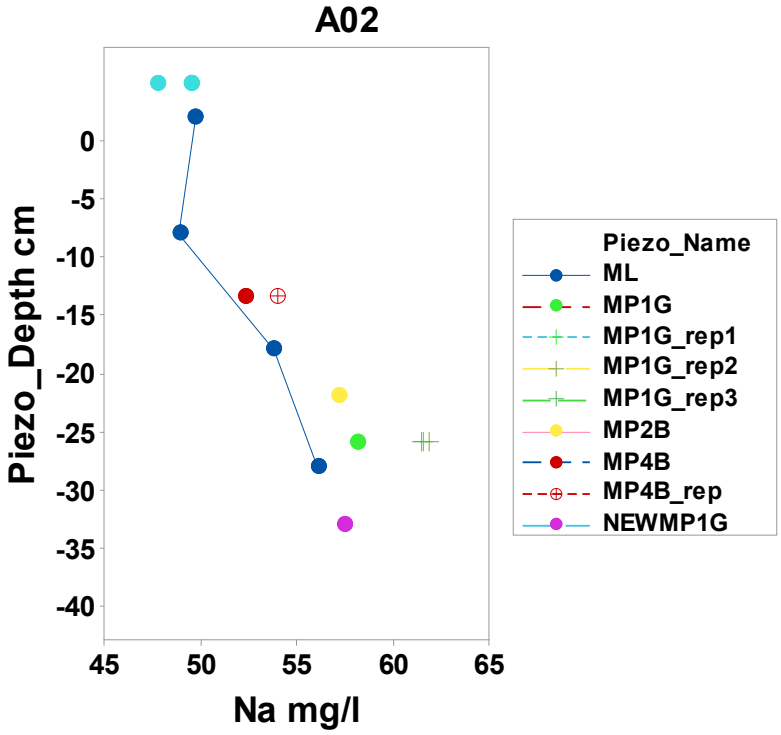

Figure 61: Depth profiles of sodium concentrations at site A02. Symbols grouped by piezometer.

7.6.4 Reactive solutes

Figure 62, Figure 63 and Figure 64 show the SW and HZ porewater vertical gradients measured in the streambed at site A02 for SO_4, N-NO_3, Mn and Fe.

N-NO_3 measurement in the SW ranged between 3.98 and 5.4 mg/l, with concentrations slightly lower than the previous JBA monitoring (7.03 to 9.5 mg/l). The N-NO_3 vertical gradient shows a sharp decrease from 15 cm sediment depth, while concentrations remained similar to the SW in the upper 15 cm of sediment. SO_4 was fairly constant throughout the riverbed (median 115 mg/l) and not dissimilar to the SW (median 106 mg/l). The Ketton Hall borehole SO_4 was much lower. The lack of a vertical gradient, as observed for Cl, suggest a mixing with waters of similar SO_4 concentrations and a conservative behaviour of SO_4. The vertical gradient of Mn in the riverbed mirrored that of N-NO_3, with a sharp increase at depth in correspondence of the decrease of N-NO_3 concentrations. Fe porewater patterns differed from the pattern of Mn distribution with values generally low, except from a very high concentration at -5 cm depth. An increase in Fe concentrations was also observed in the time repetitions of MP1G.

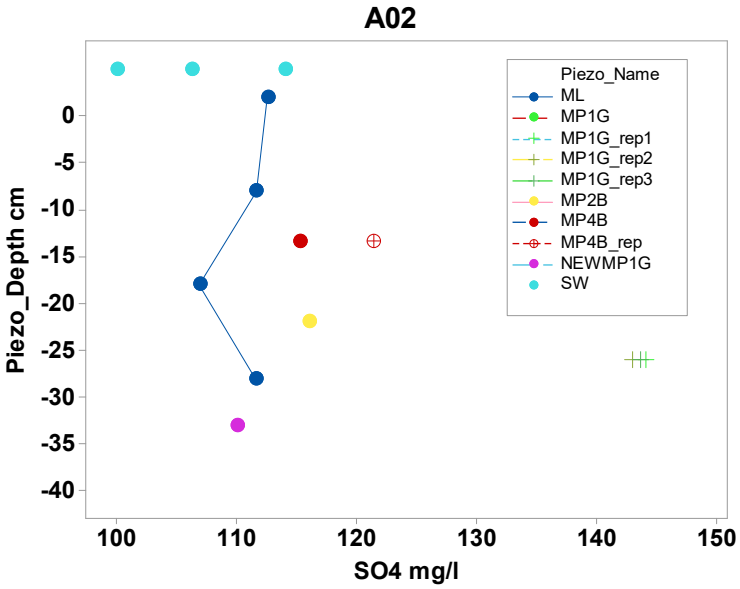

Figure 62: Depth profiles of sulphate (SO_4) concentrations. Symbols grouped by piezometer.

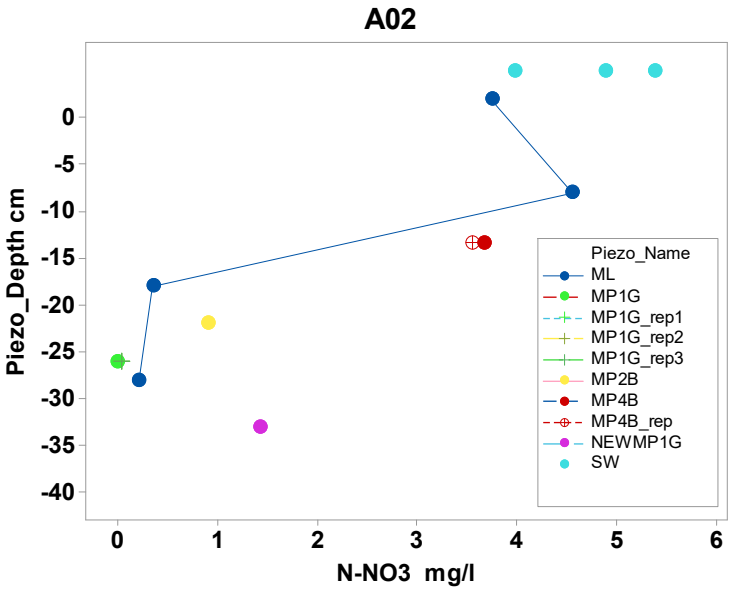

Figure 63: Depth profiles of N as nitrate (N-NO_3) concentrations. Symbols grouped by piezometer.

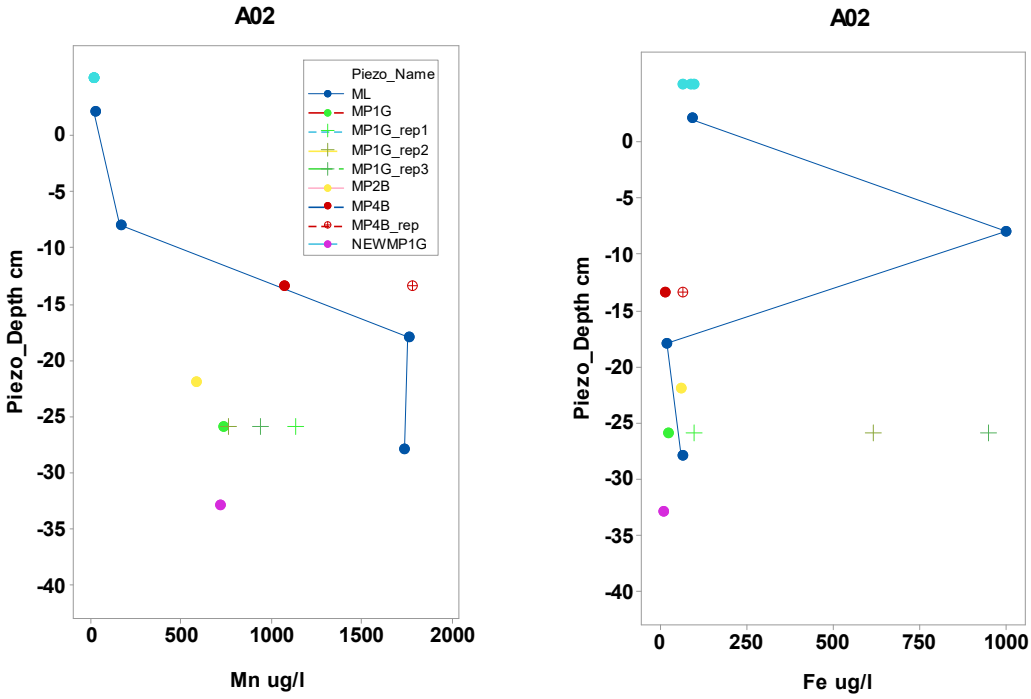

Figure 64: Depth profiles of manganese (Mn) and iron (Fe) concentrations. Symbols grouped by piezometer.

7.6.5 Summary

Figure 65 presents a schematic cross section summarising the overall solute concentrations observed at site A02. The piezometer network delineates the first 30 cm of streambed characterised by high to moderate HEF with SW, decreasing with depth. The SW mixed with relatively higher Cl groundwater defining a vertical gradient increasing with depth. In contrast, the groundwater SO_4 (median 115 mg/l) was not dissimilar to SW (median 106 mg/l) giving a homogeneous concentration profile throughout the riverbed with no evidence of SO_4 attenuation by mixing or redox reduction.

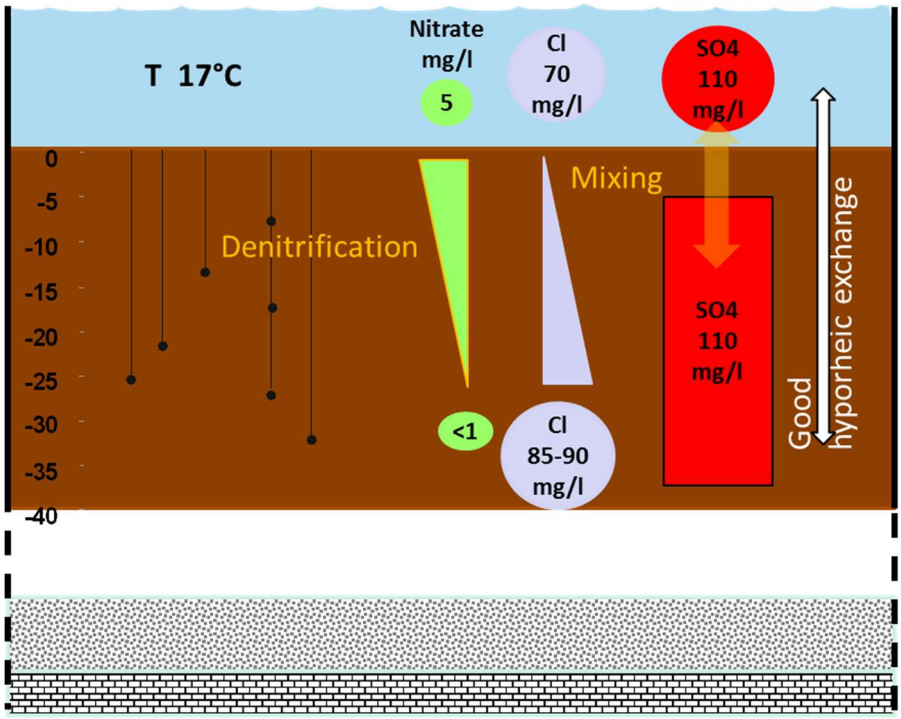

Figure 65: Schematic cross section summarising the overall solute concentrations observed at site A02.

8 Summary, Conclusions and future work

In this study we provide direct measurements of the shallow hyporheic zone composition using a network of multilevel minipiezometers at selected locations in the Skerne catchment and present a broad assessment of the hydrochemical variations of this zone observed within and across the sites. A first pass conceptual ground model of the selected sites was also derived.

The River Skerne is a tributary of the River Tees which flows through County Durham in North East England. Following the closure in 1966 of the Chilton Colliery and in 1974 of the Mainsforth and Fishburn Collieries in the Durham Coalfield Coal Measures to the south of the Butterknowle Fault, the recovery of groundwater levels has caused a sulphate rich mine water plume, from oxidation of pyrite in the abandoned workings, to migrate into the overlying Magnesian Limestone aquifer and moving eastwards. The River Skerne flows across the Magnesian Limestone for almost all of its length with superficial drift thickness (primarily Boulder Clay and Sand and Gravel deposits) significantly varying in thickness across the catchment. In areas of thinner drift deposits groundwater-surface water connectivity is likely, with surface waters either being lost to ground or receiving baseflow. The quality of surface waters is known to have been impacted, via baseflow, by the sulphate-rich water plume. This study aims at contributing to the assessment of the potential contaminant pathways in the hyporheic zone of the Skerne catchment.

The hyporheic zone sampling at the selected sites (5 locations, labelled as D01, WB, RB, AY, A02, each consisting of river stretches of 1 to 5 m long) took place on four occasions in the summer period from June to September 2017. A total of 66 hyporheic porewaters were sampled, field measurements of physico-chemical properties carried out and samples analysed for major, minor and trace element composition.

The hyporheic zone waters are mostly Ca-Mg-HCO_3 types, similar to the Magnesian Limestone groundwaters from the area. The waters are well-buffered with median pH values in the alkaline range (7.9 to 8.0). The hyporheic zone is not fully anoxic, although contains generally low concentrations of dissolved oxygen (median values ranging across the sites from 1.9 to 4.3 mg/l) and has Eh median values ranging from 120 to 390 mV, indicating moderately reducing conditions at the lowest Eh points. The electrical conductivity median values range from 920 to 1350 µS/cm. Hyporheic zone sulphate concentrations have median values ranging from 67 to 115 mg/l at the A02, AY and RB sites, while the D01 site and WB sites have, respectively, the lowest median (16 mg/l) and highest median (301 mg/l) concentrations observed. For reference, the latter value is above the maximum value of 250 mg/l permissible in drinking waters regulations. The range of nitrate-nitrogen (N-NO_3) median concentrations across the sites is 0.07–3.15 mg/l, with most of the sites having a median lower than 0.7 mg/l (well below the drinking water limit of 11 mg/l as N-NO_3). Two of the sites, A02 and RB, show relatively high total phosphorus (total P) median values of 0.2 and 0.8 mg/l with the remaining sites lower than 0.08 mg/l.

The hydrochemistry of the hyporheic zone is variable and we were able to distinguish three hydrochemical facies, on the basis of the hierarchical clustering of observations: one cluster is represented by the north west tributary of the Skerne at Foumarts Lane (D01), characterised by the lowest hyporheic zone sulphate concentrations; a second group of samples clustered around the Woodham Burn and Rushyford Beck tributaries, with distinctively high iron concentrations; a third one grouped together sites A02 and AY located in the River Skerne towards the base of the catchment and was characterised by the highest chloride and lowest iron contents.

On the basis of the vertical hydrochemical gradient observed in the hyporheic zone we estimated the hyporheic exchange flow (HEF) (Table 8). The extent of downwelling surface water in the hyporheic zone varied, and was the largest at sites AY and A02 and smallest at D01. A coarser sediment texture at AY and A02 compared to fine sediment texture at D01 might explain the variable HEF, as grain size distribution strongly governs sediment permeability and flow exchange (i.e. coarser sediment equates to higher permeability).

Hyporheic exchange is of particular importance to the chemical mass balance of a river catchment and it has been extensively shown in past studies that contaminant cycling at the groundwater-surface water interface can modify, attenuate or retard the flux of groundwater pollutants discharging into the river and vice versa. The attenuation processes at each study site are summarised in Table 8. The implication of surface-subsurface exchange for the biogeochemistry of the hyporheic zone and resulting attenuation potential of contaminants such as nitrate and sulphate is shown at site D01, where the most reducing redox level for sulphate-reduction is attained in the organic-rich silty sediments. Limited recharge rates due to low sediment permeability and higher microbial abundances recognised in fine hyporheic sediments is known to result in sub-oxic or anoxic conditions, causing the disappearance of any sulphate from porewater by reduction to sulphide and increase in alkalinity. The sulphate reducing redox level is not reached, however, at the other sites, which show low attenuation potential for sulphate. Interestingly, cultivable sulphate reducing bacteria were found in most stream bed sediments. The microbial community can be present without being necessarily active (i.e. responsible for microbial reduction of sulphate). The results might indicate that there is a potential for biostimulation for inducing sulphate attenuation in the hyporheic zone by introducing suitable electron donors, e.g. ethanol. By contrast to the sulphate fate, denitrification has been identified as a potentially important process in most of the studied hyporheic zones in the Skerne with a decrease of nitrate in the hyporheic zone compared to the surface water.

The findings of this research have been used to update the original conceptual models and re-define the areas of greatest uncertainty for each of the monitoring points:
D01: Reduction of sulphate concentrations in the soft sediment bed of the hyporheic zone. Confined mining contaminated groundwater likely recharges on faults. The key main uncertainties relate to the possible presence of transient storage in the floodplain and diffuse recharge via the glacio-fluvial sediments and the banks or stream bed. This could be addressed by installing a network of boreholes in the superficial deposit to capture shallow flow paths and a study of the nearby springs in terms of water quality and relationships with bedrock or superficial deposits.

WB2 and WB3: Some dilution of sulphate concentrations in the sand and gravel of the river bed hyporheic zone. Superficial cover suspected to be thin as it is exposed farther upsteam. The groundwater chemistry with high magnesium, calcium and bicarbonate suggests dolomitized limestone dissolution. There could be baseflow from the till, which may maintain a high flow to the stream, giving longer residence time for bedrock dissolution. Remnant uncertainties: (i) source of very high sulphate in surface water potentially from bedrock or additional sources, e.g. till, agricultural lime, or colliery waste in superficial deposits (proximity of the colliery workings may warrant further consideration) (iii) the detail of the recharge flow paths and the groundwater monitoring borehole response zones are not known.

RB: As suggested by the conceptual model here the stream bed comprised fine sand, silt, clay likely associated with the glacio-lacustrine deposits. This has influenced the hyporheic zone conditions and is associated with reducing conditions with iron and manganese enrichment,

but a low attenuation potential for sulphate. Discrete groundwater inflows were detected. The uncertainties highlighted for Woodham Burn also apply to Rushyford Beck.

AY and A02: The gravelly substrate to the stream and its oxygenated state. The data suggest that there are discrete inflows to the stream and that the groundwater has a lower sulphate content with a high chloride content. Structurally guided groundwater ingress along this stretch of the stream remains plausible. In the absence of hydrological data (groundwater levels) there remains some uncertainty with respect to this interpretation at AY. Hydraulic exchange can occur in the coarser bed materials, but the geochemical conditions do not favour significant geochemical attenuation other than by dilution.

On the basis of the present results key recommendations are:

1. Further monitoring of the hyporheic zone using multilevel minipiezometers in the riverbed:

In order to address the spatio-temporal patterns and scales of the groundwater-surface water interaction further monitoring is recommended a) to capture the hyporheic zone temporal variability expected to occur in response to seasonal controls on catchment hydrology and b) to increase the monitoring point density. The monitoring phase should be extended beyond the low flow conditions. Given the relative high sulphate concentrations in both surface water and hyporheic zone and proximity to mine workings, Woodham burn is the site recommended for further investigation.

2. Geomorphological characterisation of the river catchment to improve the assessment of the pollutant attenuation potential in sediments at the groundwater-surface interface:

Given the possibility to characterise with greater spatial coverage sediment properties such as texture with relatively low costs and time effort than required for the hyporheic zone sampling, the potential of using sediment grain size mapping for estimating potential for hyporheic zone sulphate reduction in the Skerne catchment should be explored further.

3. Reviewing existing database of water chemistry of Magnesian Limestone and coal mine boreholes and use trace elements as a fingerprint of the source of each water and the extent of water-rock interaction. Recommendations to increase the range of parameters analysed might follow.

4. Install boreholes in the superficial deposits:

The EA groundwater monitoring network does not include monitoring of groundwater levels and groundwater quality within the superficial deposits which overlie the Magnesian Limestone aquifer across the catchment, and which may also interact with the hyporheic zone and surface water in the Skerne. This represents a gap in the data collection in order to understand the relative importance of shallow and deeper groundwater in contributing to the hyporheic zone “make-up” and its capacity to attenuate potential contaminants such as nitrate or sulphate. This gap could be addressed through the installation of a number of clusters of nested piezometers to facilitate monitoring across hydrological boundaries in the superficial deposits and the underlying bedrock. If the piezometers were installed in rotary cored holes the recovered core would be valuable for pore water sampling and hydrogeological

characterisation (sediment grain-size, permeability, porosity and compressibility). It is anticipated that a tracked relatively light-weight rig, e.g. Dando Terrier would be appropriate in these ground conditions.

5. Undertaking a comparison of surface water and groundwater levels to confirm areas of connectivity at each of the study sites.

6. Characterising sulphate pools in the river catchment using sulphur isotope analysis:

Sulphate is one of the main pollutant of concern. Freshwater are generally low in sulphate, but in the Skerne catchment sulphate is one of the main pollutant of concern, present in surface water, groundwater and the hyporheic zone. Since ^{32}S is preferentially consumed compared to ^{34}S during sulphate reduction catalysed by various strains of bacteria, a higher $\delta^{34}S$ in combination with decreasing sulphate concentrations in an aquifer likely indicates sulphate reduction. Providing there is a clear difference in $\delta^{34}S$ between the local sources of sulphates and constrained flow paths, the application of sulphur and oxygen isotope analysis of sulphates has proven most useful to delineate the origin and fate of sulphate in groundwater. It is recommended that a review of potential sources in the catchment is carried out and a selection of end-members and groundwater, surface water and hyporheic zone water samples is analysed for sulphur and oxygen isotope analysis of dissolved sulphates.

Table 8: Summary of hyporheic zone characteristics at the study sites

SITE	D01	WB2	WB3	RB	AY	A02
***Riverbed monitored depth* cm**	-30 to -134	0 to -75	-85 to -115	-50 to -80	0 to -45	0 to -30
Riverbed texture	Silt clay	poorly sorted gravel—sand	poorly sorted gravel—sand	Fine-sand — silt—clay	Gravelly coarse sand	Gravelly coarse sand
HEF in shallow riverbed	Absent	Present (upper 40 cm)	No data for shallow sediment	No data for shallow sediment	Present	Present
Redox vertical gradient	Negative to positive	Negative	Negative	Positive	No gradient	Negative
***Riverbed dissolved oxygen* (mg/l)**						
Min	2.04	0.28	1.38	1.74	2.60	1.18
Median	**7.00***	**1.73**	**4.62**	**1.87**	**4.27**	**2.37**
Max	7.76*	3.21	5.81	3.32	8.50	8.91
Riverbed conductivity						
Min	846	871	1100	971	921	768
Median	**950**	**1417**	**1303**	**988**	**987**	**812**
Max	1017	1832	1692	1025	1021	1168
SO_4 in surface water (mg/l)						
Min	135	498	327	88.37	157	100
Median	**147**	**504**	**329**		**166**	**106**
Max	160	509	331		168	114
SO_4 in hyporheic zone (mg/l)						
Min	0.67	105	253	68	61	107
Median	**16**	**321**	**284**	**70**	**67**	**115**
Max	125	511	337	116	162	144
N-NO_3 in hyporheic zone (mg/l)						
Min	0.07	0.07	0.56	1.32	2.32	0.00
Median	**0.07**	**0.14**	**0.97**	**1.53**	**3.15**	**0.63**
Max	2.67	1.03	1.85	3.40	7.95	4.56
Total P in hyporheic zone (mg/l)						
Min	0.01	0.01	0.01	0.46	0.02	0.08
Median	**0.015**	**0.01**	**0.01**	**0.83**	**0.09**	**0.26**
Max	1.240	0.32	0.04	1.11	0.39	0.52
SRB bacteria presence	yes	yes	yes	yes	yes	yes
NO_3 attenuation in hyporheic zone	yes	yes	only moderate	variable	moderate	yes
Mn/Fe redox zone	yes	yes	yes	yes	no	yes
SO_4 attenuation in hyporheic zone	Attenuation in soft upper layer by redox processes; SO_4 increase at depth	Moderate attenuation by dilution (mixing of SW with GW). SO_4 much lower at depth due to either redox reduction or GW inflow	No attenuation, high SO_4 in porewater, with a moderate increase with depth. redox reduction unlikely, as oxic waters	No attenuation, High SO_4 in porewater with an increase at depth	Moderate attenuation by dilution with GW lower in SO_4.	No attenuation, high SO_4 in porewater with the presence of a high SO_4 flow at depth

*Uncertain measurements (see section 3.3.1)

Table 8 (continued): Summary of hyporheic zone characteristics at the study sites

SITES	D01	WB2	WB3	RB	AY	A02
GW dominated zone composition	SO_4-rich, but also lateral flow	Low SO_4 GW	High SO_4 GW	High SO_4 GW	Moderate SO_4 GW	High SO_4 GW
Hierarchical clustering based on chemical composition **HZ**	Cluster 1: Low SO_4 type	Cluster 4: High Fe type			Cluster 3: High Cl type	
SW	All SW in Cluster 3 except for site WB where SW forms Cluster 2: High SO4-Ca type.					

References

British Geological Survey holds most of the references listed below, and copies may be obtained via the library service subject to copyright legislation (contact libuser@bgs.ac.uk for details). The library catalogue is available at: https://envirolib.apps.nerc.ac.uk/olibcgi.

Allen, D J, Brewerton, L M, Coleby, L M, Gibbs, B R, Lewis, M A, MacDonald, A M, Wagstaff, S, and Williams, A T. 1997. The physical properties of major aquifers in England and Wales. *British Geological Survey*, WD/97/34.

Appelo, C. A. J., Postma, D. 2005. Geochemistry, groundwater and pollution. London, CRC press.

Bearcock, J.; Smedley, P.L.. 2009 *Baseline groundwater chemistry : the Magnesian Limestone of County Durham and North Yorkshire.* Nottingham, UK, British Geological Survey, 63pp. (OR/09/030) (Unpublished).

Bencala, K.E., 2011. Stream-Groundwater Interactions, in: Peter, W. (Ed.), Treatise on Water Science. Elsevier, Oxford, pp. 537-546.

Benner, S. G., Gould, W. D., & Blowes, D. W. (2000). Microbial populations associated with the generation and treatment of acid mine drainage. Chemical Geology, 169(3-4), 435-448.

Boulton, A.J., Findlay, S., Marmonier, P., Stanley, E.H. and Valett, H.M., 1998. The functional significance of the hyporheic zone in streams and rivers. . Annual Review of Ecology and Systematics 29, 59-81.

Cardenas, M.B., Wilson, J.L., 2007. Exchange across a sediment–water interface with ambient groundwater discharge. Journal of Hydrology 346, 69-80.

Conant Jr, B., Cherry, J.A., Gillham, R.W., 2004. A PCE groundwater plume discharging to a river: influence of the streambed and near-river zone on contaminant distributions. Journal of Contaminant Hydrology 73, 249-279.

Cooper, A H, and Burgess, I C. 1993. *Geology of the Country around Harrogate*. Memoirs of the British Geological Survey. No. Sheet 62 (England and Wales). (London: HMSO.)

Cooper, A H, and Gordon, J. 2000. Revised geological maps of Darlington based on new borehole information: explanation and description. British Geological Survey Technical

Engelhardt, I., Piepenbrink, M., Trauth, N., Stadler, S., Kludt, C., Schulz, M., Schüth, C., Ternes, T., 2011. Comparison of tracer methods to quantify hydrodynamic exchange within the hyporheic zone. Journal of Hydrology 400, 255-266.

Environment Agency, 2012. Hydrology Flow Investigation Stage 2. Northumbria River Basin District Investigation: NE2010-10005. Report CR/00/94.

Fernando, W. A. M., Ilankoon, I. M. S. K., Syed, T. H., & Yellishetty, M. (2018). Challenges and opportunities in the removal of sulphate ions in contaminated mine water: A review. Minerals Engineering, 117, 74-90.

Gibert, O., De Pablo, J., Cortina, J. L., & Ayora, C. (2004). Chemical characterisation of natural organic substrates for biological mitigation of acid mine drainage. Water Research, 38(19), 4186-4196.

Gu, C., Hornberger, G.M., Mills, A.L., Herman, J.S., Flewelling, S.A., 2007. Nitrate reduction in streambed sediments: Effects of flow and biogeochemical kinetics. Water Resources Research 43.

Harvey, J.W., Fuller, C.F., 1998. Effect of enhanced manganese oxidation in hyporheic zone on basin-scale geochemical mass balance. Wat. Resour. Res. 34, 623-636.

JBA 2017. Skerne Magnesian Limestone. Skerne catchment assessment, 46pp.

Kortas, L. and Younger, P.L. 2013. Fracture patterns in the Permian Magnesian Limestone Aquifer, Co. Durham, UK. Proceedings of the Yorkshire Geological Society, 59, 3, 161 – 171.

Krause, S., Hannah, D., Fleckenstein, J., Heppell, C., Kaeser, D., Pickup, R., Pinay, G., Robertson, A., Wood, P., 2011. Inter-disciplinary perspectives on processes in the hyporheic zone. Ecohydrology 4, 481-499.

Lovley, D.R., Chapelle, F.H., 1995. Deep subsurface microbial processes. Reviews of Geophysics 33, 365-381.

Mills, D A C, and Hull, J H. 1976. *Geology of the Country Around Barnard Castle*. Memoirs of the British Geological Survey. No. Sheet 32 (England and Wales). (London: HMSO.)

Mitsch, W.J. & Gosselink, J.G. 1986. Wetlands. Van Nostrand Reinhold Company IncNew York.

Nagorski, S.A., Moore, J.N., 1999. Arsenic mobilization in the hyporheic zone of a contaminated stream. Water Resources Research 35, 3441-3450.

Neymeyer, A., Williams, R.T. and Younger, P.L. 2007. Migration of polluted minewater in a public supply aquifer. Quarterly Journal of Engineering Geology and Hydrogeology. 40, 75-84.

Nordstrom and Wilde 2006, Reduction Oxidation Potential (Electrode Method): U.S. Geological Survey Techniques of Water-Resources Investigations, book 9, chap. A6., sec. 6.5, July 2006, accessed [5/12/2017], from http://pubs.water.usgs.gov/twri9A6/.

Pedersen, J.K., Bjerg, P.L., Christensen, T.H., 1991. Correlation of nitrate profiles with groundwater and sediment characteristics in a shallow sandy aquifer. Journal of Hydrology 124, 263-277.

Price, S.J., Merritt, J.E., Whitbread, K., Lawley, R.S., Banks, V., Burke, H, Irving, A.M. and Cooper, A.H. 2007. Superficial geology and hydrogeological domains between Durham and Darlington Phase 1 (Durham South). BGS Commercial Report CR/07/002 N.

Rivett, M.O., Ellis, P.A., Greswell, R.B., Ward, R.S., Roche, R.S., Cleverly, M.G., Walker, C., Conran, D., Fitzgerald, P.J., Willcox, T., Dowle, J., 2008. Cost-effective mini drive-point piezometers and multilevel samplers for monitoring the hyporheic zone. Quarterly Journal of Engineering Geology and Hydrogeology 41, 49-60.

Smith, D. B. 1989. The late Permian paleogeography of north-east England. *Proceedings of the Yorkshire Geological Society*, Vol. 47, 285-312.

Smith, D. B. 1994. *Geology of the country around Sunderland*. Memoir of the British Geological Survey. No. Sheet 21 (England and Wales). (London: HMSO.)

Smith, D. B., and Francis, E. A. 1967. *Geology of the Country between Durham and West Hartlepool. Memoirs of the Geological Survey of Great Britain. No. 27 (England and Wales). (London: HMSO.)*

Storey, R. G., Fulthorpe, R. R., & Williams, D. D. (1999). Perspectives and predictions on the microbial ecology of the hyporheic zone. Freshwater Biology, 41(1), 119-130.

Stumm, W., Morgan, J. J., 2012. Aquatic chemistry: chemical equilibria and rates in natural waters. John Wiley & Sons.

Tiedje, J. M., Ecology of dentrification and dissimilatory nitrate reduction to ammonium, in Biology of Anaerobic Microorganisms, edited by A. J. B. Zehnder, pp. 179- 244, John Wiley, New York, 1988.

Triska, F.J., Duff, J.H., Avanzino, R.J., 1993. The role of water exchange between a stream channel and its hyporheic zone in nitrogen cycling at the terrestrial—aquatic interface, Nutrient Dynamics and Retention in Land/Water Ecotones of Lowland, Temperate Lakes and Rivers. Springer, pp. 167-184.

Younger, P. L. 1995. *Chapter 11: Hydrogeology 353-359. In: Robson's Geology of North East England (Second edition).* Johnson, G A L *(editor). 56. (Newcastle upon Tyne:Transactions of the Natural History Society of Northumbria).*

Appendix 1 Borehole Records

Additional information for site D01.

Borehole log of EA-monitored borehole at D01 (Foumarts Lane)

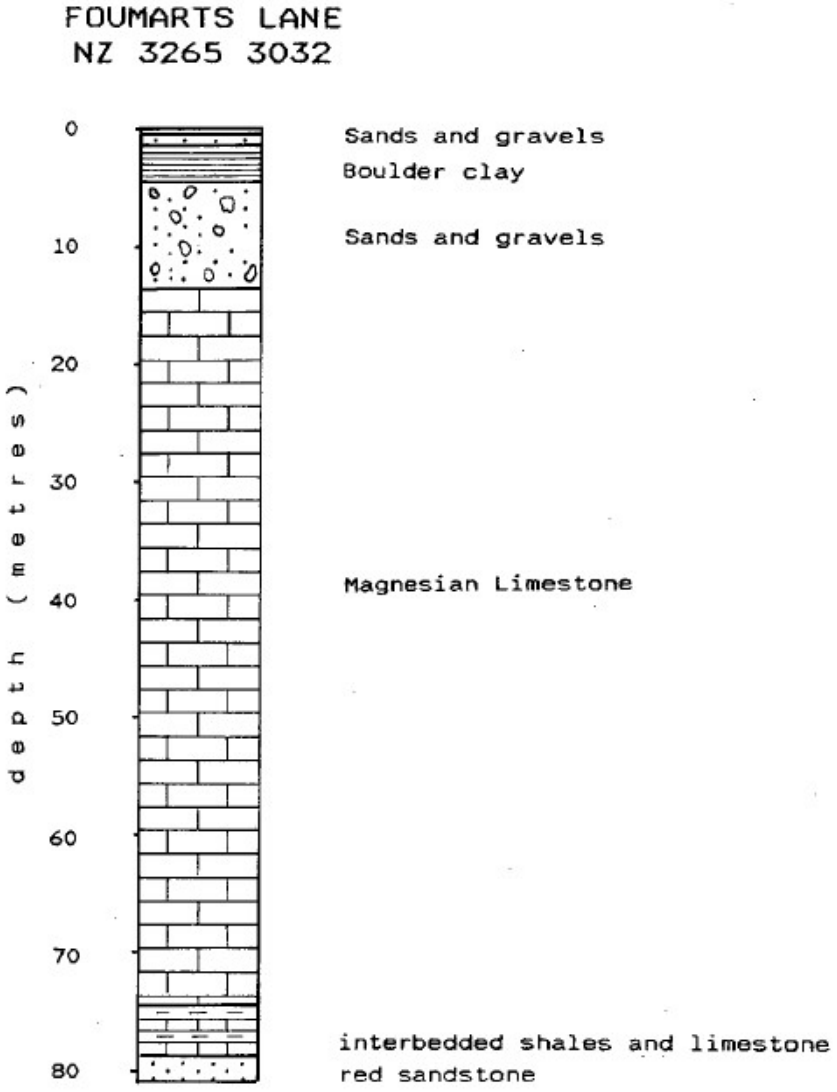

Details of the Hutton Villa borehole record available through the BGS website.

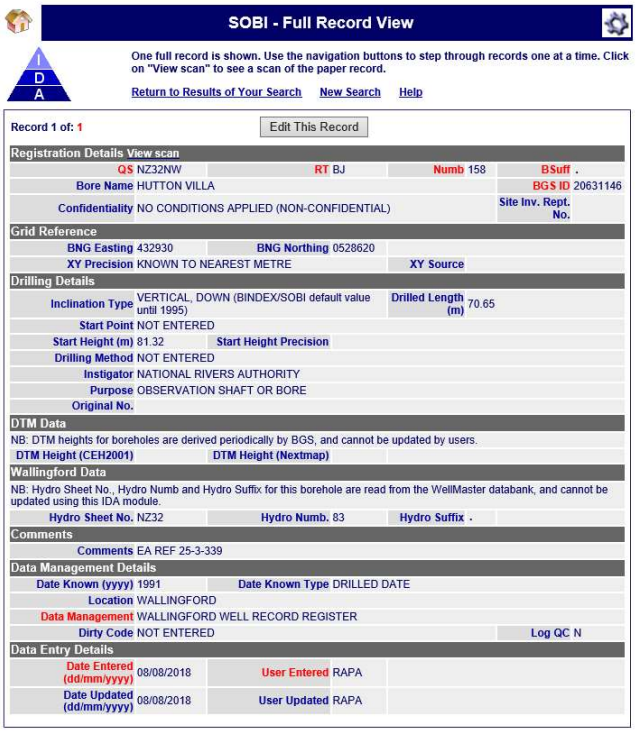

SOBI - Full Record View

One full record is shown. Use the navigation buttons to step through records one at a time. Click on "View scan" to see a scan of the paper record.

Return to Results of Your Search | New Search | Help

Record 1 of: 1 — Edit This Record

Registration Details View scan

QS	NZ32NW	RT	BJ	Numb	158	BSuff	.
Bore Name	HUTTON VILLA					BGS ID	20631146
Confidentiality	NO CONDITIONS APPLIED (NON-CONFIDENTIAL)					Site Inv. Rept. No.	

Grid Reference

BNG Easting	432930	BNG Northing	0528620		
XY Precision	KNOWN TO NEAREST METRE			XY Source	

Drilling Details

Inclination Type	VERTICAL, DOWN (BINDEX/SOBI default value until 1995)	Drilled Length (m)	70.65
Start Point	NOT ENTERED		
Start Height (m)	81.32	Start Height Precision	
Drilling Method	NOT ENTERED		
Instigator	NATIONAL RIVERS AUTHORITY		
Purpose	OBSERVATION SHAFT OR BORE		
Original No.			

DTM Data

NB: DTM heights for boreholes are derived periodically by BGS, and cannot be updated by users.

DTM Height (CEH2001)		DTM Height (Nextmap)	

Wallingford Data

NB: Hydro Sheet No., Hydro Numb and Hydro Suffix for this borehole are read from the WellMaster databank, and cannot be updated using this IDA module.

Hydro Sheet No.	NZ32	Hydro Numb.	83	Hydro Suffix	.

Comments

Comments	EA REF 25-3-339

Data Management Details

Date Known (yyyy)	1991	Date Known Type	DRILLED DATE		
Location	WALLINGFORD				
Data Management	WALLINGFORD WELL RECORD REGISTER				
Dirty Code	NOT ENTERED			Log QC	N

Data Entry Details

Date Entered (dd/mm/yyyy)	08/08/2018	User Entered	RAPA
Date Updated (dd/mm/yyyy)	08/08/2018	User Updated	RAPA

Additional information for site RB, WB2 and WB3.

Borehole Copelaw N01 reference 25-3-27

NZ 22 NE /43

NORTHUMBRIAN WATER AUTHORITY

DIRECTORATE OF PLANNING & SCIENTIFIC SERVICES

GROUNDWATER SECTION

N.W.A. REFERENCE 25-3-27 GRID REFERENCE NZ 2942 2632

BOREHOLE NO 'D' SYNOPSIS OF DRILLERS' LOG

+297.11'

DATE	FROM	TO	DETAILS OF STRATA
2 April 1968	0	25	Boulder Clay
" " "	25	48	" "
3 " "	48	88	" "
" " "	88	110	" "
" " "	110	115	Limestone +187'
4 " "	115	120	"
9 " "	120	145	"
10 " "	145	162	"
11 " "	162	181	"
16 " "	181	185	"
			Borehole Complete.

[NZ22NE BJ 43 .

NZ 22 NE/43

Northumbrian River Authority Bore 'D'

Samples examined by D. B. Smith, 15.7.68
NZ 2941 2638. O.D. + 285 (m)

Depth (ft).	
0- 5	Clay, brown, very gritty, with many small subangular to subrounded pebbles. Rock types present include Carboniferous shale, coal and limestone and Magnesian Limestone
5- 10	Clay, pale to dark brown, partly with few stones, partly with very abundant small stones. Probably represents a gravel bed in clay.
10- 15	Clay, as 0'-5' but slightly paler brown.
15- 20	Not seen
20- 25	Clay, dark brown, very gritty, with abundant small stone fragments. Magnesian Limestone is present.
25- 30	As 20' - 25'
30- 35	ditto
35- 40	"
40- 45	Not seen
45- 50	As 20' - 25'
50- 55	ditto
55- 60	" Some fragments of red sandstone
60- 65	" ditto
65- 70	Clay, as above, but very dark brown and less gritty. Some fragments of red sandstone, and generally less stony.
70- 75	As 65' - 70'
75- 80	ditto, but with slight grey tint
80-85	Not seen
85- 90	As 65' - 70'
90- 95	ditto, but with many fragments of cream dolomite.
95-100	As 90' - 95'
100-105	ditto
105-110	"
Base of drift acc. to driller → 110-115	" Magnesian Limestone abundant
115-120	" " very "
120-125	Dolomite, calcitic, buff and yellow-buff, hard, finely saccharoidal (very fine sand to silt-grade). Large chippings, Slightly porous.
125-130	As 125' - 130'
130-135	ditto
135-140	" , but with some very porous fragments.

NZ 22 NE/43

Depth (ft).

140-145	As 125' - 130', but small chippings
145-150	Dolomite calcite, grey-buff, hard, finely crystalline, small chippings.

Total depth 185 ft

Summary

Drift to c. 118'

Lower Magnesian Limestone to bottom

Rushyford NE

6 inch Map Registered No. NZ 22 NE/10

SECTION OF Surface Bore. Windlestone E.
Surface to Rusty Seam Q2.

Exact Site NZ 28750/28960
N 54° 39' 17.4"
W 01° 33' 15.3"
Level at which shaft bore drive commenced relative to O.D. 303.6

Date of sinking or boring 16/1/58 - 29/3/58.
Sinker or Borer National Coal Board. No. 4 Rig.
One Inch Geological Map
Six Inch Map (County and Quarter Sheet) 43 N.W.

Attach tracing from a map or sketch map if possible

Scale 1:10560

NATURE OF STRATA		THICKNESS		DEPTH	
Geologist's Notes	Borer's Journal	Feet	In.	Feet	In.
	Soil	1	0	1	0
	Boulder Clay	15	0	16	0
	Sand	1	6	17	6
	Boulder Clay	2	6	20	0
	Marl	2	6	22	6
	Limestone with Marl Panels.	7	6	30	0
	Limestone	176	9	206	9
Base of Permian + 91.3'O.D.	Marl Slate	5	7	212	4
	Post-red stained.	13	3	225	7
	Shale, grey sandy red-stained.	3	8	229	3
	Shale, grey with Ironstone Panels.	7	6	236	9
	Shale, dark.	4	2	240	11
	COAL +62.2' O.D.	-	6	241	5
	Shale, dark	-	9	242	2
	Shale, sandy grey.	2	7	244	9
	Shale, sandy grey with Post panels.	9	9	254	6
	COAL	-	7	255	1
	Shale, dark	1	2	256	3
	Shale, dark sandy with Post panels.	3	9	260	0

[NZ22NE BJ 10 .]

Additional information for site A02

Borehole log of EA-monitored borehole near A02 (Ketton Hall)

5. STRATA

GEOLOGICAL CLASSIFICATION	NATURE OF STRATA	THICKNESS FEET	THICKNESS IN.	DEPTH FEET	DEPTH IN.	DEPTH METRES
Drift	Boulder clay with coal traces at 98'-100'	137	–	137	–	
Upper Magnesian Lst	Broken limestone	23	–	160	–	
?	Decomposed soft limestone	10	–	170	–	
? Lower Magnesian Limestone	Alternatively hard and soft limestone	31	–	201	–	

DR DLn 46452/2(2)/360 2,500 11/66 TXL

Newton Ketton Borehole

NZ 32 SW. 45

NORTHUMBRIAN WATER AUTHORITY

DIRECTORATE OF PLANNING & SCIENTIFIC SERVICES

GROUNDWATER SECTION

N.W.A. REFERENCE 25-3-78 GRID REFERENCE NZ 3133 2067

BOREHOLE NO G SYNOPSIS OF DRILLERS' LOG

DATE	FROM	TO	DETAILS OF STRATA
11 Jan 1968	0	0'9"	Soil-Top
" " "	0'9"	1'1"	Soi-Sub
" " "	1'1"	10	Sandy Clay and Pebbles
15 " "	20	40	Sandy Clay and Boulders
15 " "	40	54	Boulders
" " "	54	68	Boulder Clay
" " "	68	74	Boulders
" " "	74	80	Boulder Clay
16 " "	80	120	Clay and Boulders
" " "	120	127	Boulder Clay
" " "	127	136'3"	Boulders
" " "	136'3"	157	Boulder Clay
" " "	157	158	Boulders
" " "	158	160	Boulder Clay
17 " "	160	162	Boulders
" " "	162	173	Limestone
23 " "	173	183	" Broken
" " "	183	203	" Hard
24 " "	203	217'6"	" "
" " "	217'6"	227	" Soft
25 " "	227	232	Marl
" " "	232	235	"
22 Feb "	235	245	"
" " "	245	248	"
" " "	248	253	Limestone
2 March "	253	267	" Hard
5 " "	267	283	" "
5 " "	283	285'6"	Limestone Hard
6 " "	285'6"	317'6"	"
" " "	317'6"	341	" With Hard Bands
7 " "	341	342	" Hard
			Borehole Completion

Additional information for site near B01

Borehole log of EA-monitored borehole near B01 (Low Copelaw)

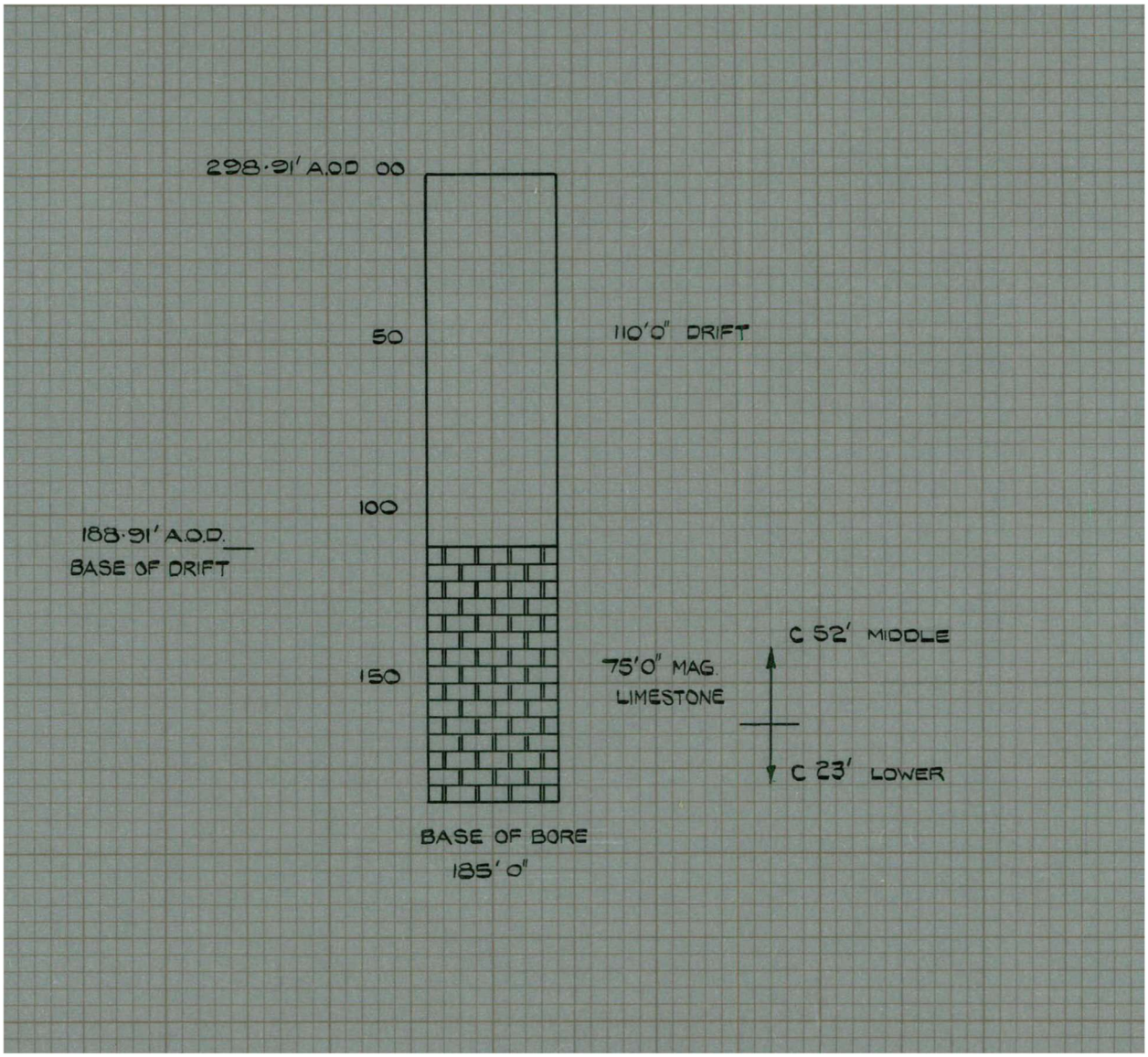

Coal mining record (near site B01)

Borehole log of EA-monitored borehole near B01 (Low Copelaw)

Field	Value
BGS_DATABASE	PLANS
PLAN_ID	29335
PLAN_TITLE	MARSKE PARISH
PLAN_DESCRIPTION	<null>
CONFIDENTIALITY	U
HORIZONTAL_SCALE	<null>
VERTICAL_SCALE	<null>
YEAR_ABANDONED	<null>
SERIES_CODE	CA
SERIES_NUMBER	N/A
SERIES_DESCRIPTION	COAL AUTHORITY ABANDONMENT PLAN DATA FROM THE HEALTH AND SAFETY EXECUTIVE
CUSTODIAN_CODE	<null>
CUSTODIAN	<null>
DONOR_OR_SOURCE_CODE	COAU
DONOR	THE COAL AUTHORITY
DONOR_EMAIL	thecoalauthority@coal.gov.uk
PLAN_TYPE_CODE	MP
PLAN_TYPE_DESC	MINE PLAN - PLAN OR PART OF PLAN OF UNDERGROUND WORKINGS. MAY BE MORE THAN ONE MINE PER PLAN.
PLAN_TYPE_TRANS	MINE PLAN
MINERAL_CODE	LEAD
MINERAL	LEAD
MINERAL_TRANS	LEAD
FEATUREID	<null>
GEOG_AREA	<null>
IMAGE_ID	<null>
IMAGE_FILE_PATH	<null>
QUARTER_SHEET	<null>
SCAN_STATUS	UNKNOWN
SWE	407081
SWN	499576

Field	Value
BGS_DATABASE	PLANS
PLAN_ID	14990
PLAN_TITLE	THE COAL SEAMS OF NORTHUMBERLAND & DURHAM. 350 VERTICAL SECTIONS OF THE GREAT NORTHERN COALFIELD SELECTED, DRAWN ANI
PLAN_DESCRIPTION	NORTHUMBERLAND & DURHAM COAL SEAMS; LITHOGRAPHED MAP SHOWING COLLIERIES, QUARRIES, RAILWAYS, POSITION OF SECTIONS AN
CONFIDENTIALITY	U
HORIZONTAL_SCALE	31680
VERTICAL_SCALE	<null>
YEAR_ABANDONED	<null>
SERIES_CODE	SP
SERIES_NUMBER	1511
SERIES_DESCRIPTION	SURVEY PLAN - LAND SURVEY PLANS HELD AT MURCHISON HOUSE
CUSTODIAN_CODE	BGS
CUSTODIAN	BRITISH GEOLOGICAL SURVEY
DONOR_OR_SOURCE_CODE	BGS
DONOR	BRITISH GEOLOGICAL SURVEY
DONOR_EMAIL	enquiries@bgs.ac.uk
PLAN_TYPE_CODE	MP
PLAN_TYPE_DESC	MINE PLAN - PLAN OR PART OF PLAN OF UNDERGROUND WORKINGS. MAY BE MORE THAN ONE MINE PER PLAN. INCLUDES COAL SEAM PLANS
PLAN_TYPE_TRANS	MINE PLAN
MINERAL_CODE	COAL
MINERAL	COAL
MINERAL_TRANS	COAL
FEATUREID	9731
GEOG_AREA	SUNDERLAND
IMAGE_ID	19822955
IMAGE_FILE_PATH	S:\SCANS\MINEPLANS\JP2_MASTER_SET\014990_01.JP2
QUARTER_SHEET	<null>
SCAN_STATUS	AWAITING SCAN
SWE	390000
SWN	0510000
NEE	465000

BGS.GDI_BRITPIT_SP
Hall Garth Pasture Gravel Pits

Location: 429,166.588 520,245.889 Meters

Field	Value
BGS_REFERENCE_NO	123897
PIT_NAME	Hall Garth Pasture Gravel Pits
PIT_STATUS	Ceased
ALTERNATIVE_NAME	<null>
PARENT_PIT	<null>
TYPE_OF_MINING_SITE	Open-pit or surface workings
EASTING	429166
NORTHING	520246
PIT_ADDRESS	Coatham Mundeville, DARLINGTON, Co. Durham
MPA_NAME	Darlington Borough Council
PLANNING_REGION	North East
OPERATOR_NAME	Unknown Operator
OPERATOR_ADDRESS	<null>
SPONSOR_ORG_CODE	BGS
WORKED_BODY_COMMODITIES	Sand and gravel, Quaternary, Glaciofluvial Deposits, Devensian, Commodity: Sand & Gravel.
SHAPE	Point
END_USE_CATEGORIES	Natural Aggregates

: Additional Material for monitoring point AY.

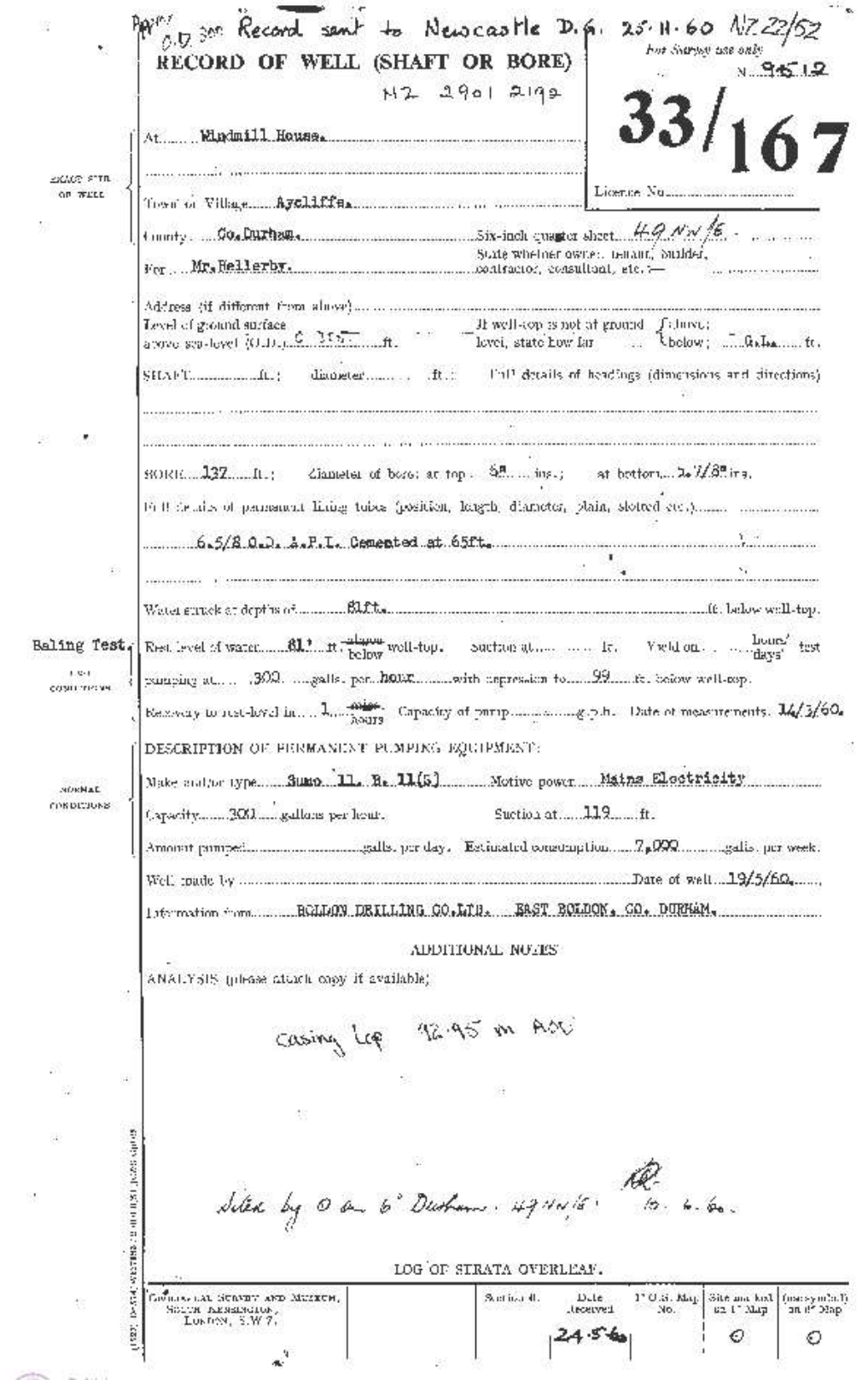

Record sent to Newcastle D.G. 25·11·60 NZ22/52

RECORD OF WELL (SHAFT OR BORE)

NZ 2901 2192

For Survey use only

N 9512

33/167

License No.

At Windmill House.

Town or Village Aycliffe.

County Co. Durham. Six-inch quarter sheet 49 NW/E

For Mr. Hellerby. State whether owner, tenant, builder, contractor, consultant, etc.:—

Address (if different from above)

Level of ground surface above sea-level (O.D.) 0 350 ft. If well-top is not at ground level, state how far above; below; 0 ins. ft.

SHAFT ft.; diameter ft.; Full details of headings (dimensions and directions)

BORE 132 ft.; Diameter of bore: at top 8" ins.; at bottom 3 7/8" ins.

Full details of permanent lining tubes (position, length, diameter, plain, slotted etc.)

6.5/8 O.D. S.P.T. Cemented at 65ft.

Water struck at depths of 81ft. ft. below well-top.

Baling Test.

Rest level of water 81' ft. above/below well-top. Suction at ft. Yield on hours/days' test pumping at 300 galls. per hour with depression to 99 ft. below well-top.

Recovery to rest-level in 1 mins./hours Capacity of pump g.p.h. Date of measurements. 14/3/60.

DESCRIPTION OF PERMANENT PUMPING EQUIPMENT:

Make and/or type Sumo 11. R. 11(5) Motive power Mains Electricity

Capacity 300 gallons per hour. Suction at 119 ft.

Amount pumped galls. per day. Estimated consumption 7,000 galls. per week.

Well made by Date of well 19/5/60.

Information from BOLDON DRILLING CO.LTD. EAST BOLDON, CO. DURHAM.

ADDITIONAL NOTES

ANALYSIS (please attach copy if available)

Casing Log 12.95 m AOD

Site by O.S. 6" Durham. 49 NW/E 15. 6. 60.

LOG OF STRATA OVERLEAF.

GEOLOGICAL SURVEY AND MUSEUM, SOUTH KENSINGTON, LONDON, S.W.7.

Section 41. Date Received 24.5.60 1" O.S. Map No. Site and boundaries on 1" Map O (necessary) on 6" Map O

: Borehole logs for additional boreholes for groundwater analysis for sulphur isotopes

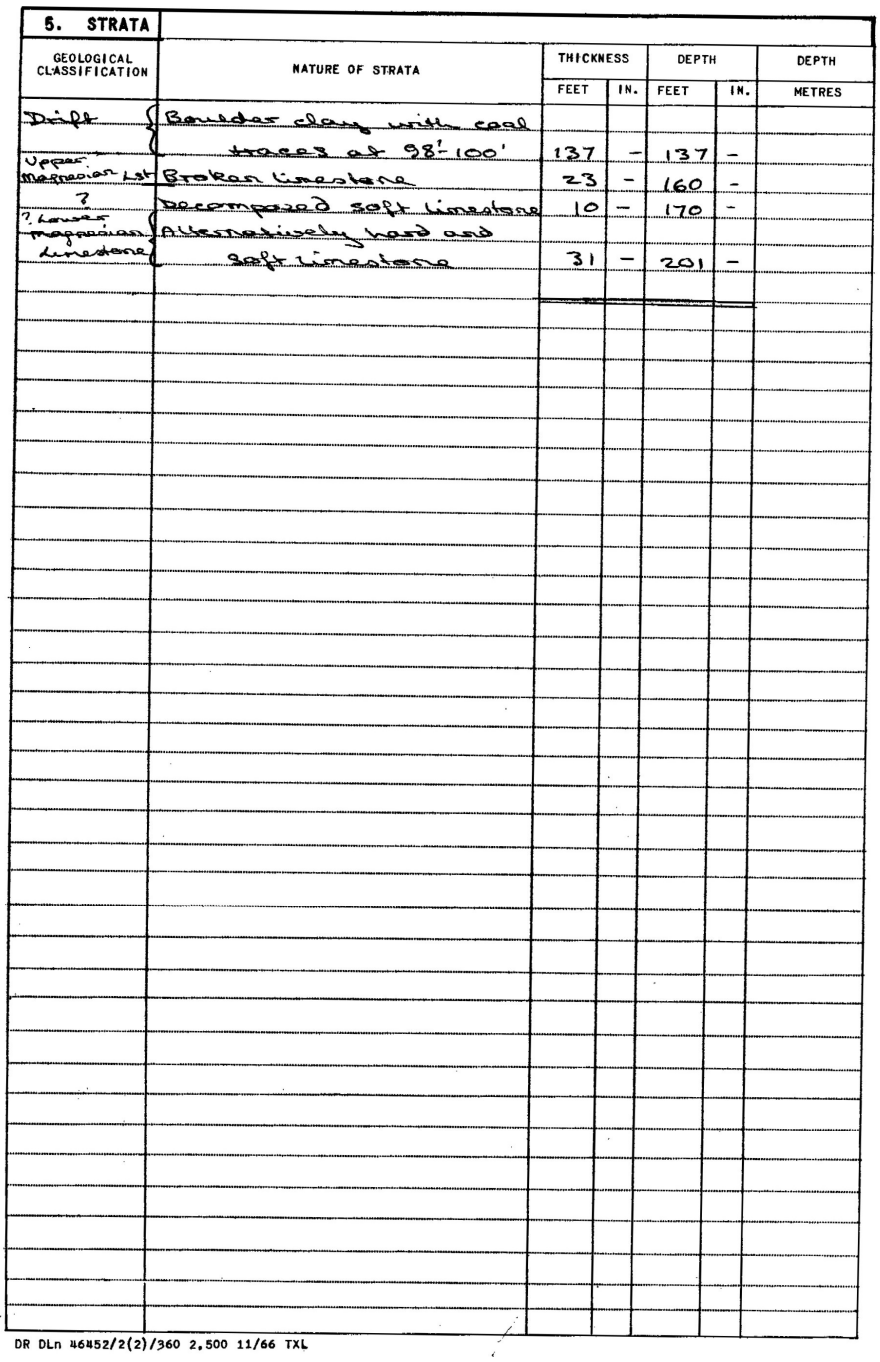

5. STRATA

GEOLOGICAL CLASSIFICATION	NATURE OF STRATA	THICKNESS FEET	THICKNESS IN.	DEPTH FEET	DEPTH IN.	DEPTH METRES
Drift	Boulder clay with coal					
	traces at 98'-100'	137	-	137	-	
Upper Magnesian Lst	Broken limestone	23	-	160	-	
?	Decomposed soft limestone	10	-	170	-	
? Lower Magnesian Limestone	Alternatively hard and soft limestone	31	-	201	-	

DR DLn 46452/2(2)/360 2,500 11/66 TXL

Borehole log for Ketton Hall (from BGS database)

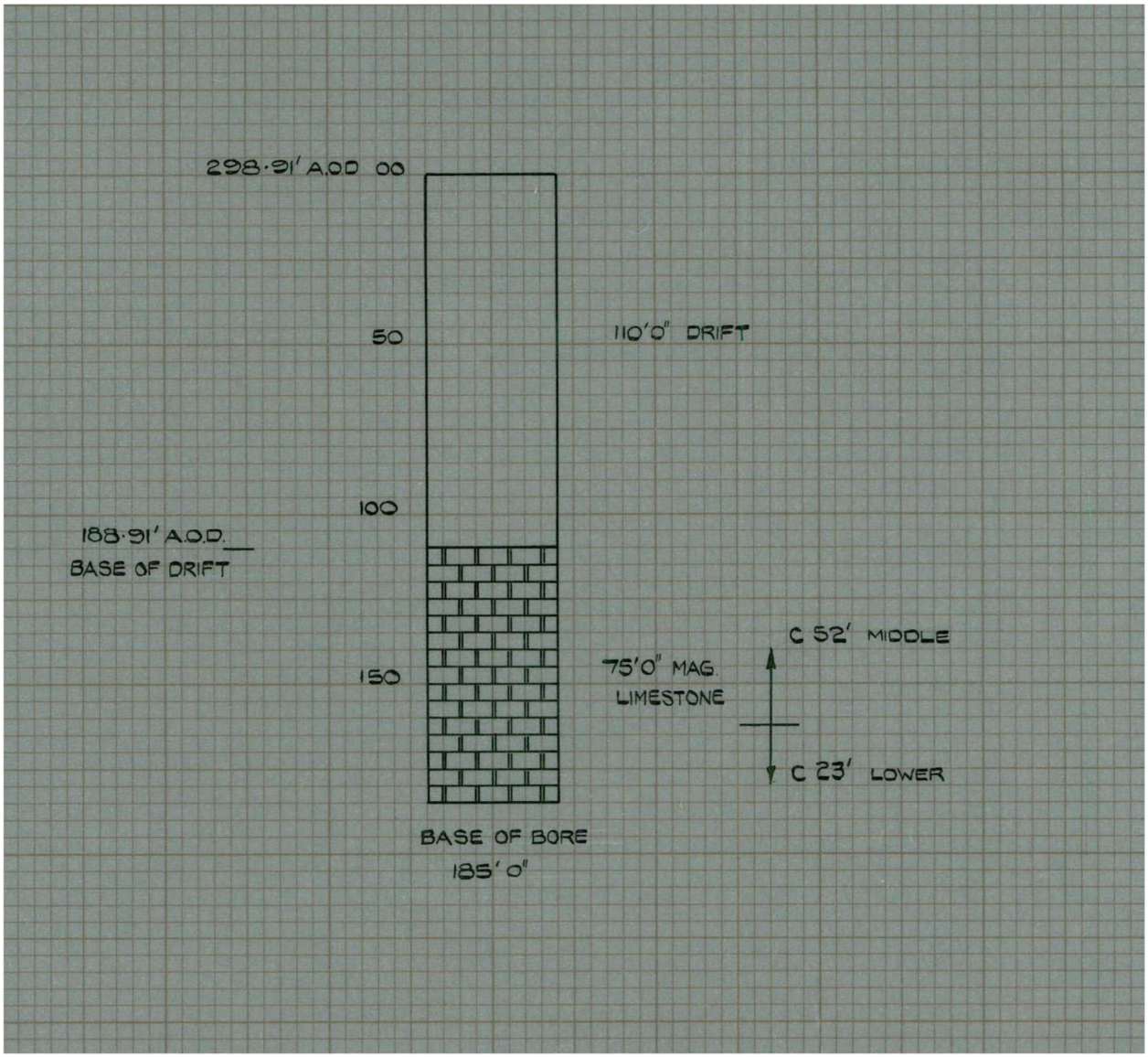

Borehole log for Low Copelaw (provided by EA)

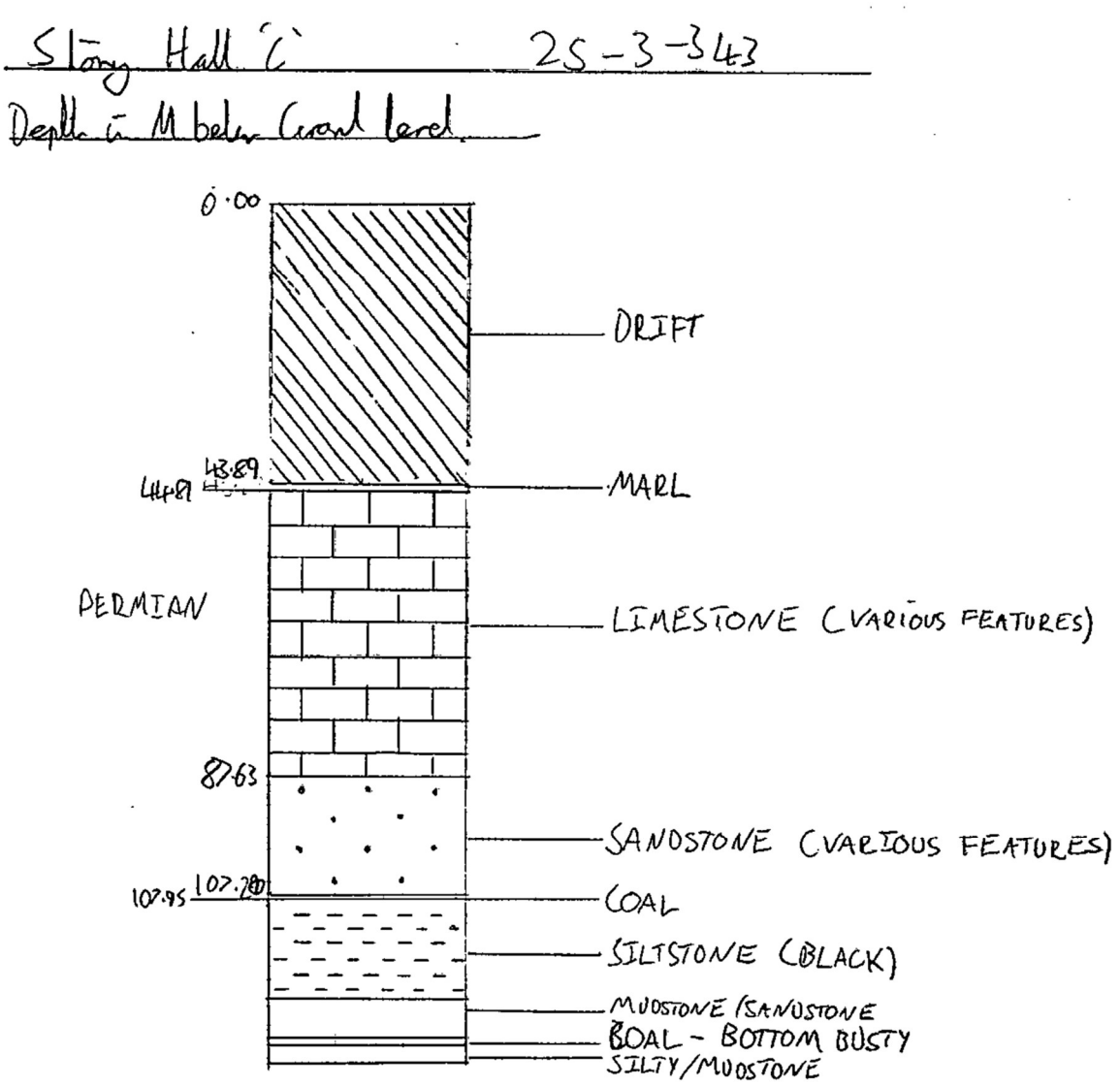

EA borehole log for Stony Hall C (provided by EA)

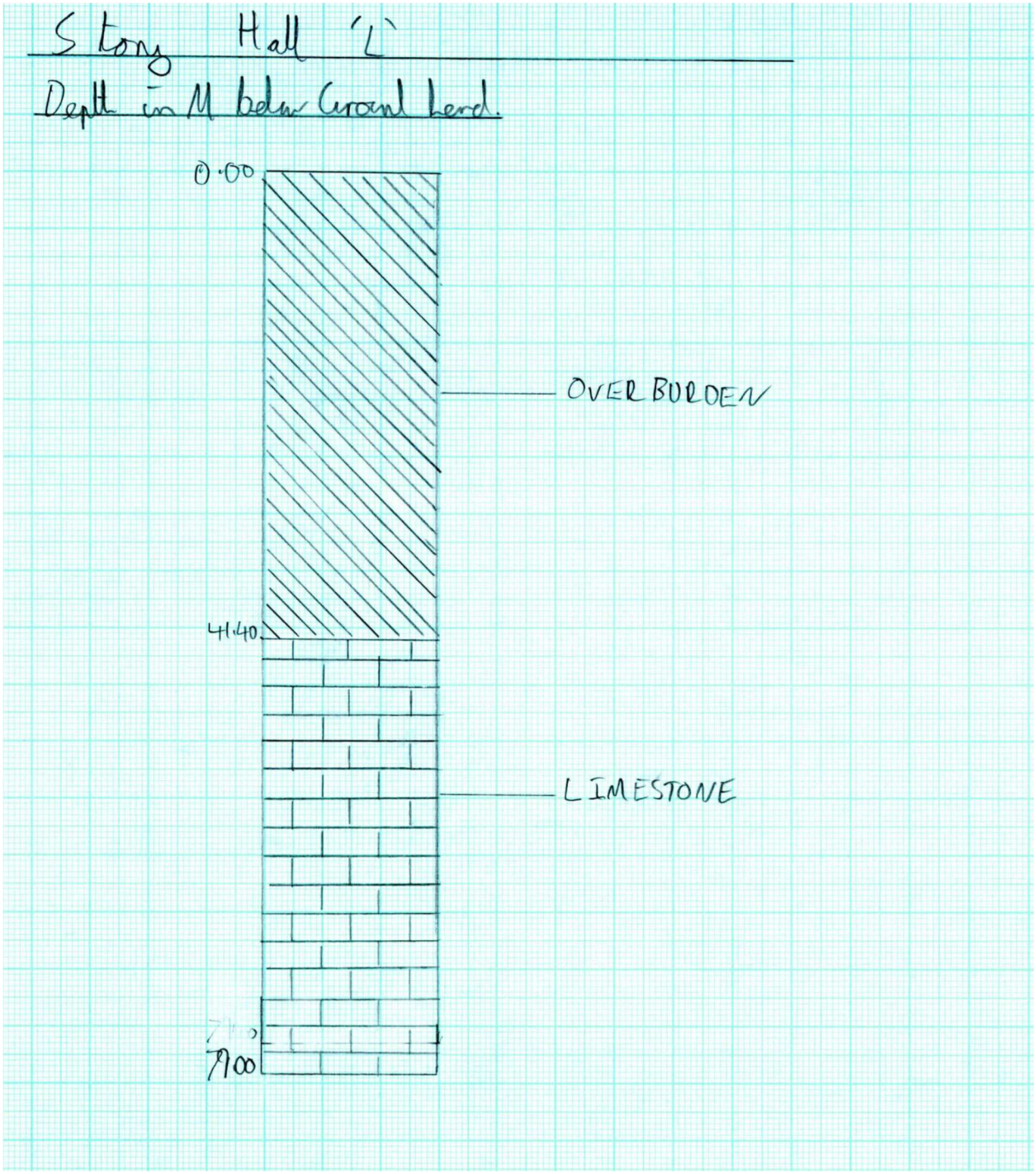

EA borehole log for Stony Hall L (provided by EA)

Appendix 2 Additional hydrogeological data

Borehole name	Easting	Northing	Elevation (m AOD)	Total depth (m)	RWL (m bgl)	Geology (number in m bgl)		EA comments
Stony Hall C	432570	529550	no data	128	no data	0-43.9	Drift	Coal Measures borehole, water level higher than the adjacent limestone borehole, high sulphate attributed to coal measures strata
						43.9-44.8	MARL	
						44.8-87.6	Magnesian LIMESTONE	
						87.6-107.3	SANDSTONE (various features)	
						107.3-108	COAL	
						108-128	SILTSTONE (black) / MUSTONE / SANDSTONE	
Stony Hall L	432570	529550	no data	79	no data	0-41.4	Drift	Magnesian Limestone borehole, high and rising sulphate, assumed impacted by underlying coal measures. Potential connectivity with adjacent coal measures borehole.
						41.4-79	Magnesian LIMESTONE	
Stillington OBH2	435400	523130	49.5	100.6	no data	0-40	Light grey-brown becoming brown, becoming dark brown silty, sandy CLAY with a little gravel	Magnesian Limestone borehole, high sulphate unknown reason, nearby boreholes understood to have intersected gypsum. Higher pH than expected.
						40-60	Dolomitic LIMESTONE	
						60-60.5	Stiff grey, becoming dark red-brown and occasionally grey mottled silty, sandy CLAY fragments of dolomitic limestone. Completely weathered calcareous MUDSTONE.	
						60.5-67.8	Slightly to faintly weathered light grey/with thinly laminated to very thinly bedded (often cross-laminated and cross-bedded and complexly folded) GYPSUM with occasional (locally abundant) lenticular and nodular dark red-brown and grey mudstone inclusions.	
						67.8-73.7	Completely weathered dark red-brown and occasionally dark brown and grey/dark grey mottled and banded silty calcareous MUDSTONE with a few thin partings and veins of gypsum (often fibrous). Weathered in parts to a firm to stiff clay.	

Detailed information on boreholes used for this study and future isotope studies (continued)

Borehole name	Easting	Northing	Elevation (m AOD)	Total depth (m)	RWL (m bgl)	Geology (number in m bgl)		EA comments
						73.7-100.6	Highly weathered, with occasional completely weathered bands yellow-brown and grey-brown banded, locally thinly and thickly laminated and cross-laminated, oolitic in parts, dolomitic LIMESTONE, very weak to moderately strong to strong with occasional (locally abundant) irregular fractures, and highly broken in parts.	
Stillington OBH4	435500	523450	48.5	115	n.d.	0-12.2	Stiff to very stiff cark brown silty CLAY, with some subangular fine gravel, some subrounded coarse gravel and some small fragments of coal, abundant in places.	Magnesian Limestone borehole, high sulphate unknown reason, nearby boreholes understood to have intersected gypsum.
						12.2-15.5	Brown sandy fine to coarse GRAVEL, subangular to subrounded, with many subangular to subrounded cobbles, with cobbles and boulders becoming abundant below 12.5 m.	
Ketton Hall NRA26	429273	519235	57	60	16	0-41	Boulder CLAY with coal traces at about 30 m below ground level.	Magnesian Limestone borehole, high sulphate unknown reason, understood to be in section which gains and loses at different times of year. Higher pH than expected.
						41-48	Upper Magnesian LIMESTONE (broken)	
Foumarts	432725	530251	~77	~81	n.d.	0-3	SAND, GRAVELS	Magnesian Limestone borehole, very orange water.
						3-5	Boulder CLAY	
						5-14	SAND, GRAVELS	
						14-75	Magnesian LIMESTONE	

Appendix 3 Hydrological data

River survey at D01

The tributary of the River Skerne at D01 was sampled at 10 m intervals from approximately 150 m upstream to about 100 m downstream of the HZ site. Measurements at the nearby pond (432690 530325), and at the confluence of the tributary with the Skerne River (and the Skerne River itself) were included. It needs to be noted that sampling was not undertaken in the same order as shown in Table 9. Instead, the sampling started at the location of the hyporheic zone (HZ) sampling (*River 15*) and continued in downstream direction to the River Skerne (*River 26)*. After a short break of approximately 15 minutes, sampling was undertaken from sample point *River 15* on in upstream direction towards the pond (*River 1)*. The inconsistency in sampling direction and the time delay (*River 14* was measured approximately 1 hour after *River 15*) may have cause slight shifts in the data – especially because it was raining during the time of the survey.

Table 9: Temperature, pH and specific electrical conductivity (SEC) measurements from the river survey at D01.

ID	Site	Grid reference	T (°C)	pH	SEC (µS/cm)
1	Pond on the eastern bank	NZ 32687 30327	14.3	9.49	337
2	River 1 (N from the bridge)	NZ 32678 30308	12.6	7.96	1056
3	River 2 (S from the bridge)	NZ 32682 30307	12.6	7.45	1055
4	River 3 (5m upstream of pond outlet)	NZ 32705 30308	12.4	7.45	1050
5	River 4 (5m downstream of pond outlet)	NZ 32716 30302	13.3	7.42	930
6	River 5	NZ 32727 30297	12.8	7.46	1001
7	River 6	NZ 32736 30293	12.8	7.45	1010
8	River 7	NZ 32746 30289	12.8	7.45	1009
9	River 8	NZ 32758 30282	12.6	7.46	1021
10	River 9	NZ 32769 30276	12.5	7.46	1023
11	River 10	NZ 30781 30271	12.7	7.46	1018
12	River 11	NZ 32792 30266	12.6	7.48	1021
13	River 12	NZ 32802 30260	12.6	7.47	1023
14	River 13	NZ 32812 30256	12.7	7.51	1015
15	River 14	NZ 32822 30252	12.7	7.51	1012
16	River 15 (location of HZ sampling)	NZ 32926 30248	12.5	7.45	1095
17	River 16	NZ 32935 30246	12.4	7.45	1082
18	River 17	NZ 32844 30239	12.4	7.48	1085
19	River 18	NZ 32856 30234	12.4	7.51	1080
20	River 19	NZ 32865 30228	12.3	7.48	1094
21	River 20	NZ 32873 30223	12.4	7.53	1086
22	River 21	NZ 32882 30217	12.3	7.51	1090
23	River 22	NZ 32896 30204	12.3	7.51	1093
24	River 23	NZ 32901 30195	12.3	7.50	1094
25	Confluence w/Skerne	NZ 33019 30011	12.1	7.59	1045
26	Skerne (downstream of confluence)	NZ 33085 30113	11.9	7.56	1039

The main observations were:

1. T, pH, and EC were relatively stable at around 12.5°C, 7.5, and 1050 µS/cm (respectively).

2. The pond (from which water is entering the stream) shows higher temperature (14.3°C) and pH (9.5), and much lower EC (337 µS/cm,) than the stream water.

3. The inflow of the pond water into the stream causes a noticeable increase in temperature (to 13.3°C) and decrease of EC (930 µS/cm) in the stream sample 5 m downstream of the point where pond water enters, but does not increase the pH.

4. T in the River Skerne was slightly lower (11.9°C), and pH slightly higher (7.6) than in the tributary.

5. EC was slightly higher between *River 15* (1095 µS/cm) and *River 28* than between *River 14* (1012 µS/cm) and *River 6*, but this might have been caused by increasing dilution from continuing rainfall (the reach upstream *River 14* was sampled about 1 hour later then *River 15*).

River survey RB

RB and WB both offered a relatively good substrate footing, so that a brief river survey could be conducted by moving up- and downstream of the sampling site. Due to the narrowness of the riverbed, the survey was only conducted along the flow path (and not across). Time constraints and heavy rainfall did not allow for a river survey in WB. The results from the brief survey at RB are shown in Table 10. The measurements were taken from about 2.5 m upstream of the (dry) sampling point MP to about 4 m downstream of MP. The distance between measurement varied between 1 to 2 m because the footing at the desired distance was not always safe.

Table 10: Temperature, pH and specific electrical conductivity (SEC) measurements from the river survey at RB.

ID	Site	T (°C)	pH	SEC (µS/cm)	DO (mg/L)	Eh (mV)
1	2.5 m upstream of MP	14.53	6.92	797	4.26	463
2	1.5 m upstream of MP	14.53	7.35	803	6.20	374
3	MP	14.53	7.22	828	5.61	317
4	1.5 m downstream of MP	14.52	7.18	831	5.57	291
5	3 m downstream of MP (below bridge)	14.53.	7.18	832	5.67	300
6	5 m downstream of MP (below bridge)	14.53	7.17	834	5.70	302
7	7 m downstream of MP	14.50	7.41	842	5.76	301

Appendix 4 Meteorological and river stage data

Location of rainfall monitoring station and river gauging stations near the HZ monitoring points

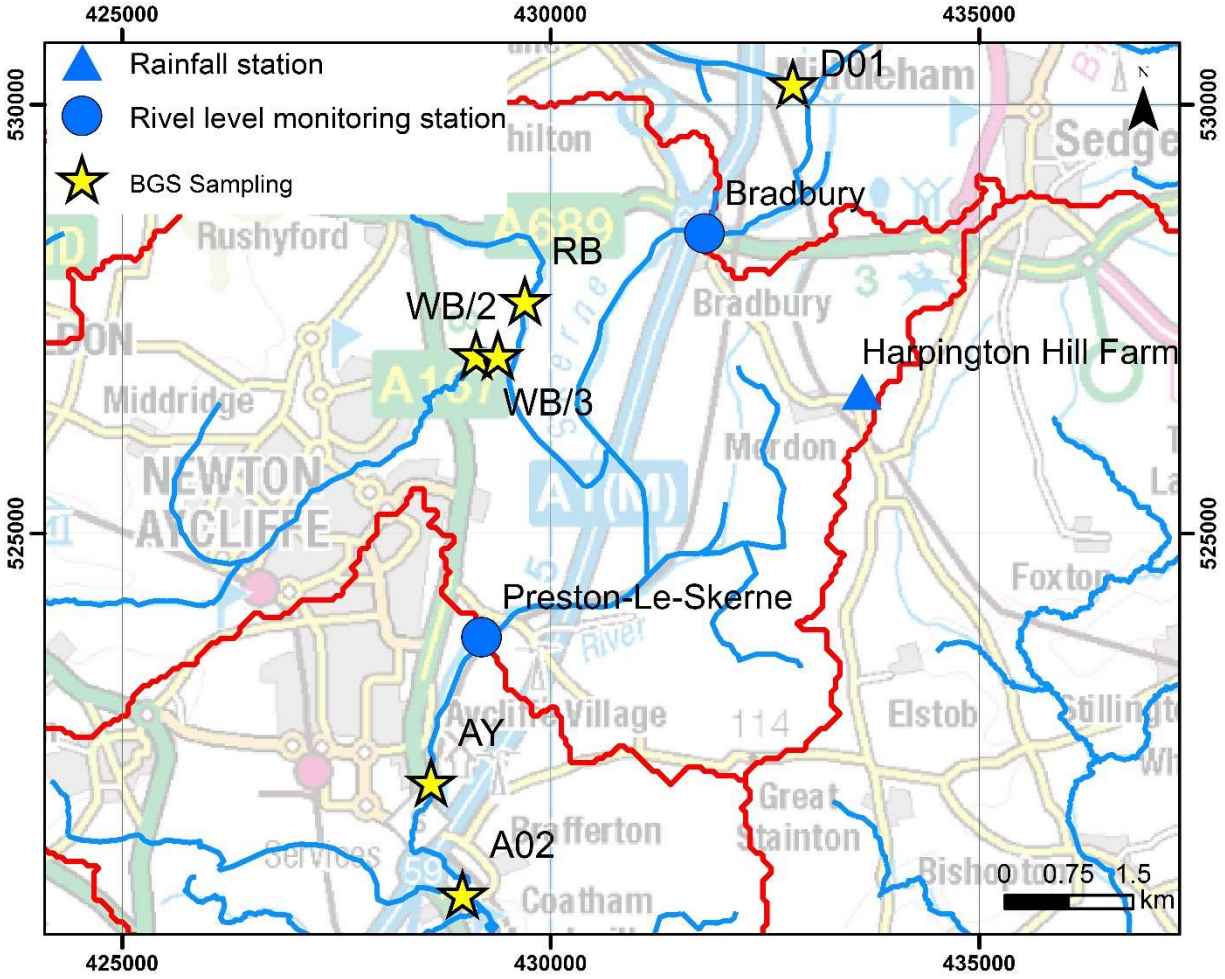

Contains Ordnance Survey data © Crown Copyright and database rights 2019. Ordnance Survey Licence no. 100021290.

Detailed figure showing precipitation and river level data at the HZ monitoring point D01 during, and seven days prior to sampling

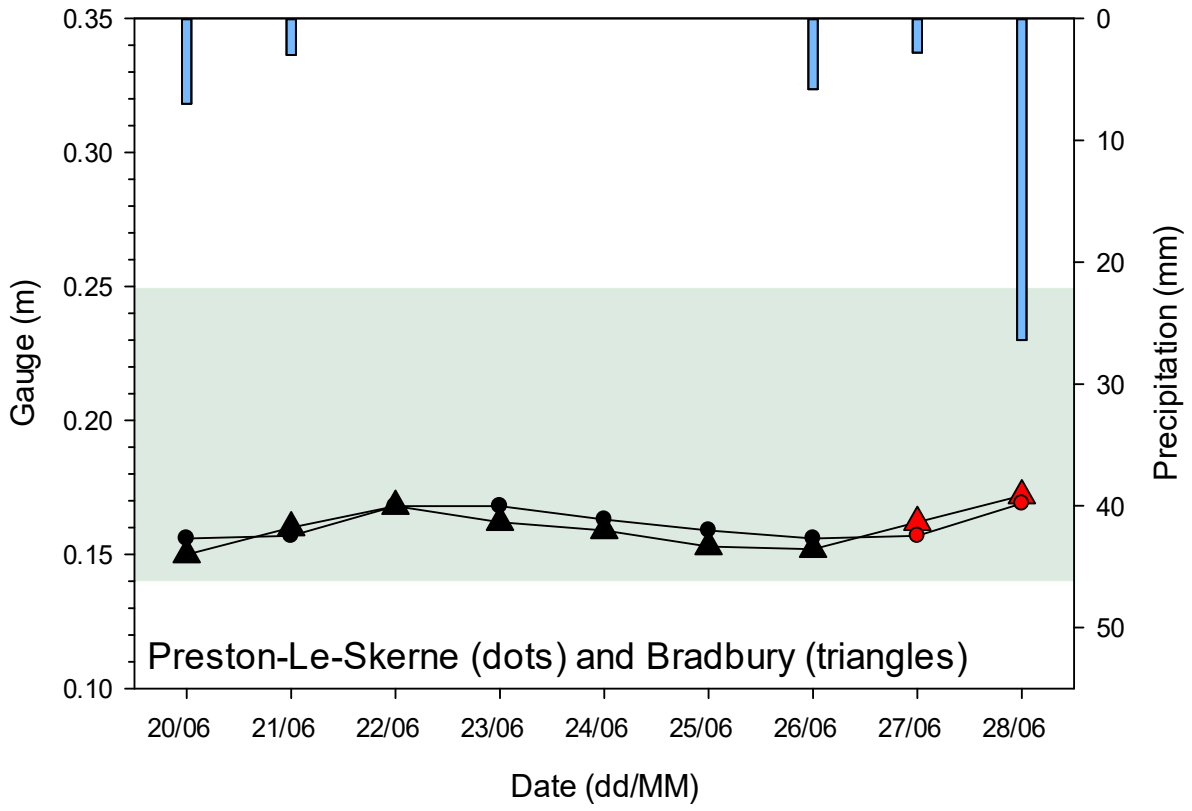

Water levels at Bradbury monitoring station from 20-28th June 2017. Red dots indicate the days on which sampling took place and green shading refers to the normal water level in average weather conditions.

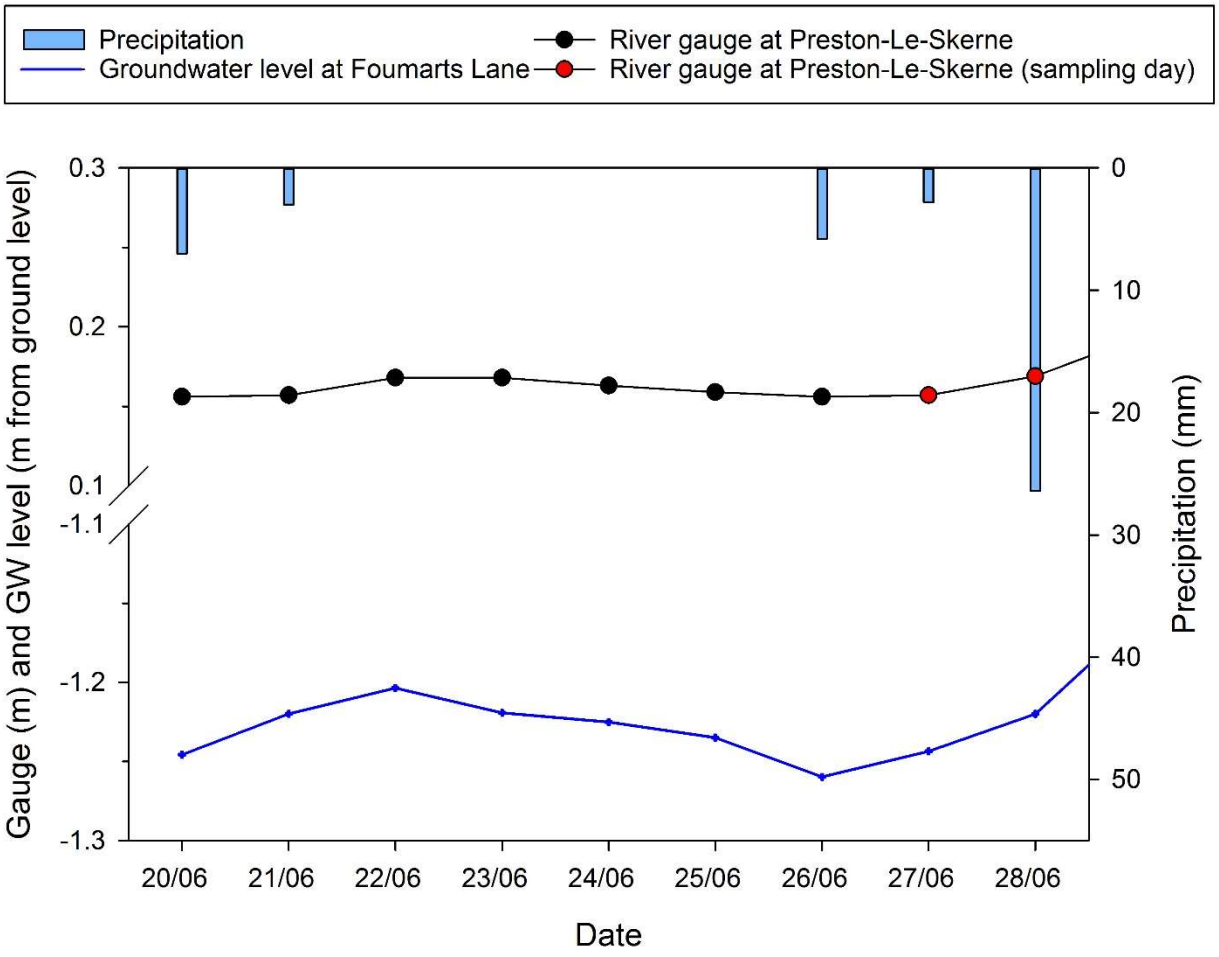

Precipitation data, water levels at Preston-Le-Skerne monitoring station, and groundwater levels at Foumarts Lane Borehole from 20-28th June 2017.

Detailed figure showing precipitation and river level data at Preston-Le-Skerne during, and seven days prior to sampling at A02

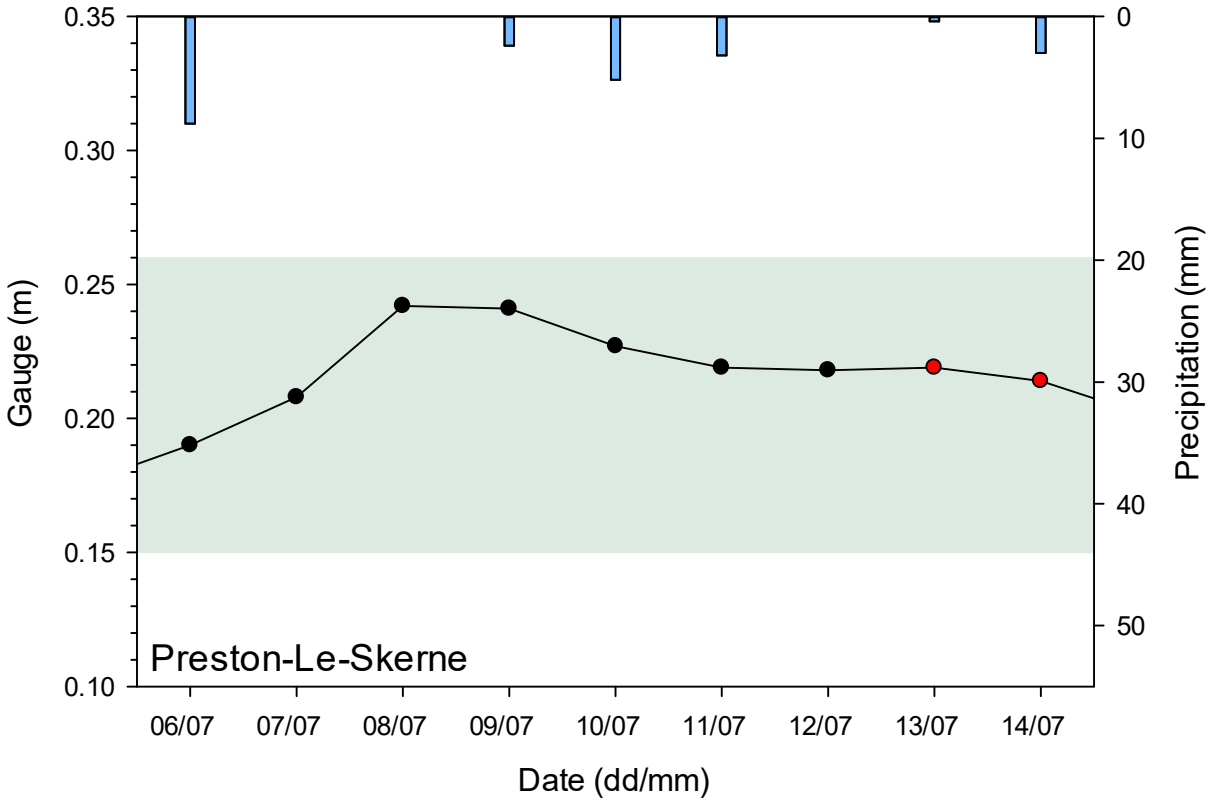

Water levels at Preston-Le-Skerne monitoring station from 6-14th September 2017. Red dots indicate the days on which sampling took place and green shading refers to the normal water level in average weather conditions.

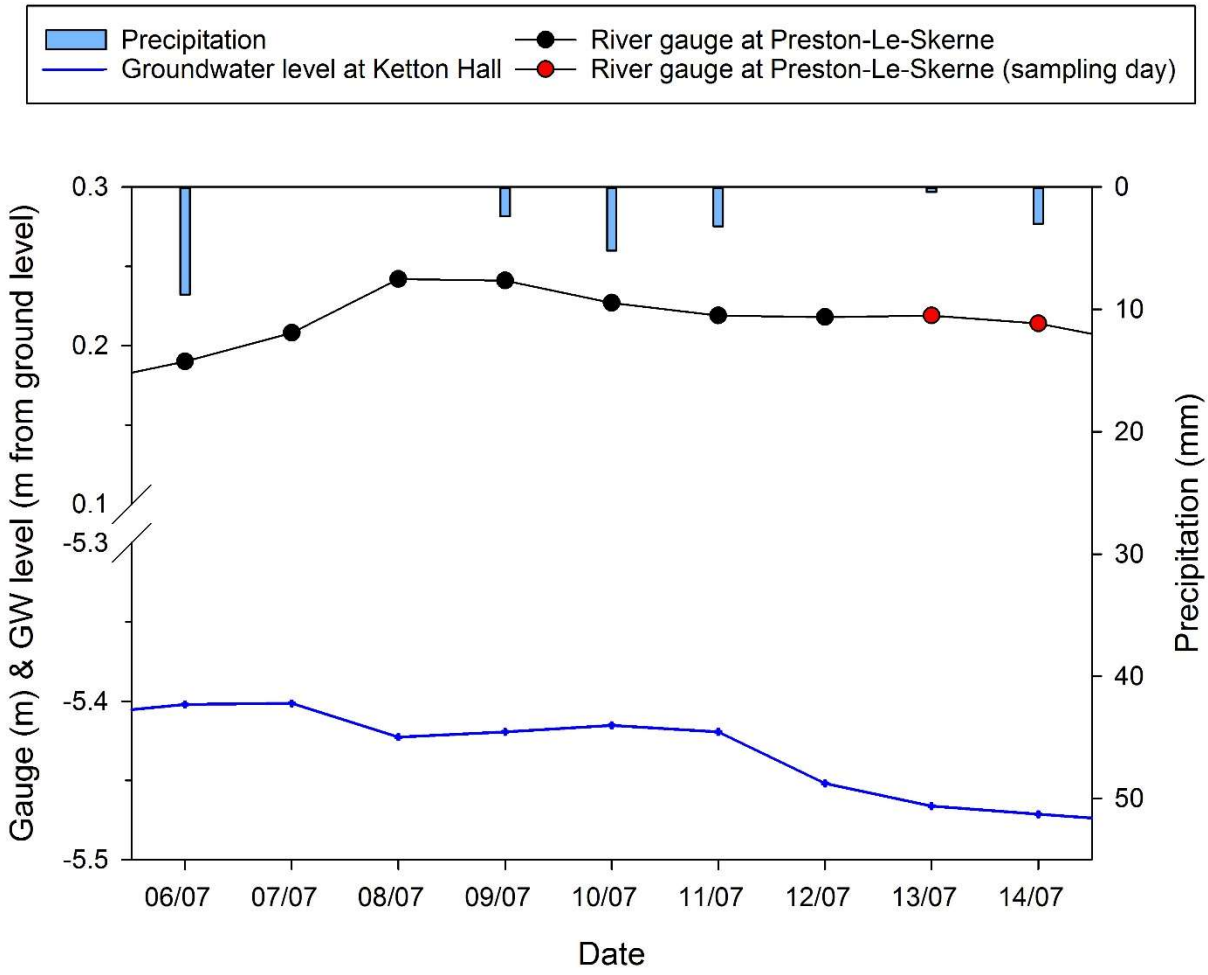

Precipitation data, water levels at Preston-Le-Skerne monitoring station, and groundwater levels at Ketton Hall Borehole from 6-14th July 2017.

Detailed figure showing precipitation and river level data at Preston-Le-Skerne during, and seven days prior to sampling at RB/WB

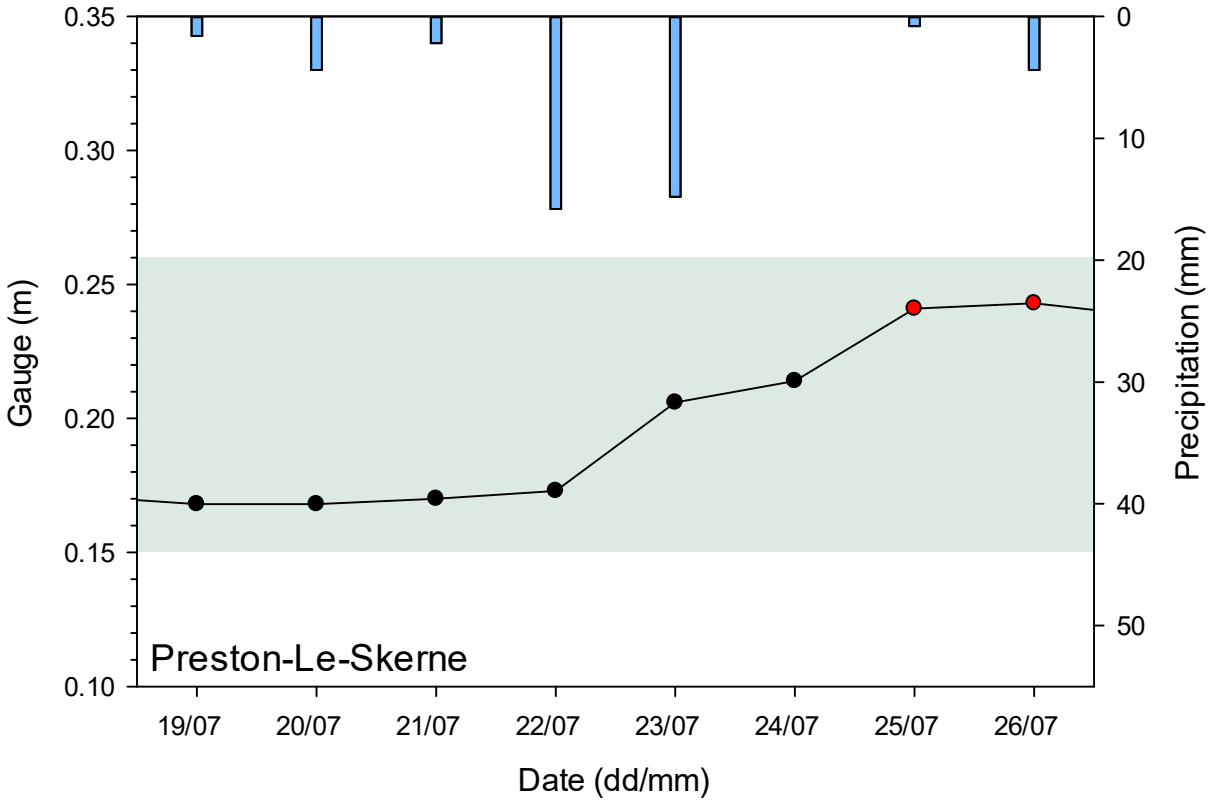

Water levels at Preston-Le-Skerne monitoring station from 18-26th September 2017. Red dots indicate the days on which sampling took place and green shading refers to the normal water level in average weather conditions.

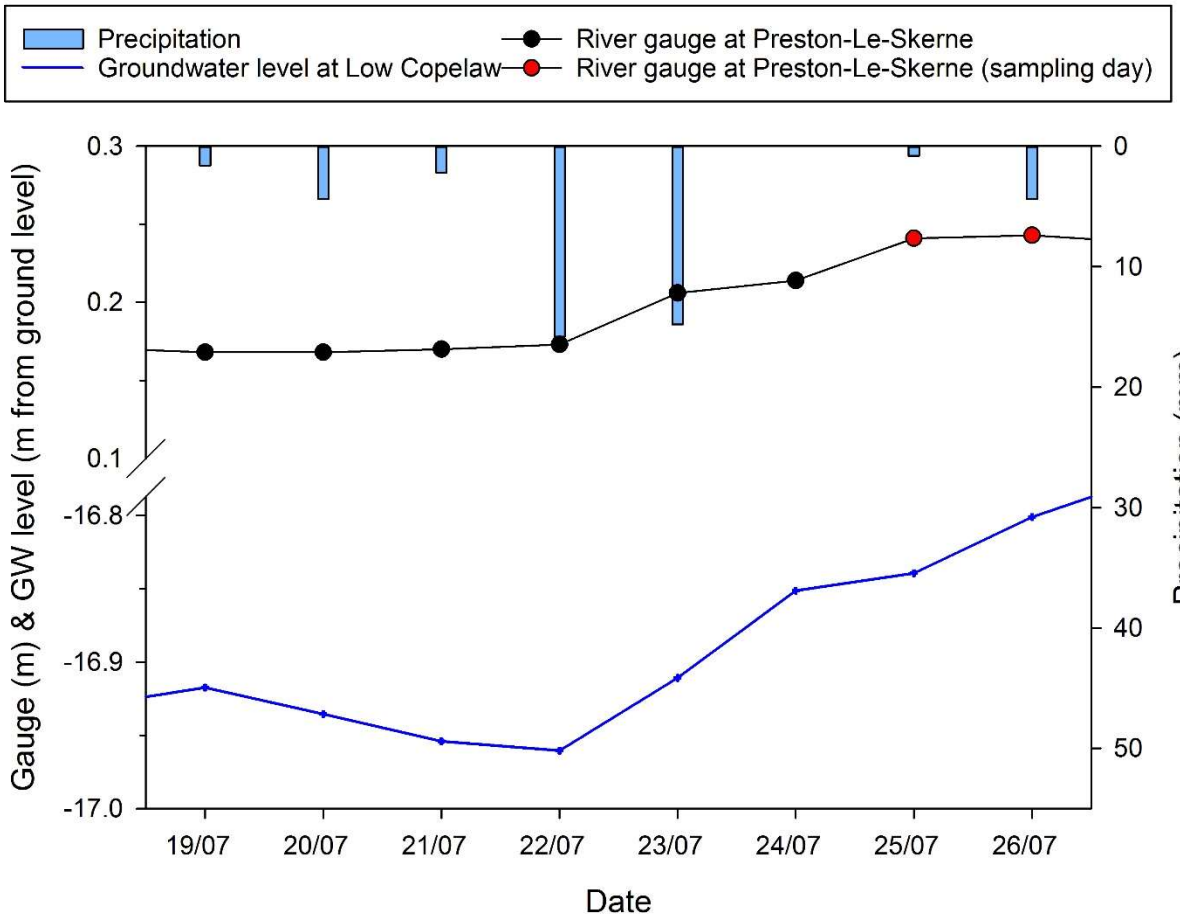

Precipitation data, water levels at Preston-Le-Skerne monitoring station, and groundwater levels at Low Copelaw No2 Borehole from 19-26th July 2017.

Detailed figure showing precipitation and river level data at Preston-Le-Skerne during, and seven days prior to sampling at AY

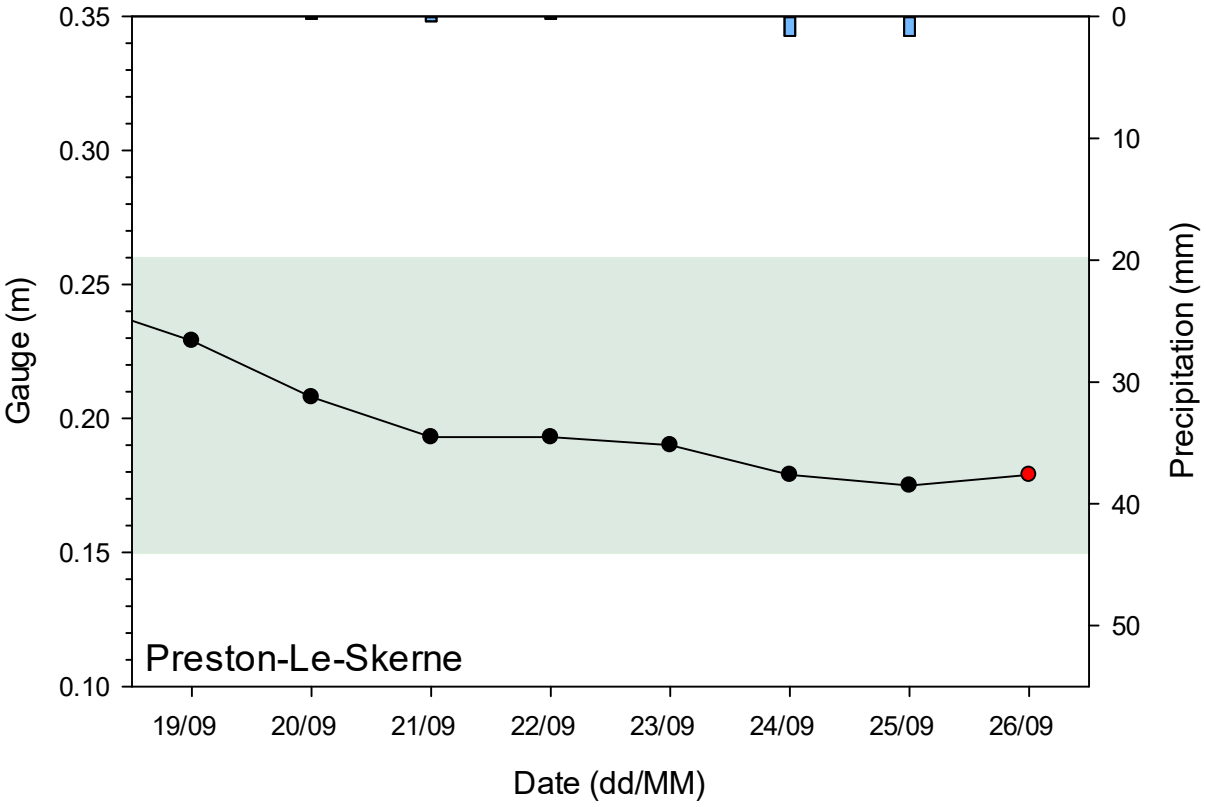

Water levels at Preston-Le-Skerne monitoring station from 19-26th September 2017. Red dots indicate the days on which sampling took place and green shading refers to the normal water level in average weather conditions.

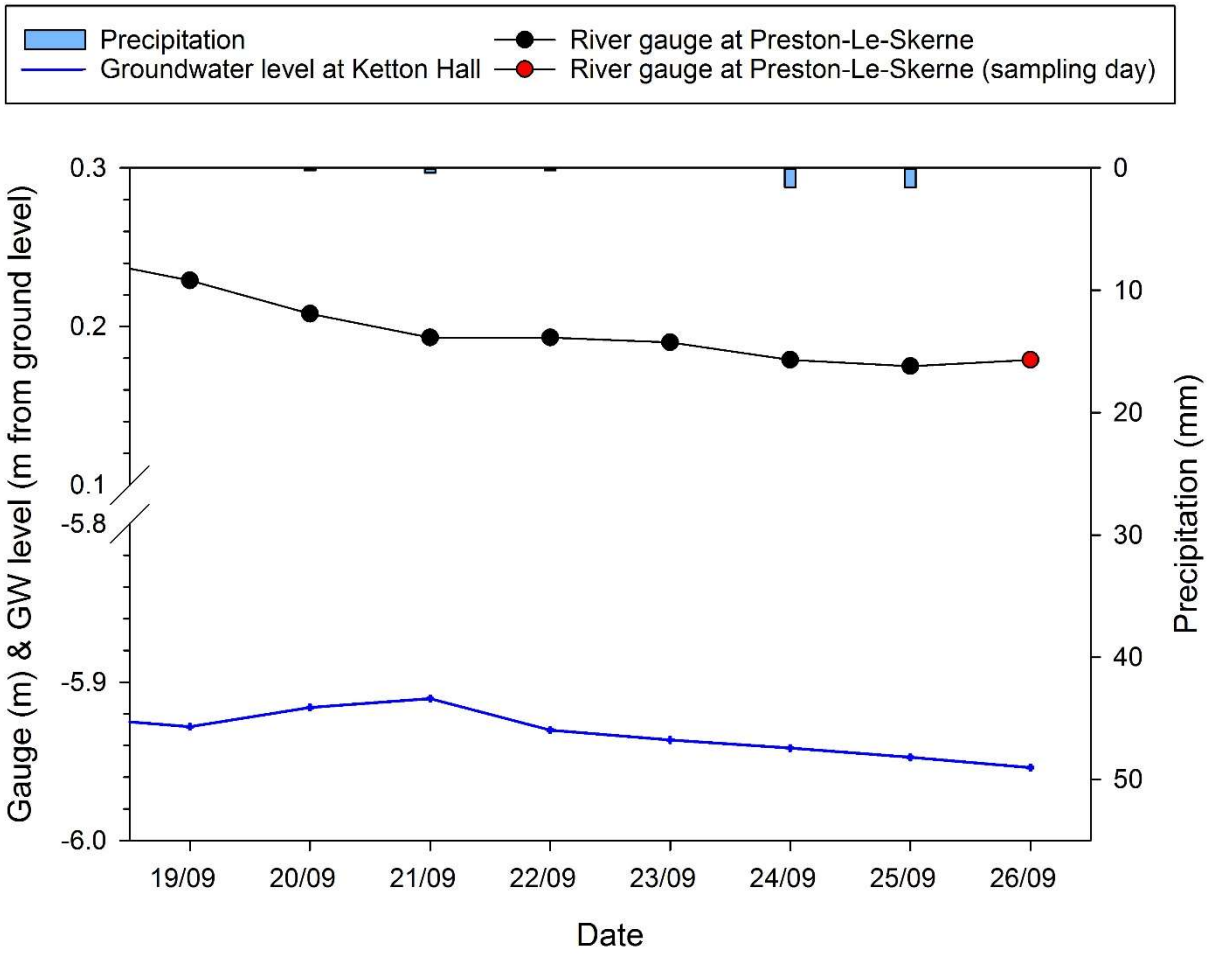

Precipitation data, water levels at Preston-Le-Skerne monitoring station, and groundwater levels at Ketton Hall Borehole from 19-26th September 2017.

Appendix 5 Cluster analysis

In order to group the samples with similar characteristics, hierarchical clustering of the 97 samples (11 GW, 17 SW, 66 HZ and 3 shallow GW) was carried out based on the geochemical data set consisting of the following elements Ca, Mg, Na, K, HCO_3, Cl, SO_4, F, Si, Ba, Sr, Mn, Fe, Li, B, Rb, U. By omitting nitrate and phosphate, potential differences among water samples due to point source anthropogenic inputs were ignored. The samples were clustered using Euclidean distance and the Ward's Linkage method. The data were standardised to convert all variables to a common scale by subtracting the means and dividing by the standard deviation before the distance matrix was calculated, to minimize the effect of scale differences. The resulting dendrogram suggested the existence of 4 distinct clusters in the data.

The results of the cluster analysis group the samples as follows:

Cluster 1, the lowest in SO_4 is made up mostly by HZ samples from D01. Borehole Foumarts lane is also part of cluster 1. The composition of Stillington and the Quarry GW fits in cluster 1.
Cluster 2, the highest in SO_4, groups the SW and GW at Woodham burn site. Only 3 HZ samples from Woodham Burn fall into the cluster.
Cluster 3, the lowest in Fe and highest in Cl, is made up by HZ samples from A02 and A03, plus SW from all sites except for WB. The boreholes: Low Copelaw, Stillington OBH2 and Ketton Hall are also part of this cluster.
Cluster 4, the highest in Fe, is made up entirely by HZ samples; they are from D01, RB and WB 2 and 3.

Table 11: Cluster Analysis of Observations: Ca, Mg, Na, K, HCO3, Cl, SO4, F, Si, Ba, Sr, Mn, Fe, Li, B, Rb, U

Standardized Variables, Euclidean Distance, Ward Linkage
Amalgamation Steps

Step	Number of clusters	Similarity level	Distance level	Clusters joined		New cluster	Number of obs. in new cluster
1	96	99.348	0.1244	89	90	89	2
2	95	99.182	0.1562	64	94	64	2
3	94	99.030	0.1851	20	21	20	2
4	93	98.955	0.1996	83	84	83	2
5	92	98.803	0.2286	71	72	71	2
6	91	98.623	0.2628	64	93	64	3
7	90	98.566	0.2737	40	85	40	2
8	89	98.399	0.3056	87	88	87	2
9	88	98.366	0.3119	74	75	74	2
10	87	98.313	0.3221	35	36	35	2
11	86	98.284	0.3276	67	68	67	2
12	85	98.188	0.3459	57	91	57	2
13	84	97.930	0.3953	64	92	64	4
14	83	97.906	0.3998	23	25	23	2
15	82	97.146	0.5448	50	51	50	2
16	81	97.044	0.5643	65	70	65	2
17	80	96.956	0.5812	16	17	16	2
18	79	96.771	0.6165	40	96	40	3
19	78	96.747	0.6211	66	69	66	2
20	77	96.722	0.6259	46	47	46	2
21	76	96.594	0.6502	15	19	15	2
22	75	96.574	0.6541	63	89	63	3
23	74	96.378	0.6916	67	74	67	4
24	73	96.203	0.7250	40	41	40	4
25	72	96.162	0.7328	81	82	81	2
26	71	95.882	0.7862	57	87	57	4
27	70	95.874	0.7878	42	43	42	2
28	69	95.767	0.8081	27	28	27	2
29	68	95.575	0.8449	71	76	71	3

30	67	95.418	0.8748	31	32	31	2
31	66	95.341	0.8896	66	67	66	6
32	65	94.935	0.9670	65	73	65	3
33	64	94.710	1.0100	40	83	40	6
34	63	94.304	1.0875	54	58	54	2
35	62	94.132	1.1204	14	18	14	2
36	61	94.038	1.1383	34	44	34	2
37	60	93.987	1.1480	45	46	45	3
38	59	93.447	1.2511	71	77	71	4
39	58	93.102	1.3169	12	16	12	3
40	57	92.831	1.3688	14	15	14	4
41	56	92.503	1.4313	55	60	55	2
42	55	92.318	1.4667	20	23	20	4
43	54	92.053	1.5173	35	39	35	3
44	53	91.994	1.5285	63	78	63	4
45	52	91.895	1.5475	13	33	13	2
46	51	91.894	1.5476	49	50	49	3
47	50	91.653	1.5936	7	8	7	2
48	49	91.619	1.6002	53	54	53	3
49	48	91.418	1.6385	37	38	37	2
50	47	90.381	1.8364	81	95	81	3
51	46	90.297	1.8526	57	97	57	5
52	45	90.029	1.9038	45	48	45	4
53	44	89.374	2.0288	49	52	49	4
54	43	89.335	2.0362	57	80	57	6
55	42	89.141	2.0732	66	71	66	10
56	41	89.139	2.0737	20	24	20	5
57	40	88.559	2.1845	13	29	13	3
58	39	88.396	2.2155	12	31	12	5
59	38	86.126	2.6488	53	55	53	5
60	37	84.911	2.8810	34	35	34	5
61	36	84.906	2.8818	37	42	37	4
62	35	84.889	2.8851	5	11	5	2
63	34	84.885	2.8858	4	9	4	2
64	33	84.089	3.0379	64	86	64	5
65	32	83.879	3.0779	56	59	56	2
66	31	83.595	3.1321	12	30	12	6
67	30	83.132	3.2205	5	6	5	3
68	29	82.864	3.2717	62	63	62	5
69	28	81.109	3.6067	65	66	65	13
70	27	80.403	3.7415	26	27	26	3
71	26	80.179	3.7844	40	79	40	7
72	25	79.538	3.9067	12	13	12	9
73	24	76.280	4.5288	1	4	1	3
74	23	73.170	5.1226	34	37	34	9
75	22	72.564	5.2383	1	14	1	7
76	21	69.780	5.7698	26	61	26	4
77	20	67.206	6.2612	40	81	40	10
78	19	61.565	7.3382	3	57	3	7
79	18	60.110	7.6159	12	20	12	14
80	17	56.493	8.3065	7	10	7	3
81	16	54.374	8.7112	45	56	45	6
82	15	53.950	8.7920	40	64	40	15
83	14	53.511	8.8760	1	12	1	21
84	13	47.394	10.0438	3	62	3	12
85	12	40.650	11.3313	5	40	5	18
86	11	38.919	11.6619	22	26	22	5
87	10	32.041	12.9750	5	34	5	27
88	9	30.987	13.1762	22	53	22	10
89	8	23.173	14.6681	22	49	22	14
90	7	14.942	16.2396	3	7	3	15
91	6	10.571	17.0743	22	45	22	20
92	5	-28.449	24.5240	5	65	5	40
93	4	-30.272	24.8721	2	3	2	16
94	3	-53.912	29.3855	1	22	1	41
95	2	-215.962	60.3250	1	2	1	57
96	1	-269.272	70.5032	1	5	1	97

Table 12: Final Partition

Number of clusters: 4

	Number of observations	Within cluster sum of squares	Average distance from centroid	Maximum distance from centroid
Cluster1	21	78.288	1.78221	3.5864
Cluster2	16	346.658	3.51770	13.8839
Cluster3	40	187.734	2.02813	4.6970
Cluster4	20	273.334	3.37690	8.2868

Table 13: Cluster Centroids

Variable	Cluster1	Cluster2	Cluster3	Cluster4	Grand centroid
Ca	-0.29873	1.52029	-0.769259	0.63595	0.0000000
Mg	-0.57277	1.71039	-0.526204	0.28550	0.0000000
Na	-0.39144	1.17490	-0.091308	-0.34630	-0.0000000
K	-1.02615	0.66752	0.660626	-0.77781	0.0000000
HCO3	0.44058	0.65433	-0.811225	0.63638	-0.0000000
Cl	-0.86318	0.16744	0.800143	-0.82790	-0.0000000
SO4	-0.68305	1.80709	-0.394996	0.06152	-0.0000000
F	0.97720	-0.78276	-0.028940	-0.34197	0.0000000
Si	0.39814	-0.38777	-0.713147	1.31846	0.0000000
Ba	-0.40305	-0.45378	-0.284298	1.35483	0.0000000
Sr	-0.11438	1.09485	-0.357272	-0.04124	-0.0000000
Mn	0.45261	-0.72475	-0.504132	1.11282	0.0000000
Fe	-0.20735	-0.14165	-0.272945	0.87693	-0.0000000
Li	-0.03290	1.66957	-0.544793	-0.21153	-0.0000000
B	0.16706	0.24457	-0.281479	0.19189	0.0000000
Rb	-0.64409	0.56723	0.331070	-0.43963	0.0000000
U	-0.61947	1.29190	-0.047101	-0.28887	0.0000000

Distances Between Cluster Centroids

	Cluster1	Cluster2	Cluster3	Cluster4
Cluster1	0.00000	5.97894	3.54363	3.12183
Cluster2	5.97894	0.00000	5.39920	5.51260
Cluster3	3.54363	5.39920	0.00000	4.65386
Cluster4	3.12183	5.51260	4.65386	0.00000

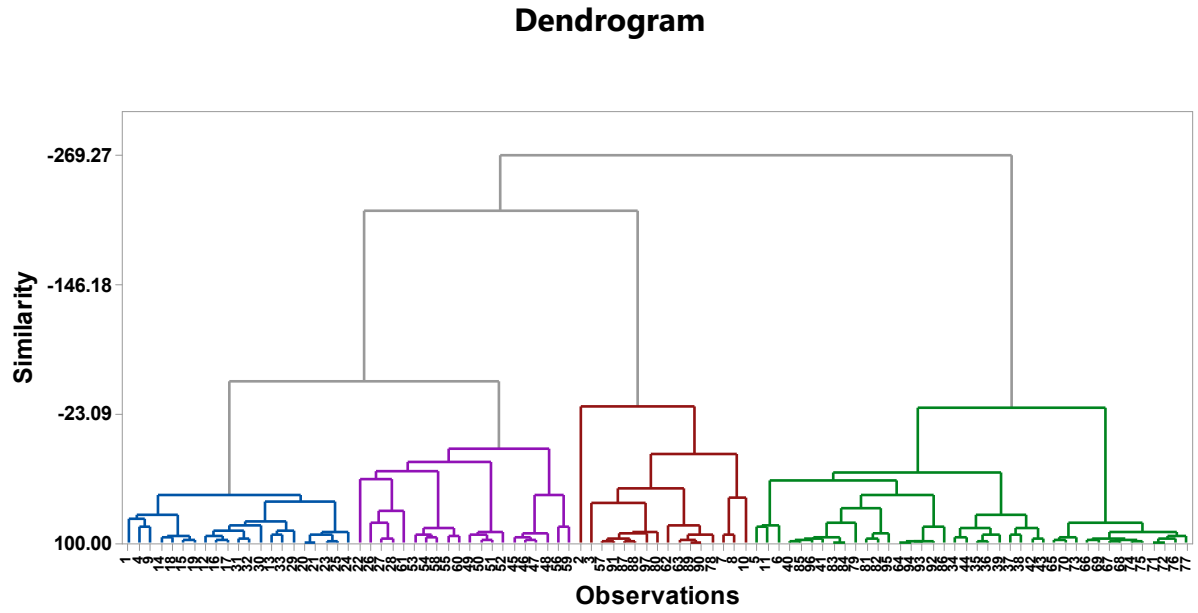

Figure 66: Cluster Observation Dendrogram showing the manner in which the different clusters of observations were formed and the composition of each cluster (observations: samples of GW, SW, HZ; variables: Ca, Mg, Na, K, HCO_3, Cl, SO_4, F, Si, Ba, Sr, Mn, Fe, Li, B, Rb, U; number of clusters: 4. Cluster analysis method: standardized variables, Euclidean distance, Ward Linkage; amalgamation steps). Cluster 1: blue; Cluster 2: red; Cluster 3: green; Cluster 4: pink.

Table 14: Composition of each cluster

ID	Cluster 1
1	Foumarts Borehole
4	Stillington OBH4 BOREHOLE
9	Quarry AYQ
12	D01 ML1B/black
13	D01 ML1B/red
14	D01 ML1B/green
15	D01 ML1B/yellow
16	D01 ML1B/black 28 June
17	D01 ML1B/red 28 June
18	D01 ML1B/green 28 June
19	D01 ML1B/yellow28 June
20	D01 MP1
21	D01 MP1/3sample
23	D01 MP2b
24	D01 MP2c
25	D01 MP2d
29	D01 ML2B/yellow
30	D01 ML1G/black
31	D01 ML1G/red
32	D01 ML1G/green
33	D01 ML1G/yellow

ID	Cluster 2
2	Stony Hall C BOREHOLE
3	Stony Hall L BOREHOLE
7	N1_SEEPAGE_5.1
8	N1_SEEPAGE_5.2
10	Bullrushes water
57	WB/2 ML2 Black
62	WB/3 MP1
63	WB/3 MP2
78	DRAIN 3_5.1
80	DRAIN 2_5.1
87	WB/1 SW
88	WB/2 SW
89	WB/3 SW
90	WB/3 SW dupl
91	WB/2 SW dupl
97	WOODHAM BURN at BENCH SITE

ID	Cluster 3
81	D01 RIVER 27/6/17
82	D01 RIVER 28/6
83	A02 Surface water
84	A02 Surface water
34	A02 MP 1 GREEN (1st time dup)
35	A02 MP 1 GREEN (2nd time dup)
36	A02 MP 1 GREEN (3rd time dup)
37	A02 MP 4 BLACK
38	A02 MP 4 BLACK (time dup)
39	A02 MP 2 BLACK
85	A02 Surface water
40	A02 ML/ BLACK
41	A02 ML/ RED
42	A02 ML/ GREEN
43	A02 ML/ YELLOW
44	A02 MP1 GREEN- new place
11	Low Copelaw BOREHOLE
5	Stillington OBH2 BOREHOLE
6	Ketton Hall BOREHOLE
86	RB/SW
92	A03_AQ SW 9:45
64	A03_AQ ML4R Black
65	A03_AQ ML4R Red
66	A03_AQ ML4R Green
67	A03_AQ ML4R Yellow
70	A03_AQ ML2G Black
71	A03_AQ ML2G Red

72	A03_AQ ML2G Green
73	A03_AQ ML2G Yellow
93	A03_AQ SW 12:00
74	A03_AQ MP1Y
75	A03_AQ MP1Y REP
76	A03_AQ MP2Y
94	A03_AQ SW 16:00
77	A03_AQ MP2R
68	A03_AQ ML4R Yellow REP
69	A03_AQ ML4R Green REP
79	DRAIN 1_5.1
95	BRAD.B
96	A02

ID	Cluster 4
22	D01 MP2a
26	D01 ML2B/black
27	D01 ML2B/red
28	D01 ML2B/green
45	RB/ML Black
46	RB/ML Red
47	RB/ML Green
48	RB/ML Yellow
49	WB/3 ML Black
50	WB/3 ML Red
51	WB/3 ML Green
52	WB/3 ML Yellow
53	WB/2 ML1 Black
54	WB/2 ML1 Red
55	WB/2 ML1 Green
56	WB/2 ML1 Yellow
58	WB/2 ML2 Red
59	WB/2 ML2 Green
60	WB/2 ML2 Yellow
61	WB/2 MP1

Table 15: Descriptive Statistics of selected elements by clusters: Ca, Na, Cl, SO_4, F, Fe, Mn, Ba, U

Variable	Clusters	N	N*	Mean	Minimum	Q1	Median	Q3	Maximum
Ca mg/l	1	21	0	103.61	86.00	92.30	101.90	109.85	145.20
	2	16	0	183.08	125.20	145.82	183.45	204.98	263.10
	3	40	0	83.05	5.00	79.25	88.50	93.80	110.80
	4	20	0	144.44	100.30	138.42	143.30	160.10	172.10
Na mg/l	1	21	0	43.00	16.00	37.85	46.60	48.45	52.80
	2	16	0	90.5	59.2	64.6	71.0	82.5	303.9
	3	40	0	52.11	21.10	46.50	52.80	58.17	77.60
	4	20	0	44.38	28.40	38.85	46.20	50.60	57.60
Cl mg/l	1	21	0	42.36	25.00	33.95	41.76	50.02	61.09
	2	16	0	61.67	36.80	54.98	64.84	69.26	78.44
	3	40	0	73.52	21.08	69.15	73.94	77.80	97.80
	4	20	0	43.02	22.17	28.96	39.12	61.40	68.74
SO4 mg/l	1	21	0	52.87	0.67	3.33	59.34	96.73	125.20
	2	16	0	522.1	265.1	332.1	503.6	658.8	839.8
	3	40	0	107.15	27.09	68.79	111.65	134.80	168.14
	4	20	0	193.2	1.9	68.2	265.4	312.1	385.7
F mg/l	1	21	0	0.7971	0.4795	0.6268	0.7641	0.9405	1.4112
	2	16	0	0.3503	0.1250	0.3196	0.3686	0.3940	0.4826
	3	40	0	0.5417	0.1000	0.3593	0.5376	0.7420	0.8981
	4	20	0	0.4622	0.2197	0.2797	0.3702	0.6281	1.0290
Fe ug/l	1	21	0	376	4	12	46	236	2455
	2	16	0	552	1	8	26	76	5192
	3	40	0	200.3	5.0	16.0	39.5	88.5	3466.0
	4	20	0	3282	5	39	224	7180	18814
Mn ug/l	1	21	0	1071	1	552	1256	1439	2512
	2	16	0	173.7	1.0	54.3	70.5	209.3	847.4
	3	40	0	341.8	10.6	22.5	102.1	529.1	1775.3
	4	20	0	1574	764	1063	1331	2042	3358
Ba ug/l	1	21	0	72.16	31.70	40.40	51.20	99.40	197.10
	2	16	0	66.7	12.2	27.3	56.5	70.7	244.9
	3	40	0	85.05	1.50	60.63	90.00	116.15	134.50
	4	20	0	263.0	74.5	153.9	190.2	436.0	588.0
U ug/l	1	21	0	0.599	0.003	0.069	0.540	0.930	1.582
	2	16	0	3.340	0.150	2.611	3.141	3.838	10.753
	3	40	0	1.420	0.020	1.065	1.238	1.544	4.660
	4	20	0	1.073	0.187	0.438	0.766	1.962	2.239

Appendix 6 Additional plots of analytical results

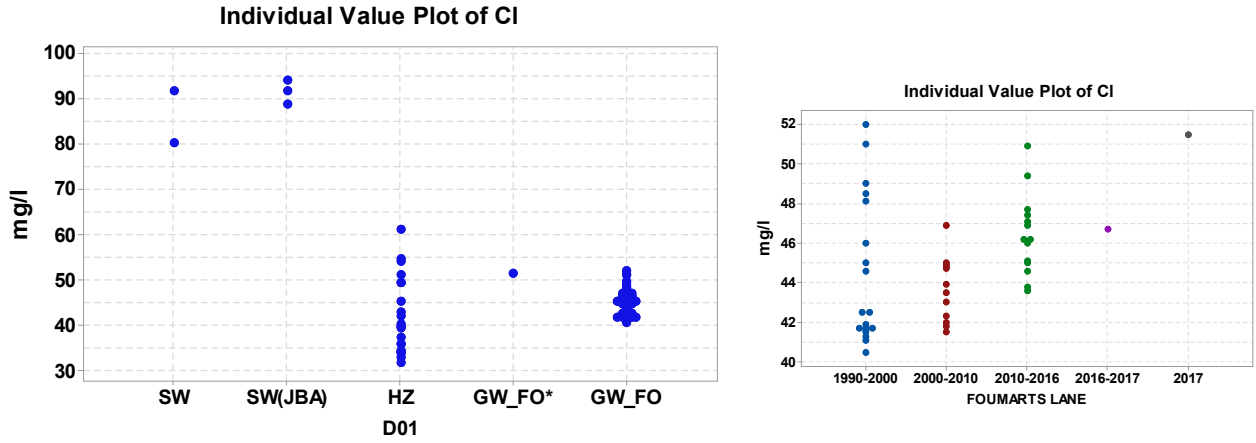

GW_FO=FOUMARTS LANE

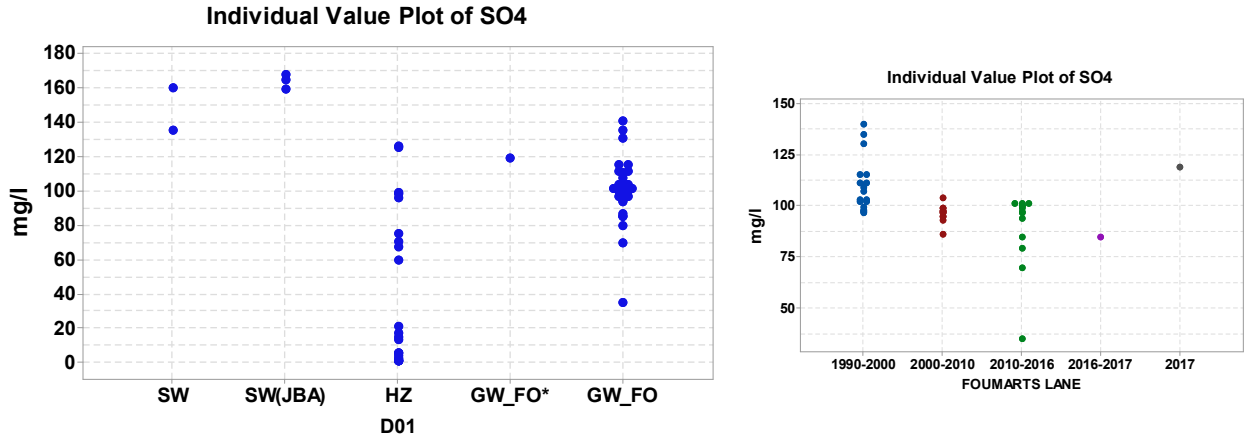

GW_FO=FOUMARTS LANE

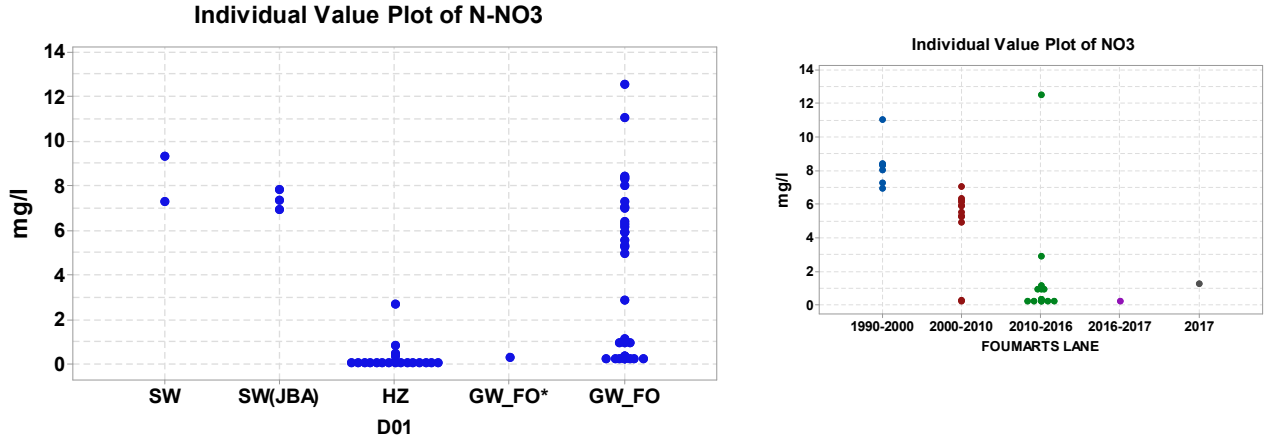

GW_FO=FOUMARTS LANE

Figure 67: Left: Individual value plot of Cl, SO_4 and NO_3 (mg/l) distribution in surface water (SW), hyporheic porewater (HZ) and groundwater (GW) at site D01. GW_FO = EA data for BOREHOLE 25-3-330 FOUMARTS LANE (date of collection 10/6/1992 to 27/2/2017). GW_FO* = BGS data of BOREHOLE 25-3-330 FOUMARTS LANE collected at the same time of SW/HZ. SW(JBA) = EA/JBA surface water data (collected on 24/1, 27/2 and 31/5 2017). Right: Distribution in BOREHOLE 25-3-330 FOUMARTS LANE groundwater across years of sampling.

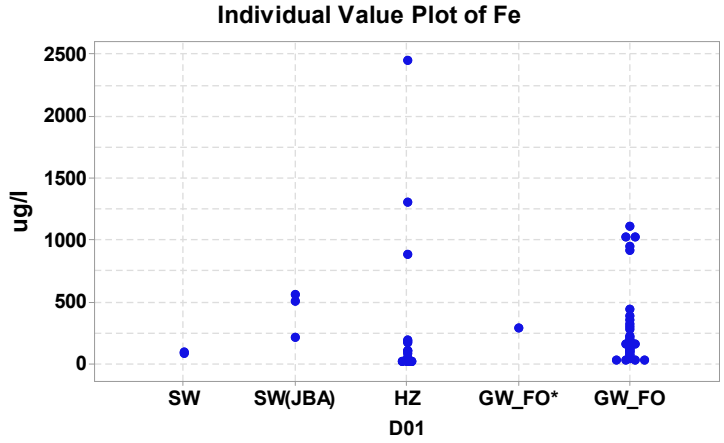

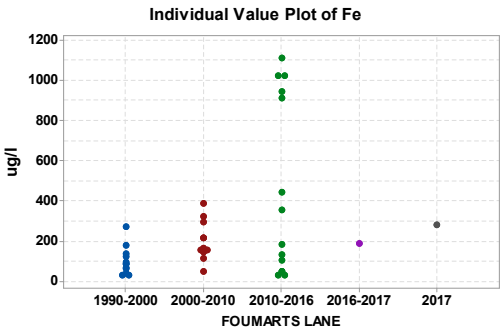

GW_FO=FOUMARTS LANE

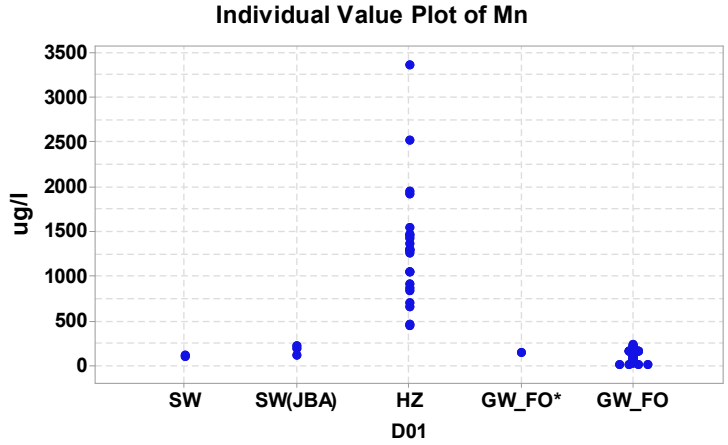

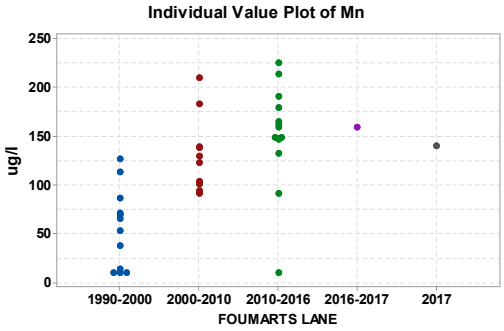

GW_FO=FOUMARTS LANE

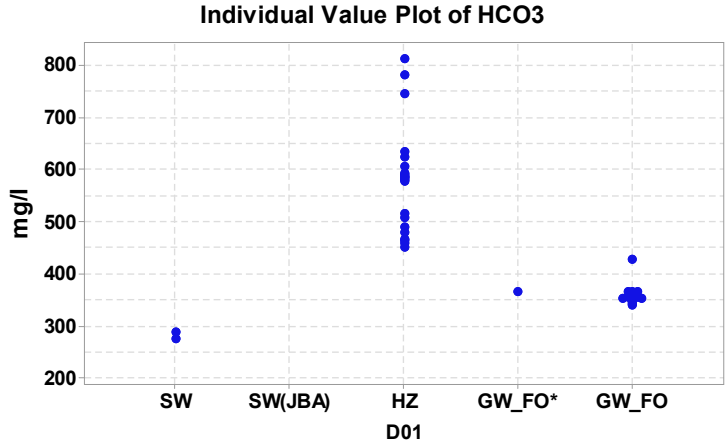

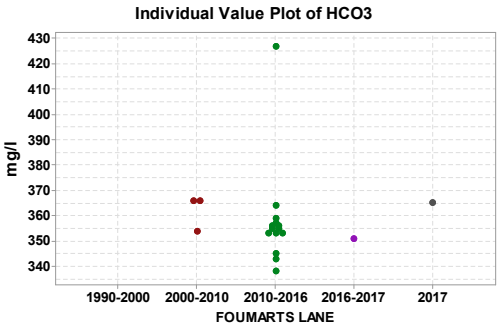

GW_FO=FOUMARTS LANE

Figure 68: Left: Individual value plot of Fe, Mn, HCO_3 distribution in surface water (SW), hyporheic porewater (HZ) and groundwater (GW) at site D01. GW_FO = EA data for BOREHOLE 25-3-330 FOUMARTS LANE (date of collection 10/6/1992 to 27/2/2017). GW_FO* = BGS data of BOREHOLE 25-3-330 FOUMARTS LANE collected at the same time of SW/HZ. SW(JBA) = EA/JBA surface water data (collected on 24/1, 27/2 and 31/5 2017). Right: Distribution in BOREHOLE 25-3-330 FOUMARTS LANE groundwater across years of sampling.

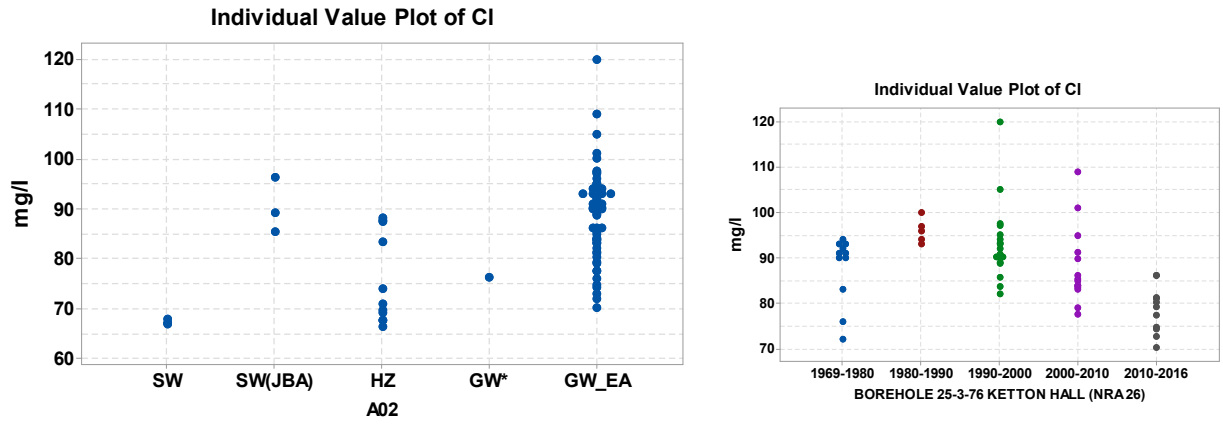

Borehole Ketton hall

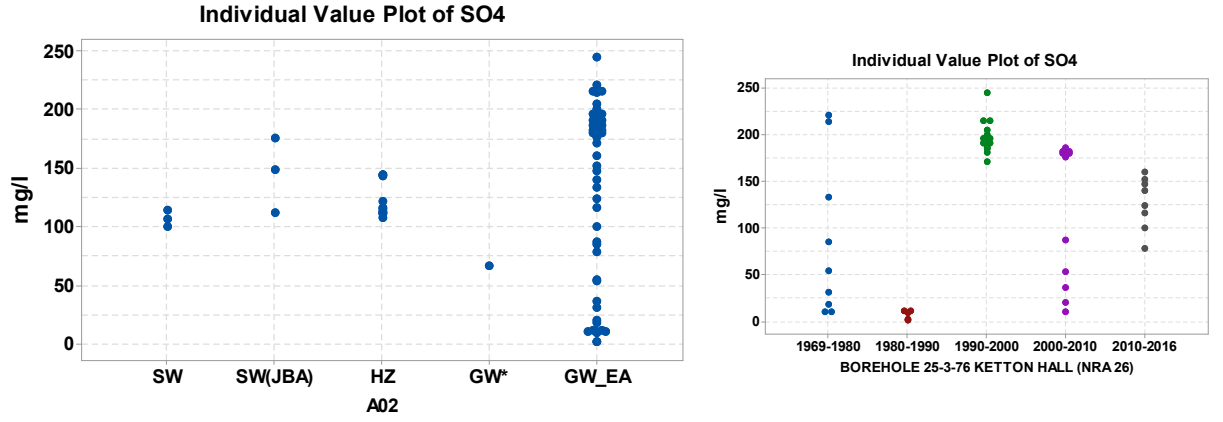

Borehole Ketton hall

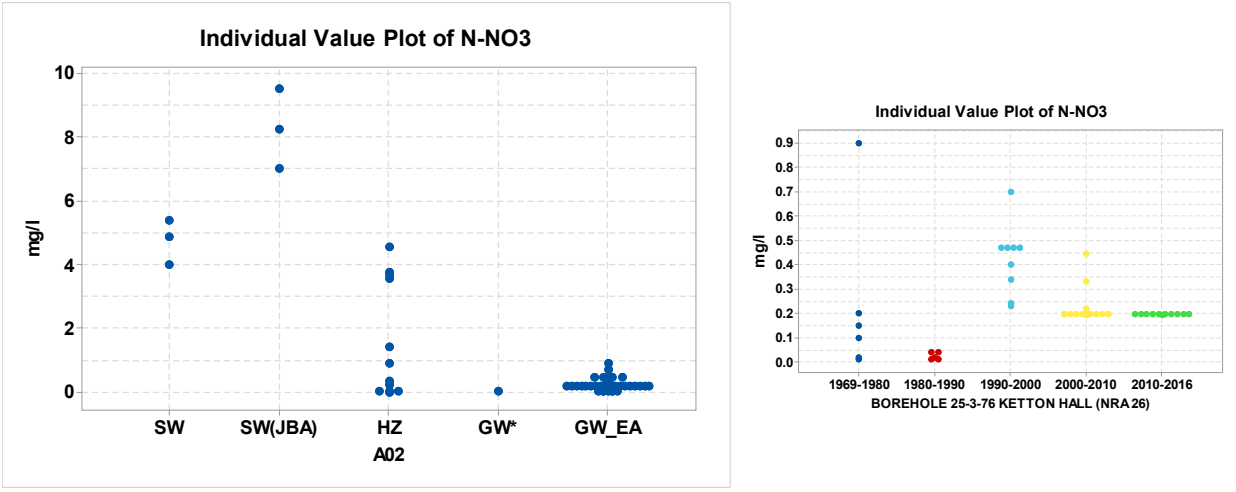

Figure 69: Left: Individual value plot of Cl, SO4 and N-NO3 (mg/l) distribution in surface water (SW), hyporheic porewater (HZ) and groundwater (GW) at site A02. GW_FO = EA data for BOREHOLE 25-3-76 KETTON HALL (date of collection 10/6/1992 to 27/2/2017). GW * = BGS data of BOREHOLE KETTON HALL collected at the same time of SW/HZ. SW(JBA) = EA/JBA surface water data (collected on 24/1, 27/2 and 31/5 2017). Right: Distribution in BOREHOLE KETTON HALL groundwater across years of sampling.

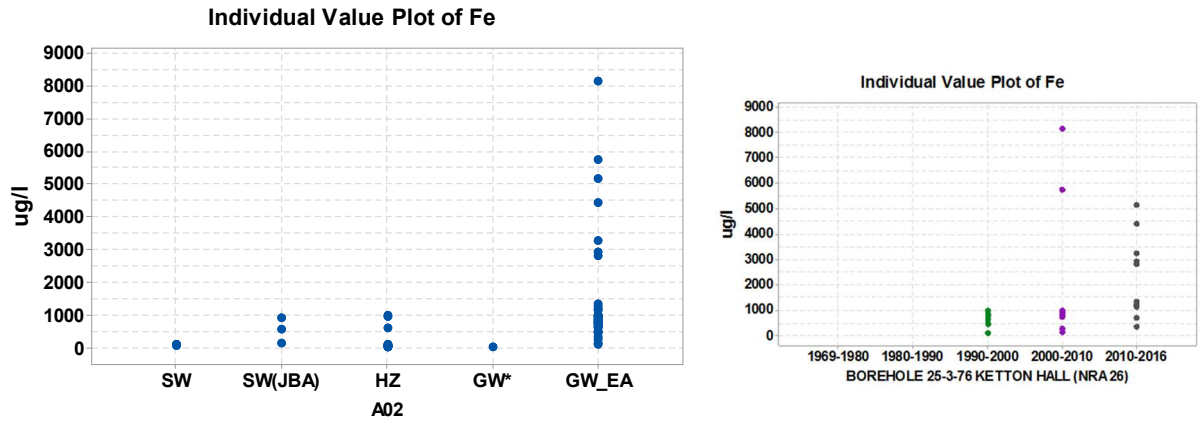

Borehole Ketton hall

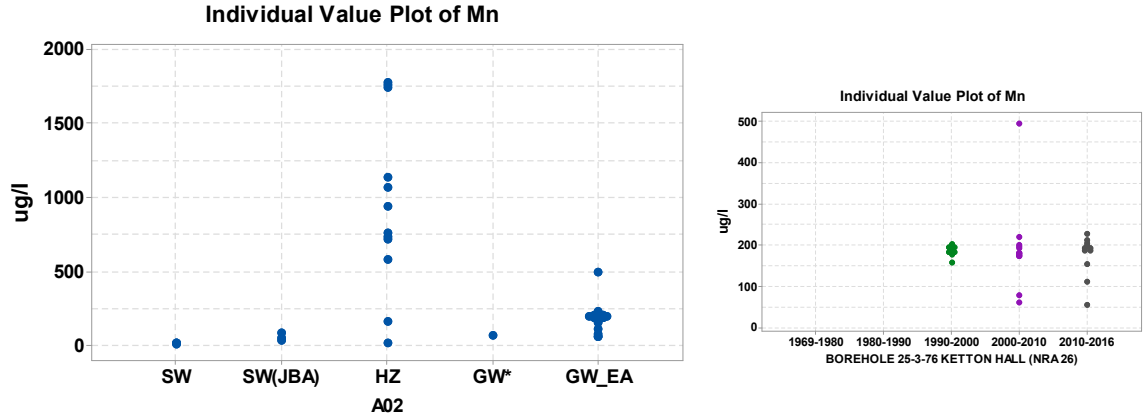

Borehole Ketton hall

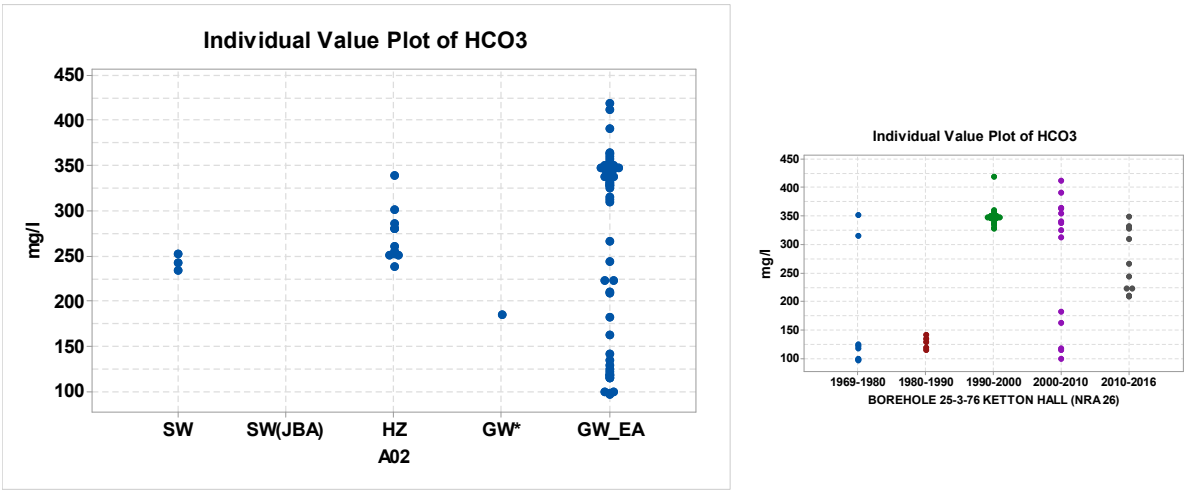

Figure 70: Left: Individual value plot of Fe, Mn and HCO3 distribution in surface water (SW), hyporheic porewater (HZ) and groundwater (GW) at site A02. GW_FO = EA data for BOREHOLE 25-3-76 KETTON HALL (date of collection 10/6/1992 to 27/2/2017). GW * = BGS data of BOREHOLE KETTON HALL collected at the same time of SW/HZ. SW(JBA) = EA/JBA surface water data (collected on 24/1, 27/2 and 31/5 2017). Right: Distribution in BOREHOLE KETTON HALL groundwater across years of sampling.

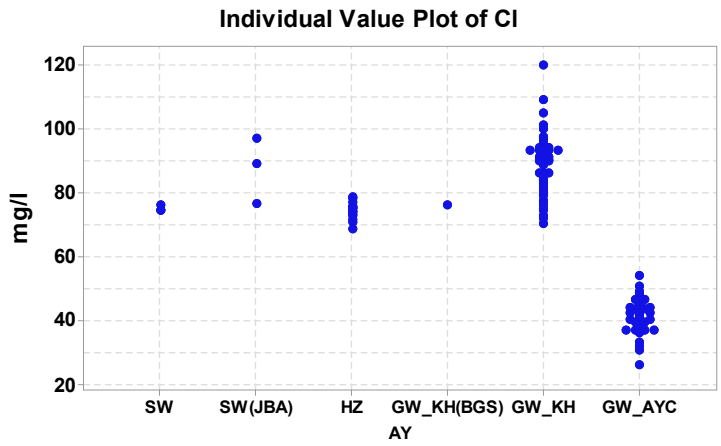

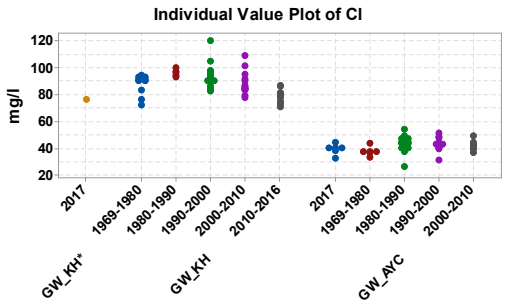

GW_KH=KETTON HALL; GW_AYC=AYCLIFFE

GW KH=KETTON HALL: GW AY=AYCLIFFE

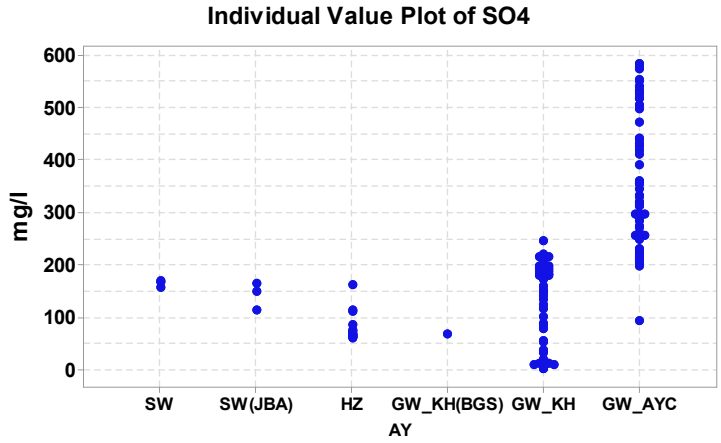

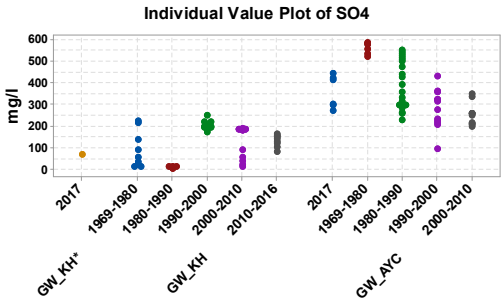

GW_KH=KETTON HALL; GW_AYC=AYCLIFFE

GW_KH=KETTON HALL; GW_AY=AYCLIFFE

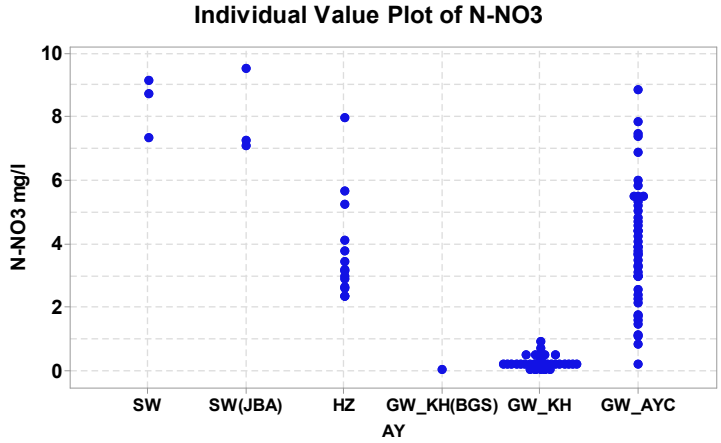

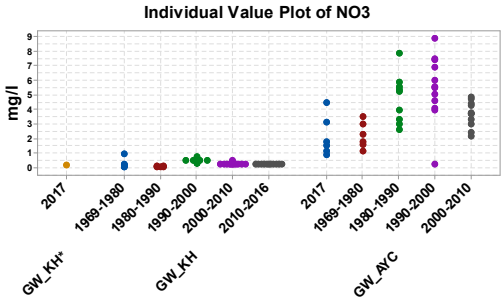

GW_KH=KETTON HALL; GW_AYC=AYCLIFFE

GW_KH=KETTON HALL; GW_AY=AYCLIFFE

Figure 71: Individual value plot of Cl, SO4, N-NO3 distribution in surface water (SW), hyporheic porewater (HZ) and groundwater (GW) at site AY. GW_FO = EA data for Borehole 25-3-76 Ketton Hall (date of collection 10/6/1992 to 27/2/2017). GW * = BGS data of Borehole Ketton Hall collected at the same time of SW/HZ. SW(JBA) = EA/JBA surface water data (collected on 24/1, 27/2 and 31/5 2017). GW_AYC = EA data for Borehole 25-3-41 Aycliffe (NRA 2). Right: distribution across years of groundwater sampling.

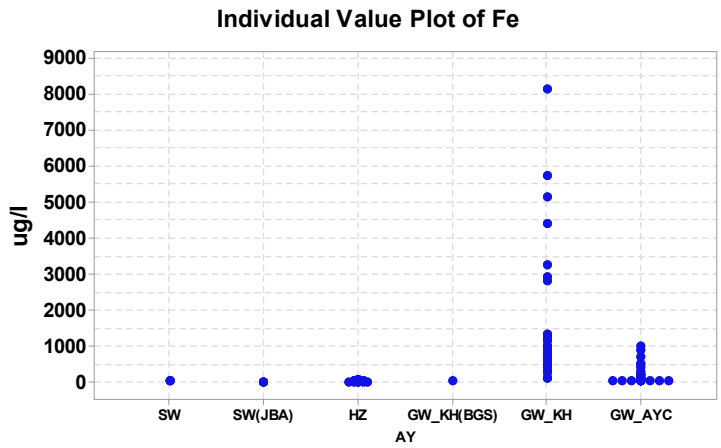

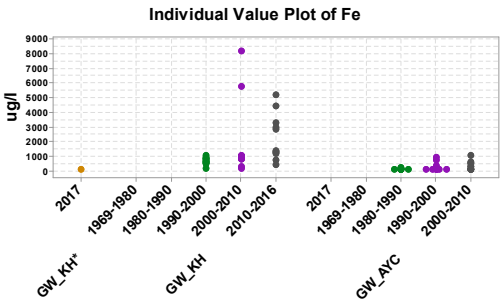

GW_KH=KETTON HALL; GW_AYC=AYCLIFFE

GW KH=KETTON HALL: GW AY=AYCLIFFE

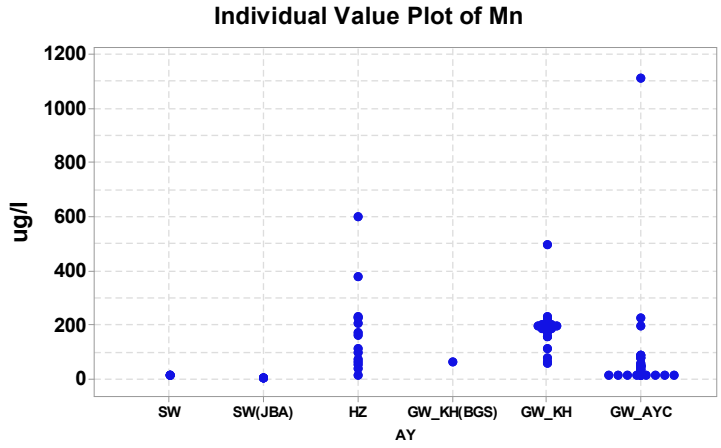

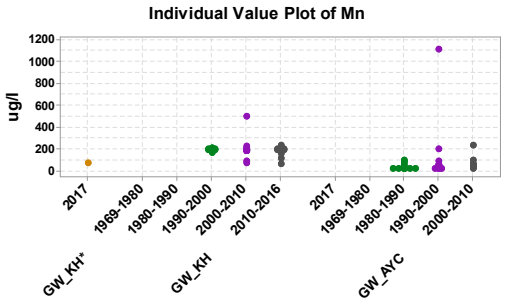

GW_KH=KETTON HALL; GW_AYC=AYCLIFFE

GW_KH=KETTON HALL; GW_AY=AYCLIFFE

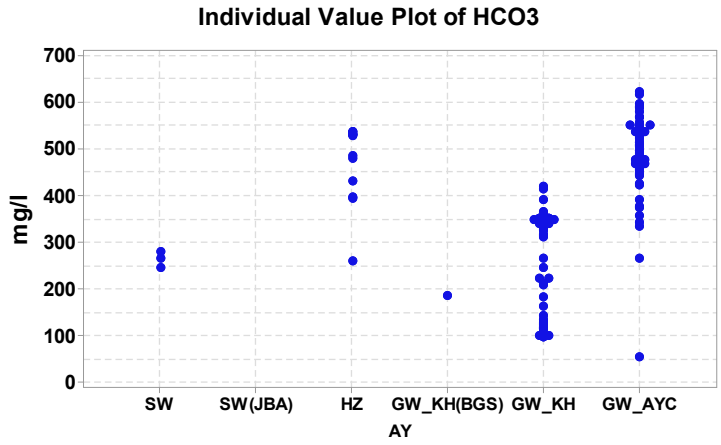

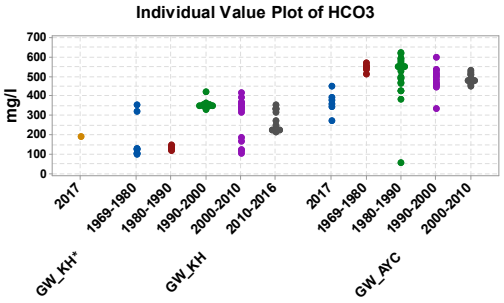

GW_KH=KETTON HALL; GW_AYC=AYCLIFFE

GW_KH=KETTON HALL; GW_AY=AYCLIFFE

Figure 72: Individual value plot of Fe, Mn, HCO3 distribution in surface water (SW), hyporheic porewater (HZ) and groundwater (GW) at site AY. GW_FO = EA data for Borehole 25-3-76 Ketton Hall (date of collection 10/6/1992 to 27/2/2017). GW * = BGS data of Borehole Ketton Hall collected at the same time of SW/HZ. SW(JBA) = EA/JBA surface water data (collected on 24/1, 27/2 and 31/5 2017). GW_AYC = EA data for Borehole 25-3-41 Aycliffe (NRA 2). Right: distribution across years of groundwater sampling.

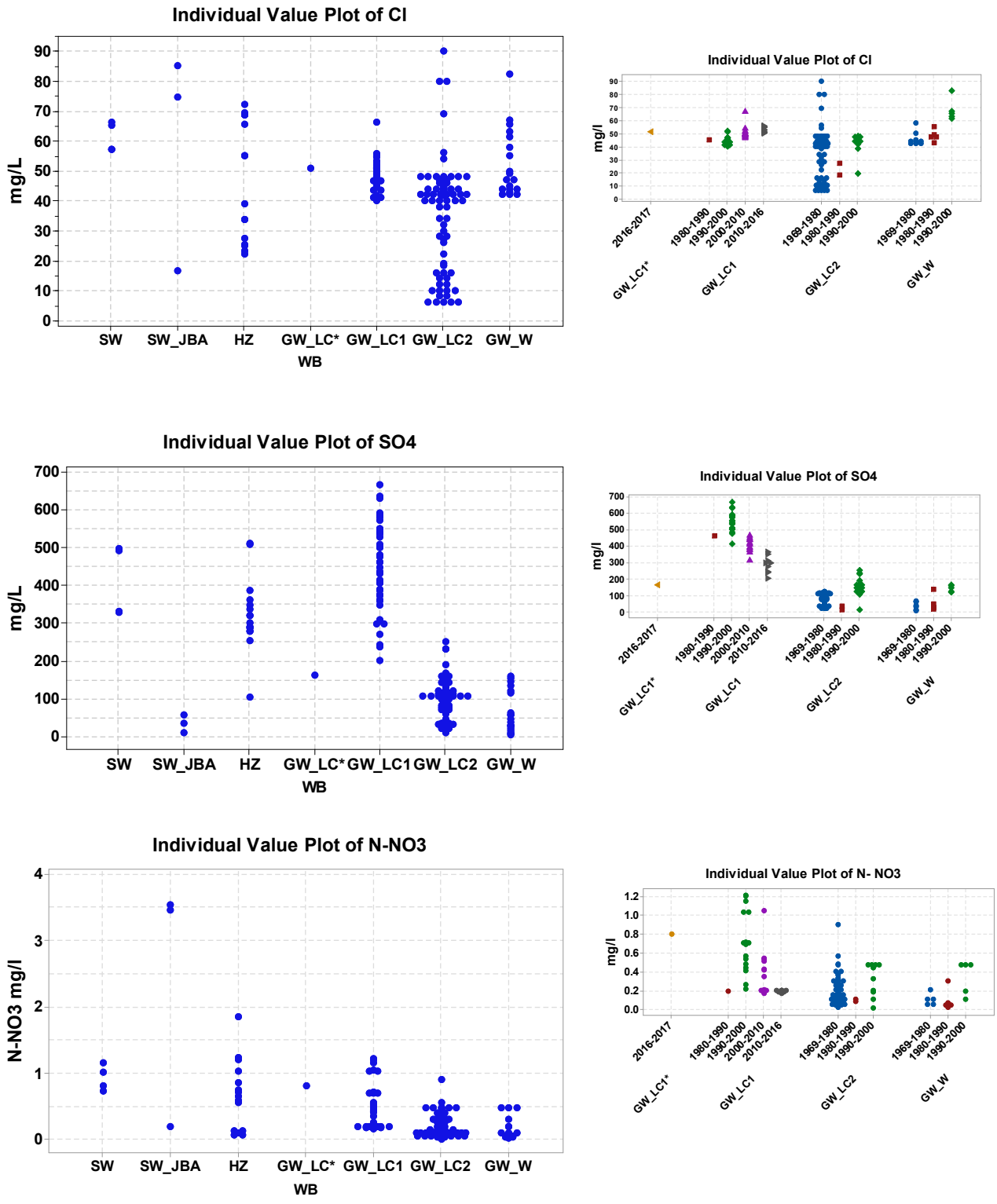

Figure 73: Individual value plot of Cl, SO4, N-NO3 distribution in surface water (SW), hyporheic porewater (HZ) and groundwater (GW) at sites WB2 and 3. Legend: SW at WB1,2,3 SW(JBA): JBA sites B01, B02, B03; GW_LC*= Borehole 25-3-27 Low Copelaw N01 (NRA D)/BGS analysis; GW_LC1= borehole 25-3-27 Low Copelaw N01 (NRA D)/EA analysis; GW_LC2= Borehole 25-3-28 Low Copelaw N02 (NRA 7)/EA analysis; GW_W= Borehole 25-3-26 Woodham (NRA 5)/EA analysis. Right: distribution across years of groundwater sampling.

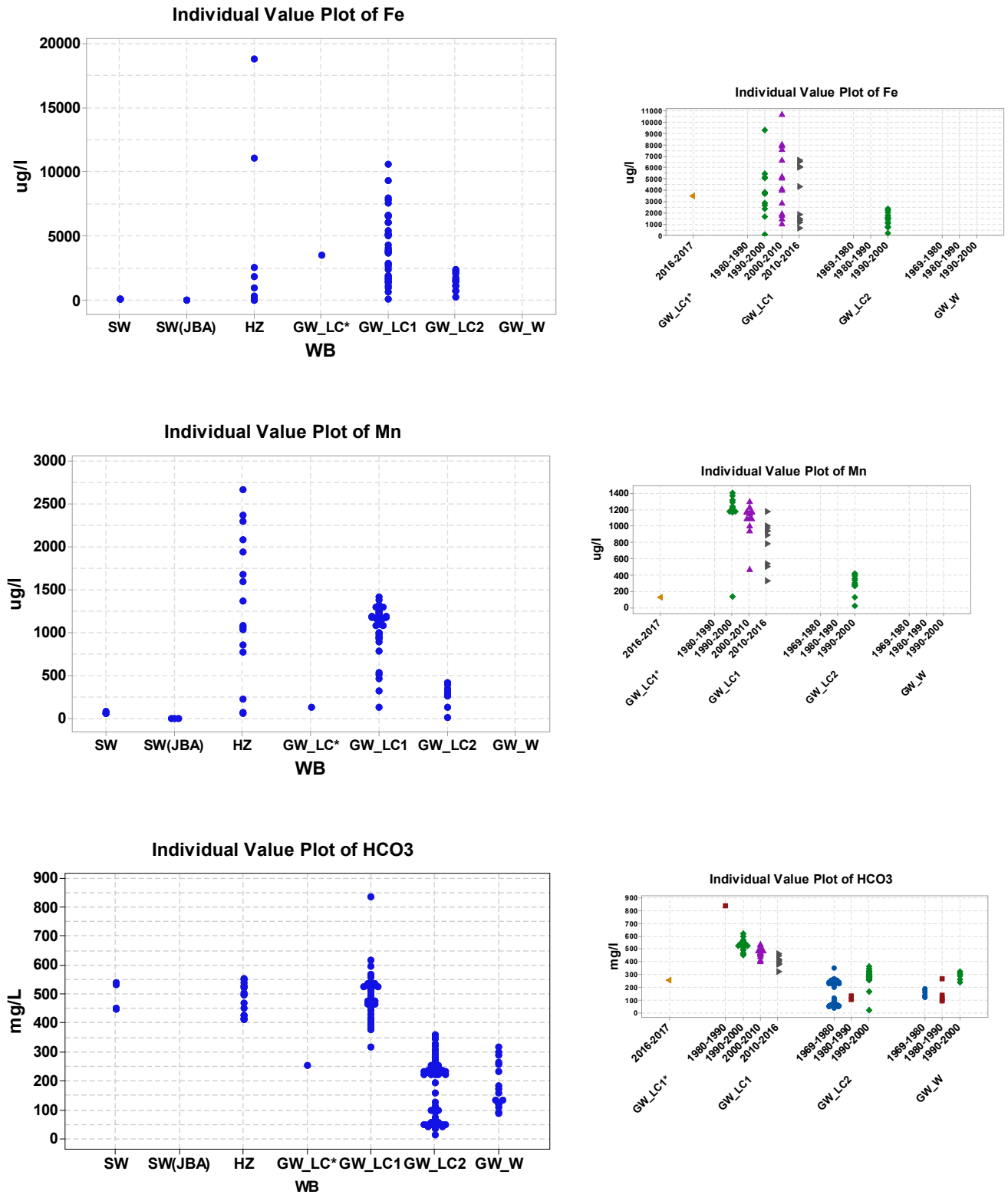

Figure 74: Individual value plot of Fe, Mn, HCO3 distribution in surface water (SW), hyporheic porewater (HZ) and groundwater (GW) at sites WB2 and 3. Legend: SW at WB1,2,3 SW(JBA): JBA sites B01, B02, B03; GW_LC*= Borehole 25-3-27 Low Copelaw N01 (NRA D)/BGS analysis; GW_LC1= borehole 25-3-27 Low Copelaw N01 (NRA D)/EA analysis; GW_LC2= Borehole 25-3-28 Low Copelaw N02 (NRA 7)/EA analysis; GW_W= Borehole 25-3-26 Woodham (NRA 5)/EA analysis. Right: distribution across years of groundwater sampling.

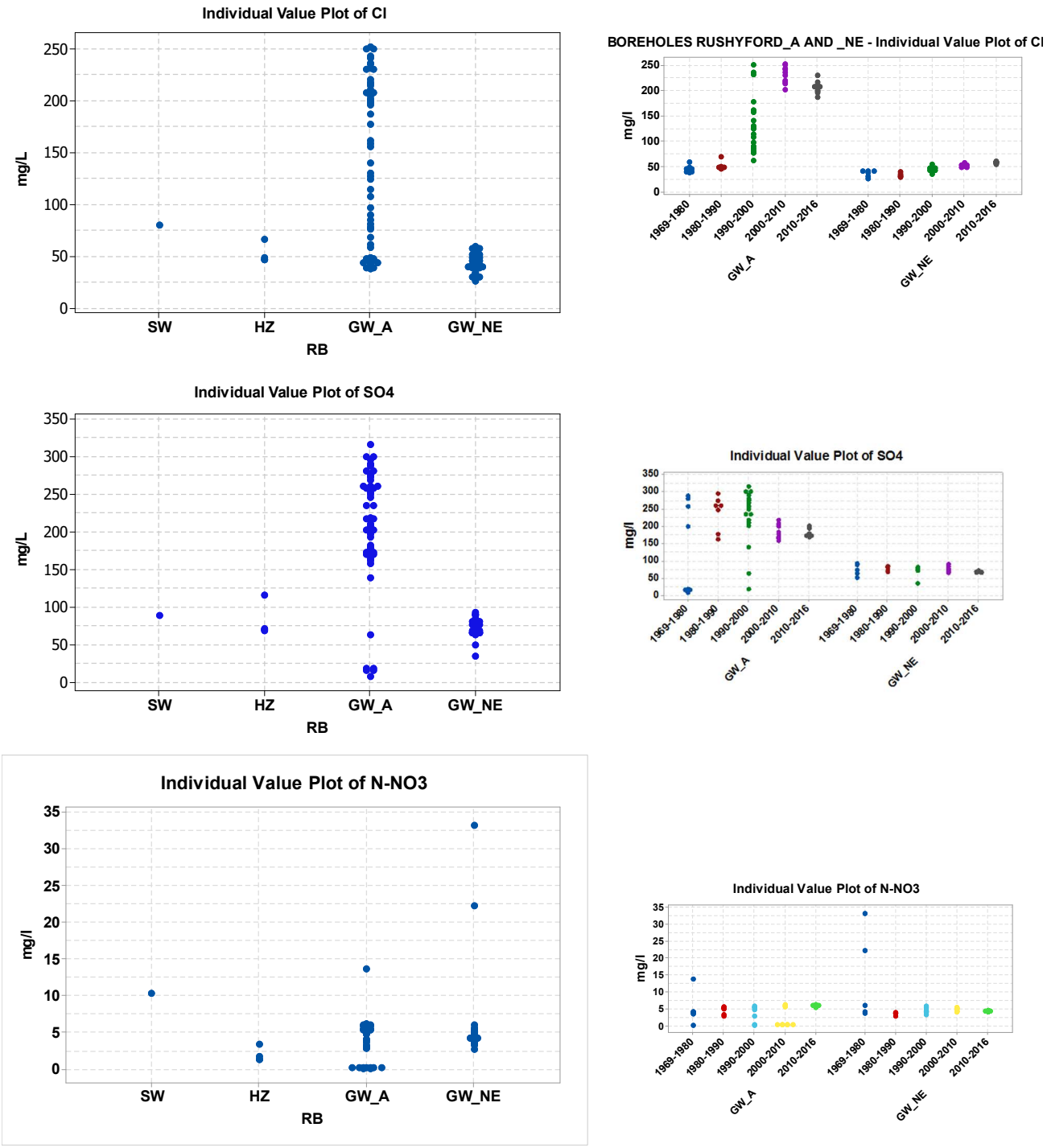

Figure 75: Individual value plot of Cl, SO4, N-NO3 distribution in surface water (SW), hyporheic porewater (HZ) and groundwater (GW) at site RB. Legend: GW_A= Borehole 25-3-21 Rushyford_A , GW_NE= Borehole 25-3-22 Rushyford_NE. Right: distribution across years of groundwater sampling.

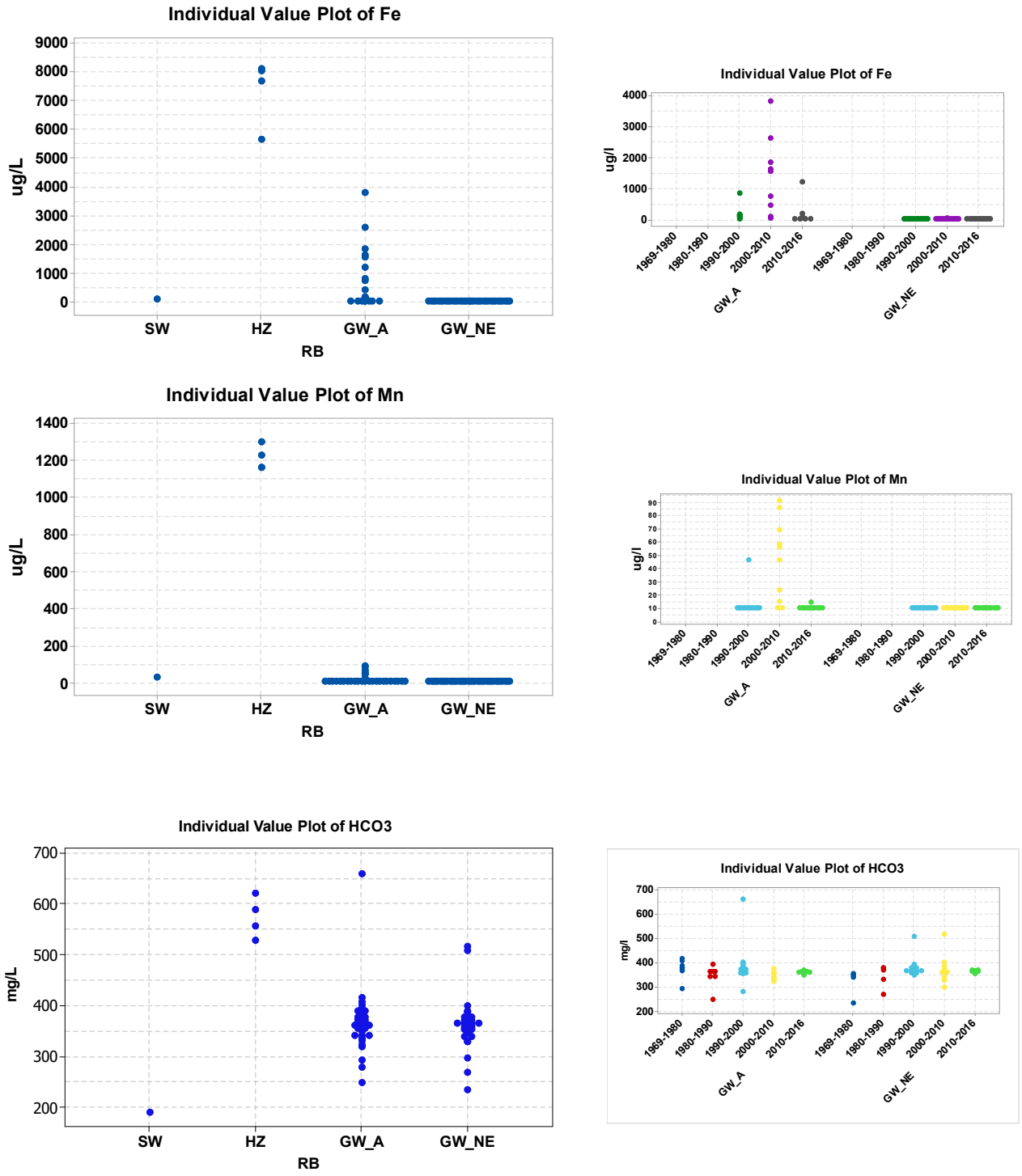

Figure 76: Individual value plot of Fe, Mn, HCO3 distribution in surface water (SW), hyporheic porewater (HZ) and groundwater (GW) at site RB. Legend: GW_A= Borehole 25-3-21 Rushyford_A , GW_NE= Borehole 25-3-22 Rushyford_NE. Right: distribution across years of groundwater sampling.

Appendix 7 Analytical Data

Table 16: Field parameters, range of major and minor elements in the hyporheic zone of site D01

D01 POREWATER		**All Depths (N=14)**				
		Mean	**SD**	**Min**	**Max**	***ICP-MS DL***
Sediment Depth (cm)		**-86**	n/a	-135	-30	
Conductivity	uS cm-1	**973**	94	884	1145	
DO2	mg l-1					
Temp	°C	**14.6**	1.1	13.7	16.3	
Eh	mVolt	**199**	43	150	264	
pH		**7.89**	0.18	7.57	8.32	
Ca	mg l-1	**116.5**	18.25	91.0	147.3	*0.6*
Mg	mg l-1	**40.56**	6.01	34.33	51.85	*0.02*
Na	mg l-1	**45.29**	5.57	33.20	52.80	*0.2*
K	mg l-1	**4.98**	2.22	2.84	8.89	*0.02*
HCO_3	mg l-1	**602**	112	456	811	
Cl	mg l-1	**43.90**	8.16	33.78	61.09	
SO_4	mg l-1	**37.0**	41.9	1.0	125	
NO_3	mg l-1	**1.42**	3.04	0.30	11.8	
Br	mg l-1	**0.26**	0.07	0.17	0.37	
NO_2	mg l-1	**0.10**	0.13	0.05	0.52	
HPO_4	mg l-1	**0.339**	0.797	0.100	3.100	
F	mg l-1	**0.777**	0.126	0.599	1.01	
NPOC	mg l-1	**6.36**	1.89	3.88	9.46	
Total P	mg l-1	**0.15**	0.34	0.01	1.16	*0.01*
Total S	mg l-1	**13.36**	12.51	4.00	36.00	*4*
Si	mg l-1	**8.81**	2.13	6.08	12.98	*0.05*

Table 17: Trace element concentrations in the hyporheic zone of site D01

D01 POREWATER		**All Depths (N=14)**				
		Mean	**SD**	**Min**	**Max**	***ICP-MS DL***
Ba	ug l-1	**136**	141	32	485	*0.1*
Sr	ug l-1	**344**	104	204	519	*0.2*
Mn	ug l-1	**1295**	553	448	2512	*0.2*
Total Fe	ug l-1	**228**	342	13	1234	*1*
Li	ug l-1	**48**	13	27	63	*3*
Be	ug l-1	**0.01**	0.00	0.01	0.01	*0.01*
B	ug l-1	**238**	148	118	709	*50*
Al	ug l-1	**3.43**	2.15	2.00	8.00	*2*
Ti	ug l-1	**0.11**	0.05	0.06	0.24	*0.06*
V	ug l-1	**0.54**	0.11	0.50	0.90	*0.5*
Cr	ug l-1	**0.23**	0.21	0.07	0.77	*0.07*
Co	ug l-1	**1.14**	0.37	0.40	1.74	*0.02*
Ni	ug l-1	**2.61**	1.14	1.40	5.70	*0.1*
Cu	ug l-1	**0.59**	0.23	0.50	1.30	*0.5*
Zn	ug l-1	**4.27**	2.80	3.00	11.00	*3*
Ga	ug l-1	**0.20**	0.01	0.20	0.25	*0.2*
As	ug l-1	**1.50**	0.91	0.60	2.98	*0.06*
Se	ug l-1	**0.52**	0.08	0.50	0.80	*0.5*
Rb	ug l-1	**2.56**	0.96	0.72	4.04	*0.02*
Y	ug l-1	**0.020**	0.010	0.008	0.042	*0.005*
Zr	ug l-1	**0.150**	0.046	0.090	0.240	*0.05*
Nb	ug l-1	**0.020**	0.000	0.020	0.020	*0.02*
Mo	ug l-1	**0.591**	0.315	0.200	1.400	*0.2*
Ag	ug l-1	**0.070**	0.000	0.070	0.070	*0.07*
Cd	ug l-1	**0.044**	0.015	0.040	0.095	*0.04*
Sn	ug l-1	**0.050**	0.022	0.040	0.120	*0.04*
Sb	ug l-1	**0.206**	0.118	0.090	0.460	*0.03*
Cs	ug l-1	**0.032**	0.016	0.007	0.057	*0.007*
La	ug l-1	**0.004**	0.002	0.002	0.009	*0.002*
Ce	ug l-1	**0.005**	0.003	0.002	0.011	*0.002*
Pr	ug l-1	**0.002**	0.000	0.002	0.002	*0.002*
Nd	ug l-1	**0.034**	0.013	0.030	0.080	*0.03*
Sm	ug l-1	**0.005**	0.000	0.005	0.007	*0.005*
Eu	ug l-1	**0.008**	0.016	0.004	0.066	*0.004*
Gd	ug l-1	**0.003**	0.001	0.003	0.005	*0.003*
Tb	ug l-1	**0.002**	0.001	0.002	0.004	*0.002*
Dy	ug l-1	**0.003**	0.001	0.002	0.005	*0.002*
Ho	ug l-1	**0.002**	0.000	0.002	0.004	*0.002*
Er	ug l-1	**0.003**	0.002	0.002	0.008	*0.002*
Tm	ug l-1	**0.002**	0.001	0.002	0.004	*0.002*
Yb	ug l-1	**0.006**	0.004	0.002	0.015	*0.002*

Lu	ug l-1	**0.002**	0.001	0.002	0.006	*0.002*
Hf	ug l-1	**0.010**	0.000	0.010	0.010	*0.01*
Ta	ug l-1	**0.020**	0.000	0.020	0.020	*0.02*
W	ug l-1	**0.071**	0.002	0.070	0.078	*0.07*
Tl	ug l-1	**0.010**	0.000	0.010	0.010	*0.01*
Pb	ug l-1	**0.136**	0.063	0.100	0.300	*0.1*
Th	ug l-1	**0.005**	0.001	0.005	0.008	*0.005*
U	ug l-1	**0.53**	0.35	0.02	1.23	*0.002*

Table 18: Field parameters, range of major and minor elements in the hyporheic zone of site RB

		RB POREWATER (N=4)				
		Mean	**SD**	**Min**	**Max**	***ICP-MS DL***
Sediment Depth (cm)		**-64.0**		-79	-49	
Conductivity	uS cm-1	**993**	25	971	1025	
DO2	mg l-1	**2.2**	0.8	1.74	3.32	
Temp	°C	**17.3**	0.5	16.5	17.7	
Eh	mVolt	**126**	18	111	152	
pH		**7.89**	0.06	7.82	7.95	
Ca	mg l-1	**140**	5.39	133	146	*0.3*
Mg	mg l-1	**49.3**	1.92	46.7	51.2	*0.01*
Na	mg l-1	**39.0**	10.1	29.5	53.1	*0.2*
K	mg l-1	**4.24**	0.59	3.59	5.01	*0.03*
HCO_3	mg l-1	**573**	40.3	528	620	
Cl	mg l-1	**51.9**	9.35	46.4	65.9	
SO_4	mg l-1	**81.1**	23.4	67.7	116	
NO_3	mg l-1	**8.61**	4.38	5.84	15.1	
Br	mg l-1	**0.12**	0.01	0.11	0.13	
NO_2	mg l-1	**0.12**	0.11	0.05	0.29	
HPO_4	mg l-1	**0.10**	0.00	0.10	0.10	
F	mg l-1	**0.37**	0.01	0.36	0.38	
NPOC	mg l-1	**4.74**	1.05	4.05	6.30	
Total P	mg l-1	**0.81**	0.28	0.46	1.11	*0.01*
Total S	mg l-1	**34**	10	26	49	*1*
Si	mg l-1	**9.03**	0.40	8.49	9.46	*0.05*

Table 19: Trace element concentrations in the hyporheic zone of site RB

		RB POREWATER (N=4)				
		Mean	**SD**	**Min**	**Max**	***ICP-MS DL***
Ba	ug l-1	**170**	27.3	132	195	*0.2*
Sr	ug l-1	**265**	12.0	251	278	*0.1*
Mn	ug l-1	**1211**	64.7	1161	1297	*0.2*
Total Fe	ug l-1	**7371**	1151	5666	8114	*1*
Li	ug l-1	**22**	4.7	19	29	*2*
Be	ug l-1	**0.02**	0.02	0.01	0.05	*0.01*
B	ug l-1	**98**	5	92	105	*10*
Al	ug l-1	**74**	127	2	265	*1*
Ti	ug l-1	**1.30**	1.98	0.13	4.25	*0.05*
V	ug l-1	**1.1**	0.4	0.7	1.6	*0.2*
Cr	ug l-1	**0.31**	0.24	0.14	0.66	*0.05*
Co	ug l-1	**0.87**	0.20	0.64	1.11	*0.02*
Ni	ug l-1	**1.8**	0.3	1.4	2.1	*0.1*
Cu	ug l-1	**13.5**	16.1	0.4	35.3	*0.4*
Zn	ug l-1	**13.4**	6.6	4.7	19.2	*0.6*
Ga	ug l-1	**0.10**	0.02	0.09	0.13	*0.09*
As	ug l-1	**3.0**	0.5	2.5	3.6	*0.03*
Se	ug l-1	**0.15**	0.06	0.10	0.20	*0.1*
Rb	ug l-1	**2.98**	0.41	2.74	3.60	*0.02*
Y	ug l-1	**0.13**	0.18	0.03	0.39	*0.005*
Zr	ug l-1	**0.09**	0.04	0.06	0.15	*0.05*
Nb	ug l-1	**0.02**	0.00	0.02	0.02	*0.02*
Mo	ug l-1	**0.61**	0.28	0.24	0.85	*0.03*
Ag	ug l-1	**0.05**	0.00	0.05	0.05	*0.05*
Cd	ug l-1	**0.02**	0.01	0.01	0.04	*0.01*
Sn	ug l-1	**0.06**	0.05	0.03	0.14	*0.02*
Sb	ug l-1	**0.26**	0.09	0.17	0.39	*0.009*
Cs	ug l-1	**0.06**	0.04	0.024	0.12	*0.005*
La	ug l-1	**0.11**	0.17	0.007	0.37	*0.004*
Ce	ug l-1	**0.25**	0.43	0.012	0.90	*0.005*
Pr	ug l-1	**0.03**	0.05	0.006	0.11	*0.006*
Nd	ug l-1	**0.13**	0.21	0.020	0.45	*0.02*
Sm	ug l-1	**0.03**	0.05	0.005	0.11	*0.005*
Eu	ug l-1	**0.01**	0.01	0.004	0.03	*0.004*
Gd	ug l-1	**0.04**	0.06	0.005	0.12	*0.004*
Tb	ug l-1	**0.01**	0.01	0.004	0.02	*0.004*
Dy	ug l-1	**0.03**	0.04	0.004	0.09	*0.004*
Ho	ug l-1	**0.01**	0.01	0.004	0.02	*0.004*
Er	ug l-1	**0.01**	0.02	0.004	0.04	*0.004*
Tm	ug l-1	**0.005**	0.00	0.004	0.01	*0.004*
Yb	ug l-1	**0.01**	0.01	0.004	0.03	*0.004*

Lu	ug l-1	**0.004**	0.00	0.004	0.01	*0.004*
Hf	ug l-1	**0.01**	0.00	0.010	0.01	*0.01*
Ta	ug l-1	**0.02**	0.00	0.020	0.02	*0.02*
W	ug l-1	**0.06**	0.01	0.050	0.08	*0.05*
Tl	ug l-1	**0.01**	0.00	0.010	0.01	*0.01*
Pb	ug l-1	**1.53**	2.35	0.120	5.02	*0.02*
Th	ug l-1	**0.02**	0.03	0.005	0.07	*0.005*
U	ug l-1	**0.47**	0.06	0.43	0.56	*0.002*

Table 20: Field parameters, range of major and minor elements in the hyporheic zone of sites WB

		WB/2 PORWATER (N=9)					WB/3 POREWATER (N=6)				
		Mean	**SD**	**Min**	**Max**		**Mean**	**SD**	**Min**	**Max**	***ICP-MS DL***
Sediment Depth (cm)		**-25.9**	22.1	-75	0		-99.9	10.2	-115	-85	
Conductivity	µS/cm	**1408**	346	871	1832		1355	257	1100	1692	
DO2	mg/l	**1.8**	1.1	0	3		4.1	2.0	1	6	
Temp	°C	**13.9**	0.6	13	15		17.7	2.1	16	20	
Eh	mV	**166**	35	125	229		175	40	134	222	
pH		**7.53**	0.45	6.97	8.21		8.05	0.33	7.80	8.70	
Ca	mg/l	**159**	21.7	109	190		142	2.21	141	146	*0.3*
Mg	mg/l	**80.1**	17.1	49	113		69.0	4.76	63.9	76.9	*0.01*
Na	mg/l	**46.2**	13.4	28	74		55.7	7.45	47.0	67.9	*0.2*
K	mg/l	**3.75**	2.08	1.52	8.42		5.19	1.64	3.57	7.80	*0.03*
HCO_3	mg/l	**515**	25.4	469	550		423	14.5	412	450	
Cl	mg/l	**31.6**	10.5	22.2	55.1		68.9	2.13	65.7	72.3	
SO_4	mg/l	**325**	107	105	511		290	28.0	253	337	
NO_3	mg/l	**1.82**	1.70	0.30	4.56		4.59	2.16	2.49	8.19	
Br	mg/l	**0.23**	0.16	0.08	0.50		0.12	0.04	0.10	0.20	
NO_2	mg/l	**0.11**	0.08	0.03	0.25		0.09	0.06	0.05	0.22	
HPO_4	mg/l	**0.23**	0.16	0.05	0.50		0.12	0.04	0.10	0.20	
F	mg/l	**0.37**	0.14	0.25	0.68		0.34	0.09	0.22	0.45	
NPOC	mg/l	**5.56**	1.91	1.60	7.35		5.08	1.52	3.53	6.73	
Total P	mg/l	**0.05**	0.10	0.01	0.32		0.02	0.01	0.01	0.04	*0.01*
Total S	mg/l	**122**	40	38	189		106	10	93	122	*1*
Si	mg/l	**10.80**	3.53	5.08	17.69		6.40	1.61	4.38	8.63	*0.05*

Table 21: Trace element concentrations in the hyporheic zone of sites WB

		WB/2 POREWATER (N=9)					WB/3 POREWATER (N=6)				
		Mean	**SD**	**Min**	**Max**		**Mean**	**SD**	**Min**	**Max**	***ICP-MS DL***
Ba	µg/l	**172**	49.7	71	233		**382**	190	69	588	*0.2*
Sr	µg/l	**403**	126	258	680		**391**	32.1	357	451	*0.1*
Mn	µg/l	**1697**	800	217	2663		**957**	522	56	1670	*0.2*
Total Fe	µg/l	**3653**	6734	5	18814		**534**	734	24.0	1848	*1*
Li	µg/l	**37.8**	29.0	10	105		**47.7**	12.7	32	68	*2*
Be	µg/l	**0.01**	0.01	0.01	0.04		**0.01**	0.01	0.01	0.02	*0.01*
B	µg/l	**108**	26	83	172		**108**	6	98	116	*10*
Al	µg/l	**3**	2	1	6		**35**	34	10	99	*1*
Ti	µg/l	**0.12**	0.13	0.05	0.44		**0.66**	0.85	0.05	2.34	*0.05*
V	µg/l	**0.6**	0.6	0.2	1.9		**0.4**	0.2	0.2	0.6	*0.2*
Cr	µg/l	**0.14**	0.10	0.05	0.38		**0.35**	0.19	0.13	0.68	*0.05*
Co	µg/l	**0.97**	0.78	0.16	2.30		**1.84**	0.96	0.54	3.32	*0.02*
Ni	µg/l	**2.0**	1.5	0.4	3.9		**4.2**	0.8	3.1	5.4	*0.1*
Cu	µg/l	**0.4**	0.0	0.4	0.4		**9.5**	17.0	0.4	44	*0.4*
Zn	µg/l	**7.3**	3.3	2.9	13		**23.8**	33.4	7.7	92	*0.6*
Ga	µg/l	**0.12**	0.02	0.09	0.15		**0.10**	0.02	0.09	0.14	*0.09*
As	µg/l	**1.3**	1.1	0.3	3.5		**2.8**	1.6	0.4	4.3	*0.03*
Se	µg/l	**0.30**	0.09	0.20	0.40		**0.43**	0.15	0.30	0.70	*0.1*
Rb	µg/l	**2.31**	0.99	1.05	4.44		**3.07**	0.51	2.61	4.03	*0.02*
Y	µg/l	**0.05**	0.03	0.03	0.12		**0.09**	0.04	0.07	0.17	*0.005*
Zr	µg/l	**0.08**	0.03	0.05	0.16		**0.06**	0.02	0.05	0.10	*0.05*
Nb	µg/l	**0.02**	0.00	0.02	0.02		**0.02**	0.00	0.02	0.02	*0.02*
Mo	µg/l	**1.00**	1.19	0.13	4.02		**2.92**	1.95	1.43	6.71	*0.03*
Ag	µg/l	**0.05**	0.00	0.05	0.05		**0.05**	0.00	0.05	0.05	*0.05*
Cd	µg/l	**0.01**	0.00	0.01	0.01		**0.04**	0.06	0.01	0.16	*0.01*
Sn	µg/l	**0.03**	0.02	0.02	0.08		**0.14**	0.17	0.05	0.48	*0.02*
Sb	µg/l	**0.32**	0.38	0.06	1.31		**0.69**	0.28	0.34	1.17	*0.009*
Cs	µg/l	**0.02**	0.01	0.008	0.05		**0.03**	0.01	0.01	0.04	*0.005*
La	µg/l	**0.01**	0.01	0.005	0.03		**0.05**	0.05	0.01	0.15	*0.004*
Ce	µg/l	**0.02**	0.02	0.005	0.06		**0.12**	0.15	0.03	0.41	*0.005*
Pr	µg/l	**0.01**	0.0004	0.006	0.01		**0.02**	0.02	0.01	0.05	*0.006*
Nd	µg/l	**0.02**	0.01	0.02	0.04		**0.06**	0.06	0.02	0.19	*0.02*
Sm	µg/l	**0.01**	0.003	0.005	0.014		**0.021**	0.017	0.010	0.055	*0.005*
Eu	µg/l	**0.004**	0.001	0.004	0.006		**0.006**	0.004	0.004	0.014	*0.004*
Gd	µg/l	**0.01**	0.005	0.004	0.019		**0.023**	0.016	0.011	0.053	*0.004*
Tb	µg/l	**0.004**	0	0.004	0.004		**0.007**	0.005	0.004	0.016	*0.004*
Dy	µg/l	**0.01**	0.004	0.004	0.015		**0.019**	0.011	0.009	0.038	*0.004*
Ho	µg/l	**0.004**	0	0.004	0.004		**0.007**	0.005	0.004	0.017	*0.004*
Er	µg/l	**0.01**	0.002	0.004	0.010		**0.011**	0.006	0.006	0.020	*0.004*
Tm	µg/l	**0.004**	0	0.004	0.004		**0.006**	0.004	0.004	0.015	*0.004*

Yb	µg/l	**0.01**	0.003	0.004	0.012		**0.012**	0.006	0.008	0.023	*0.004*
Lu	µg/l	**0.004**	0	0.004	0.004		**0.006**	0.004	0.004	0.015	*0.004*
Hf	µg/l	**0.01**	0	0.010	0.010		**0.012**	0.004	0.010	0.020	*0.01*
Ta	µg/l	**0.02**	0	0.020	0.020		**0.020**	0.000	0.020	0.020	*0.02*
W	µg/l	**0.05**	0.003	0.050	0.060		**0.250**	0.366	0.050	0.980	*0.05*
Tl	µg/l	**0.01**	0.01	0.010	0.030		**0.020**	0.024	0.010	0.070	*0.01*
Pb	µg/l	**0.09**	0.06	0.020	0.210		**0.748**	0.680	0.250	1.870	*0.02*
Th	µg/l	**0.01**	0.00	0.005	0.010		**0.012**	0.010	0.005	0.031	*0.005*
U	µg/l	**1.36**	0.92	0.19	3.26		**2.53**	0.72	2.04	3.93	*0.002*

Table 22: Field parameters, range of major and minor elements in the hyporheic zone of site AY

AY POREWATER			All Depths (N=11)				
			Mean	**SD**	**Min**	**Max**	***ICP-MS DL***
Sediment Depth (cm)			**-19.64**		-44.00	1.00	
Conductivity	µS/cm		**982**	28	921	1012	
DO2	mg/l		**4.7**	1.8	2.6	8.5	
Field Temp	°C		**16.3**	0.9	15.2	18.4	
Field Eh	mV		**388**	12	370	405	
pH			**8.01**	0.16	7.76	8.22	
Ca	mg/l		**93.8**	4.62	85.0	102	*0.6*
Mg	mg/l		**51.9**	8.31	32.0	60.6	*0.01*
Na	mg/l		**48.9**	4.96	44.3	60.3	*0.2*
K	mg/l		**8.89**	0.69	8.22	10.5	*0.03*
HCO_3	mg/l		**463**	87	260	536	
Cl	mg/l		**74.9**	2.50	70.7	78.5	
SO_4	mg/l		**84.5**	31.7	61.8	162	
NO_3	mg/l		**17.1**	7.69	10.3	35.2	
Br	mg/l		**0.19**	0.01	0.17	0.22	
NO_2	mg/l		**0.18**	0.15	0.03	0.50	
HPO_4	mg/l		**0.11**	0.11	0.05	0.37	
F	mg/l		**0.77**	0.11	0.53	0.90	
NPOC	mg/l		**2.92**	1.18	1.62	5.01	
Total P	mg/l		**0.13**	0.11	0.02	0.39	*0.01*
Total S	mg/l		**28.23**	10.51	21.00	54.00	*1.00*
Si	mg/l		**4.87**	0.63	3.43	5.75	*0.05*

Table 23: Trace element concentrations in the hyporheic zone of site AY

AY POREWATER			**All Depths (N=11)**				
			Mean	**SD**	**Min**	**Max**	***ICP-MS DL***
Ba	µg/l		**110**	21	61	135	*0.1*
Sr	µg/l		**219**	15	190	245	*0.1*
Mn	µg/l		**187**	171	11	596	*0.2*
Total Fe	µg/l		**19**	17	5	66	*1*
Li	µg/l		**17**	4	13	28	*2*
Be	µg/l		**0.01**	0.00	0.01	0.01	*0.01*
B	µg/l		**103**	19	71	148	*11*
Al	µg/l		**13.8**	15.0	3.0	56.0	*2*
Ti	µg/l		**0.19**	0.15	0.05	0.46	*0.05*
V	µg/l		**0.36**	0.17	0.10	0.60	*0.1*
Cr	µg/l		**0.19**	0.17	0.03	0.64	*0.05*
Co	µg/l		**0.48**	0.43	0.16	1.55	*0.02*
Ni	µg/l		**2.32**	0.93	1.10	4.20	*0.2*
Cu	µg/l		**3.81**	1.84	1.40	6.80	*0.4*
Zn	µg/l		**15.7**	9.1	5.1	33.4	*0.5*
Ga	µg/l		**0.04**	0.03	0.03	0.11	*0.06*
As	µg/l		**0.33**	0.16	0.13	0.73	*0.03*
Se	µg/l		**1.24**	0.72	0.50	2.45	*0.1*
Rb	µg/l		**4.57**	1.98	2.13	9.26	*0.04*
Y	µg/l		**0.02**	0.02	0.02	0.07	*0.005*
Zr	µg/l		**0.03**	0.01	0.03	0.06	*0.05*
Nb	µg/l		**0.01**	0.00	0.01	0.01	*0.02*
Mo	µg/l		**2.46**	1.55	0.81	5.97	*0.03*
Ag	µg/l		**0.03**	0.00	0.03	0.03	*0.05*
Cd	µg/l		**0.04**	0.02	0.02	0.07	*0.01*
Sn	µg/l		**0.18**	0.18	0.03	0.58	*0.02*
Sb	µg/l		**0.36**	0.23	0.09	0.88	*0.005*
Cs	µg/l		**0.02**	0.01	0.01	0.04	*0.005*
La	µg/l		**0.01**	0.01	0.01	0.06	*0.002*
Ce	µg/l		**0.02**	0.04	0.01	0.13	*0.006*
Pr	µg/l		**0.01**	0.00	0.00	0.02	*0.008*
Nd	µg/l		**0.02**	0.01	0.01	0.06	*0.02*
Sm	µg/l		**0.00**	0.00	0.00	0.02	*0.003*
Eu	µg/l		**0.00**	0.00	0.00	0.01	*0.002*
Gd	µg/l		**0.01**	0.01	0.01	0.02	*0.002*
Tb	µg/l		**0.00**	0.00	0.00	0.00	*0.002*
Dy	µg/l		**0.00**	0.00	0.00	0.01	*0.002*
Ho	µg/l		**0.00**	0.00	0.00	0.00	*0.002*
Er	µg/l		**0.00**	0.00	0.00	0.01	*0.002*
Tm	µg/l		**0.00**	0.00	0.00	0.00	*0.002*
Yb	µg/l		**0.00**	0.00	0.00	0.01	*0.002*

Lu	µg/l		**0.00**	0.00	0.00	0.00	*0.002*
Hf	ug l-1		**0.01**	0.00	0.01	0.01	*0.01*
Ta	ug l-1		**0.01**	0.00	0.01	0.01	*0.02*
W	ug l-1		**0.03**	0.01	0.03	0.06	*0.05*
Tl	ug l-1		**0.05**	0.04	0.02	0.13	*0.01*
Pb	ug l-1		**0.15**	0.09	0.06	0.41	*0.02*
Th	ug l-1		**0.00**	0.00	0.00	0.02	*0.005*
U	ug l-1		**1.38**	0.17	1.11	1.65	*0.003*

Table 24: Field parameters, range of major and minor elements in the hyporheic zone of site A02

A02 POREWATER		All Depths (N=7)				
		Mean	**SD**	**Min**	**Max**	***ICP-MS DL***
Sediment Depth (cm)		**-21**		-33	-8	
Conductivity	µS/cm	**904**	171	768	1153	
DO2	mg/l	**3.24**	2.76	1.18	8.78	
Temp	°C	**19.7**	3.2	16.2	22.9	
Eh	mV	**285**	87	170	354	
pH		**7.98**	0.12	7.84	8.15	
Ca	mg/l	**82.36**	5.62	77	92	*2*
Mg	mg/l	**31.91**	2.93	29.37	37.66	*0.07*
Na	mg/l	**55.35**	3.81	48.9	60.8	*0.2*
K	mg/l	**9.01**	0.37	8.5	9.41	*0.04*
HCO_3	mg/l	**275.17**	35.29	237.5	339.3	
Cl	mg/l	**74.30**	8.08	67.46	87.69	
SO_4	mg/l	**117**	12	107	144	
NO_3	mg/l	**7.03**	7.93	0.15	20.19	
Br	mg/l	**0.34**	0.34	0.11	1.01	
NO_2	mg/l	**0.29**	0.61	0.025	1.67	
HPO_4	mg/l	**0.49**	0.35	0.05	0.91	
F	mg/l	**0.46**	0.11	0.28	0.55	
NPOC	mg/l	**8.13**	2.60	4.39	12.89	
Total P	mg/l	**0.32**	0.15	0.11	0.52	*0.04*
Total S	mg/l	**40.43**	3.27	38	47.5	*2*
Si	mg/l	**5.15**	0.93	3.73	6.3	*0.07*

Table 25: Trace element concentrations in the hyporheic zone of site A02

A02 POREWATER		**All Depths (N=7)**				
		Mean	**SD**	**Min**	**Max**	***ICP-MS DL***
Ba	µg/l	**92.36**	19.06	67.2	115	*0.2*
Sr	µg/l	**217**	17.84	202.45	250	*0.2*
Mn	µg/l	**1037**	612	162	1757	*0.2*
Total Fe	µg/l	**228**	370	7.00	1000	*1*
Li	µg/l	**21.50**	1.19	20	23	*3*
Be	µg/l	**0.03**	0.03	0.02	0.09	*0.02*
B	µg/l	**139**	123	55	398	*35*
Al	µg/l	**74.14**	136.81	7	383	*1*
Ti	µg/l	**1.80**	3.58	0.2	9.9	*0.2*
V	µg/l	**1.21**	0.39	1	2	*1*
Cr	µg/l	**0.42**	0.43	0.0975	1.33	*0.05*
Co	µg/l	**0.98**	0.55	0.2675	1.65	*0.01*
Ni	µg/l	**3.89**	1.19	1.75	5.3	*0.1*
Cu	µg/l	**4.46**	3.26	0.5	10.1	*0.4*
Zn	µg/l	**15.32**	10.83	3.5	37	*2*
Ga	µg/l	**0.21**	0.10	0.1	0.34	*0.08*
As	µg/l	**1.12**	0.66	0.54	2.345	*0.03*
Se	µg/l	**0.44**	0.14	0.275	0.7	*0.2*
Rb	µg/l	**4.84**	0.77	3.66	6.04	*0.02*
Y	µg/l	**0.14**	0.24	0.032	0.694	*0.008*
Zr	µg/l	**0.10**	0.11	0.05	0.34	*0.05*
Nb	µg/l	**0.02**	0.00	0.02	0.02	*0.02*
Mo	µg/l	**9.79**	2.51	6.12	13.25	*0.08*
Ag	µg/l	**0.05**	0.00	0.05	0.06	*0.05*
Cd	µg/l	**0.04**	0.03	0.02	0.09	*0.02*
Sn	µg/l	**0.47**	0.37	0.18	1.27	*0.02*
Sb	µg/l	**0.62**	0.28	0.25	1.04	*0.01*
Cs	µg/l	**0.02**	0.02	0.006	0.075	*0.005*
La	µg/l	**0.10**	0.20	0.012	0.547	*0.009*
Ce	µg/l	**0.24**	0.49	0.017	1.359	*0.009*
Pr	µg/l	**0.03**	0.06	0.008	0.173	*0.008*
Nd	µg/l	**0.15**	0.27	0.04	0.75	*0.04*
Sm	µg/l	**0.03**	0.06	0.009	0.182	*0.009*
Eu	µg/l	**0.01**	0.02	0.007	0.051	*0.007*
Gd	µg/l	**0.05**	0.07	0.013	0.212	*0.009*
Tb	µg/l	**0.01**	0.01	0.009	0.03	*0.009*
Dy	µg/l	**0.03**	0.05	0.009	0.145	*0.009*
Ho	µg/l	**0.01**	0.01	0.008	0.029	*0.008*
Er	µg/l	**0.02**	0.02	0.008	0.072	*0.008*
Tm	µg/l	**0.01**	0.00	0.01	0.01	*0.01*
Yb	µg/l	**0.02**	0.02	0.004	0.059	*0.002*

Lu	µg/l	**0.01**	0.00	0.009	0.011	*0.009*
Hf	µg/l	**0.01**	0.00	0.01	0.01	*0.01*
Ta	µg/l	**0.02**	0.00	0.02	0.02	*0.02*
W	µg/l	**0.11**	0.07	0.07	0.26	*0.07*
Tl	µg/l	**0.02**	0.01	0.01	0.04	*0.01*
Pb	µg/l	**2.66**	4.48	0.24	12.6	*0.02*
Th	µg/l	**0.02**	0.01	0.02	0.04	*0.02*
U	µg/l	**2.46**	1.43	1.21	4.66	*0.02*

Table 26: Field parameters, range of major and minor elements in selected boreholes

LIMS Code		14061-0026	14067-0016	14067-0017	14067-0018	14067-0019	14067-0020	14067-0021	14283-0060
Sample Name		**Foumarts Lane**	**Stony Hall C**	**Stony Hall L**	**Low Copelaw**	**Stillington OBH4**	**Stillington OBH2**	**Ketton Hall**	**Aycliffe Quarry**
Easting		432713	432570	432570	429400	435500	435400	429450	429524
Northing		530321	529550	529550	526300	523450	523130	519300	522571
Date Sampled		29/6/17	12/7/17	12/7/17	12/7/17	12/7/17	12/7/17	12/7/17	17/7/18
Time		09:00	10:53	11:30	12:47	13:58	14:37	15:35	-
Field Temp	°C	nd	11	10.9	10.9	11.5	11.6	11.6	nd
Field pH		nd	7.14	7.09	8.15	7.21	8.4	9.04	nd
DO2	mg/l	nd	n/a	0.019	0.015	0.015	0.016	0.013	nd
Conductivity	µS/cm	965	2540	2010	822	775	433	652	835
pH		8.02	n/a	n/a	n/a	n/a	n/a	n/a	8.17
Ca	mg/l	90.2	185	178	55	86	13	5	87.9
Mg	mg/l	41.07	78.57	81.02	45.32	38.69	33.07	43.34	48.8
Na	mg/l	29.2	303.9	155.5	36.6	34.1	21.1	54.2	16.0
K	mg/l	1.5	12.68	4.27	6.25	2.42	2.6	2.72	2.33
HCO_3	mg/l	365	661	539	253	380	197	186	415
Cl	mg/l	51.4	78.4	77.2	51.0	48.4	21.1	76.1	25.0
SO_4	mg/l	119	751	570	162	46	27	67	68.7
NO_3	mg/l	1.23	2.92	4.64	3.54	3.33	<0.15	<0.15	16.3
Br	mg/l	0.153	<0.5	<0.5	<0.2	<0.2	0.059	0.324	0.060
NO_2	mg/l	<0.05	<0.25	<0.25	<0.1	<0.1	<0.025	<0.025	<0.025
HPO_4	mg/l	<0.1	<0.5	<0.5	<0.2	<0.2	<0.05	<0.05	<0.05
F	mg/l	1.411	<0.25	0.330	<0.1	0.479	0.279	0.198	0.527
NPOC	mg/l	0.584	n/a	n/a	n/a	n/a	n/a	n/a	0.45
Total P	mg/l	<0.01	<0.04	<0.04	<0.04	<0.04	<0.04	<0.04	<0.04
Total S	mg/l	35	271	207	61	19	11	25	23
Si	mg/l	3.85	5.39	7.11	1.49	4.16	0.99	0.88	4.18

Table 27: Trace element concentrations in selected boreholes

LIMS Code		14061-0026	14067-0016	14067-0017	14067-0018	14067-0019	14067-0020	14067-0021	14283-0060
Sample Name		**Foumarts Lane**	**Stony Hall C**	**Stony Hall L**	**Low Copelaw**	**Stillington OBH4**	**Stillington OBH2**	**Ketton Hall**	**Aycliffe Quarry**
Ba	µg/l	67.2	21	12.2	26.4	51.2	4.1	1.5	197
Sr	µg/l	226.8	4976.7	1331.2	219.3	807.2	55.5	22.5	149
Mn	µg/l	140.1	319.9	187	123	101.5	43.7	63.4	<2
Total Fe	µg/l	282	3222	5192	3466	2088	485	38	<7
Li	µg/l	9	242	118	34	58	26	63	10
Be	µg/l	<0.01	0.04	0.04	<0.02	<0.02	<0.02	<0.02	<0.5
B	µg/l	62	1255	224	101	39	42	67	27
Al	µg/l	<2	<1	<1	<1	<1	<1	<1	10
Ti	µg/l	<0.06	<0.2	<0.2	<0.2	<0.2	<0.2	<0.2	<0.2
V	µg/l	<0.5	<1	<1	<1	<1	<1	<1	<0.1
Cr	µg/l	<0.07	<0.05	<0.05	<0.05	0.07	<0.05	<0.05	<0.3
Co	µg/l	0.19	5.97	0.25	0.07	0.07	<0.01	<0.01	<0.05
Ni	µg/l	0.6	6.9	0.6	0.7	0.3	<0.1	<0.1	<0.1
Cu	µg/l	<0.5	<0.4	<0.4	<0.4	<0.4	<0.4	<0.4	<1
Zn	µg/l	8	9	6	<2	<2	21	<2	10
Ga	µg/l	<0.2	<0.08	<0.08	<0.08	<0.08	<0.08	<0.08	<0.08
As	µg/l	0.16	0.45	0.12	0.08	0.1	0.03	0.15	0.08
Se	µg/l	<0.5	<0.2	<0.2	<0.2	<0.2	<0.2	<0.2	1.2
Rb	µg/l	0.77	22.9	3.81	2.84	2.22	2.07	0.89	1.43
Y	µg/l	<0.005	0.059	0.03	<0.008	0.01	<0.008	<0.008	<0.02
Zr	µg/l	0.09	<0.05	<0.05	<0.05	<0.05	<0.05	<0.05	<0.05
Nb	µg/l	<0.02	<0.02	<0.02	<0.02	<0.02	<0.02	<0.02	<0.02
Mo	µg/l	0.6	0.33	0.5	1.46	1.49	0.17	4.47	<0.3
Ag	µg/l	<0.07	<0.05	<0.05	<0.05	<0.05	<0.05	<0.05	<0.05
Cd	µg/l	<0.04	<0.02	<0.02	<0.02	<0.02	<0.02	<0.02	<0.04
Sn	µg/l	<0.04	<0.02	<0.02	<0.02	<0.02	0.6	<0.02	<0.04
Sb	µg/l	0.12	0.13	0.1	0.09	0.12	0.12	0.1	<0.05
Cs	µg/l	<0.007	0.809	0.076	0.008	0.025	0.008	<0.005	<0.02
La	µg/l	<0.002	<0.009	<0.009	<0.009	<0.009	<0.009	<0.009	<0.03
Ce	µg/l	<0.002	<0.009	<0.009	<0.009	<0.009	<0.009	<0.009	<0.04
Pr	µg/l	<0.002	<0.008	<0.008	<0.008	<0.008	<0.008	<0.008	<0.05
Nd	µg/l	<0.03	<0.04	<0.04	<0.04	<0.04	<0.04	<0.04	<0.2
Sm	µg/l	<0.005	<0.009	<0.009	<0.009	<0.009	<0.009	<0.009	<0.03
Eu	µg/l	<0.004	<0.007	<0.007	<0.007	<0.007	<0.007	<0.007	<0.008
Gd	µg/l	<0.003	<0.009	<0.009	<0.009	<0.009	<0.009	<0.009	<0.007
Tb	µg/l	<0.002	<0.009	<0.009	<0.009	<0.009	<0.009	<0.009	<0.007
Dy	µg/l	<0.002	<0.009	<0.009	<0.009	<0.009	<0.009	<0.009	<0.007
Ho	µg/l	<0.002	<0.008	<0.008	<0.008	<0.008	<0.008	<0.008	<0.007
Er	µg/l	<0.002	<0.008	<0.008	<0.008	<0.008	<0.008	<0.008	<0.008
Tm	µg/l	<0.002	<0.01	<0.01	<0.01	<0.01	<0.01	<0.01	<0.007
Yb	µg/l	<0.002	<0.002	0.005	<0.002	<0.002	<0.002	<0.002	<0.008
Lu	µg/l	<0.002	<0.009	<0.009	<0.009	<0.009	<0.009	<0.009	<0.007

Hf	µg/l	<0.01	<0.01	<0.01	<0.01	<0.01	<0.01	<0.01	<0.01
Ta	µg/l	<0.02	<0.02	<0.02	<0.02	<0.02	<0.02	<0.02	<0.02
W	µg/l	<0.07	<0.07	<0.07	<0.07	<0.07	<0.07	<0.07	<0.05
Tl	µg/l	0.14	<0.01	0.01	<0.01	<0.01	<0.01	<0.01	<0.01
Pb	µg/l	<0.1	0.02	0.03	<0.02	<0.02	<0.02	<0.02	<0.02
Th	µg/l	<0.005	<0.02	<0.02	<0.02	<0.02	<0.02	<0.02	<0.009
U	µg/l	1.11	0.15	0.65	0.24	0.54	<0.02	<0.02	1.58

Table 28: Field parameters, range of major and minor elements in selected samples from the Woodham Burn site

LIMS Code		*ICP-MS DL*	14231-0056	14231-0057	14231-0009	14283-0061	14231-0010	14283-0062
Sample Code			Woodham Burn- bank seepage 1	Woodham Burn- bank seepage 2	Woodham Burn- bank seepage 3	Woodham Burn- standing water in waterlogged area	Woodham Burn spring	N1_SEEPAGE
Easting			429105	429083	429083	429528	429172	429172
Northing			527014	526975	526975	527127	527145	527145
Conductivity	µS/cm		-	-	-	2133	-	2443
pH			-	-	-	7.39	-	7.14
Ca	mg/l	*0.7*	111	209	125	210	253	263
Mg	mg/l	*0.01*	39.0	122	67.9	138	168	158
Na	mg/l	*0.3*	41.4	69.8	59.2	64.2	93.2	85.2
K	mg/l	*0.03*	8.71	8.60	5.97	11.9	11.6	11.9
HCO_3^-	mg/l		328	623	419	649	724	736
Cl^-	mg/l		97.8	52.4	68.4	68.6	43.0	36.8
SO_4^{2-}	mg/l		100	660	265	654.5	840	839.7
NO_3^-	mg/l		52.6	3.11	4.12	6.00	0.957	<1.5
Br^-	mg/l		0.106	<0.2	<0.1	<0.2	<0.2	<0.5
NO_2^-	mg/l		0.424	<0.1	<0.05	<0.1	<0.1	<0.25
HPO_4^{2-}	mg/l		1.21	<0.2	<0.1	<0.2	12	<0.5
F^-	mg/l		0.152	0.367	0.316	0.339	0.427	<0.25
NPOC	mg/l		11.0	1.07	1.25	12.7	2.09	2.05
Total P	mg/l	*0.04*	0.47	<0.04	<0.04	<0.04	<0.04	<0.04
Total S	mg/l	*2*	33	216	90	214	290	288
Si	mg/l	*0.05*	4.57	5.59	4.30	6.64	5.80	5.82

Table 29: Trace element concentrations in selected samples from the Woodham Burn site

LIMS Code		*ICP-MS DL*	14231-0056	14231-0057	14231-0009	14283-0061	14231-0010	14283-0062
Sample Code			Woodham Burn- bank seepage 1	Woodham Burn- bank seepage 2	Woodham Burn- bank seepage 3	Woodham Burn- standing water in waterlogged area	Woodham Burn spring	N1_SEEPAGE
Ba	µg/l	*0.1*	104	27.2	27.6	162	26.2	27.7
Sr	µg/l	*0.2*	204	759	334	635	1071	1192
Mn	µg/l	*0.3*	16.9	29.8	88.4	601	4.3	<2
Fe	µg/l	*2*	134	4	<2	79	7	<7
Li	µg/l	*3*	8	107	56	91	206	178
Be	µg/l	*0.01*	<0.01	<0.01	<0.01	<0.5	<0.01	<0.5
B	µg/l	*18*	45	155	123	47	253	182
Al	µg/l	*2*	9	2	<2	5	4	2
Ti	µg/l	*0.2*	1.0	<0.2	<0.2	<0.2	<0.2	<0.2
V	µg/l	*0.1*	0.8	<0.1	<0.1	0.2	<0.1	<0.1
Cr	µg/l	*0.2*	0.5	<0.2	<0.2	<0.3	<0.2	<0.3
Co	µg/l	*0.02*	0.49	0.09	0.11	0.18	0.03	<0.05
Ni	µg/l	*0.1*	5.8	0.9	2.0	0.7	0.4	0.3
Cu	µg/l	*0.6*	2.8	0.9	0.8	<1	0.7	<1
Zn	µg/l	*0.8*	14.5	9.2	15.1	<2	15.0	7
Ga	µg/l	*0.05*	<0.05	<0.05	<0.05	0.26	<0.05	<0.08
As	µg/l	*0.06*	1.33	<0.06	0.13	1.14	<0.06	<0.07
Se	µg/l	*0.1*	0.2	0.1	0.1	0.1	<0.1	<0.1
Rb	µg/l	*0.01*	2.15	3.64	2.81	1.31	7.91	7.93
Y	µg/l	*0.01*	0.09	0.03	<0.01	0.02	0.03	<0.02
Zr	µg/l	*0.09*	0.10	<0.09	<0.09	0.18	<0.09	<0.05
Nb	µg/l	*0.02*	<0.02	<0.02	<0.02	<0.02	<0.02	<0.02
Mo	µg/l	*0.08*	0.75	0.18	0.24	<0.3	<0.08	<0.3
Ag	µg/l	*0.05*	<0.05	<0.05	<0.05	<0.05	<0.05	<0.05
Cd	µg/l	*0.02*	0.03	0.03	<0.02	<0.04	0.02	<0.04
Sn	µg/l	*0.03*	0.11	0.11	0.08	0.49	<0.03	<0.04
Sb	µg/l	*0.02*	0.28	0.05	0.04	0.12	<0.02	<0.05
Cs	µg/l	*0.005*	<0.005	0.009	0.008	<0.02	0.015	<0.02
La	µg/l	*0.005*	0.067	0.008	<0.005	<0.03	0.018	<0.03
Ce	µg/l	*0.03*	0.08	<0.03	<0.03	<0.04	<0.03	<0.04
Pr	µg/l	*0.04*	<0.04	<0.04	<0.04	<0.05	<0.04	<0.05
Nd	µg/l	*0.07*	0.07	<0.07	<0.07	<0.2	<0.07	<0.2
Sm	µg/l	*0.006*	0.011	<0.006	<0.006	<0.03	<0.006	<0.03
Eu	µg/l	*0.002*	<0.002	<0.002	<0.002	<0.008	0.003	<0.008
Gd	µg/l	*0.003*	0.018	0.005	<0.003	<0.007	0.006	<0.007

Tb	µg/l	*0.002*	<0.002	<0.002	<0.002	<0.007	<0.002	<0.007
Dy	µg/l	*0.005*	0.014	<0.005	<0.005	<0.007	<0.005	<0.007
Ho	µg/l	*0.002*	0.004	<0.002	<0.002	<0.007	<0.002	<0.007
Er	µg/l	*0.002*	0.017	0.002	0.003	<0.008	0.003	<0.008
Tm	µg/l	*0.002*	0.003	<0.002	<0.002	<0.007	<0.002	<0.007
Yb	µg/l	*0.004*	0.026	0.006	<0.004	<0.008	<0.004	<0.008
Lu	µg/l	*0.002*	0.004	<0.002	<0.002	<0.007	<0.002	<0.007
Hf	µg/l	*0.01*	<0.01	<0.01	<0.01	<0.01	<0.01	<0.01
Ta	µg/l	*0.02*	<0.02	<0.02	<0.02	<0.02	<0.02	<0.02
W	µg/l	*0.05*	<0.05	<0.05	<0.05	<0.05	<0.05	<0.05
Tl	µg/l	*0.02*	<0.02	0.17	0.36	<0.01	0.09	0.06
Pb	µg/l	*0.04*	0.32	0.04	0.05	0.02	0.11	<0.02
Th	µg/l	*0.005*	0.01	<0.005	<0.005	<0.009	<0.005	<0.009
U	µg/l	*0.01*	0.980	3.57	2.27	10.8	4.33	3.97